

ESTABLISHING VISUAL BASED AND DATUM BASED SHORELINES AND  
SHORELINE UNCERTAINTIES ON A SANDY COAST: CAPE CANAVERAL, FLORIDA

By

RICHARD ALLEN MacKENZIE III

A DISSERTATION PRESENTED TO THE GRADUATE SCHOOL  
OF THE UNIVERSITY OF FLORIDA IN PARTIAL FULFILLMENT  
OF THE REQUIREMENTS FOR THE DEGREE OF  
DOCTOR OF PHILOSOPHY

UNIVERSITY OF FLORIDA

2012

UMI Number: 3585194

All rights reserved

INFORMATION TO ALL USERS

The quality of this reproduction is dependent upon the quality of the copy submitted.

In the unlikely event that the author did not send a complete manuscript and there are missing pages, these will be noted. Also, if material had to be removed, a note will indicate the deletion.



UMI 3585194

Published by ProQuest LLC (2014). Copyright in the Dissertation held by the Author.

Microform Edition © ProQuest LLC.

All rights reserved. This work is protected against unauthorized copying under Title 17, United States Code



ProQuest LLC.  
789 East Eisenhower Parkway  
P.O. Box 1346  
Ann Arbor, MI 48106 - 1346

© 2012 Richard Allen MacKenzie III

To my children, who have sacrificed much for me to get here, to mother who has supported me through the many years of finishing my education, to my family and friends whose support has been absolutely critical to this project, and to my father and Yolande Eve whom we lost along the way, you have been sorely missed.

## ACKNOWLEDGMENTS

I would like to thank my advisors John Jaeger and Peter Adams and my supervisory committee Robert Dean, Neil Opdyke, Michael Perfit, Mark Brenner, Joann Mossa, and Jane Southworth. My nine member supervisory committee, whom I have affectionately referred to as the, “The “Justice League” has provided innumerable assistance, advice and thoughts throughout this entire project. Besides my committee I would like to thank my mentors at Mott College (Frederick DeGroot), The University of Toledo (Timothy Fisher), and Bowling Green State University (Peg Yacobucci). They have also provided good advice and encouragement whenever it was required, which was a lot. I would also like to thank the staff at the University of Florida Department of Geological Sciences, without which none of this would have been possible; Nita Fahm, Dow Van Arnam, Carrie Williams, Pam Haines, and Susan Lukowe. I would also like to thank Christian Russell and Ray Thomas for the frequent electronic interventions they performed to keep me working, without which this project would have certainly taken another 5 years to complete.

I would like to thank the folks at NASA (John and Krista Shaffer, and Don and Mary Dankert) and Innovative Health Applications (Carlton Hall, Jane ad Marc Provancha, Ron Schaub, Shanon Gann, Tim Kozusko, Donna Oddy, Eric Reyier, and Doug Scheidt) for all of the friendship and support they have provided. I would also like to thank the folks on the Dune Vulnerability Team (DVT) that have provided guidance and support including Nathaniel Plant and Cheryl Hapke (USGS), Don George and Angy Chambers (U.S. Air Force), Ralph Llyod, James Lyon, and Steve Trull (U.S. Fish and Wildlife).

This research was supported by data and grants from NASA Environmental Programs Branch - Kennedy Space Center, The Geoeye Foundation, Innovative Health Applications, Ocean Weather Inc., Geological Society of America (Graduate Student Research Grant), Sedimentary Society for Sedimentary Geology (Dr. Mary Kraus SEPM President's Student Research Grant), The University of Florida Department of Geological Sciences, The University of Florida Graduate College, The George A. Smathers Library, and The University of Florida Office of Research, The U.S. Department of Agriculture, and The Florida Department of Environmental Protection.

Finally, I would like to thank my fellow students and friends who have influenced this project or my journey to the completion of this project. To the best field crew ever, Bianca Maibauer, Tim Kirchner, and Albert Carmenate, thank you for ALL of the avoided disasters. I would like to acknowledge my UF graduate student cohort; Mary Beth Day, Julie Mathis, and Marie Kurz, for all the support and advice they have offered and for all of the complaining I have done throughout this dissertation. This is especially true for Mary Beth Day, Annette Farah, and John Ezell who were, by no fault of their own, forced to share an office with me as some sort of punishment. I would like to acknowledge the post-doc's that provided advice, editing, encouragement, and scooter rides to campus if needed, Adam Goss (Dr. Metro) and Amanda Waite, thank you! To Derrick, who has had to endure more complaining and whining than anyone else during this process, "Thanks Bro!". I would also like to acknowledge team Sedimentology; Dylan Loss and Tania Villasenor, and team Coastal Shaun Kline, Jessica Lovering, JD Lovering, and Katherine Malone the best lab groups at UF! I want to thank all of my military friends especially Paul Bremner, "Chair Force!", for all of the time keeping these

“Academics” on the straight and level. I would also like to acknowledge the Anthropology group especially JD Pampush and Los for evolutionary advice and other advice that was tossed my way.

## TABLE OF CONTENTS

	<u>page</u>
ACKNOWLEDGMENTS.....	4
LIST OF TABLES.....	10
LIST OF FIGURES.....	11
LIST OF ABBREVIATIONS.....	18
ABSTRACT .....	20
CHAPTER	
1 INTRODUCTION .....	25
1.1 Motivation for this Dissertation .....	25
1.2 Local Questions with Broader Impacts.....	29
2 GEOMORPHIC SETTING OF CAPES AND THE CAPE CANAVERAL SYSTEM..	37
2.1 Formation.....	37
2.2 Ridges and Migration .....	38
2.3 Similarities and Differences with Other Capes .....	40
3 USING RTK-GPS TO MONITOR SIMPLE AND COMPLEX SANDY SHORELINES AT CAPE CANAVERAL, FLORIDA .....	49
3.1 Introduction .....	49
3.2 Study Area .....	51
3.3 Background.....	53
3.3.1 Global Navigation Satellite System (GNSS).....	53
3.3.2 Global Positioning System (GPS).....	53
3.3.2 Real-Time Kinematic Global Positioning System (RTK-GPS) .....	54
3.3.2 GPS Beach Monitoring and Surveying .....	55
3.4 Methods .....	56
3.4.1 GPS.....	56
3.4.2 Slope Break DBS Survey Style and SWASH MHW Contours .....	58
3.4.3 Survey Style .....	61
3.5 Results.....	61
3.5.1 Static Testing of RTK-GPS Data Acquisition .....	61
3.5.2 Field Data Acquisition Experiments-Slope Break Versus SWASH .....	64
3.5.3 Other Field Data Acquisition Experiments .....	65
3.6 Discussion .....	66
3.6.1 Testing of RTK-GPS Data Acquisition .....	66
3.6.2 Field Data Acquisition Experiments .....	70

3.7 Conclusions .....	73
<b>4 ANNUAL VARIANCE IN DATUM BASED SHORELINE POSITION .....</b>	<b>93</b>
4.1 Introduction .....	93
4.2 Physical Setting .....	98
4.3 Methods and Data Overview.....	101
4.3.1 Wave Data.....	101
4.3.2 Survey, Datum and Definitions .....	101
4.4 Results.....	104
4.4.1 Wave Data During Survey Periods.....	104
4.4.2 Slope .....	105
4.4.3 Net Shoreline Change .....	106
4.4.4 Shoreline Change Envelope .....	108
4.4.5 Slope Versus Shoreline Change Envelope (SCE).....	109
4.4.6 Seasonal Variation in Shoreline Change Envelope .....	110
4.5 Discussion .....	111
4.5.1 Spatial Trends in Shoreline Behavior and Morphology.....	111
4.5.2 Net Shoreline and Annual Reversals.....	112
4.5.3 Annual Shoreline Uncertainties .....	113
4.5.4 Three-Month Variation in Shoreline Change .....	114
4.6 Conclusions .....	115
<b>5 IMPROVEMENTS OF VISUALLY BASED SHORELINE (VBSL) ACCURACY FROM SIMULTANEOUS SATELLITE IMAGERY COLLECTION AND DIFFERENTIAL RTK-GPS SURVEYS: CAPE CANAVERAL, FLORIDA.....</b>	<b>134</b>
5.1 Introduction .....	134
5.2 Study Area .....	137
5.3 Delineating Shoreline Proxies and Uncertainty .....	138
5.3.1 Datum-Based Shoreline (DBSL) Proxies.....	138
5.3.2 Visual Based Shoreline (VBSL) Proxies .....	139
5.3.3 VBSL/DBSL Bias Corrections.....	141
5.4 Methods .....	143
5.4.1 Remotely Sensed Image Capture and Analysis .....	143
5.4.2 RTK-GPS Surveys.....	144
5.4.3 HW Geomorphology .....	145
5.4.4 Water Level, Wave Height, and Wave Length .....	146
5.4.5 Slope .....	146
5.4.6 DBSL MHW – VBSL HWL Offset Calculation.....	147
5.5 Results.....	149
5.5.1 Visual-Based Versus Datum-Based Shorelines .....	149
5.5.2 DBSL Versus Wet/Dry VBSL .....	150
5.5.3 DBSL Versus HW VBSL.....	150
5.5.4 DBSL Versus HWL offsets .....	151
5.5.6 VBSL/DBSL Offset Versus Beach Morphology .....	154
5.6 Discussion .....	155

5.6.1 Offsets .....	155
5.6.2 Simultaneous Image Capture and RTK-GPS Surveys .....	158
5.7 Conclusions .....	159
<b>6 CONCLUSIONS .....</b>	<b>179</b>
<b>APPENDIX</b>	
A TABLE OF SURVEYS AND SURVEY QUALITY .....	183
B TRIMBLE DATA COLLECTER DATA EXTRACTION.....	185
C POINT, TIN, RASTER, AND MEAN HIGH WATER SHAPFILE GENERATION.	193
D CAPE CANAVERAL WAVE CLIMATE .....	231
LIST OF REFERENCES .....	250
BIOGRAPHICAL SKETCH.....	259

## LIST OF TABLES

<u>Table</u>		<u>page</u>
3-1	Results of static testing of RTK-GPS with collection at 1 second intervals for 600 seconds. RTK-GPS tests were conducted with different distances between base station and rover and different dates.....	88
3-2	Results of a test of using multiple GPS Signals (L1 & L2, L2C) and GNSS (NAVSTAR & GLONASS) RTK-GPS data was collected at 1 second intervals for 600 seconds for each test. ....	89
3-3	The difference between a walked across shore transect location of the MHW DBSL and a MHW DBSL extracted from a raster DEM created by the Slope break survey style.....	90
3-4	Table showing the difference in elevations between different 3-dimensional surfaces constructed from a simple TIN for each of the different survey RTK-GPS collection strategies on a simple concave-up beach. ....	91
3-5	Table showing the difference in elevations between different 3-dimensional surfaces constructed via a simple TIN for each of the different survey RTK-GPS collection strategies for a complex beach with cusps and berm.....	92
4-1	Table of survey dates .....	130
4-2	Standard deviation of average significant wave height ( $H_s$ ) .....	131
4-3	Net change values for three-month intervals for May 2009 – June 2011.....	132
4-4	Shoreline change envelope values for three-month intervals for May 2009 – June 2011.....	133
5-1	Average beach slopes calculated at 1 km intervals and used for HW VBSL offset corrections. ....	178
A-1	Dates of surveys and survey quality .....	183
D-1	Standard deviation of average significant wave height ( $H_s$ ) .....	247
D-2	Standard deviation of dominant wave period ( $T_P$ ).....	248
D-3	Standard deviation of average wave period ( $T_{AVE}$ ) .....	249

## LIST OF FIGURES

<u>Figure</u>		<u>page</u>
1-1	Coastal change operators and their spatial and temporal scales after Cowell and Thom, (1994). Red box illustrates the spatial and temporal scales of operators addressed in this manuscript.....	33
1-2	Bathymetry and topography of Cape Canaveral and adjacent coastal region. ..	34
1-3	Long-term shoreline change rates for study area after Absalonsen and Dean, (2010).....	35
1-4	Dates of historic imagery used in long-term shoreline change rate analysis in this dissertation.....	36
2-1	The Cape Canaveral – Merritt Island salient protrudes ~20 km from a normally straight Florida coastline. ....	43
2-2	Cape formation of fixed latitude over time on the Florida coast. Red oval indicate areas of possible capes located off shore as part of a massive Cape "retreat" massif. After White (1970) and Pirkle et al. (1972). ....	44
2-3	Absolute Dating records in the Cape Canaveral region. Osmond et al., and Brooks used Uranium/Thorium dating methods while others used OSL dating methods.....	45
2-4	Absolute Dating records logged in the Cape Canaveral study area. Brooks used Uranium/Thorium dating methods while others used OSL dating methods.....	46
2-5	Eustatic sea level trends for the last ~125 ka (Miller et al., 2005). Superimposed are characteristic periods of Cape Canaveral shoreline development according to interpretation from dates in Figure 2-4.....	47
2-6	Late Pleistocene to modern shoreline and geomorphic features that form the Cape Canaveral - Merritt Island Sedimentary Complex. Ages of features from Figure 2-4.....	48
3-1	Kennedy Space Center - False Cape study area with associated launch complex coastal infrastructure .....	76
3-2	ATV towed RTK-GPS trailer shown in three different configurations (2, 3, and 5 roving antennas). GPS trailer is equipped with tires purposely built for operation in sand. ....	77
3-3	The MHW tidal datum for Cape Canaveral is 0.28 m (NAVD88), MSL is -0.23 m and MLW is -0.68 m. ....	78

3-4	Representative RTK-GPS survey collection density, TIN of collected points, and TIN-generated elevation model.....	79
3-5	Raster DEM ( $1 \text{ m}^2$ ) constructed from TIN with 0.25 elevation contours (NAVD88). Mean High Water (MHW) Datum Based Shoreline (DBSL) shown by red line at 0.28 m NAVD88.....	80
3-6	Map of static RTK-GPS data collected at NGS benchmark KAREN on five different test dates with vertical NADV88 data displayed on "Y" axis with UTM 17N Easting displayed on "X" axis.....	81
3-7	Distribution and cumulative frequency plot of vertical RTK-GPS elevation data (NADV88) collected at 1 second intervals for 5 hours at a static point 9.7 km from base station .....	82
3-8	Results of a five-hour GPS acquisition test with data collected at 1 second intervals with 9.7 km between RTK-GPS base station and rover .....	83
3-9	Comparison of across shore MHW (0.28 m) locations derived from RTK-GPS walked transects following Morton (1993) and MHW locations derived from RTK-GPS Slope break survey style (colored lines) .....	84
3-10	Comparison of across shore MHW (0.28 m) locations (0 axis) derived from RTK-GPS walked transects following Morton (1993) and MHW locations derived from RTK-GPS.....	85
3-11	Comparison of survey styles on a simple concave-up beach. Panel 1 is in upper left corner. ....	86
3-12	Comparison of survey styles on a complex beach with cusps and berm. Panel numbering same as Fig. 3-11.....	87
4-1	Area of study including NASA critical coastal launch facilities.....	117
4-2	Long-term shoreline change rates for study area after Absalonsen and Dean (2010) .....	118
4-3	Example of data collection strategy and relevant vertical datums. Tidal datum for Cape Canaveral MHW is 0.28 m, MSL is -0.23 m and MLW is -0.68 m.....	119
4-4	Monthly average significant wave heights measured ~37.04 km east of Cape Canaveral in a water depth of 44.2 m.....	120
4-5	Average significant wave heights for the period of 1 April 2009 through 2 May 2010 with GPS survey times in red.....	121
4-6	Average significant wave heights for the period of 2 May 2010 through 2May 2011 with GPS surveys noted in red .....	122

4-7	Average slope and deviation of the slope of the foreshore (0.25 m – 0.75 m contours) for surveys conducted from May 2009 through April 2011 (25 individual surveys) .....	123
4-8	Average slope of the foreshore (0.25 m – 0.75 m contours) for surveys conducted from May 2009 through April 2010 and May 2010 through April 2011. ....	124
4-9	Annual shoreline change for the two survey periods of May 2009 – April 2010 and May 2010 – April 2011 .....	125
4-10	Comparison of the 2 year (May 2009 – April 2010 and May 2010 – April 2011) shoreline change envelope (SCE).....	126
4-11	Comparison of the average beach slope and the SCE for the survey period May 2009 – April 2010.....	127
4-12	Comparison of the average beach slope and the SCE for the survey period May 2010 – April 2011.....	128
4-13	Three-month interval shoreline change envelopes (blue) with maximum individual transect SCE values (green).....	129
5-1	NASA coastal property at Kennedy Space Center consists of Merritt Island Capes .....	160
5-2	Historic shoreline change rates derived from Florida DEP across shore surveys at 1,000 ft intervals, after Absalonsen and Dean (2010) .....	161
5-3	Historic and modern aerial and satellite imagery available for use in decadal-scale coastal change studies at the Kennedy Space Center, Cape Canaveral, Florida. ....	162
5-4	Examples of visual based shorelines (VBSLs) from previous studies .....	163
5-5	VBSLs visible in different types of imagery from the Kennedy Space Center, Cape Canaveral, Florida.....	164
5-6	Tidal datum for Cape Canaveral MHW 0.28 m, MSL -0.23 m and MLW -0.68 m. ....	165
5-7	Water conditions found on the concurrent RTK-GPS survey and Geoeye I image capture on 28 July 2010.....	166
5-8	Average beach slopes for the period for 32 RTK-GPS surveys conducted between May 2009 - May 2011(blue), and the beach slope recorded on 28 July 2010 during the concurrent RTK-GPS survey and Geoeye 1 image.....	167

5-9	Different VBSLs and DBSLs from concurrent image capture and RTK-GPS survey conducted on 28 July 2010.....	168
5-10	Offset digitized between the tonal change wet/dry VBSL and the MHW DBSL produced by RTK-GPS survey .....	169
5-11	Offset between the HW VBSL traced on the ground during the RTK-GPS survey and the Geoeye I HW VBSL digitized at 10 m intervals. Both image capture and RTK-GPS survey were conducted on 28 July 2010.....	170
5-12	Offset between the geomorphically guided VBSL, and the MHW DBSL (red); offset between the HW VBSL with directly measured water levels and slopes measured at 10 intervals and the MHW DBSL (blue).....	171
5-13	Offset between geomorphically guided tonal wet/dry VBSL and MHW DBSL vs. beach slope and further dived by beach regions on 28 July 2010. ....	172
5-14	Offset between HW VBSL with offset correction applied using slopes calculated at 10 m intervals and measured water levels and MHW DBSL vs. slope and further divided by beach regions on 28 July 2010. ....	173
5-15	Offset between HW VBSL with offset correction applied using median slopes calculated at 1 km intervals and with MHW and MHW DBSL vs. slope and further divided by beach regions on 28 July 2010. ....	174
5-16	Offset between geomorphically guided tonal wet/dry VBSL and MHW DBSL vs. beach slope and further divided by beach morphology on 28 July 2010....	175
5-17	Offset between HW VBSL with offset correction applied using slopes calculated at 10 m intervals and measured water levels and MHW DBSL vs. slope and further divided by beach morphology on 28 July 2010. ....	176
5-18	Offset between HW VBSL with offset correction applied using average slopes calculated at 1 km intervals and with MHW and MHW DBSL vs. slope and further divided by beach morphology on 28 July 2010. ....	177
B-1	Screen capture of data collector connection to PC.....	185
B-2	Data controller destination configuration. ....	186
B-3	Data collector files and icon structure.....	187
B-4	Trimble Office GPS project screen shot. ....	189
B-5	Typical text file structure from Trimble Business Report Generator.....	191
B-6	DOP report generated by Trimble Business Job Report Generator.....	192
C-1	ArcGIS screen shot of steps to add GPS data.....	193

C-2	Screen shot of ArcGIS demonstrating export of data. ....	194
C-3	Screen shot depicting how to open the desired point shape file.....	196
C-4	Point shape file as it appears in ArcMap 9.3.....	197
C-5	Demonstration of converting data points to lines using XTools Pro.....	198
C-6	Selection box for making a Polyline from Points.....	199
C-7	An example of the polylines created from the point shape file.....	200
C-8	Creation of a Polyline in XTools Pro .....	201
C-9	Drawing a line that cuts across the Polyline at each end of the data set. In this case at the northern extent of the data as as shown in this figure cutting across the souther data extent. ....	202
C-10	Drawing a ling cutting across the data at both “ends” of the data. This example shows a line cutting through the northern extent of the data. Make sure both lines are “Deselected” by clicking outside of the drawing box.....	203
C-11	Use XTools Pro to convert both of the “drawn” lines to shapefiles by selecting “Layer Operations” in the XTools Pro drop down menu. Then by selecting “Convert Graphics to Shapes” in the “Layer Operations” drop down menu. ....	204
C-12	Selection of the “drawn” lines. Make sure both of the drawn polylines are selected, save the shapefiles in a work folder and add to the map.....	205
C-13	Instructions for splitting the single data poly line with the two drawn shapefiles created in the previous step. ....	206
C-14	Select the single polyline created from the data in step C-13, select the work folder for the data and name the Polyline shapefile that will be created. ....	207
C-15	Splitting of the single Polyline.....	208
C-16	Using the Edit tool to delete line segments internal to the outer lines surrounding the data.....	209
C-17	Removal of extra line segments in ArcGIS .....	210
C-18	Checking of the single Polyline in ArcGIS .....	211
C-19	Conversion of Polyline to a Polygon in ArcGIS. Under the XTools Pro drop down menu select “Feature Conversions” then “Make One Polygon from Polylines”.....	212

C-20	Screens shot of Polygon creation settings. Use the Polyline created in the previous steps that surround the point shapefile data. Name and save the Polygon in the work folder. ....	213
C-21	Error message if spurious points are not eliminated .....	214
C-22	Screen shot of location of extra line segments. The location of the extra line segments will be highlighted by red circles as shown above.....	215
C-23	Removal of extra line segments in ArcGIS .....	216
C-24	Screen shot of polygon with spurious data. ....	217
C-25	Removal of polygon intersections.....	218
C-26	Review the polygon that was created to ensure the polygon that contains all of the data points that are to be included in the construction of the TIN. ....	219
C-27	Adjustment of the polygon to cover all GPS data .....	220
C-28	Turing the GPS data into a TIN in ArcGIS .....	221
C-29	Setting the height source in ArcGIS.....	222
C-30.	Screen shot of clipping polygon settings .....	223
C-31	Removal of spurious data from GPS data. Once the TIN is created in ArcMap review its contents for pyramids or data artifacts .....	224
C-32	Final TIN generated from GPS points.....	225
C-33	Conversion of TIN to raster.....	226
C-34	Selecting the TIN used to create the raster. Under “Cell size” set size to 1.00. This sets the raster to build a grid of 1 m by 1 m squares. Save the Raster....	227
C-35	Screen shot of contour settings in ArcGIS.....	228
C-36	Setting ArcGIS to set contour elevation. Under the “Contour” menu set the contour interval greater than the range of elevations .....	229
C-37	MHW contour intersection with TIN .....	230
D-1	Wave buoy and hindcast locations. ....	240
D-2	Monthly average significant wave heights measured ~20 nm east of Cape Canaveral in a water depth of 44.2 m.....	241

D-3	Monthly comparison of average significant wave heights from NOAA Buoy 41009 collected (1988-2008) and the two annual study cycles (May 2009 - May 2010, May 2010 - May 2011). ....	242
D-4	Monthly comparison of dominant wave period from the WIS hindcast study (1988-2008) and the two annual study cycles (May 2009 - May 2010, May 2010 - May 2011). ....	243
D-5	Monthly comparison of average wave period from the WIS hindcast study (1988-2008) and the two annual study cycles (May 2009 - May 2010, May 2010 - May 2011). ....	244
D-6	Average significant wave heights for the period of April 1, 2009 through May 2, 2010 with GPS surveys lined in red. ....	245
D-7	Average significant wave heights for the period of May 2, 2010 through May 2, 2011 with GPS surveys lined in red. ....	246

## LIST OF ABBREVIATIONS

ATV	All – Terrain Vehicle
DEM	Digital Elevation Model
DVT	Dune Vulnerability Team
DBSL	Datum Based Shoreline
DSAS	Digital Shoreline Analysis System
GNSS	Global Navigation Satellite Systems
GPS	Global Positioning System
HWL	High Water Line
KSC	Kennedy Space Center
LIDAR	Light Detection and Ranging
MHW	Mean High Water
MLW	Mean Low Water
MSL	Mean Sea Level
NASA	National Aeronautics and Space Administration
NGS	National Geodetic Survey
NOAA	National Oceanic and Atmospheric Administration
NOS	National Ocean Service
OSL	Optically Stimulated Luminescence
PC	Personal Computer
PDOP	Position Dilution of Precision
QA/QC	Quality Assurance / Quality Control
RTK-GPS	Real Time Kinematic – Global Positioning System
SCE	Shoreline Change Envelope
SWASH	Surveying Wide – Area Shorelines

TIN	Triangulated Irregular Network
USGS	United States Geological Survey
VBSL	Visual Based Shoreline

Abstract of Dissertation Presented to the Graduate School  
of the University of Florida in Partial Fulfillment of the  
Requirements for the Degree of Doctor of Philosophy

ESTABLISHING VISUAL BASED AND DATUM BASED SHORELINES AND  
SHORELINE UNCERTAINTIES ON A SANDY COAST: CAPE CANAVERAL, FLORIDA

By

Richard A. MacKenzie III

August 2012

Chair: John M. Jaeger  
Cochair: Peter N. Adams  
Major: Geology

Shoreline change rates are used by scientists, coastal managers, and coastal municipal agencies to study and manage coasts; but the uncertainties associated with establishing shoreline positions are poorly understood and remain undocumented. These uncertainties arise through data collection, data processing, merging of different data types, and distinguishing short-term shoreline change “noise” from the long term shoreline trend signals. This dissertation examines these sources of uncertainty along the NASA-Kennedy Space Center coast, near Cape Canaveral Florida.

Several methods have been used to collect data to develop datum-based shoreline (DBSL): standard across shore transit surveys, Global Positioning System (GPS), and Light Detection And Ranging (LIDAR). Real Time Kinematic (RTK-GPS) survey methods and data collection strategies can include: across shore transect surveys, dual-track alongshore surveys, and multi-pass alongshore surveys (e.g. slope break, sawtooth, diamond, and square patterns). Field testing of the accuracy and precision of RTK-GPS systems in the coastal environment has largely consisted of the collection of a few tracks of data along a surface of known elevation. Little information is

available on the uncertainties (i.e. “point cloud size”) and growth of the GPS uncertainties over the course of a typical survey or those uncertainties that arise from the use of multiple Global Navigation Satellite System (GNSS) systems. Little data are available on the effectiveness of the various surveying spatial patterns and data collection strategies on a complex sandy beach with cuspatate and berm morphologies. Numerous tests were conducted using single and multiple GNSS systems at different base station-to-rover distances to establish the uncertainties associated with RTK-GPS topographical coastal surveys. Different survey methods and data collection strategies were tested to compare and contrast their performance in reproducing a geomorphic surface. RTK-GPS elevation uncertainties averaged 5.4 cm (95% confidence) for 22 individual ten minute tests with a data collection frequency of 1 Hz. Cumulative RTK-GPS elevation uncertainties for a five-hour test were ~9.0 cm (95% confidence) for the same data collection frequency. Our RTK-GPS survey, data collection strategy which follows beach face slope breaks in the along shore direction produced a Mean High Water (MHW) DBSL within 2 m of a backpack mounted across shore transect MHW elevation survey. The Slope Break method of collecting topographic data produced more cells within  $\pm$  10 cm of the reference surface than any of the other data collection strategies I tested. This result held true for both complex (cusps and berm) and simple (concave-up) sandy beaches.

Another source of uncertainty in establishing trends in shoreline change is the short-term variability (i.e. event-based, monthly, and seasonal) in shoreline position, which can be documented in shoreline change envelopes (SCE). Both seasonal and annual SCEs must be established to produce meaningful shoreline change rates;

however, the uncertainties associated with seasonal and annual change rates have been understudied due to the time and expense required. Additionally the seasonal uncertainties associated with the SCE are necessary to understand the uncertainties involved in the timing of both historical and planned shoreline data acquisition. To test the annual and seasonal shoreline change envelope two years of monthly and rapid-response storm RTK-GPS surveys were conducted along the 10 km coastal reach of the NASA-KSC site. During the first annual survey period, the average SCE over the entire study area was 13.0 m with a standard deviation of 3.3 m. During the second annual survey period the average SCE was 11.8 m with a standard deviation of 5.2 m. The SCEs for each of the annual study periods also revealed, not unexpectedly, that areas with more net change (either accretion or retreat) have the largest SCE. Three-month running means of SCEs over the two year period show that the months of April, May, and June have the lowest values (3 month SCE <3 m) than those collected during any other 3 month period.

Several methods each with their own sampling density, interval, and uncertainties, are currently used in decadal-scale coastal change studies. LIDAR has rapidly become the preferred tool for coastal studies with its high data density and moderate accuracy (15 – 30cm), but the typical sampling interval between LIDAR surveys is ~5 years. Coastal GPS studies have a higher accuracy (10 cm) and may be conducted at more frequent intervals than LIDAR, but data density is lower and the surveyed coastline length is minimized because of the effort required to collect the data. Remotely sensed imagery can provide insight into geomorphic evolution and system dynamics that may be difficult to extract from datum based shoreline DBSL survey methods. Remotely-

sensed imagery is attractive for long-term coastal change studies because of its historical significance and long duration of observation (decades), but it is the least accurate. A high degree of uncertainty associated with remotely sensed imagery revolves around the difficulty in choosing an appropriate visual shoreline proxy. This is due, in part, to the fact that specific visual based shoreline (VBSL) proxies (e.g. vegetation line, debris line, high water mark, wet/dry line, low water mark) are not visible on all beaches at all times. Geomorphic clues from remotely sensed imagery combined with knowledge of coastal morphology from DBS surveys can minimize uncertainties in using VBS proxies. In order to establish a relationship between VBS and DBS, I conducted 32 kinematic differential GPS surveys over a two-year period at the NASA-KSC site. Two Geoeye I (0.5 m resolution) satellite images were collected 3 days post DBS survey on June 9, 2009 and during a DBS survey on July 28, 2010. June and July beach states were selected for image collection because they have the lowest mean monthly significant wave height ( $H_s$ ) and least variability in  $H_s$ , providing the highest likelihood of stable beach morphology.

The 10-km study reach exhibits various slope characteristics, beach morphologic states and stability histories. A 2.0 km historically stable beach that is towards a reflective end member, with relatively high slopes (~ 0.10) is found in the northern portion of the study area. The 4.6 km central portion is characterized by an intermediate beach state and has been historically retreating. The 2.4 km False Cape region comprises a near dissipative beach, with low slopes (~ 0.06) and is historically accreting. The southernmost 1.0 km region has a mixed history of accretion and retreat, is an intermediate beach, and is characterized by relatively low slopes (~0.05).

During the July survey, the visual high water mark was traced with the GPS system, which revealed that the surveyed high water wet/dry line, did not correspond to the wet/dry line on the image. Further analysis shows that a wet/dry line related to grain size, composition and/or groundwater seepage, that is visible in all images, provides the most accurate VBS proxy. Direct comparison of this proxy with the image collected three days after the survey in June 2009 reveals a 5.9 m RMS offset of the VBS landward of the DBS and maximum offset 13.4 m landward of the DBS with an apparent inverse relationship between offset and beach slope. Comparison of the image collected concurrently with the DBS survey in July 2010 showed RMS and maximum offsets of 3.57 m and 8.9 m, respectively, with the VBS landward of DBS and an apparent positive correlation between offset and beach slope. Maximum excursions for both surveys appear to relate to dynamic morphology (i.e. bar welding, berm overwash) and minimum offsets appear to relate to stable unchanging states.

Although the decreased uncertainties make DBS techniques more desirable for coastal change studies, the economic trade off associated with increased cost and sampling frequency is, in some cases, insurmountable. Although LIDAR has become the widely accepted tool for coastal change studies, the combination of satellite imagery and a detailed documentation of its uncertainties is a valuable tool, because it offers the advantage of having an effectively instantaneous collection interval, a precise collection time, and a short return interval (~ 3 days).

## CHAPTER 1 INTRODUCTION

### 1.1 Motivation for this Dissertation

Coasts are among the most dynamic landforms on the Earth's surface, changing over a range of temporal and spatial scales. To better relate how different processes influence coasts, Cowell and Thom (1994) developed a convenient framework to depict spatial and temporal geomorphic coastal change (Figure 1-1). Bruun (1962, 1988) related coastal change at geologic timescales to sea level fluctuations. Named for him, Bruun's rule describes the movement of the coastal zone landward and upward as sea level rises, and seaward and downward as it falls through erosional and accretionary sedimentary processes. Wright and Short (2002; 1983, 1984) related seasonal and decadal beach morphologic change to fluctuations in beach states. The six states of beaches range from fully dissipative to highly reflective, and are related to the morphology, circulation, surf behavior, and resonant frequencies of the beach (Wright and Short, 1983, 1984). Stive (2004) described decadal shoreline position changes for high energy coasts on the eastern seaboard of the U.S. as being dominated principally by alongshore transport processes, and to a lesser extent, by across shore transport and anthropogenic changes. Graham (2005; 2001), Inman et al. (1996), and Seymour et al. (1984) demonstrated that climate variability plays a role in coastal change by showing that decadal shoreline position change in California was related to climate forcing through the El Nino Southern Oscillation (ENSO) phenomenon. The authors related observed morphologic changes to variation in the deep-water wave climate from changes in ENSO conditions from 1948-1998. Anthropogenic change is another important forcing agent on modern coasts operating at multiple spatial and temporal

scales. Examples of these changes include the construction of inlets, jetties, piers, and the nourishment of beaches (Woodroffe, 2002).

Determining the dominant decadal to centennial coastal forcing agents acting on the coast is a significant challenge. Most studies have observational durations of days or, at best, a few years, making decadal variability difficult to quantify. Experiments measuring the role of long-term processes such as sea level change have been contentious and quantifying the change caused by these processes has met with mixed results (Stive, 2004). Bird (1985) suggested that 70% of coastlines are eroding from anthropogenically induced sea-level rise following Bruun's rule. Although Bruun's rule is thought to act over geologic timescales, it has been suggested that decadal change at coasts is related to anthropogenic sea level rise (Leatherman et al., 2000). Several coasts, however have been accreting or eroding at greater rates than those predicted by application of Bruun's Rule, providing evidence that other forcing agents can override the "Bruun Effect" (Stive, 2004).

Cape Canaveral is an enigmatic coastal feature; it is a salient protruding from a normally straight, 400-km long sandy coast and its formation is thought to arise a combination of several geomorphic and geologic influences. Cape Canaveral is a barrier island – strand plain complex cape with no major associated fluvial system. The Cape Canaveral-Merritt Island complex is comprised of several ridge sets or strand plains formed during sea level high stands over the past ~100,000 years (Brooks, 1972; Rink and Forrest, 2005), accompanied by a complex bathymetry composed of numerous sandy shoals on a gently-sloped inner shelf (Figure 1-2). Historic aerial photography and modern satellite imagery suggest that several capes have nucleated

and persisted at this location since at least the Pleistocene. Questions relating to the formation of the cape, the conditions that brought about its formation, the modern forcing that affects the system, and the processes that allow capes to repeatedly nucleate in this location are the motivating themes of this research. Dean (1998) and Absalonsen and Dean (2010) showed that Cape Canaveral has a sinusoidal pattern of shoreline change over a 30 km reach, with growth and retreat often in opposition with older trends in shoreline change indicated by the prevalent ridge and swale topography of the cape (Figure 1-3). Understanding how short-term processes influence Holocene modification of the Cape requires data analysis of shoreline indicators reflecting a range of timescales, from short-term events (nor'easter storms and hurricanes) to decades of sea-level rise. Explaining how the coast in this area demonstrates both erosion and accretion over decadal timescales has been problematic, because the influences of storms, sea level rise, onshore/offshore sediment transport, and anthropogenic change have not been quantified.

Cape Canaveral, however, is also home to the John F. Kennedy Space Center and Cape Canaveral Air Force Station, which house a significant portion of the United States' space launch and support infrastructure. Recently a presidential initiative was passed to improve, expand, and modernize the Kennedy Space Center and its associated infrastructure. Launch operational imperatives, however, will keep much of that infrastructure within 500 m of the Atlantic coastline making it vulnerable to shoreline retreat. For example, during the week of May 17, 2009 a nor'easter storm impacted the Cape producing waves with a deep water height of 3-4 m for ~ 37 hours. This moderate storm over-topped and damaged several hundred meters of dunes that had been

repaired by NASA after the energetic 2004 hurricane season. The University of Florida's Cape Canaveral project was added to NASA's KSC Dune Vulnerability Team (DVT) as a consequence of NASA's concerns from the damage caused by this moderate storm. Following this storm, there was a desire to monitor the shoreline and dunes monthly, as a means of quantifying threats to endangered species habitat and infrastructure. The first task of the monitoring effort was to develop a method for quantifying monthly shoreline change along the 10 km reach of KSC property using RTK-GPS with stringent quality control. The second task involved the analysis of a large dataset of aerial photography and satellite imagery collected by the University of Florida and NASA's environmental contractor Innovative Health Application (IHA) (Figure 1-4). Monthly and storm RTK-GPS surveys were used to document shoreline position uncertainty associated with the annual variation in shoreline position or annual shoreline change envelope (SCE). The monthly and storm surveys can be used to derive seasonal SCEs, which provide guidance in analysis of aerial photography and satellite imagery and provide guidance on a preferred 3-month period to acquire shoreline data. The third task was to test the applicability of visual-based shoreline (VBSL) proxies, visible in remotely-sensed imagery, in the analysis of shoreline change. The testing involved identifying a VBSL proxy, common to all of the collected imagery, which has reduced uncertainties, and can be related to a datum based proxy such as Mean High Water (MHW).

It is anticipated that understanding the uncertainties associated with both VBSLs and DBSLs will provide a more accurate rate of shoreline change along the entire 10 km KSC coastal reach. Reducing the uncertainties associated with the use of historic aerial

imagery allows for shoreline retreat rates to be calculated using larger dataset, with a greater degree of confidence, than shoreline change rates calculated from DBSL proxies alone. The use of additional datasets by the inclusion of historical imagery also reduces the potential short-term trend bias associated with using only a few available DBSL datasets. Finally, it is anticipated that the shoreline change rates derived from combination of VBSP and DBSL data will provide insight into drivers of coastal change over the last two centuries. It is hoped that the questions addressed in this dissertation and those which arise from the results provide the foundation for further work to quantify and model the migration evolution of cape systems worldwide.

## **1.2 Local Questions with Broader Impacts**

The questions posed and addressed in this dissertation have local practical applications, but also serve to foster thought on broadly scoped implications about shoreline change studies. Coastal change studies have historically relied on aerial imagery (Boak and Turner, 2005; Crowell et al., 1991; Fletcher et al., 2003; Frazer et al., 2010; Genz et al., 2007; Moore, 2000; Moore et al., 2006b; Romine et al., 2009; Ruggiero and Lists, 2009; Smith and Zarillo, 1990) or across shore topographic surveys (Dail et al., 2000; Huang, 2002; Morton et al., 1993) to determine shoreline position, but new technologies have brought about a paradigm shift to methods that produce a datum based shoreline position (e.g. LIDAR and RTK-GPS) (Baganha Baptista et al., 2011; Barnard et al., 2009; Dail et al., 2000; Huang, 2002; List and Farris, 1999; Robertson et al., 2004; Ruggiero et al., 2010; Ruggiero et al., 2005; Sallenger et al., 2003; Stockdon et al., 2002). Although many studies have used RTK-GPS for shoreline change investigation, the uncertainties associated with the use of this method in coastal studies have had very little discussion. To establish GPS accuracy, Barnard (2007) tested a

single point of known elevation every survey. Baptista (2011) used a portion of a parking surface near a beach as a reference. However, most studies cite the instrument's reported potential precision (Huang, 2002) rather than independently establishing the precision in the field. The uncertainties associated with the use of RTK-GPS have seriously implications for modern coastal topographic surveys. LIDAR, for instance, uses a GPS receiver in the aircraft to relate to position of the LIDAR instrument to the ground. The uncertainties associated with the use of vehicle-mounted GPS instruments determine the amount of change that can be measured. The tests described in Chapter 3 of this dissertation provide information on the uncertainties associated with the use of RTK-GPS in any coastal study. As the use of RTK-GPS in coastal topographic studies increases, establishment of the uncertainties associated with the use of these instruments becomes increasingly relevant.

The use of RTK-GPS systems mounted on all-terrain vehicles have allowed coastal scientists and engineers to construct three-dimensional models of the foreshore and backshore from which changes in beach volume and datum-based shoreline position may be extracted (Baganha Baptista et al., 2011; Barnard et al., 2009; Barnard et al., 2007; Dail et al., 2000; Hansen and Barnard, 2009, 2010; Ruggiero et al., 2005). Several different data collection strategies have been used to collect these data including: multiple across shore transects (Morton et al., 1993), a single alongshore pass (List and Farris, 1999; List et al., 2006), multiple alongshore passes (Barnard et al., 2009; Hansen and Barnard, 2010; Ruggiero et al., 2005), alongshore square wave (Malone, 2011), or multiple alongshore passes following slope breaks (this study). Each of the aforementioned data collection strategies each have an associated cost in terms

of: (1) time per survey, (2) distance covered in during the survey, and (3) data collection density. To establish uncertainties associated with each data collection strategy, I describe, in Chapter 2, how different data acquisition strategies were tested. I test a volumetric data collection strategy's ability to reproduce a three-dimensional idealized foreshore and backshore surfaces. I also test each volumetric model for interpolation artifacts using a simple triangulated network of survey points. Testing each of these data collection methods will assist researchers in selecting the most cost-effective method to extract the pertinent shoreline position data.

There are a multitude of coastal studies using both visual based shoreline proxies, such as those extracted from aerial or satellite imagery (Boak and Turner, 2005; Crowell et al., 1991; Fletcher et al., 2003; Frazer et al., 2010; Genz et al., 2007; Moore, 2000; Moore et al., 2006b; Romine et al., 2009; Ruggiero and Lists, 2009; Smith and Zarillo, 1990), and datum based shoreline proxies, such as those gathered by LIDAR (Brock et al., 2002; Klemas, 2011; Robertson et al., 2004; Sallenger et al., 2003; Stockdon et al., 2002; Young and Ashford, 2006) or GPS (Baganha Baptista et al., 2011; Barnard et al., 2009; Barnard et al., 2007; Dail et al., 2000; Hansen and Barnard, 2009, 2010; Ruggiero et al., 2005) . Regardless of the method used to extract a shoreline, the uncertainties associated with the annual change in shoreline position, also known as a shoreline change envelope (SCE), are poorly understood. To measure the annual shoreline change envelope, monthly and storm (rapid-response) surveys must be conducted, which is a time consuming and expensive undertaking (Moore, 2000). Many studies have estimated the SCE from one image taken in summer and one image taken in winter (Fletcher et al., 2003; Genz et al., 2007; Romine et al., 2009), while others

suggest the exclusion of all imagery collected around the times of storms or use only spring and summer images (Moore, 2000). In Chapter 4, I describe a study that establishes the shoreline change envelope (monthly and storm) for two years and relate the findings to beach morphology. Uncertainties associated with the change in shoreline position provide information on the optimal time of year to collect shoreline position data, and therefore help to establish the uncertainties associated with historic shoreline position data.

There are multiple visual shoreline based proxies (VBSL) used to extract a shoreline position from aerial and satellite imagery (Boak and Turner, 2005). Many of these proxies share the same name, but reflect different vertical and/or horizontal position on the beach, thereby adding uncertainty to shoreline position studies (Boak and Turner, 2005). The high water level (HWL) mark has been used in the United States since the 1800's to delineate shoreline positions on nautical charts, and many studies using VBSL proxies use a HWL mark to identify shoreline position. Several authors have attempted to use offsets to compensate or shift the HWL to coincide with the mean high water (MHW) datum used in more modern studies. In Chapter 5, I examine which proxy best reduces uncertainty associated with VSBLs. In the last 10 years there has been a concentrated effort to use modern DBSL which, unfortunately, excludes data from historical imagery. A goal of this study is to test methods that might minimize uncertainty in shoreline position determination, thereby providing full utilization of data sources to examine for the processes responsible for shoreline change over a range of timescales.

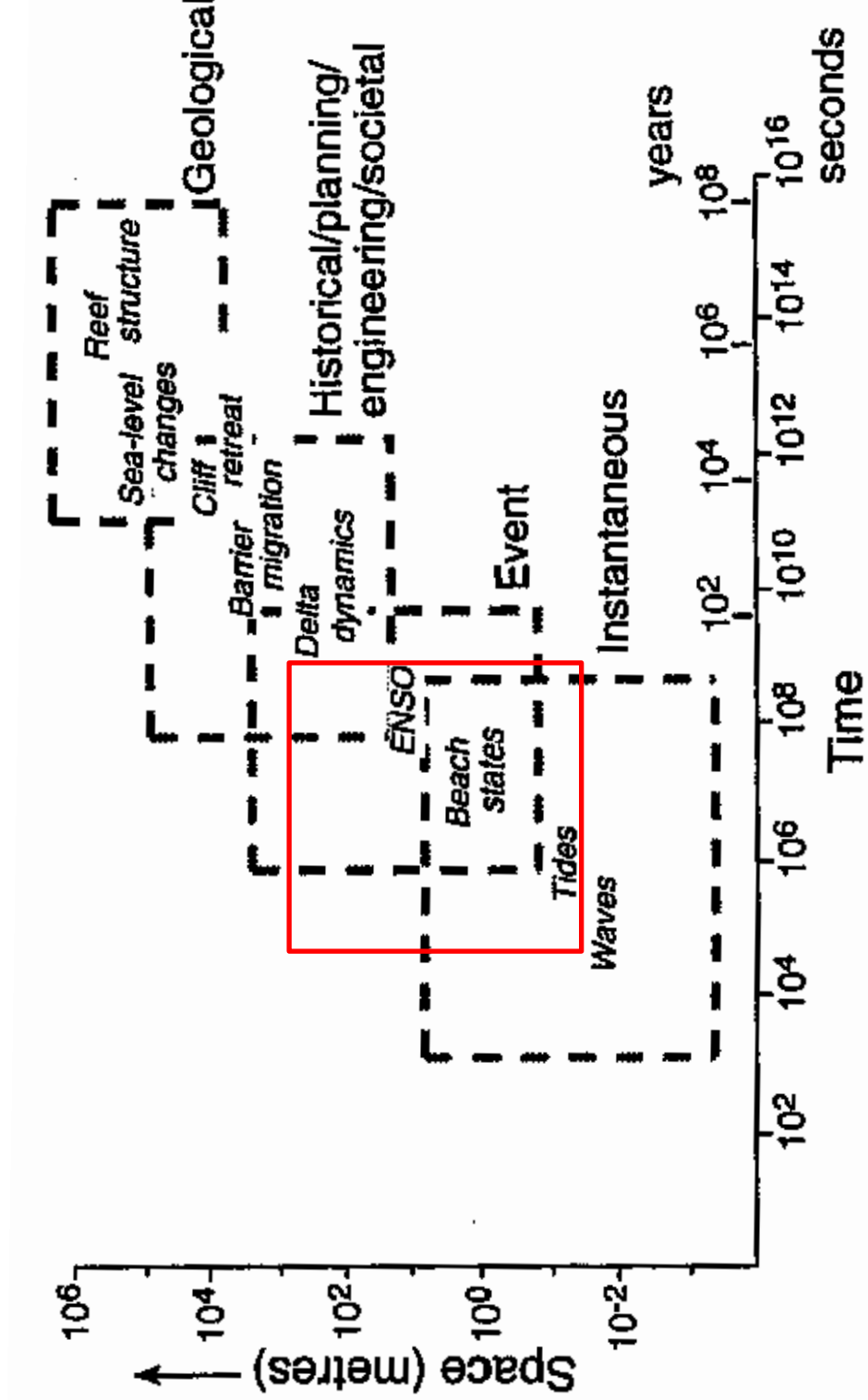


Figure 1-1. Coastal change operators and their spatial and temporal scales after Cowell and Thom, (1994). Red box illustrates the spatial and temporal scales of operators addressed in this manuscript.

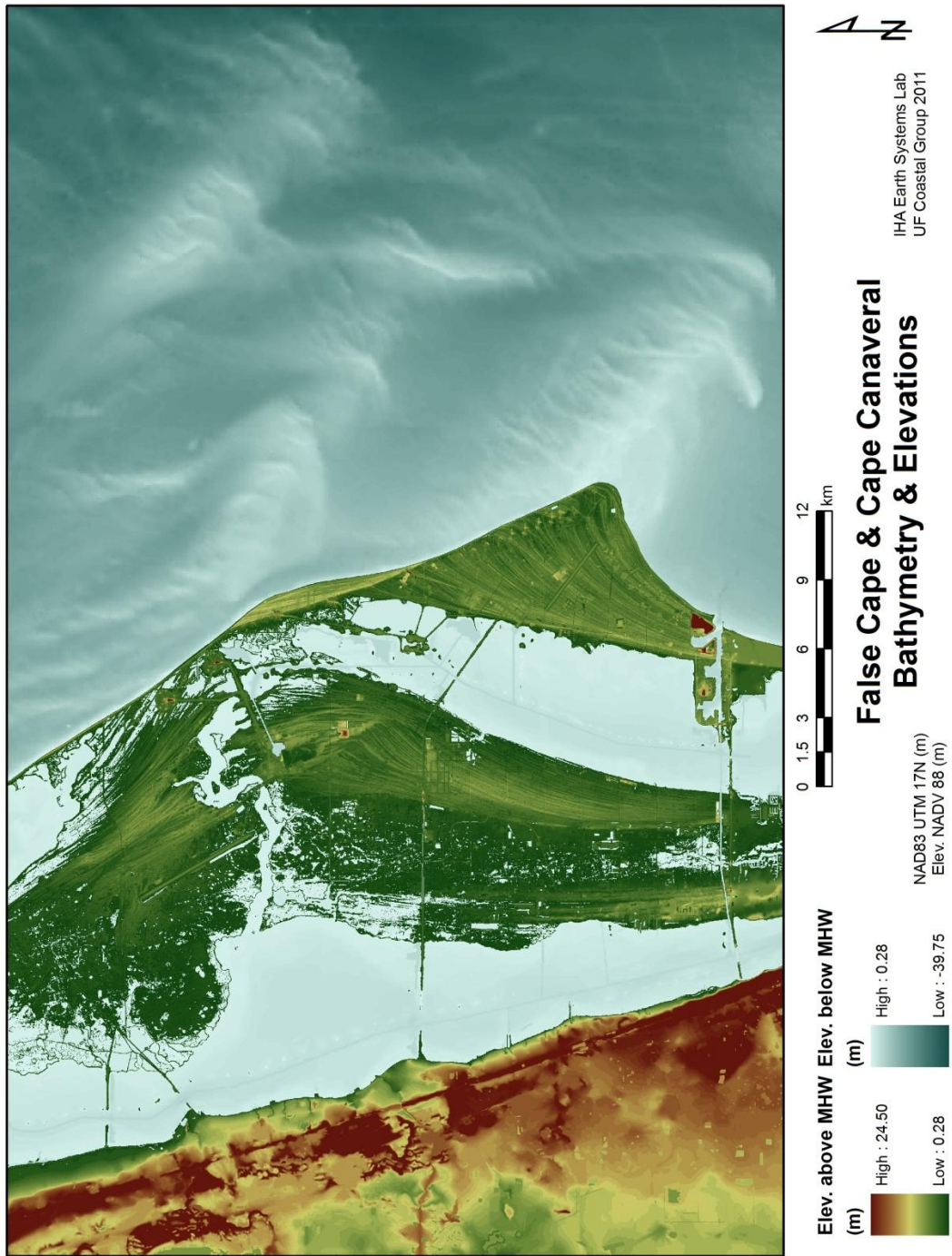


Figure 1-2. Bathymetry and topography of Cape Canaveral and adjacent coastal region. All elevations above mean high water (0.28 m NAVD88) are colored as subaerial topography and were obtained from a LiDAR survey (2007). Bathymetry is derived from composite surveys conducted by NOS/NOAA.

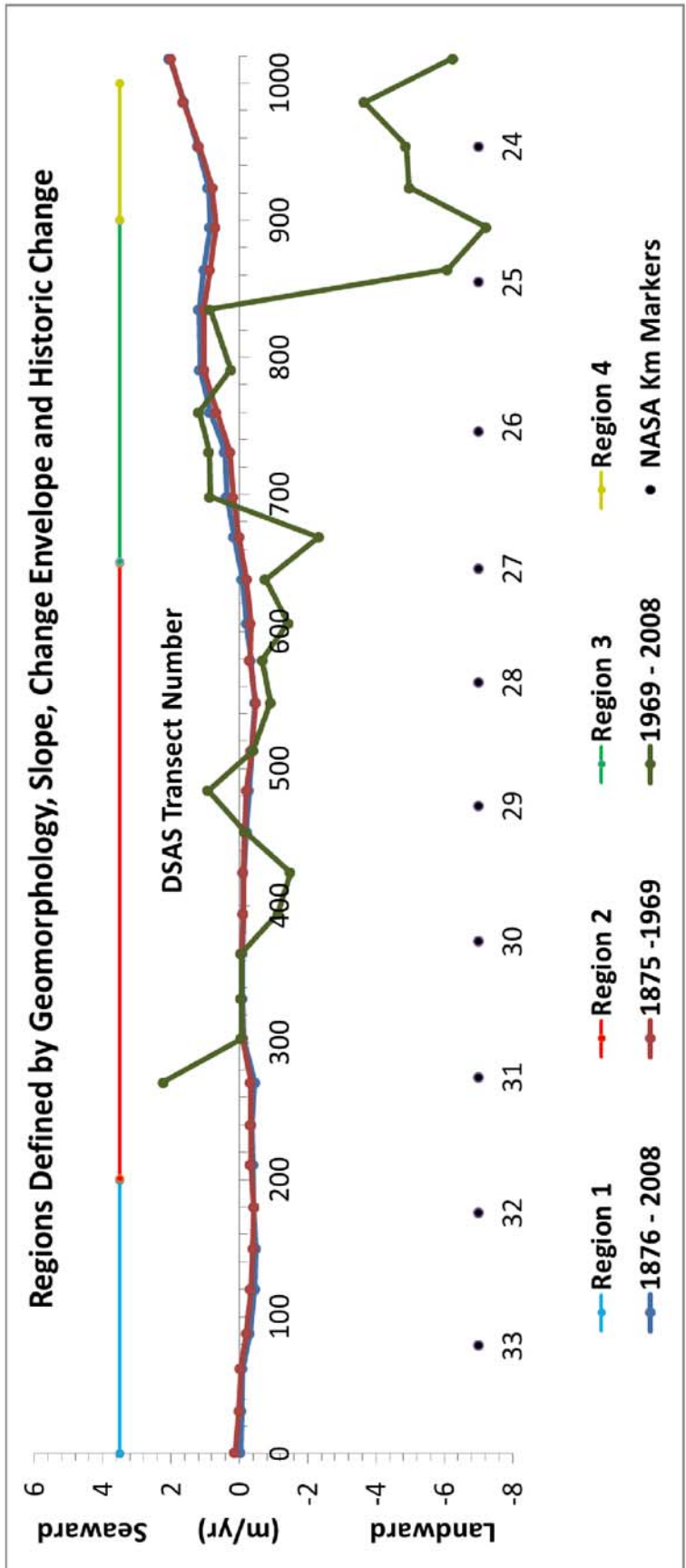


Figure 1-3. Long-term shoreline change rates for study area after Absalonsen and Dean, (2010). The more recent change rates (1969-2008) do not reflect the longer-term rates (1876-2008). Long-term change rate data is sporadic at this site after 1943 due to Kennedy Space Center's designation as a federal facility bordered by a National Seashore and a U.S. Air Force Base.

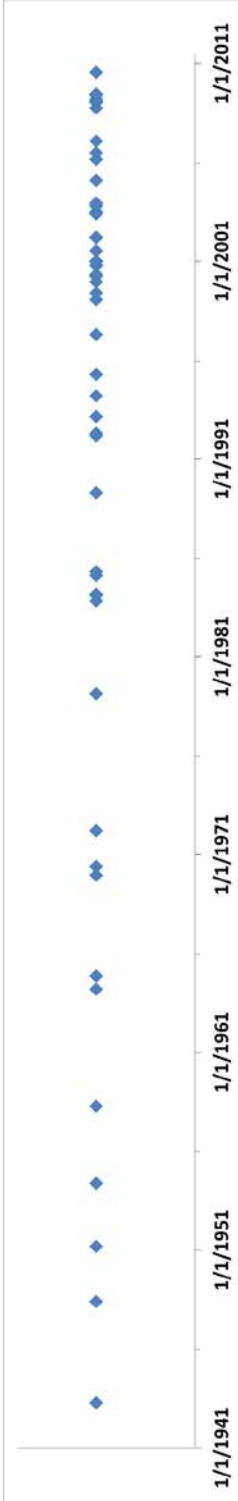


Figure 1-4. Dates of historic imagery used in long-term shoreline change rate analysis in this dissertation.

## CHAPTER 2

### GEOMORPHIC SETTING OF CAPES AND THE CAPE CANAVERAL SYSTEM

Cape Canaveral-Merritt Island sedimentary system is a depositional geomorphic feature that protrudes abruptly from a remarkably straight, sand-dominated, divergent margin coast (Figure 2-1). The coastal landmass comprising the Canaveral-Merritt Island region consists of regularly spaced, shore-parallel beach ridges that record a monotonic depositional history of sea level high stands, that indicates persistence of the Cape over several tens of thousands of years (Figure 2-1). Several hypotheses have been offered to account for the formation and maintenance of this large geomorphic feature including (1) antecedent topography, (2) alternating obliquely-approaching wave fields, (3) convergent littoral cells, and (4) slow, alongshore migration of sediment pulses. This chapter provides an overview of the geomorphic and geologic setting at Cape Canaveral and discusses the processes responsible for cape formation along sandy shorelines.

#### **2.1 Formation**

Cape Canaveral is one of the most recognizable coastal geomorphic features along the east coast of North America, but its geomorphic history is not well known. Several competing theories of paleo- and modern cape formation in this area have been argued and published over the last several decades. White (1958, 1970) was the first to suggest that several capes have formed at the same latitude of the modern cape during the Holocene from sea level fluctuations (Figure 2-2). Pirkle et al. (1972) described the paleo-cape on Merritt Island as an eastward or seaward progressive cape, as opposed to the southward progressing modern cape. He attributes this variation to eustatic sea level changes related to glacial and interglacial periods. White (1958, 1970), Vernon

(1951), and Brown et al., (1962), argue for a structural geological component to the formation of the Cape, but Meisburger and Duane (1971) found no evidence of faulting in the surrounding subsurface to account for a significant structural component. Both transgressional and regressive sea level fluctuations have been argued as probable causes for the Cape's formation (Brooks, 1972; May, 1972; Pirkle et al., 1972). Another theory suggests that the convergence of a major southward-moving littoral cell and a minor northward moving cell could cause the cape to form in its present location (Field and Duane, 1974b; Kofoed, 1963). Antecedent geology has also been suggested as a factor in cape formation (Randazzo and Jones, 1997). The Sanford High, located a few kilometers to the northwest of the complex, has a higher lithologic strength than the surrounding rocks, which could provide a deflection point for alongshore currents. Recently, a numerical model developed by Ashton et al., (2001) was able to simulate cape-like features produced by instabilities induced by high-angle wave-fields.

## **2.2 Ridges and Migration**

Aerial orthographic quadrangle photos taken prior to the construction of the Kennedy Space Center on Cape Canaveral indicate the presence of four to eleven individual beach ridge sets (Brooks, 1972). Each set exhibits a characteristic orientation, wavelength, period, and amplitude that may reflect the wave climate and sea level conditions responsible for ridge set formation (Brooks, 1972; Rink and Forrest, 2005). Aerial photos also reveal the recent migration history of the cape, from northwest to southeast (Shepard and Wanless, 1971). However, the details of the modern processes involved in cape migration are poorly defined. As the Cape migrates seaward to the southeast, portions of older ridges on the north side are eroded while new ridges accrete seaward south of the existing shoreline. It is unclear whether the sediments

eroded from the paleo-cape account for a large portion of sediment supply to the littoral cell, the sediment is supplied by a positive divergence of drift, or if sediment is provided by alongshore transport.

The first absolute dates for the beach ridges on the Cape Canaveral-Merritt Island complex were provided by Osmond et al., (1970) using  $^{232}\text{U}/^{225}\text{Th}$  dating techniques on shell material found in local quarries and beach ridges. The results demonstrated an age of 2.87-10.33 ka for samples collected at Patrick Air Force Base and Eau Gallie Beach in a coastal area south of the modern cape Figures 2-3 and 2-4. Samples from the Banana River on the South Shore of Merritt Island produced an age of ~30,000 ka, and test on a coquina from the Titusville quarry produced an age of ~110,000 ka. Brooks (1972) produced a series of dates on the modern cape using  $^{14}\text{C}$  dating on reworked shell material recovered from cores (Figures 2-3 and 2-4). The dates showed that ridges became progressively younger from the northwest to the southeast, with the oldest ridges at 7,670 ka to the youngest ridges at 1,980 ka near the tip of the modern cape position. Rink and Forrest (2005) suggested these dates were too old due to the reworking of the shell material and heavy isotopic signature in modern bivalves found on the cape. The Optically Stimulated Luminescence (OSL) method used by Rink and Forrest (2005) provided dates along a northwest-southeast track similar to that of Brooks (1972). OSL dates for the oldest ridges were found to be 4,020 years B.P. and the youngest dates near the tip of the cape at 150 years B.P. Rink and Forrest also recovered a date of 43,750 ka from north Merritt Island and an age of 8,070 ka from a location near the Titusville Quarry (Figures 2-3 and 2-4). These dates demonstrate that sea level may have reached a level near modern sea level between 7.67 and 4.02 ka in

order for the oldest ridges to form and be preserved. Figures 2-5 and 2-6 compare sea-level history to the  $^{14}\text{C}$ ,  $^{232}\text{U}/^{225}\text{Th}$ , and OSL dates found on Merritt Island, Cape Canaveral, and the surrounding area. These dates indicate that the modern cape-preserved ridges have formed since the LGM, whereas the Merritt Island ridges possibly formed during the oxygen isotopic 3a or 3c sea level high stands. This is problematic since the ridges are ~2-3 m higher than the modern cape ridges while sea level then is thought to be ~40 m lower than current sea level. The oldest date at ~110,000 ka may be associated with the Princess Ann Shoreline at the oxygen isotopic 5e sea level high stand. This shoreline shows no cape formation and follows the normal northwest-southeast trend of the Florida coast, suggesting this may be an erosional high stand coastline.

### **2.3 Similarities and Differences with Other Capes**

The Cape Canaveral-Merritt Island sedimentary system is a large cuspat foreland on the Florida Atlantic Coast that contains a series of accretional beach ridge and swale sets projecting 20 km seaward of the regional coastal trend. The Cape is part of a series of large cuspat forms on the southeast coast of the North America that also includes the capes on the Outer Banks of North and South Carolina including Capes: Hatteras, Lookout, Fear, and Romain. Cuspat features are a ubiquitous geomorphic form that can occur along river channels, elongate bays, or on outer coast shorelines (Dean and Dalrymple, 2002). The presence of these cuspat shorelines on the outer coasts of the southeastern North America has given rise to a highly variable shoreline configuration with variable susceptibility to erosion (Dolan, 1971; Dolan and Ferm, 1968; Dolan and Hayden, 1981; Dolan et al., 1977). The processes involved in the accretion, erosion, location, and movement of these features is poorly understood, making it difficult to

predict how changing climatic conditions will affect their appearance and position. The largest cuspat forms of the southeastern United States coasts in the hierarchy of Dolan and Ferm (1968) are the capes found in the Carolinas, Georgia, and Florida. These capes include Hatteras, Lookout, Fear, Romain, Tybee Island, and Canaveral. The capes are associated with seaward shoals extending several kilometers off shore with depths of ~10 m, and are part of the barrier island system fringing the coast (Komar, 1998). The formation and semi-regular 100 km spacing of the capes is poorly understood. The earliest hypotheses regarding the origin of the capes involved secondary rotational cells or eddies in the Gulf Stream (Abbe, 1895; Tuomey, 1848) . A study by Bumpus (1955) found no evidence to support the circulation cell hypotheses, and promoted a wind-driven rise in sea level on the south sides of the capes forming an offshore current transporting sediments towards the shoals. Cooke (1936) suggested that wave fields remove sediment in the arcs between capes then deposit material on the capes proper maintaining a “smoothly curved shoreline”. Zenkovitch (1967) proposed that the capes were formed by oblique wave fields changing from the north and south seasonally. However, cape forming theories that involve a direct wave formation component have recently been rejected since wave energy refraction should erode the promontories (capes) and straighten the coast (Komar, 1998). White (1966) stressed the importance of shoals located seaward of the capes in maintaining cape form and position, but did not address the origin of the shoals.

Although Cape Canaveral shares many features with these other capes, such as cape related shoals, paleo-capes, and near-orthogonal limbs, it also has several striking differences that make it an interesting site for study. The capes of North Carolina have

been thought to migrate landward since the last glacial maximum (LGM). This is not true of Cape Canaveral, which has generally accreted seaward for at least the last 4,000 years (Hayes, 1994; Hoyt and Henry, 1971; Komar, 1998). The Carolina capes are constructed of a single ridge or dune, making it difficult to document their formation history since the LGM. Cape Canaveral on the other hand, has a well-preserved set of ridges documenting its formation and migration not only since the LGM, but possibly through the late Holocene. Furthermore, the capes of the Carolinas are all associated with rivers, while Cape Canaveral has no related river to supply large quantities of sediment.

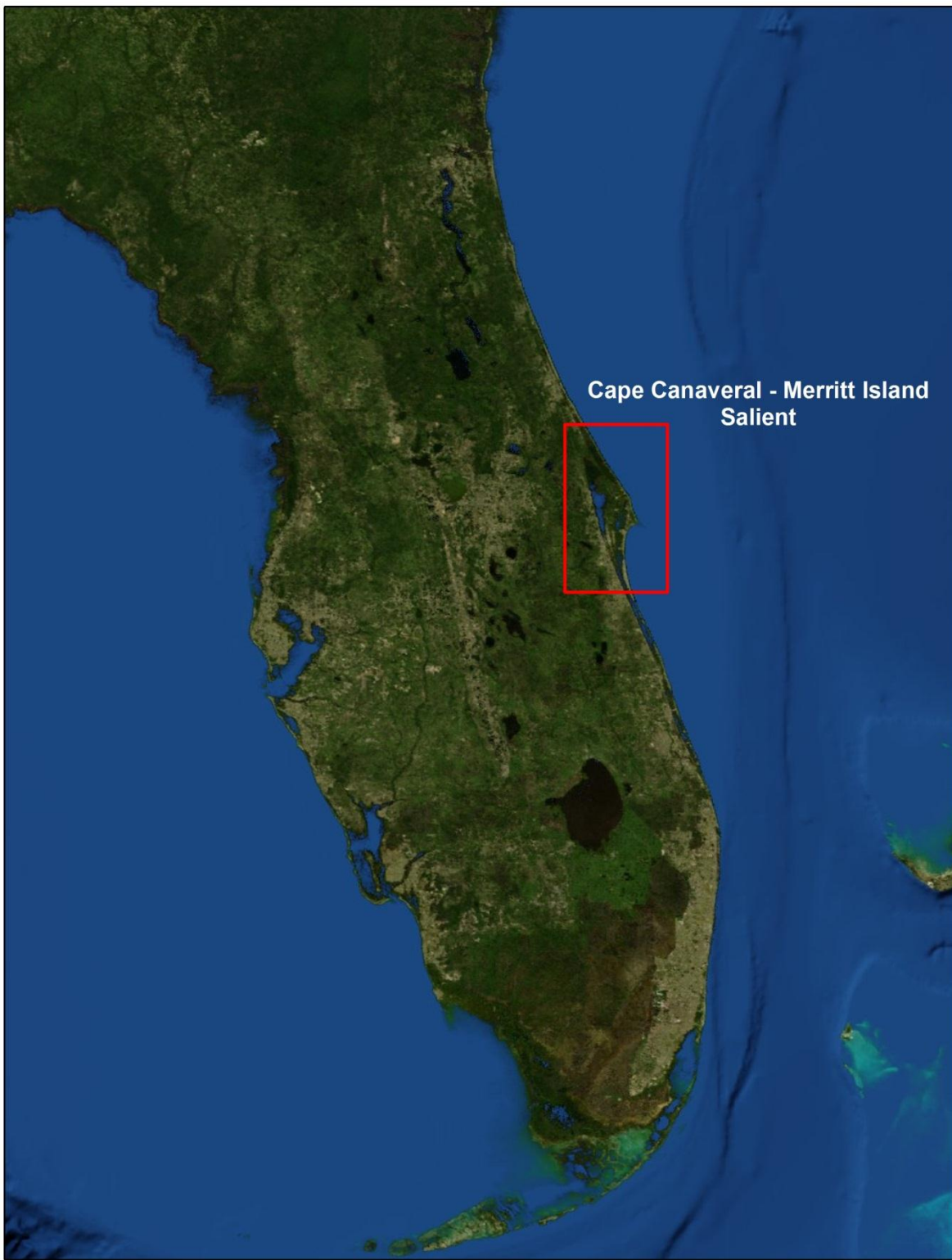


Figure 2-1. The Cape Canaveral – Merritt Island salient protrudes ~20 km from a normally straight Florida coastline.

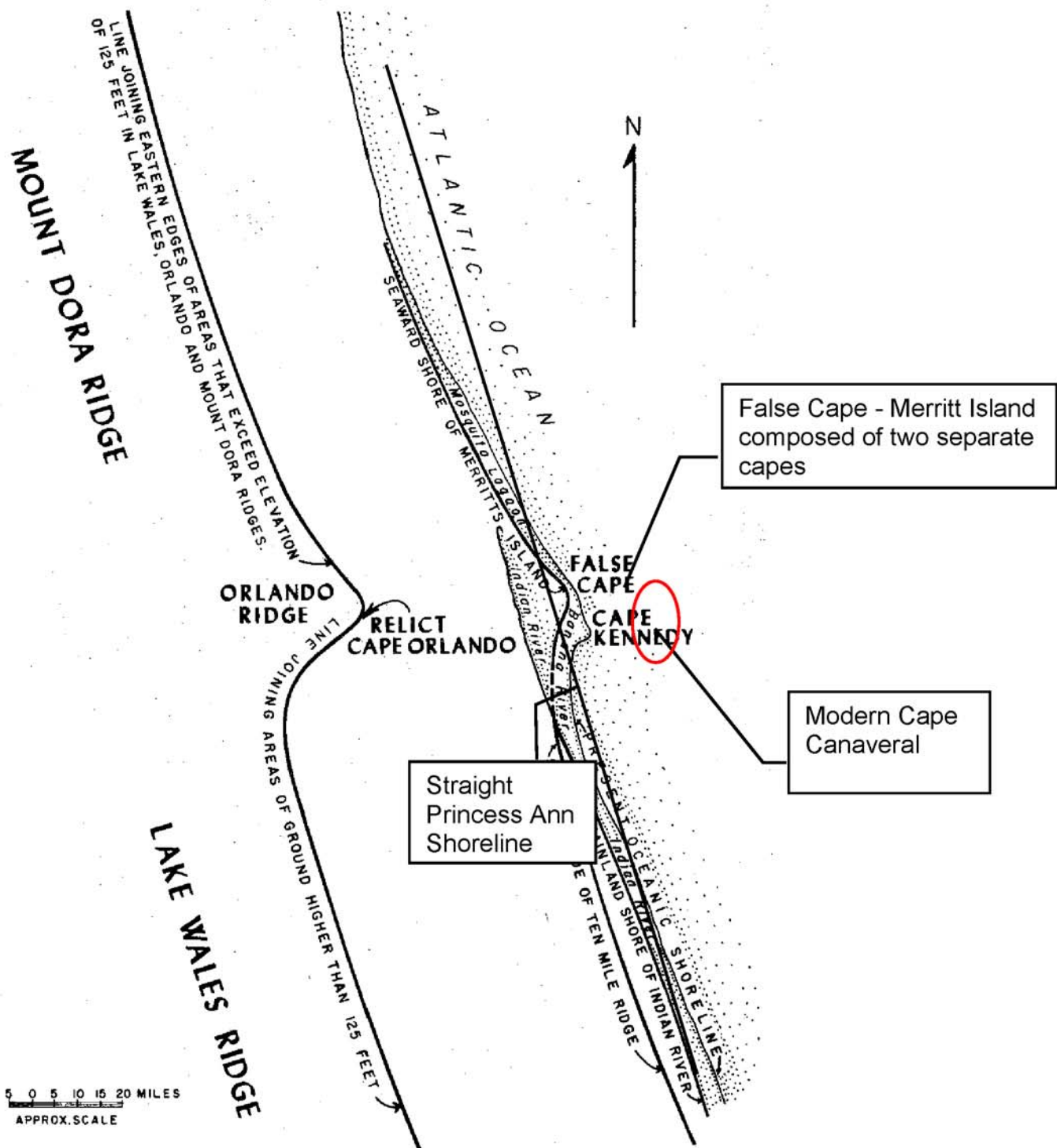


Figure 2-2. Cape formation of fixed latitude over time on the Florida coast. Red oval indicate areas of possible capes located off shore as part of a massive Cape "retreat" massif. After White (1970) and Pirkle et al. (1972).

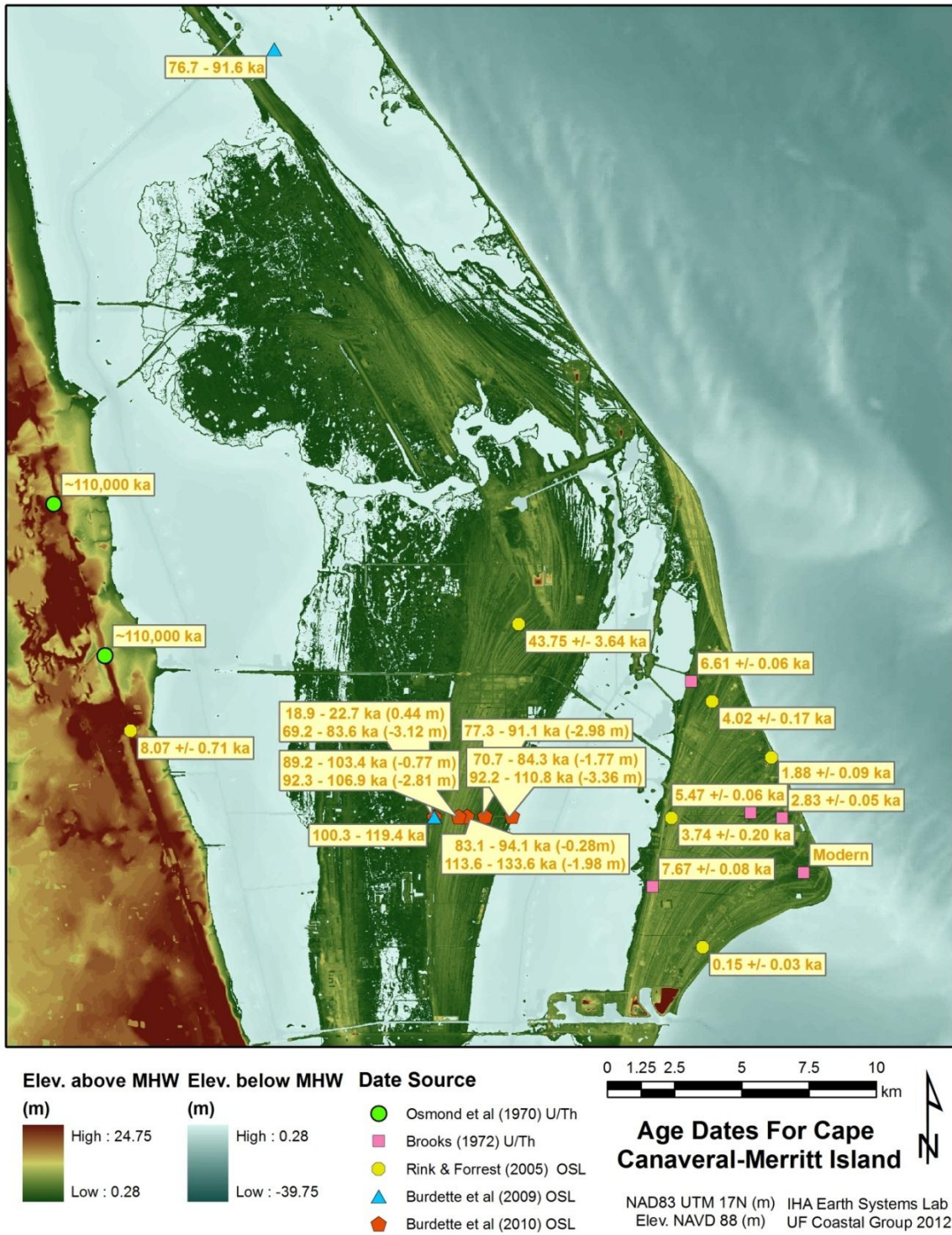


Figure 2-3. Absolute Dating records in the Cape Canaveral region. Osmond et al., and Brooks used Uranium/Thorium dating methods while others used OSL dating methods.

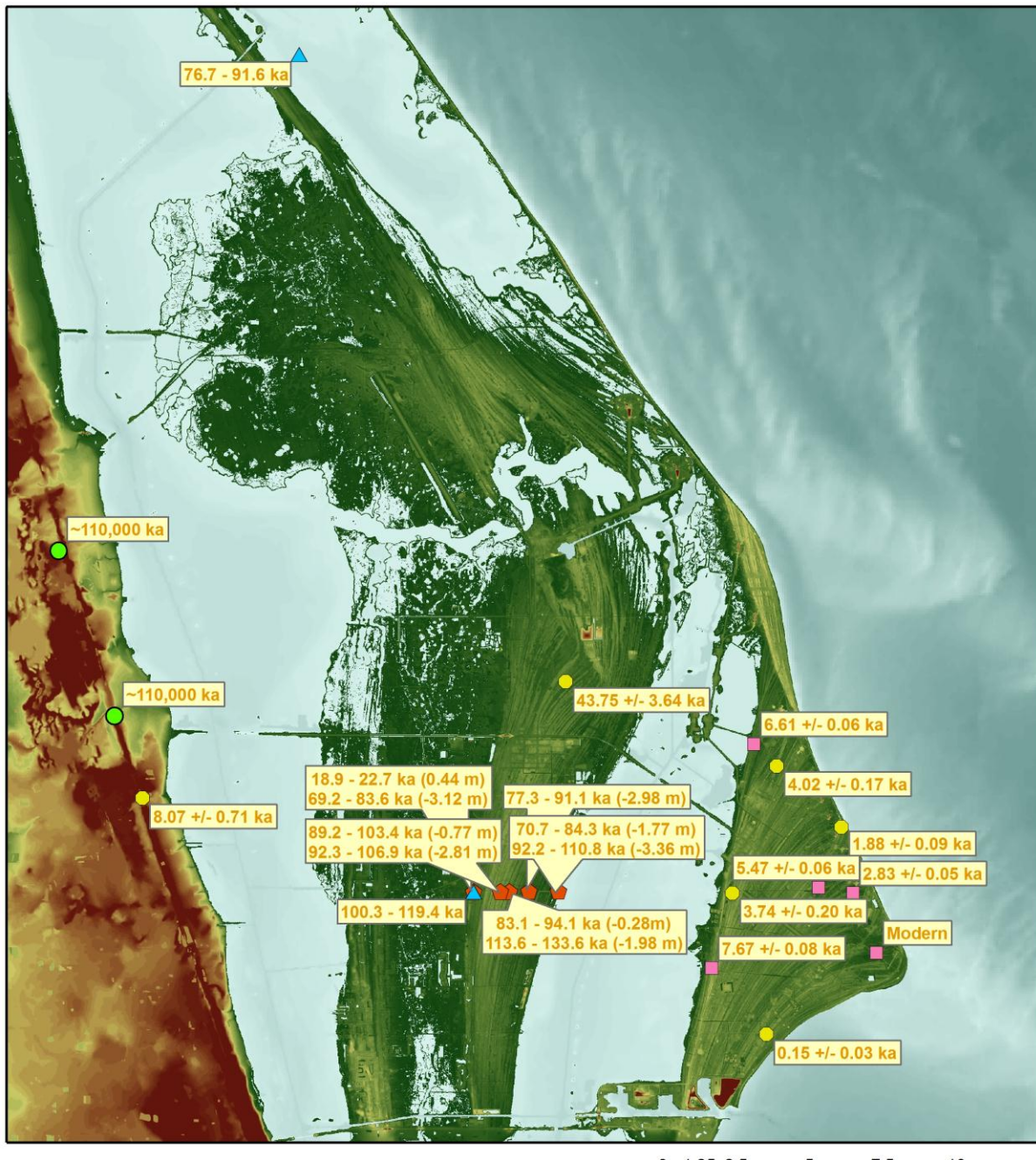


Figure 2-4. Absolute Dating records logged in the Cape Canaveral study area. Brooks used Uranium/Thorium dating methods while others used OSL dating methods.

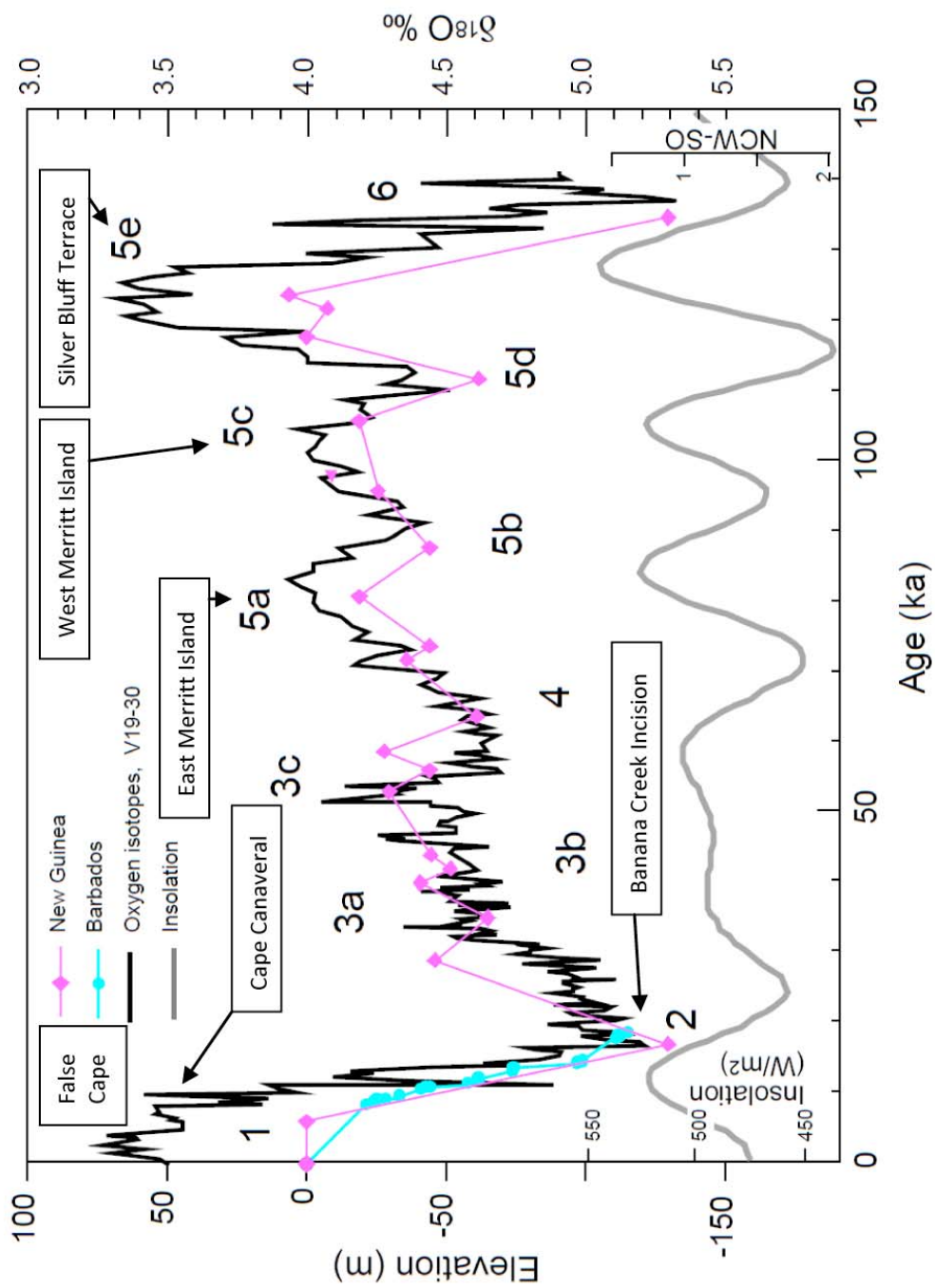


Figure 2-5. Eustatic sea level trends for the last ~125 ka (Miller et al., 2005). Superimposed are characteristic periods of Cape Canaveral shoreline development according to interpretation from dates in Figure 2-4.

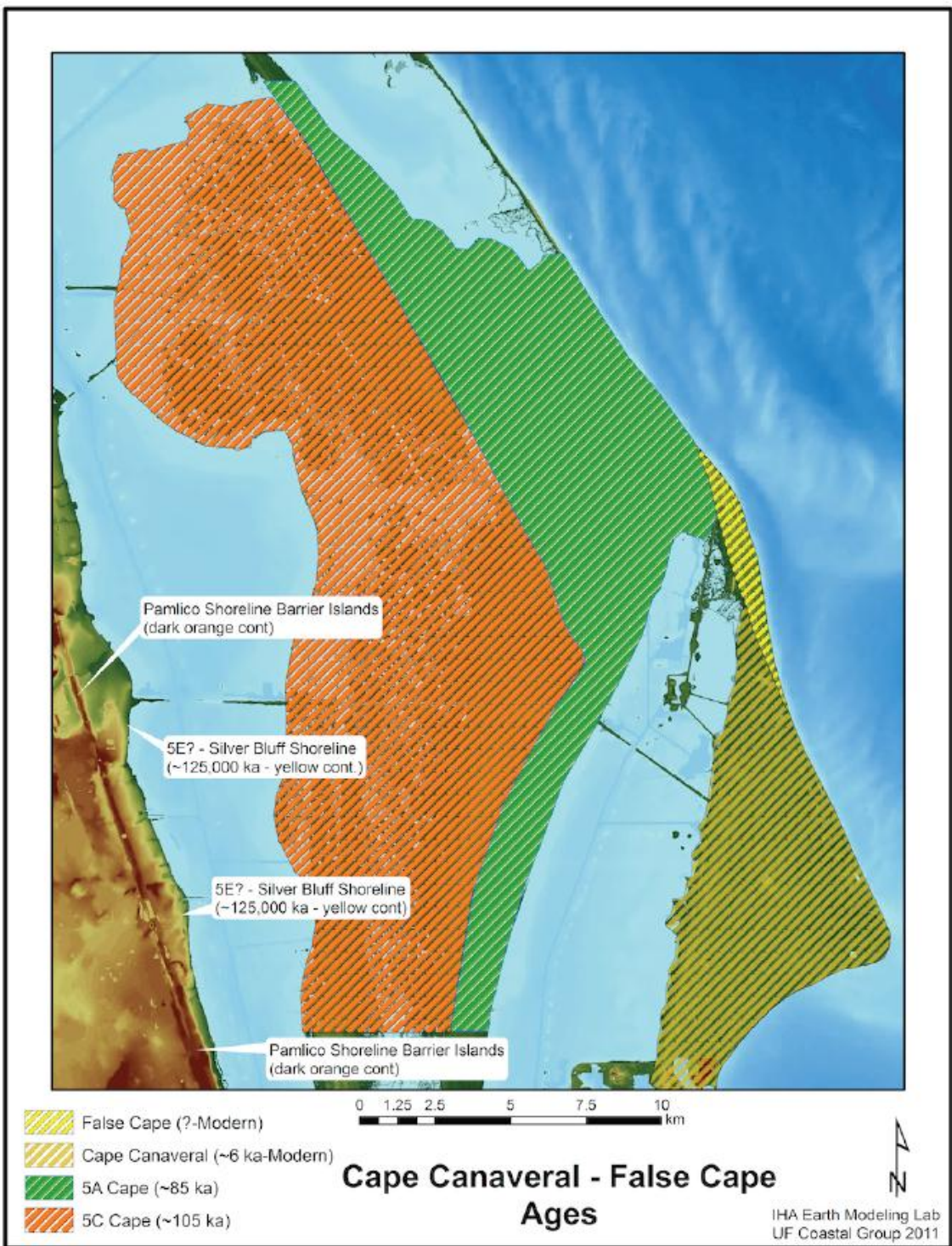


Figure 2-6. Late Pleistocene to modern shoreline and geomorphic features that form the Cape Canaveral - Merritt Island Sedimentary Complex. Ages of features from Figure 2-4.

# CHAPTER 3

## USING RTK-GPS TO MONITOR SIMPLE AND COMPLEX SANDY SHORELINES AT CAPE CANAVERAL, FLORIDA

### **3.1 Introduction**

With concerns over sea level rise and coastal flooding growing, documenting coastal morphodynamics and monitoring critical coastal infrastructure have become increasingly important. Real Time Kinematic – Global Positioning System (RTK-GPS) surveys have been increasingly used to provide both two-dimensional across shore transects and 3-dimensional geomorphic surfaces from which vertical datum such as Mean High Water (MHW) can then be extracted. For three-dimensional surveys, RTK-GPS generally can provide elevation data to generate geomorphic surfaces over a few tens of kilometers of alongshore spatial coverage. In comparison to other datum-based coastal surveying techniques such as LIDAR, RTK-GPS surveying results in a higher vertical resolution of 5-8 cm and is more cost-effective over a few 10s of kilometers, which can result in a much higher temporal frequency (monthly or greater) of data collection. This allows for documentation of shoreline response to short-term events.

Numerous spatial surveying strategies or data collection techniques have been used to collect topographic data on beaches, with each method chosen to minimize data collection effort while attempting to effectively capture key morphologic features. These methods include cross-shore transects (Dail et al., 2000; Dornbusch, 2010; Morton et al., 1993), alongshore transects straddling the MHW shoreline (List et al., 2006), sawtooth (Malone, 2011) , and square wave (Malone, 2011). Although each survey style has potential advantages, for example along shore surveys can be driven in a vehicle while across shore or square tooth surveys require a walking pattern (Dail et al., 2000; Malone, 2011), uncertainties in topographic accuracy, arising from the

interpolation required to evaluate morphologic change between discrete point measurements using different survey patterns, have not been quantified. RTK-GPS surveys using these different methods have then been used to provide high-resolution spatial data for event-, seasonal-, and decadal-scale studies of coastal change (Barnard et al., 2007; 2008; Dail et al., 2000; Hansen and Barnard, 2010; List et al., 2006; Ruggiero et al., 2003). Lastly, several studies have used RTK-GPS in a coastal environment with tested continuous (vertical  $1\sigma$  uncertainties of 1 to 3 cm (Dail et al., 2000; Dornbusch, 2010; Huang, 2002). However, no coastal studies have determined how the precision and accuracy of coastal RTK-GPS elevation measurements if affected by the use of multiple GPS signals (NAVSTAR GPS signals combined with additional Global Navigation Satellite Systems (GNSS) systems), the effect of using multiple base station locations, and uncertainties of rapid (1 second or 1 meter intervals) GPS measurements.

To address the influence of different survey patterns and multiple data acquisition strategies on coastal RTK-GPS surveys, a field site with minimal human interference coupled with a varying morphology is preferred. The 10 km of coastline at the Kennedy Space Center (KSC), Cape Canaveral Florida provides an ideal location to study an undeveloped coast with little associated anthropogenic influence, as the beach is closed to the public. The beach at the KSC has areas with several different intermediate beach states, a wide variety of beach slopes (0.014 - 0.227) as defined by the elevations 0.25 – 0.75 m NAVD 88, and areas of complex (cuspatate features and berms) and simple (concave-up) geomorphologies.

The main effort of this manuscript is to provide the results of a stringent Quality Assurance/Quality Control (QA/QC) requirement (RTK-GPS instrument vertical and horizontal errors of  $\pm$  5 cm, and shoreline position errors of  $\pm$  1.5 m) by the NASA Environmental Programs Division tasked with coastal monitoring of NASA's Kennedy Space Center's Cape Canaveral coast. This experiment was undertaken as part of a larger project to study geomorphic change at KSC, several quality assurance/quality control (QA/QC) surveys were conducted from May 2009 through April 2011, to test the uncertainties associated with the use of a RTK-GPS survey system with rapid point data collection (1 sec. or 1 m intervals) and with no additional post processing. These QA/QC tests involved two basic components: a test of data accuracy and precision under different acquisition parameters (e.g., multiple GPS signals, different acquisition times, etc.); and different field survey patterns. Different topographic survey styles were also tested on both a simple concave beach and on a complex beach with cuspat features, multiple berms, and multiple slope breaks to compare and contrast the methods for differences in the volumes calculated and artifacts relating to the processing of the data. A new method of surveying that incorporates alongshore surveying of multiple slope breaks (e.g. berm crest, dune toe, etc.) is described that produce both datum based MHW shoreline extraction and 3-dimensional topographic surfaces.

### **3.2 Study Area**

Cape Canaveral comprises  $\sim$  32 km of shoreline protruding seaward from a generally straight eastern Florida coastline (Figure 3-1). It is formed by two dominant geomorphic features: Cape Canaveral proper, a cuspat foreland  $\sim$ 15 km in length and Merritt Island. On the seaward side of Merritt Island lies False Cape, an area  $\sim$ 10 km in length that contains all of NASA's coastal infrastructure including Launch Complexes

41, 39A and 39B. The 10 km False Cape study area exhibits various shoreline stability histories and beach morphologic states. In the northern 1 km of the study area a historically stable shoreline (Absalonsen and Dean, 2010; Dean et al., 1998) with relatively high foreshore (0.25 m to 0.75 m elevations NADV 88) slopes ( $\sim 0.12$ ) is found. The area frequently has cusp features with amplitudes of  $\sim 1.25 - 2.0$  m and is towards the reflective end member described by Wright and Short (1984). The central six km is characterized by an intermediate beach morphology that is historically retreating at an average of  $\sim 0.33$  m/yr (Absalonsen and Dean, 2010; Dean et al., 1998). Cuspate features are less frequently observed and this region has a wide variety of average beach slopes ranging from 0.11 to 0.06. The two km that comprise the shoreline aspect change at False Cape is comprised of a historically accreting beach towards the dissipative end member of Wright and Short (1984), with low slopes ( $\sim 0.06$ ). Cusps are less frequently found here and have smaller amplitudes ( $\sim 0.75 - 1.25$  m) than those further to the north. In high wave conditions during the winter and early spring, the beach exhibits a simple concave-up profile through most of the area, while a berm forms along much of the 10 km in the early spring and summer.

Distributed throughout the Kennedy Space Center Complex are over 300 different National Geodetic Survey (NGS) benchmarks (NGS, 2011). Of these 300 NGS benchmarks there are 27 NGS markers with first or second order classifications found within a 100 m of the shoreline and located within the study area. There are three B order (1 part per million (ppm) horizontal and first order vertical (10 ppm) NGS benchmarks located in the study area: KAREN, BUDROE and WARD (Figure 3-1). These markers are located on camera pads that were surveyed in the 1960s to provide

telemetry and visual tracking of rocket launches. Benchmark KAREN was resurveyed by Brevard County, Florida using modern GPS methods on July 26, 2004 with 95% confidence to 0.76 cm northing, 0.69 cm easting and 1.57 cm ellipsoidal heights. Benchmarks BUDROE and WARD along with the 6 other associated benchmarks were then surveyed with 95% confidence to better than 3 cm in the northing, easting and elevation dimensions by differential GPS methods for use in the study. All survey benchmark locations can be found in Figure 3-1.

### **3.3 Background**

#### **3.3.1 Global Navigation Satellite System (GNSS)**

GNSSs are comprised of a constellation of satellites that provide timing information to ground-based receivers. The NAVSTAR global positioning system is the United States component of the global navigation satellite systems. The U.S. GPS system is designed to provide passive, accurate, continuous, world-wide, 3-d position and velocity measurements using a constellation of 24 satellites in 6 orbital planes with four satellites in each plane (Kaplan and Hegarty, 2006). The Russian counterpart to the American GPS system is the Global Navigation Satellite System (GLONASS). In 2004, the United States and the Russian federation issued a joint statement of cooperation. The objective of this agreement was to provide interoperability between the U.S. and Russian systems and maintaining cooperative efforts in both GNSS.

#### **3.3.2 Global Positioning System (GPS)**

Current NAVSTAR satellites broadcast in two frequencies known as L1 (1,575.42 MHz) and L2 (1,227.6 MHz) (Kaplan and Hegarty, 2006). These signals or codes are broadcast in code division multiple access or (CDMA) and are comprised of two parts: a short code C/A for course adjustments and acquisition; and a long code denoted as the

P(Y) code (Kaplan and Hegarty, 2006). Newer NAVSTAR satellites have two additional signals added to them and improved L2 frequency signal L2C and a L5 signal at 1,176.45 MHZ. The combined use of all of these signals (L1, L2C and L5) will allow GPS users the ability to better correct for atmospheric distortion providing for better accuracy (Kaplan and Hegarty, 2006).

There are two general modes of GPS tracking used to determine the distance between a GPS satellite and receiver antenna: Code Phase Pseudorange Tracking and Carrier Phase Tracking (USACE, 2004). Code Pseudorange Tracking uses a single phase comparison of a code transmitted by the GPS satellite to determine the distance between the satellite and the ground base antennas. This method is primarily used to calculate the relative differences between two points and provides “meter-level” positional accuracies (USACE, 2004). Carrier Phase Tracking uses variations in the carrier frequency’s phase to determine the distance between the satellite and ground. This method is most often used to produce sub-decimeter results for engineering and surveying, and is used in RTK-GPS surveying the methods described in this manuscript.

### **3.3.2 Real-Time Kinematic Global Positioning System (RTK-GPS)**

NAVSTAR RTK-GPS surveys result in sub-decimeter vertical and horizontal accurate surveys in real-time without the necessity of post processing, which is a method that requires position corrections to be collected at one location and then later applied to the data collected by the rovers using additional software (USACE, 2004). The RTK-GPS technique involves two components: a base antenna positioned on a known location, and one or more rovers receiving signals from both GPS satellites and the base antenna. This technique allows the roving antenna/receiver to gather sub-

decimeter position/velocity data while it is in motion after the initial integer ambiguity (time it takes the receiver to distinguish the phase differences in the codes used for timing) and the timing between satellites and receiver have been resolved (initialization). In order to provide sub-decimeter positioning in three dimensions, both the base and roving antennas must maintain a lock on at least 4 satellites. If this lock is lost, the roving receiver must reinitialize to resolve signal phase ambiguities. Loss of rover antenna initialization can also be caused by quality control residuals that fail to meet user defined criteria. In either case, the roving receiver must reinitialize before sub-decimeter data can be obtained (USACE, 2004, 2006, 2010, 2011) This becomes important during a continuous topographic RTK-GPS survey when initialization is lost and data point uncertainties increase to unacceptable levels (normally greater than 1m in both the vertical and horizontal. RTK-GPS operations are discussed in more detail in Dail (2000).

### **3.3.2 GPS Beach Monitoring and Surveying**

GPS has been used to study sandy beaches and morphology since the 1990s (Baganha Baptista et al., 2011; Byrnes and Hiland, 1995; Dornbusch, 2010; Gorman et al., 1998; Huang, 2002; List et al., 2006; Morton et al., 1993). Initial applications of GPS included improving the accuracies of aerial photogrammetric surveys and to support multiple topographic surveys by establishing benchmarks for across shore transects (Byrnes et al., 1994; Gorman et al., 1998). Morton et al. (1993) used GPS methodologies as standalone techniques to study coastal morphologies and morphodynamics by using GPS to produce across shore transects. Huang et al. (2002) compared Total Station and RTK-GPS techniques and found that both systems produced static one standard deviation ( $1\sigma$ ) results of one centimeter horizontal and two

cm vertical single point measurement accuracy. Huang et al. (2002) also used a vehicle mounted RTK-GPS system in a “continuous” operational mode, they concluded that the vehicle mounted system improved survey time but only speculated on the systems accuracy. List et al., (2006) used two GPS antennas mounted on an all-terrain vehicle (ATV) to produce shore-parallel transects on the foreshore over alongshore distances of 10s of km. These shore parallel transects were then used to produce a foreshore slope at defined intervals and then intersect a vertical datum. No mention is made in this study of the relative accuracy and precision of this method. Baptista et al., (2008) improved on vehicle mounted GPS units by incorporating a laser elevation measurement tool and tested its use in long-term (annual or storm) cost effective (thousands of data points vs tens to hundreds of thousands points for LIDAR) studies with resulting vertical accuracies of 10 cm. Methods of surveying that best captured the relevant beach topography with minimal effort were tested by Dornbusch (2010) using a GPS antenna mounted on a pole with a bike wheel. He determined that across shore transects where the best survey method to study morphologic changes in mixed sand and gravel beaches where topographic changes were most pronounced in a cross-shore direction.

### **3.4 Methods**

#### **3.4.1 GPS**

GPS signal clouds, defined by an ovoid shape with poles of an x (easting), y (northing), and z (elevation) length, were tested by using both Trimble 5800 and Trimble R8 RTK-GPS systems. Testing of GPS signals and multiple GNSS were conducted at static points collected at 1-second intervals identical to field collection conditions to simulate “Continuous Topographic” operational mode. All GPS point northing and easting measurements are reported in UTM 17N NAD83 GRS80 meters and elevations

are recorded in NADV88 meters. For static GPS point testing, a baseline was set using the NGS first-order horizontal and first-order class II vertical benchmark KAREN (Figure 3-1). GPS points were then collected at different distances between the base and rover, and for different collection durations to show the effects of using multiple base station locations and data collection times. The corner marker of Heli Pad 5 located at the northern most extent of monthly surveys and a reference marker on LC-14 were also used as test benchmarks for base to rover distances of greater than 9 km (maximum survey distance).

In order to test the spread of positions (i.e., growth of the GPS point cloud) over the duration of a typical multiple-hour survey, a long duration survey was conducted on 6/12/2011 using a Trimble 5800 base station and rover occupying two static points. The base station was placed on NGS benchmark WARD and the rover antenna was placed on a weighted tripod 9.68 km away at Launch Complex 14. This distance represents the maximum distance between the base and rover during any survey conducted at KSC. Test points were collected at one-second intervals for 19,868 seconds or 315 minutes. The test was terminated at this point due to lightning within 5 km of the GPS antennas. After data points were collected, QA/QC was performed by removing any data point that was collected without initialization as reported by the instrument.

To test the use of multiple GNSS (NAVSTAR and GLONASS) and multiple NAVSTAR GPS signals (L1/L2, L2C), experiments were performed using a Trimble R8 base antenna and R8 Trimble rover antenna. Testing of the use of multiple GNSS systems and GPS signals took place on 7/30/2010 with the RTK-GPS base station set on NGS benchmark WARD and the roving antenna set on NGS bench mark BUDROE

(Figure 3-1). Points were collected at 1 second intervals for 500 seconds twice for each of the following signal configurations: NAVSTAR L1/L2 and L2C; NAVSTAR L1/L2, L2C and GLONASS L1/L2; and NAVSTAR L1/L2. The two individual test of each configuration were conducted in reverse order to prevent satellite configuration changes to skew results. For example a configuration using the NAVSTAR L1 & L2 signals was tested first for 600 epochs, and then the second test of the NAVBSTAR L1 & L2 signals was conducted last in the sequence of the 4 different configurations tested. After data collection the same QA/QC analysis as mentioned above was performed on data.

### **3.4.2 Slope Break DBS Survey Style and SWASH MHW Contours**

Topographic surveys were performed using a wood trailer outfitted with dual GPS antennas towed by an ATV. The trailer was outfitted with tires that were specifically designed for use in a sand environment. In the standard configuration, 2 roving GPS antennas were towed 2.25 m apart at an elevation of 1.4 meters, but configurations of 3 antennas 1.125 m apart and 5 antennas ~ 1 m apart were also used in testing (Figure 3-2).

The Slope break method developed in this study incorporates RTK-GPS surveys following alongshore slope breaks. The GPS trailer was towed along the shore collecting data points at 0.5 m horizontal intervals or as rapidly as data collector would allow. A “pass” consisted of a single trip up and back the entire 10 km study area; this would produce 4 lines of data. A typical survey consisted of 2-3 passes with additional data collected in areas with additional topographic relief. On each “pass”, a slope break in the beach was tracked visually and one trailer tire was placed to follow this feature (Figure 3-3). Slope breaks of morphologic features included: the trough landward of the berm; the berm crest; the mid-slope of foreshore; and the beach toe (Figure 3-3). Areas

with additional topographic relief such as top and bottom of scarps or beach cusps were also surveyed. Survey “passes” were bounded shoreward by the vegetation line and seaward by the furthest distance that low-tide surf conditions would allow.

After each survey, GPS data points were extracted from data collectors using Trimble Data Transfer and Trimble Office software and placed into text files. Individual text files were imported and combined in Microsoft EXCEL for QA/QC analysis (full procedures for GPS data processing and file structure of data available in Appendices 1, 2, and 3). The x,y,z data were then imported into a GIS and converted to an ESRI point shapefile (Figure 3-4). Further QA/QC analysis is then performed on the data ensuring that all points collected along a transect maintained a constant distance between receivers, as transient data drops (e.g., loss of signal from base station) would result in rapid horizontal jumps between points and any visually identified outliers were removed from data. A polygon was then created in ArcGIS to use the outermost data points collected as a clip, or limit, on the topographic model. Once the clipping polygons were set, the point data was formed into a simple three-dimensional meshed triangulated irregular network (TIN) model (Figure 3-4). As simple TINs have been used in previous coastal studies to generate topographic surfaces from RTK-GPS survey data (Dornbusch, 2010; Baptista et al., 2008; Hansen and Barnard, 2010) this method was selected to produce a 3-D surface from the backpack mounted RTK-GPS and slope break surveys. The TIN routine in Arc GIS 9.3 was used, which is a Delaunay triangulation method. The TIN was then converted in the GIS to a 1 m by 1 m raster (Figure 3-5). From the raster model, a set of contours or a single contour at the MHW elevation (0.28 m in study area) was then extracted (Figure 3-5). Full details for GPS

data processing in GIS, data acronyms and file structures are provided in Appendices 1, 2, and 3.

To test the relative spatial distance between MHW extracted using the Slope break (multiple passes and lines) versus the SWASH style (single pass with 2 lines) (List et al., 2006), a single alongshore survey transit towing the dual GPS antenna array was made during three test surveys. Using methodology similar to (List et al., 2006) a single transit was performed by making a visual determination of the most likely across shore position for the location of the MHW contour and keeping this position between the GPA antennas. Unlike List et al. (2006) and List and Farris (1999), where the GPS antennas were ~1.5 m apart attached to the ATV and a tilt meter was used to determine the relative slope between receivers, our tests were conducted with the GPS rovers mounted on our trailer at a distance of 2.25 m apart and without a tilt meter.

To conduct a performance analysis on the Slope break style's MHW contour and to compare the Slope break style versus the SWASH method, 14 across shore test transects were conducted following Morton et al. (1993) . Because of the higher horizontal (x, y) resolution of the backpack surveys, it was assumed that this technique produced the most accurate position of the MHW and was used as the standard against which the MHW extracted from other techniques was compared. Transects were performed walking over the crest of the first continuous dune and out to a chest high wading depth at low tide during monthly surveys. The GPS antenna was mounted on a backpack and walked. QA/QC of these data followed previous procedures. The horizontal offset of the MHW position between the walked transect and both alongshore styles were then compared.

### **3.4.3 Survey Style**

To test the ability of the various methods beyond the SWASH and Slope- Break methods to accurately reproduce a topographic surface or datum in a coastal environment, surveys on simple and complex beach morphologies were conducted on 2/18/2011. The “complex” beach tested was 330 m in length and averages 33 m in across shore width and consisted of cusps and multiple slope breaks. The “simple” beach measured 350 m in length and averaged 33 m in width and consisted of a simple concave-up profile. A reference or idealized surface was constructed using data collected from all survey styles with the addition of 12 additional along shorelines collected randomly to maximize the number of data points used to generate a surface and to compare and evaluate the different survey methods (Figure 3-11 and Figure 3-12). To quantify the differences in the survey styles, difference maps were produced in GIS by subtracting each survey types raster from the idealized raster (Figure 3-11 and Figure 3-12). Each surface was also visually inspected to identify data artifacts or systematic errors from the simple TIN interpolation routine.

## **3.5 Results**

### **3.5.1 Static Testing of RTK-GPS Data Acquisition**

Testing of the RTK-GPS instrument on a point at one second intervals produces a point cloud or spheroid that can be defined by the resultant size of its poles; in this case the poles are defined as the northing, easting, and elevation values. GNSS were designed to primarily provide accurate horizontal locations; as a result the uncertainties associated with vertical measurements are always higher than those of horizontal. Testing the uncertainties associated with performing multiple RTK-GPS surveys on different days and using different base station locations was conducted using the L1/L2

GPS signals on various dates and at different distances between base and test point to determine the size of the poles (N,E, elevation) that contain 95% of the GPS point cloud data. Figure 2-6 provides examples of using one GPS testing location along with the clouds for individual tests at different distances. This example shows all RTK-GPS test data (2,800 points) collected at NGS location KAREN using multiple base station locations. The GPS data for all different tests at this location (Figure 3-6) project into an x,y,z point cloud containing 95% of the data and results in maximum x,y,z pole sizes of 6.3 cm (northing), 4.2 cm (easting) and 7.5 cm (elevation). The difference between the maximum value and the minimum value for each northing, easting and elevation pole values are 11.3, 7.8, and 13.0 cm respectively. The maximum 95% pole lengths for individual 600 epoch (10 min.) tests, irrespective of the date the test was conducted, are 4.9 cm northing, 4.3 cm easting, and 10.4 cm elevation (Table 3-1). The effect of using multiple base station locations and conducting surveys on multiple dates may be defined by the difference in northing, easting, and elevation between the centroids of each 600 epoch point cloud tested at a specific location. Additional uncertainty may arise by using multiple base station locations and conducting multiple surveys. The maximum difference between centroids at NGS KAREN using different base stations was 1.2 cm easting, 0.9 cm northing, and 1.5 cm elevation.

Different GPS signal configurations were tested twice with 600 epochs in each test (1200 epochs in total) using the same Trimble R8 base and rover instrument. The two individual tests of each configuration were conducted in reverse order to prevent satellite configuration changes that could skew results. For example, a configuration using the NAVSTAR L1 & L2 signals was tested first for 600 epochs, and then the

second test of the NAVSTAR L1 & L2 signals was conducted last of the 4 different configurations tested. In the basic L1/L2 configuration the 95% confidence poles were 1.8 cm, 1.4 cm and 3.6 cm for northing, easting and elevation, respectively (Table 3-2). The difference between the maximum and minimum values for northing, easting and elevation were 2.9 cm, 2.2 cm, and 6.3 cm, respectively. In the L1/L2 and L2C configuration, the 1200 epoch 95% confidence poles were 1.6 cm, 1.5 cm and 3.4 cm for northing, easting and elevation, respectively. The difference between the maximum and minimum values for the L1/L2 and L2C configuration were 2.3 cm, 2.3 cm and 5.9 cm, respectively. In the L1/L2 configuration, with the addition of the L1/L2 GLONASS signals the 95% confidence poles for northing, easting and elevation were 1.8, 1.5 cm and 3.4 cm. Differences between the maximum and minimum values for this signal configuration were 2.7 cm, 2.2 cm, and 7.4 cm for northing, easting and elevation. With all available signals (L1/L2, L2C, and the GLONASS L1/L2) the 95% confidence poles for northing, easting and elevation were 1.6 cm, 1.9 cm and 3.9 cm. The maximum differences in northing, easting and elevation for all 1200 epochs with all signals are 2.9 cm, 2.7 cm and 6.4 cm (Table 3-2).

Testing the effects of long-term (> 1 hour) data collection (similar to topographic survey duration) on the size of the RTK-GPS point cloud was conducted for a five-hour time interval with cumulative pole-size results calculated every minute. At the conclusion of the test, the 95% pole sizes were 4.3 cm, 4.1 and 8.6 cm (N, E, Elev.) with average standard deviations of 1.1 cm, 1.0 cm and 2.1 cm respectively. Maximum 95% pole sizes for northing, easting and elevation occurred at different times during the test with northing, easting and elevation results of 4.9 cm, 4.9 cm and 10.4 cm (Figure 3-8).

Cumulative errors between the maximum and minimum values for northing, easting, and elevation during the five-hour test were 7.8 cm, 7.0 cm and 17.6 cm respectively (Table 3-8). Northing and easting 95% poles reached their maximum sizes after about 40 minutes, while the elevation 95% pole reached its maximum size after ~120 minutes. During the test, average cumulative Position Dilution of Precision (PDOP) calculated from satellite constellation configuration remained relatively steady at 2.0 with a recorded minimum PDOP of 1.4 and a maximum PDOP of 4.4. There was an average of 8.8 satellites used by the RTK-GPS system to determine positions during this test.

### **3.5.2 Field Data Acquisition Experiments-Slope Break Versus SWASH**

To test the ability of different survey patterns and data processing methods to accurately establish the location of the MHW contour location, different techniques were compared to across shore backpack GPS transects at 14 different locations along the 10 km study area (Figure 3-1). Positive values were observations where the Slope break-survey-technique MHW was seaward of the across shore-survey MHW location, and negative values were landward. The average difference for all 106 comparisons was +52.8 cm (Table 3-3). The maximum difference between the backpack survey and the Slope break MHW shorelines was +1.92 meters seaward, of the across shore-survey MHW measured at transect UF 80 (Figure 3-9). Several locations had differences of less than 10 cm between the two MHW locations.

For three test surveys, a comparison was performed between MHW locations derived from across shore surveys, the Slope break survey style and the SWASH method (List and Farris, 1999; List et al., 2006). Again, the across shore GPS survey was used as the reference for the comparison (Figure 3-9). The average absolute difference between the across shore surveys and Slope break style was 52.8 cm. The

average difference between the across shore surveys and the MHW point derived using the SWASH method was 1.8 m. The maximum difference between the backpack method and slope break method was 1.4 m at UF test transect 100. The maximum difference between the backpack style and the SWASH method was 11.1 m at UF Test Transect 105 (Figure 3-9).

### **3.5.3 Other Field Data Acquisition Experiments**

Different survey methods were tested against an idealized beach surface developed from a combination of the data collected for all survey styles and an additional 10 alongshore transects (Figure 3-11 and Figure 3-12). Experiments were conducted along ~300 m of shoreline of both a simple concave-up beach and on a complex beach with several slope breaks and cusps (Figure 3-11 and Figure 3-12). Nominal conditions (areas defined as no difference between idealized surface and surface under test) were defined as being within  $\pm$  5 cm (95% vertical measurement confidence). Difference maps between the idealized surface and the surface under test were constructed using “Raster Calculator” in ArcGIS (ESRI, 2009).

On the simple concave-up beach, the Slope break survey method had the most 1 m by 1 m cells in the user defined  $\pm$  5cm range with 11,461 of 12,337 (93%) (Figure 3-11 and Table 3-4). The diamond method of surveying produced the second best results with 7,103 cells of 11,756 cells (60%) in the nominal range, and had areas that both underestimate and overestimated the elevation of the idealized surface. Surveying using transects along only the dune base, berm crest and low water mark produced 4,740 of 12,219 cells in the nominal range or 39%, while over-estimating the elevation of the idealized surface. The sawtooth and transect methods produced similar results with ~36% percent of their cells in the nominal range. The square-tooth survey style

performed the poorest of all survey styles tested with 4,228 cells falling into the nominal range and having the widest range of values deviating from the idealized surface (0.85 m to -0.85 m) (Figure 3-11 and Table 3-4). The square-tooth method also underestimated the height of the idealized surface.

Testing the different survey styles on a complex beach produced different results (Figure 3-11 and Table 3-5). The Slope break method had the closest agreement to the idealized surface with 9,107 of 10,993 cells (83%) within the RTK-GPS instrument precision of  $\pm$  5 cm. The cells with uncertainty outside the RTK-GPS instrument range tend to underestimate the elevation of the idealized surface. The dune base, berm crest and low water mark survey method produced 4,807 of 10,955 cells (44%) in the nominal five-cm range, while underestimating the elevation of the idealized surface. The diamond survey style produced the lowest number of cells within the nominal value; 2,274 of 10,298 (22%), and underestimated the elevation of the idealized surface (Figure 3-11 and Table 3-5).

### **3.6 Discussion**

#### **3.6.1 Testing of RTK-GPS Data Acquisition**

The ability to minimize uncertainty in beach topography using RTK-GPS depends on maximizing acceptable precision but with minimal, cost-effective effort in the field. Precision can be maximized, but usually with a time penalty and the use of more complex receiver combinations. The level of precision required depends on the purpose of surveying and the beach morphology. For example, for a given vertical uncertainty, the relative uncertainty in the position of an extrapolated MHW position increases for flatter, more dissipative beaches (Fig. 3-1). Given that annual changes in the position of the MHW may be only a few 10s of meters (Hansen and Barnard, 2010),

the impacts of the uncertainty created by poor RTK-GPS data acquisition can be substantial. Also, if the goal is to capture subtle beach morphology (e.g., cusps), higher precision is required for flatter beaches.

Several methods have been tested to determine the relative uncertainty created by different RTK-GPS acquisition parameters. A common approach to determining relative vertical precision is to survey a relatively flat surface within the study region (e.g., parking lots (Dornbusch, 2010). I also used a section of road to test vertical uncertainties and a narrow beach access point surveyed multiple times to test horizontal uncertainties as initial or quick QA/QC data check. However, I felt that testing on a static point with a known position would provide a better understanding of the uncertainties in RTK-GPS measurements. Testing on a static point isolates the uncertainties associated with the RTK-GPS instrument from the uncertainties associated with the mounting system. RTK-GPS instruments can be set to collect in a continuous manner over a set distance or for a set time interval. Either way, the instrument is collecting data at an instantaneous epoch without averaging multiple measurements, so the results for collecting data at a fixed distance or for data collected at a fixed time interval at a static point are comparable.

Other studies involving the use of RTK-GPS report horizontal instrument uncertainties of ~2-3 cm and vertical uncertainties of 3-5 cm (Dail et al., 2000; Dornbusch, 2010; Huang, 2002). This agrees with our testing of the RTK-GPS at 10 minute intervals on several dates (22) with different distances between base and rover antennas. The average pole sizes with 95% confidence are 2.8 cm northing, 2.5 cm easting, and 5.4 cm elevation (Table 3-1). Even when removing all points that have a

reported instrument error of greater than 5 cm, the difference between the maximum and minimum reported values can be almost twice that of the 95% confidence poles with maximum 95% confidence pole sizes for an individual 10 min test were 4.9 cm northing, 4.3 cm easting, and 10.4 cm elevation. The differences between the maximum and minimum values during an individual 10 minute test for northing and easting averages about 3.8 cm, but can climb to over 7 cm, while the difference between maximum and minimum elevation during an individual test averages about 6.7 cm but can be as much as 11.5 cm. The distance between the rover and the base seemed to have little influence on the size of the poles up to the ~ 10 km test interval (Table 3-1). This would indicate that surveys with the base centered at 20 km are possible without degradation of the pole size beyond the uncertainty of the instruments reported in this manuscript.

The five-hour long interval testing of a static point 9.7 km away from the base station produced results that were consistent with the 600-second test. Our study demonstrates that within a 40 minute period with ~9.5 km between the base station and roving antenna, the uncertainties associated with horizontal measurements of 95% confidence reach a near maximum size of ~ 4.4 cm, while after 120 minutes the uncertainties associated with vertical measurements with 95% confidence reach a maximum of ~8.6 cm (Figure 3-8). This means that the longer the time spent collecting data, the greater the possible accumulated error, although this tends to level out after two hours. Although the 95% confidence elevation pole measured was 8.6 cm, the difference between the maximum and minimum elevation was 17.6 cm. It is difficult to eliminate these outliers from being used in the development of the three-dimensional

TIN surface as these points had instrument reported vertical errors of less than 5 cm. Even though there are few points with this uncertainty, the errors associated with these points are not averaged together, but are used as individual points to produce the three-dimensional surface. This indicates that even though 95% of the vertical data have uncertainties of less than 10 cm, individual points with higher uncertainties may be incorporated during the creation of a three-dimensional surface if proper QA/QC is not performed. Therefore, care must be taken when measuring surficial changes from multiple surveys, especially when the magnitude of the changes are smaller than the uncertainty of the data and are being attributed to external environmental forcing of beach morphology and not the uncertainty of the data.

Testing the use of multiple GNSS signals to improve accuracy proved to be difficult or at best inconclusive. Basic L1/L2 signals produced poles and a minimum and maximum vertical and horizontal error comparable to the poles and min/max vertical and horizontal errors produced by using an additional GNSS (GLONASS) and additional signals (L2C). No combination proved to provide any real improvement over any of the others (Table 3-2). Two improvements observed anecdotally when using the GLONASS constellation were the number of satellites used in observations and an improvement in the time the RTK-GPS needed to initialize. This is not unexpected since two different constellations of satellites are used. The increased amount of satellites available for an initialized solution using multiple GNSS may allow for the use of shorter antenna pole heights on the towed array and therefore shorter moment arms, and less error due to instrument tilting on slopes. The reduction in the time to instrument initialization would

also significantly reduce data lost when initialization is lost during topographic surveys, and reduces the time spent waiting for antennas to gain initializations.

### **3.6.2 Field Data Acquisition Experiments**

After establishing the relative precision of RTK-GPS measurements, a method of surveying the beach was needed to produce both a DBS MHW contour and a three-dimensional surface of the beach that minimized uncertainty in the extraction of a datum based shoreline. The implications of the different survey approaches are discussed below.

Walked across shore transects using the methods described in Morton (1993) were used as a QA/QC test of DBS extracted using the Slope break and SWASH methods. Even though backpack-mounted across shore transects have their own measurement artifacts associated with it (e.g., sway of person acquiring the data), comparisons between across shore and alongshore MHW approaches are useful. During the eight tests shown in Figure 3-9, the difference between the walked across shore transects and the MHW contour extracted from elevation grids was never greater than  $\pm 2$  m in the horizontal for all test points using the Slope break technique. This level of uncertainty is within the annual noise of shoreline movement of  $\sim 15$  m along this beach (Chapter 4). Most of the DBS MHW points using the Slope break technique were seaward of the walked MHW points, most likely due to the MHW being very low in the shoreface and the Slope break technique not capturing the full curvature of the shoreline in the area of the MHW.

When comparing the across shore transects with the MWH DBS generated from both the Slope break style and the SWASH methods, the Slope break method had an average offset of 0.52 m while the SWASH method had an average offset of 1.82 m.

The differences between the SWASH method and backpack-mounted methods were greatest on the flat low slope areas of the beach (Figure 3-10). This is especially true when the two lines of the SWASH method are seaward of the MHW contour. When seaward of the MHW contour, the SWASH method projects a MHW contour along the flatter slope much further landward. Unlike the SWASH method, the Slope break method produces a MWH DBS that is constrained by data on both the seaward and landward side of the selected datum, unlike the SWASH method where that may not be constrained.

During a previous backpack mounted RTK-GPS coastal study performed at Matanzas Inlet, FL, elevation artifacts associated with the data collection strategy were found in the three-dimensional TIN models (Malone, 2011). These artifacts manifested themselves as TIN facet elevation and orientations associated with the data collection strategy and not the observed orientation and elevation of the beach morphology (Malone, 2011).

During our study, several data collection strategies were tested including the Slope break and SWASH methods and several walked backpack mounted methods including: sawtooth, diamond, and square (Figures 3-11 and 3-12). Regardless if the GPS receivers are mounted on a trailer, vehicle, or backpack, the collection of the data is not a random process, therefore the data will always be biased in the direction of movement of the GPS antenna. Since the data are not being collected in a random manner, care needs to be taken to understand the relationship between the data collection routine and the routine use to interpolate that data. Collecting data with a higher density along the slope breaks forces the TIN framework to bend along those slope breaks. While I

agree that most beaches (both mixed sand and gravel and sandy beaches) show more variation across shore than alongshore, it is not necessary to survey only in that direction to reproduce the beach morphology. While it is true that the beach profile changes most across shore, areas of slope breaks such as a berm crest also propagate alongshore (Baptista et al., 2008). Collection of point data with the highest sampling density alongshore forces the TIN to bend along the slope breaks producing a realistic representation of the beach morphology. Adding across shore transects or mixing data collection strategies may have unexpected results and cause the facets of the TIN to form in a less realistic manner as shown in Figures 3-11 and 3-12. The Slope break survey method is recommend for surveys with an alongshore distance of greater than 500 m, especially on complex beaches with cusps or berms. While the use of a predefined “mesh” or survey strategy developed before the survey may have merit for areas of <500 m alongshore (Baptista et al., 2008), when confronted with a survey of several km and a variety of beach states, data collection strategies and densities should be dictated by beach morphology in order to best reproduce the 3-dimensional surface.

The use of a towed RTK-GPS array mounted on a trailer with tires designed especially for use in sand allowed for the most efficient and economic design. During initial testing in loose dry sand these tires never made depressions greater than 0.75 cm, while under the same conditions the ATV made depressions of up to 17 cm. The towed trailer configuration allowed the RTK-GPS antennas to be mounted directly above the tires at different elevations (typical 1.3 m) this allowed for the direct measurement of data without having to correct for the suspension of the AVT, the depth of penetration of the ATV or the tilt of the GPS antennas. Even on the highest average

beach slopes in the study area (0.16) the elevation difference from the tilt of the trailer is about ~1 cm well within the measurement error of ~10 cm discussed in this manuscript. The trailer was normally towed in its standard two antenna configuration allowing for the best avoidance of obstacles. Although the three and five antenna configurations allowed for the collection of 5 points of data per alongshore meter with a an across shore spacing of ~ 5.75 m, these configurations proved difficult on the upper beach where the spacing of the slope breaks and the abundance of obstacles made following the slope breaks difficult.

### **3.7 Conclusions**

The goal of this study is to provide an improved understanding of the methods employed during the collection of RTK-GPS in coastal settings under “real-world” field test conditions. Maximum values for RTK-GPS horizontal 95% confidence uncertainties are reached after ~40 minutes of surveying and are ~5 cm, while vertical 95% confidence uncertainties are reached after ~120 minutes and are ~10 cm. The maximum horizontal uncertainties associated with RTK-GPS measurements are ~7 cm, while maximum vertical uncertainties are ~20 cm. The use of multiple base station location and multiple surveys add an additional 1.5 cm to RTK-GPS uncertainties. These results would indicate that RTK-GPS surveys without additional post processing can provide elevation differences on the order of 20 cm, with the understanding that individual point elevation measurements with vertical uncertainties of up to 20 cm could potentially be used in generation of the surface if more detailed QA/QC is not performed. While the addition of the extra GNSS (GLONASS) and extra signal (L2C) provided no improvement on the size of the GPS uncertainty poles, anecdotally they did

provide a more rapid initialization time therefore less data and time lost to initialization loss.

The Slope break RTK-GPS method has proven to be an effective method for the monitoring and measurement of coastal changes at many scales and intervals, especially on sandy coastlines with complex beaches. This method along with a trailer designed specifically to operate in loose dry sand provides a means to economically monitor and survey up to 20 km of shoreline in one day. The Slope break survey method provides landward and seaward constraints on the MHW DBS that the SWASH may not, although this is accomplished with additional alongshore survey data and time. The Slope break method produced MHW DBSL with average uncertainties of less ~ 0.5 m and maximum uncertainties of less than 2 m, while the SWASH method produced average uncertainties of 1.8m and maximum uncertainties of greater than 10 m. It is important to note that while testing Slope break versus SWASH methodologies, it was discovered that when using the SWASH method to generate DBSLs it is important to stay as close to or above the MHW as possible as stated in List and Ferris (1999) and List et al. (2006) . However this may prove difficult if the driver of the GPS system has no previous knowledge of the beach they are testing. Surveying below the MHW can produce higher differences between the measured MHW line and the actual MHW especially on beaches with low slopes, surveying below the MHW DBSL will project a MHW DBSL that is landward of the actual MHW datum.

Surveying along slope breaks forces a simple TIN to bend along the alongshore survey axis, allowing for an understanding of how the TIN will form while surveying. Other methods of survey styles have the possibility to form artifacts in the data, from

unintended consequence of data interpolation. It is important to understand how the data collection strategy and sampling interval affects the sampling routine. Defining the length of beach to study or monitor, knowledge of the beach morphology and knowledge of the beach response to forcing are all critical elements for developing a survey technique and interpolation routine that will work the best.

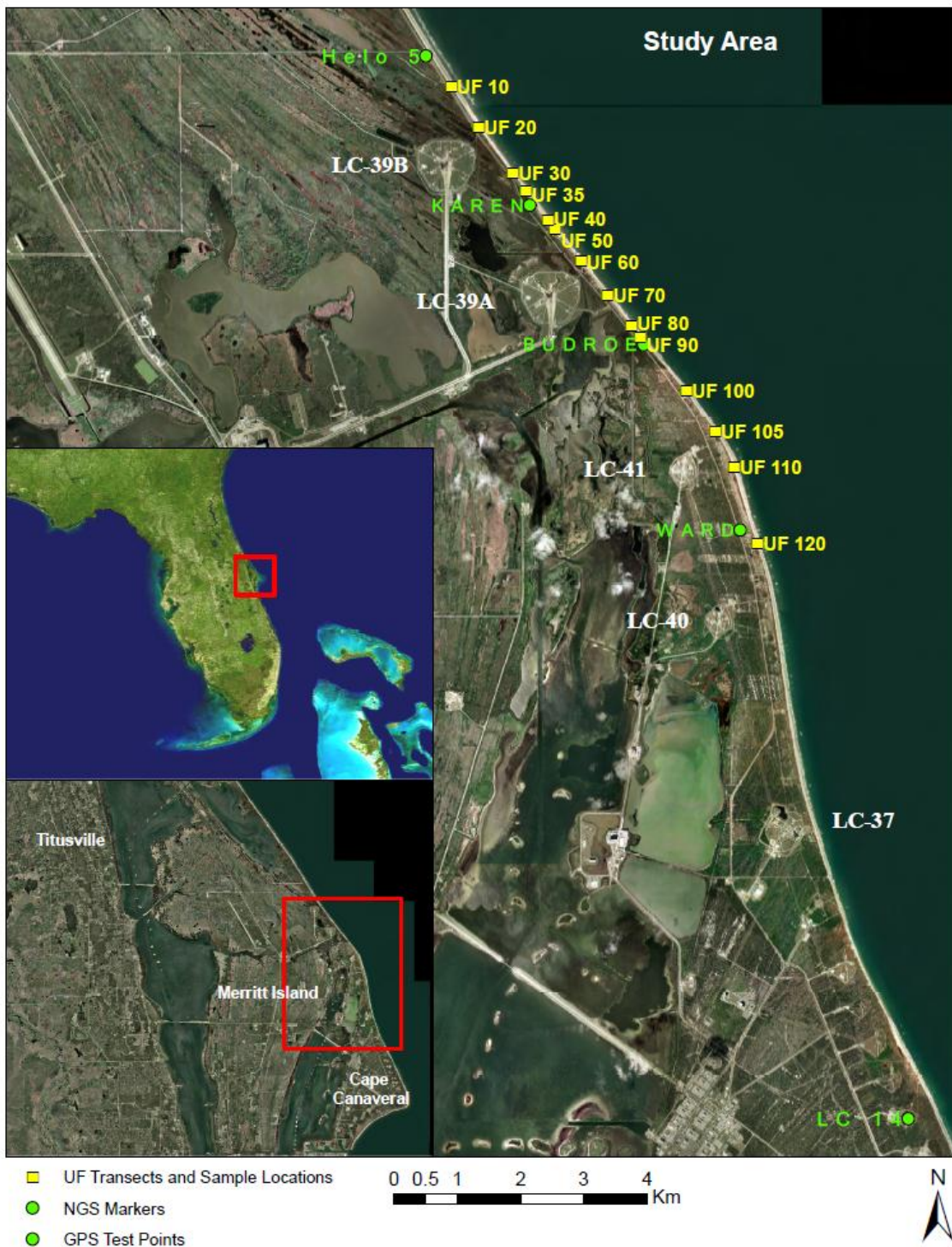


Figure 3-1. Kennedy Space Center - False Cape study area with associated launch complex coastal infrastructure. University of Florida across shore transects locations are indicated in yellow. NGS benchmarks and GPS test locations are indicated in green.



Figure 3-2. ATV towed RTK-GPS trailer shown in three different configurations (2, 3, and 5 roving antennas). GPS trailer is equipped with tires purposely built for operation in sand.

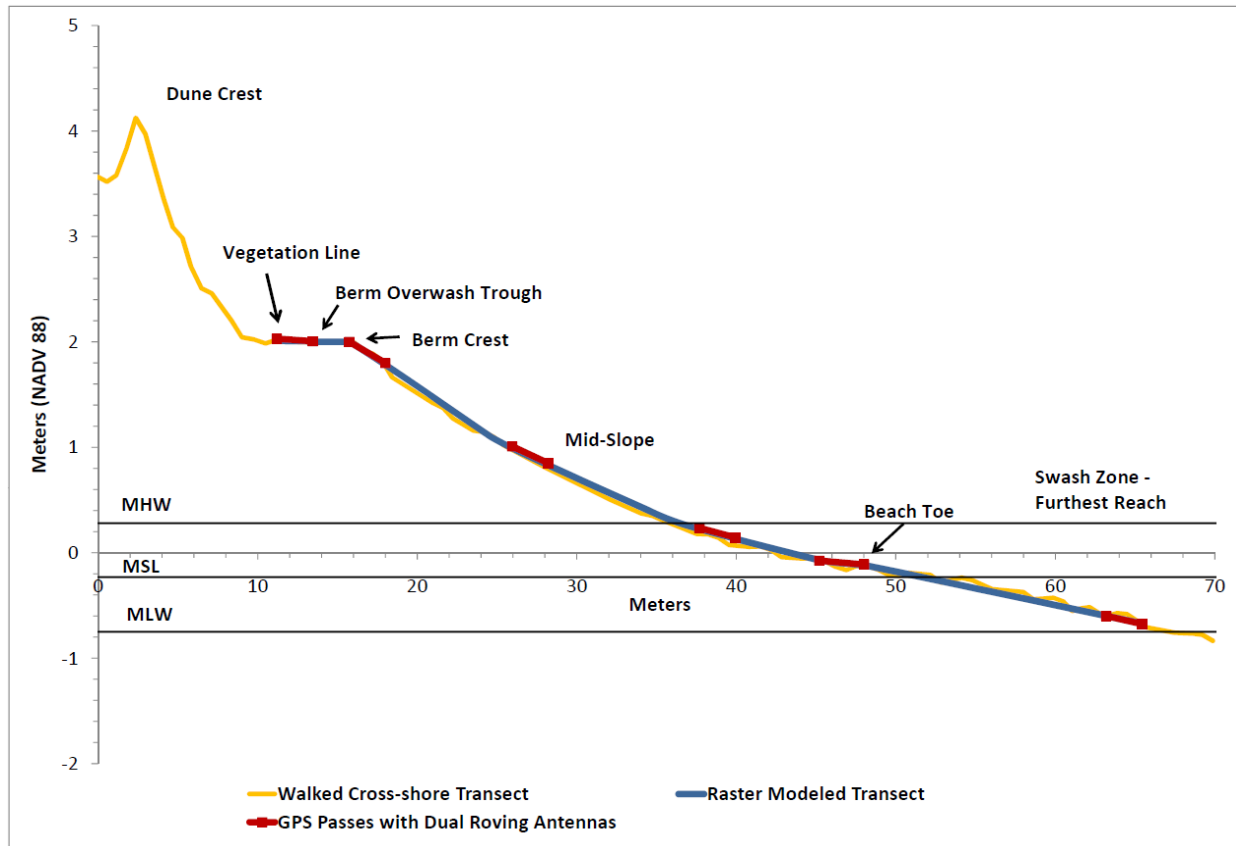


Figure 3-3. The MHW tidal datum for Cape Canaveral is 0.28 m (NAVD88), MSL is -0.23 m and MLW is -0.68 m. Red segments represent the two measurements taken by the GPS trailer at each slope break. The blue line indicates the across shore profile generated from the GPS measurements modeled with a TIN converted to a raster. Orange line indicates a profile measured with a backpack mounted GPS receiver along a UF sampling transect measured from the first continuous dune out to wading depth.

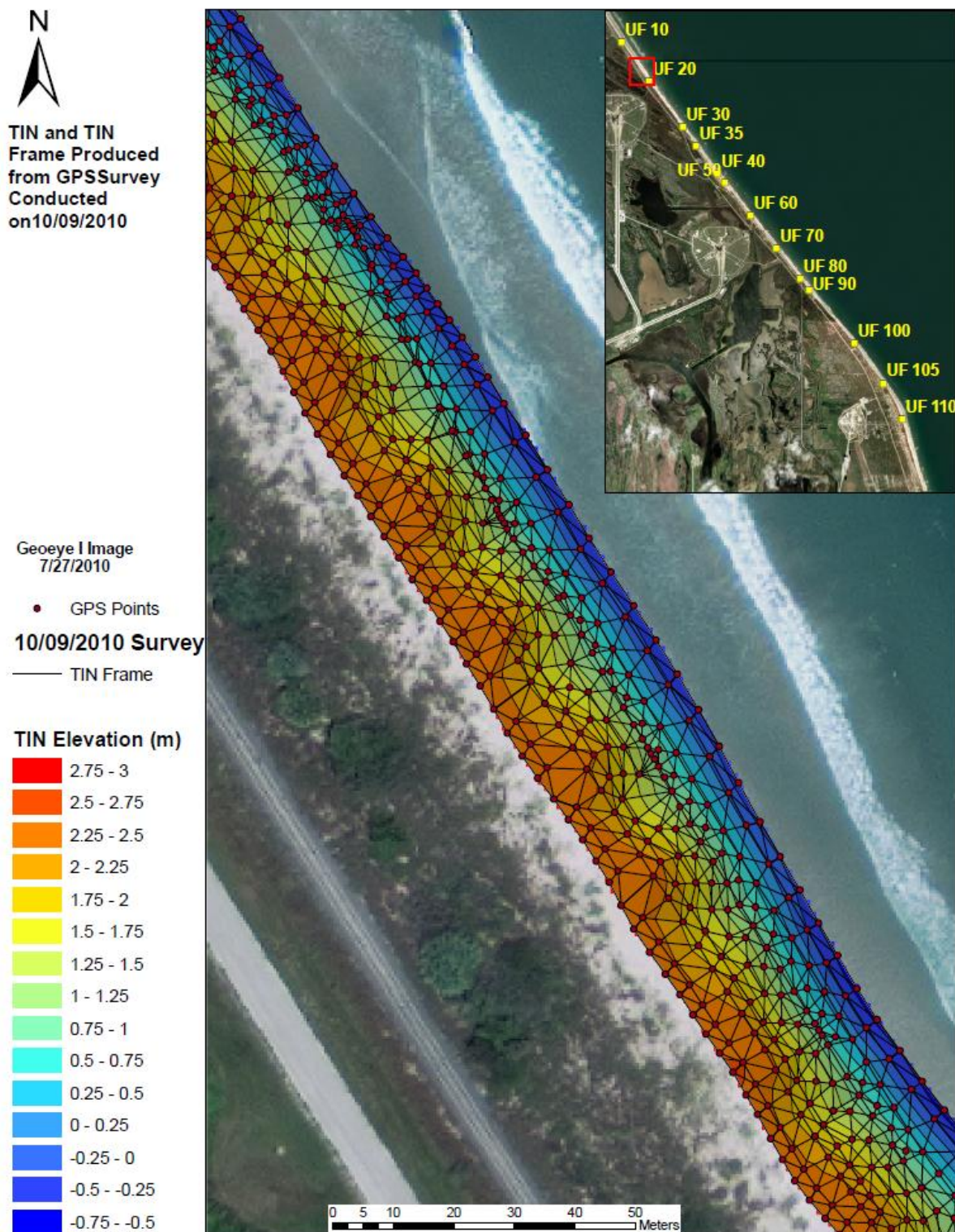


Figure 3-4. Representative RTK-GPS survey collection density, TIN of collected points, and TIN-generated elevation model.

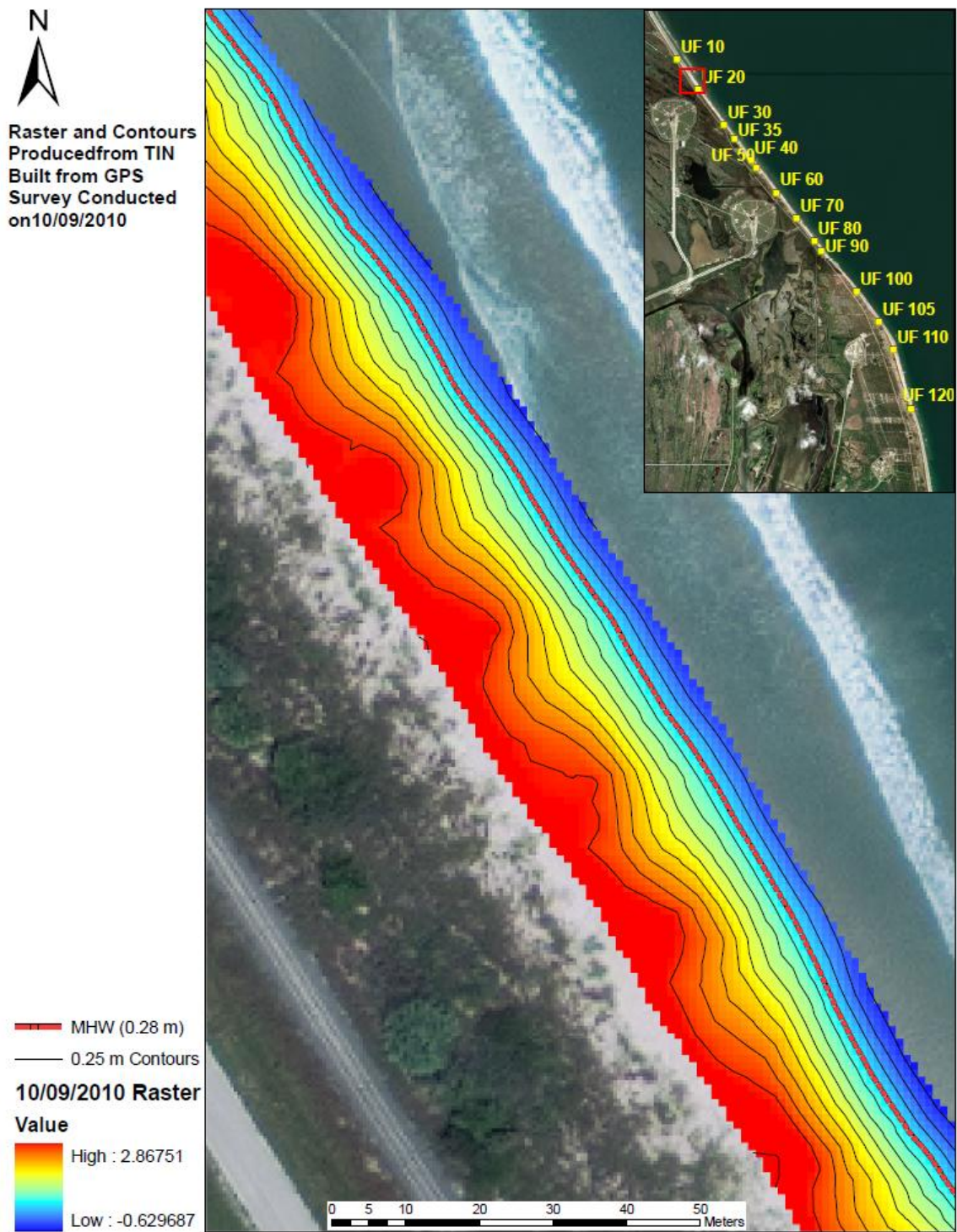
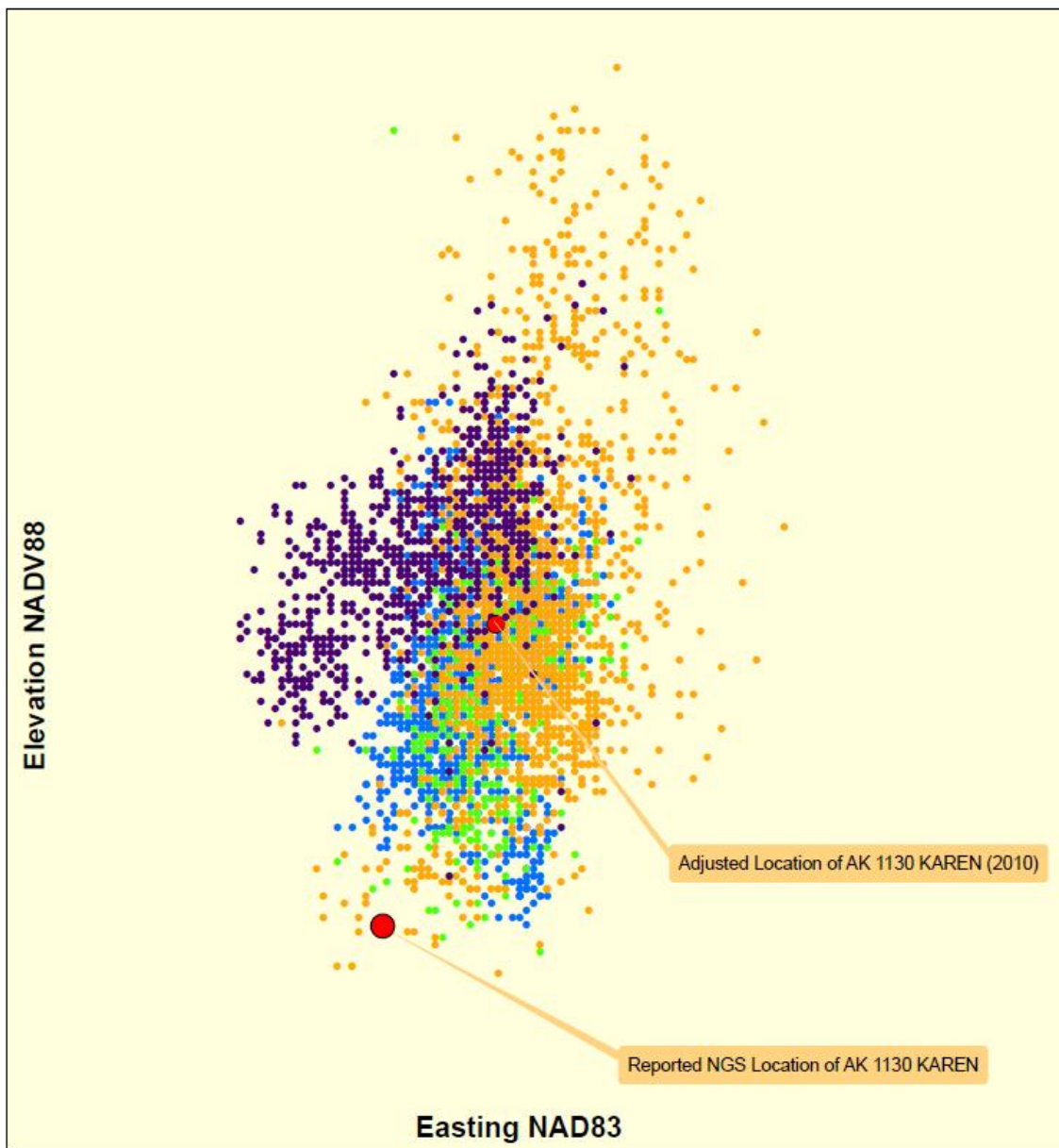


Figure 3-5. Raster DEM ( $1 \text{ m}^2$ ) constructed from TIN with 0.25 elevation contours (NAVD88). Mean High Water (MHW) Datum Based Shoreline (DBSL) shown by red line at 0.28 m NAVD88.



### GPS Quality Control Test at NGS Point AK1130 KAREN

Figure 3-6. Map of static RTK-GPS data collected at NGS benchmark KAREN on five different test dates with vertical NADV88 data displayed on “Y” axis with UTM 17N Easting displayed on “X” axis. Large red circles show location of NGS reported point location and Brevard County surveyed location in 2005. Scale bar is same for both horizontal and vertical error.

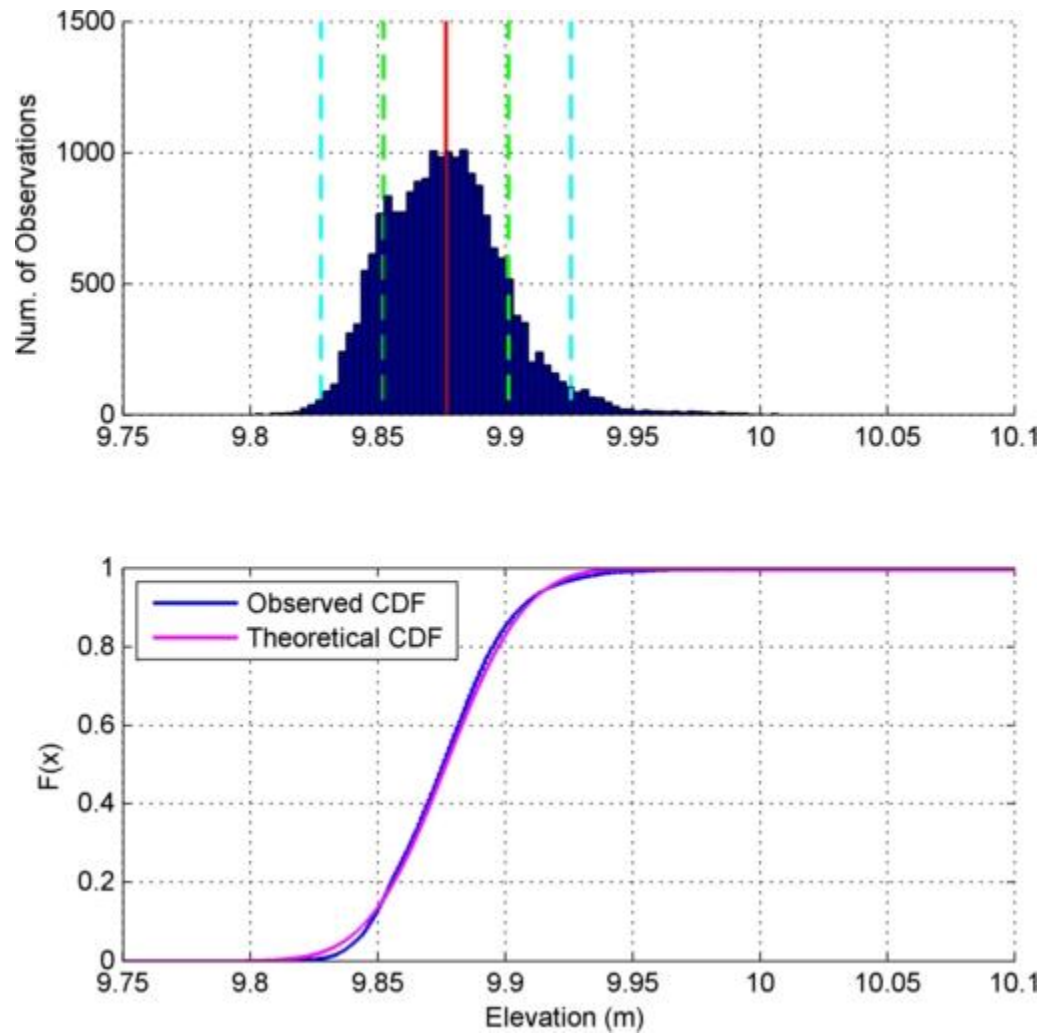


Figure 3-7. Distribution and cumulative frequency plot of vertical RTK-GPS elevation data (NADV88) collected at 1 second intervals for 5 hours at a static point 9.7 km from base station. Data follow CDF Gaussian distribution (purple). Red, green, and cyan lines in top panel represent mean, and 1 and 2 standard deviations, respectively.

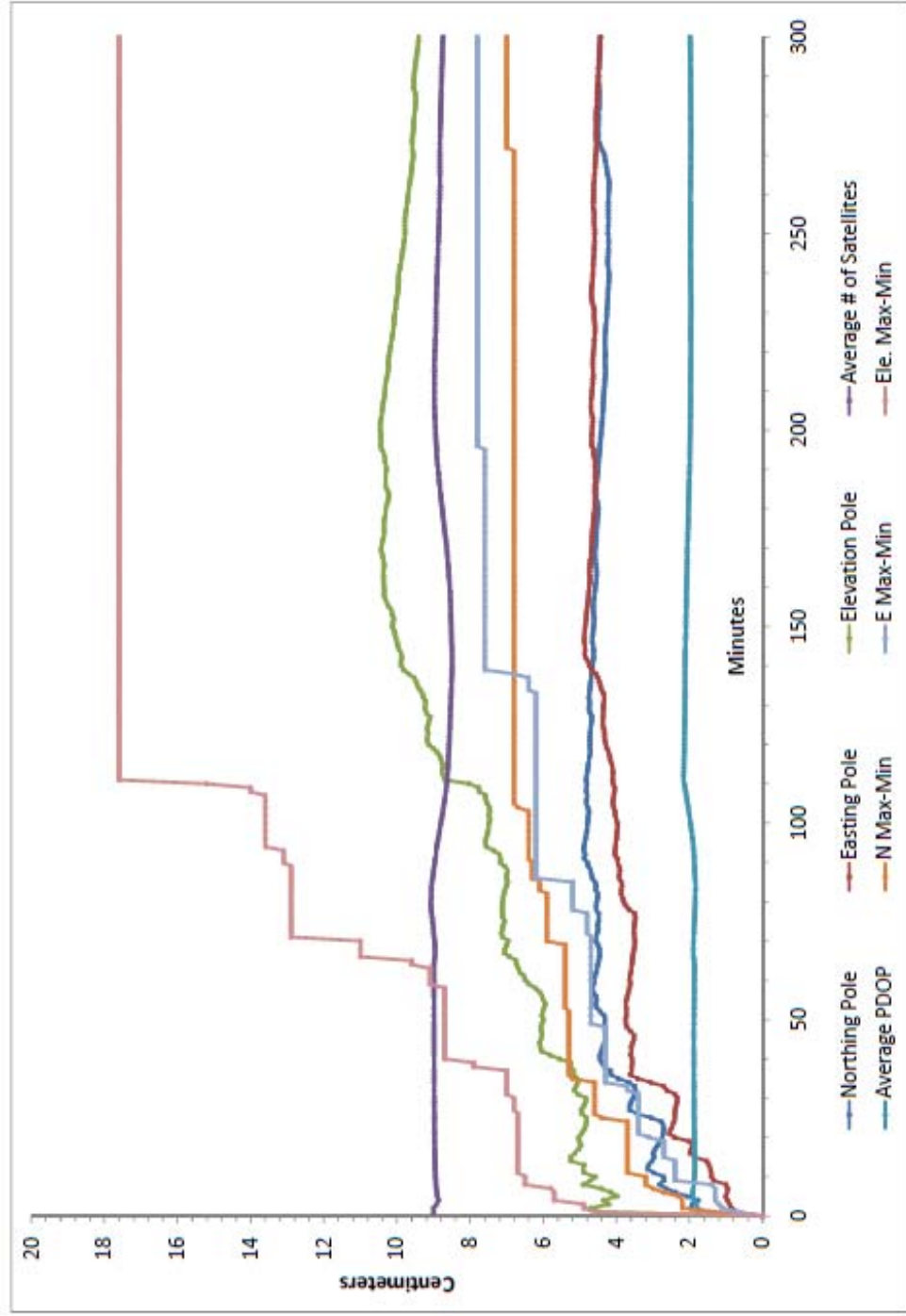


Figure 3-8. Results of a five-hour GPS acquisition test with data collected at 1 second intervals with 9.7 km between RTK-GPS base station and rover. Northing and Easting 95% confidence poles reach the maximum values of ~4 cm at ~40 minutes into test while the elevation 95% confidence pole continues to increase in length to ~9 cm ~150 minutes into the test.

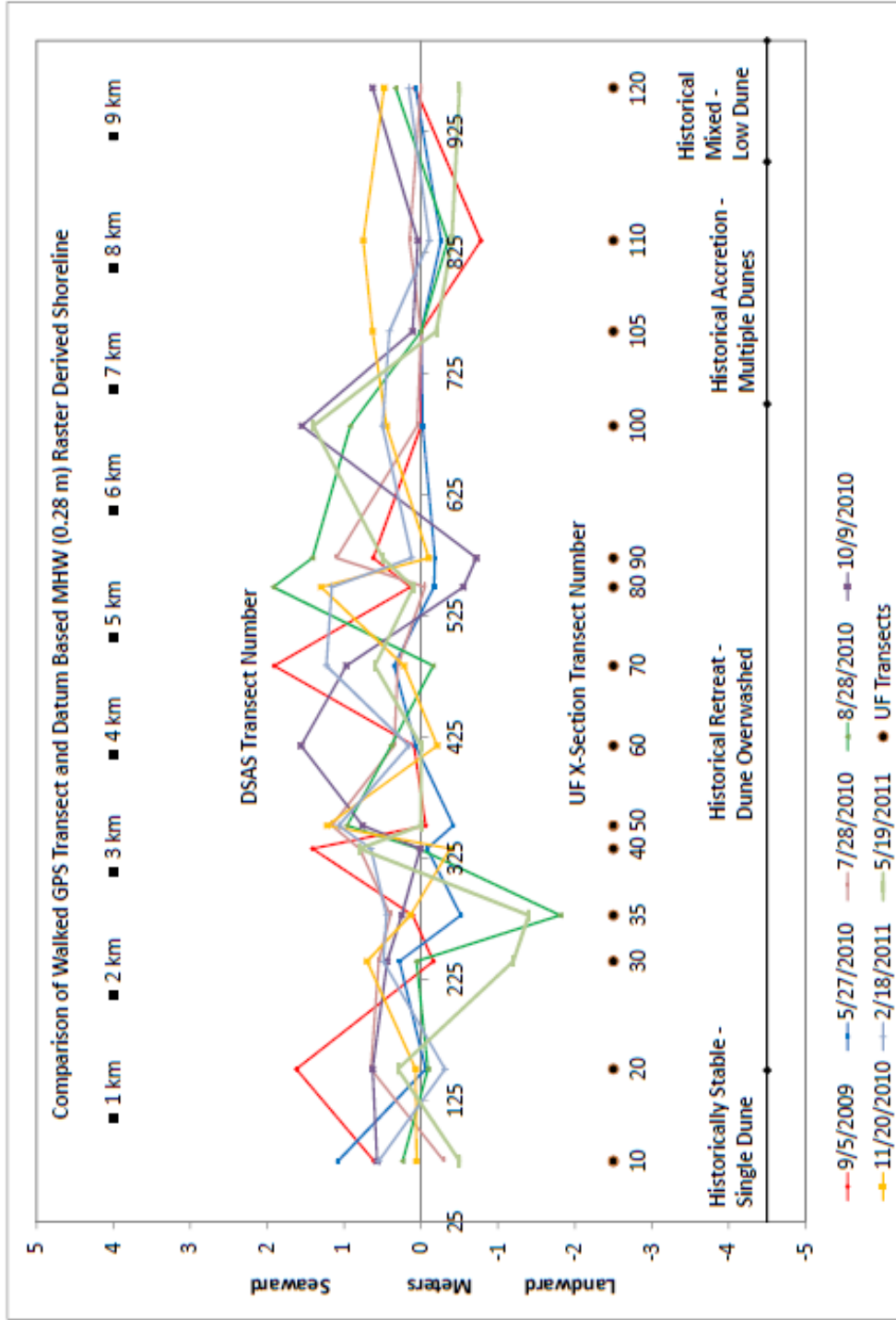


Figure 3-9. Comparison of across shore MHW (0.28 m) locations derived from RTK-GPS walked transects following Morton (1993) and MHW locations derived from RTK-GPS Slope break survey style (colored lines). Distance along the KSC shoreline is noted at top of figure referenced to northern boundary. DSAS transect number is higher-density (10 m spaced) across shore transect used in other parts of this study.

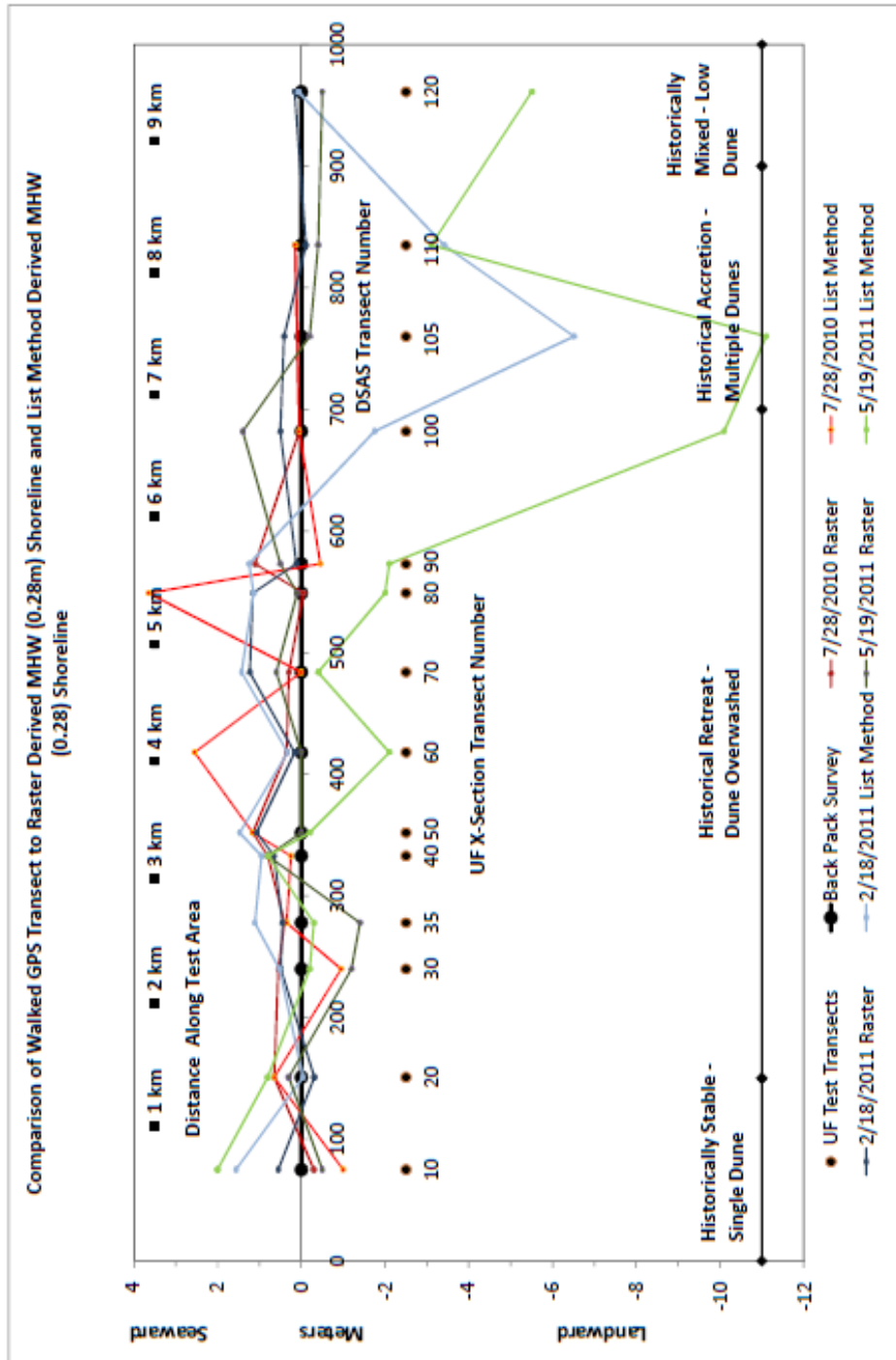


Figure 3-10. Comparison of across shore MHW (0.28 m) locations (0 axis) derived from RTK-GPS walked transects following Morton (1993) and MHW locations derived from RTK-GPS Slope break survey style (colored lines) and those extracted from the List et al. (2006) method (colored lines).

### Difference Between Idealized Raster and Different Survey Styles on A Simple Concave Up Beach

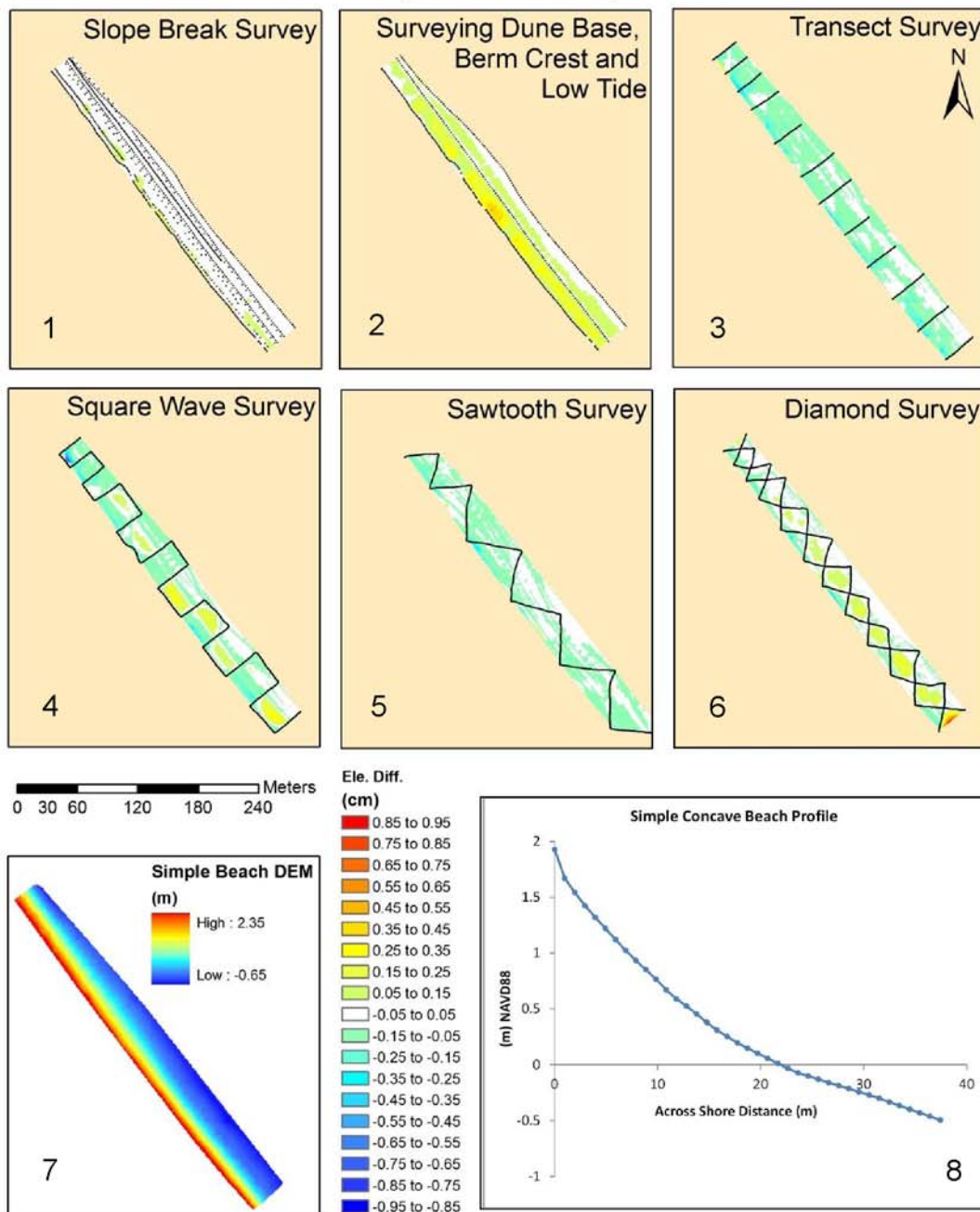


Figure 3-11. Comparison of survey styles on a simple concave-up beach. Panel 1 is in upper left corner. Panel 7 displays the “idealized” beach using data from all methods and additional alongshore transects. Panel 8 displays the simple concave-up profile of the beach in this region. Top six panels show the elevation difference between each type of survey style and the idealized elevation surface.

### Difference Between Idealized Raster and Different Survey Styles on A Complex Beach with Cusps and Berm

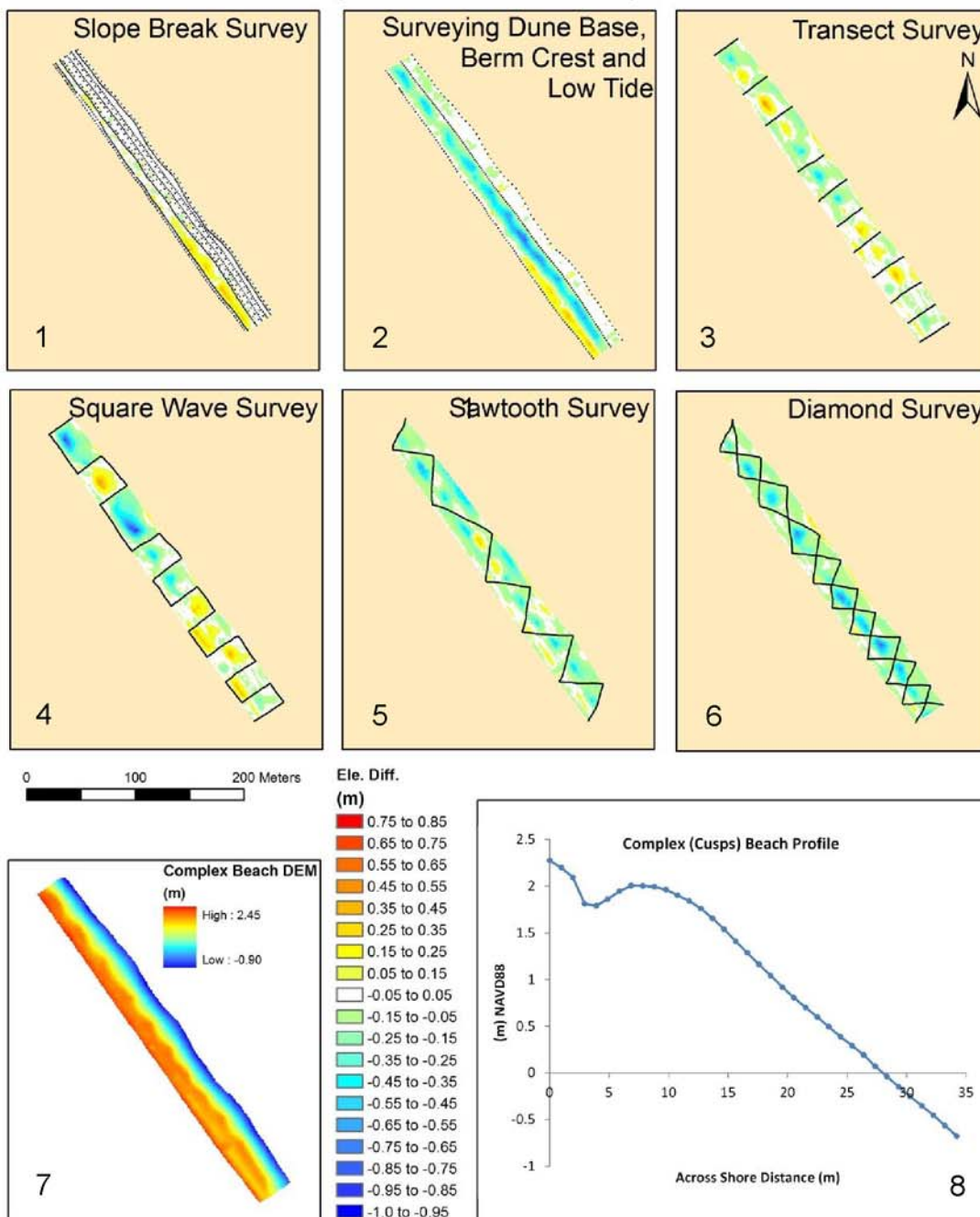


Figure 3-12. Comparison of survey styles on a complex beach with cusps and berm. Panel numbering same as Fig. 3-11. Panel 7 displays the “idealized” beach using data from all methods and additional alongshore transects. Panel 8 displays the complex beach across shore profile of the beach in this region. Top six panels show the elevation difference between each type of survey style and the idealized elevation surface.

Table 3-1. Results of static testing of RTK-GPS with collection at 1 second intervals for 600 seconds. RTK-GPS tests were conducted with different distances between base station and rover and different dates. Results of testing are presented in 95% confidences poles and poles corresponding to the maximum differences found in the x (easting), y (northing), and z (elevation) distances. IS PDOP defined somewhere?

Date	Distance (km)	Ave. # of Satellites	Ave. PDOP	Length N-Pole (cm)	Length E-Pole (cm)	Length Ele-Pole (cm)	N Max- Min (cm)	E Max- Min (cm)	Elev. Max- Min (cm)
2/28/2010	2.84	8.93	1.83	4.9	3.4	3.7	6.3	4.5	4.8
2/28/2010	2.84	8.08	3.47	4.2	3.1	4.0	5.1	4.8	5.9
2/17/2011	3.3	7.81	2.58	1.9	1.8	10.4	3.3	2.3	10.5
2/17/2011	3.3	7.47	2.70	2.6	1.0	6.2	3.5	1.6	7.3
2/17/2011	3.3	8.00	2.00	1.1	1.1	2.5	1.6	1.9	4.6
7/24/2010	3.3	7.53	2.02	1.9	2.3	8.7	2.7	2.9	9.7
2/17/2011	6.12	9.51	1.90	1.4	2.0	4.1	2.6	2.6	4.9
2/17/2011	6.12	9.00	1.98	1.5	2.6	6.9	2.2	3.3	7.7
2/17/2011	6.12	7.00	2.20	2.1	1.6	3.1	2.6	2.2	5.3
3/25/2010	6.12	9.98	2.01	3.7	3.5	4.4	6.1	5.8	5.7
3/26/2010	6.12	9.58	2.24	3.6	3.3	6.7	7.8	6.9	11.5
3/26/2010	6.12	8.88	1.83	4.4	4.1	9.4	6.1	5.8	5.7
5/26/2010	6.12	10.40	1.93	4.7	2.7	6.0	6.1	4.6	6.9
2/17/2011	8.98	8.03	2.09	2.9	2.3	4.1	4.4	3.2	5.4
2/17/2011	8.98	8.04	2.09	2.9	2.0	4.1	3.9	2.8	5.6
2/17/2011	8.98	8.00	2.10	2.8	1.8	4.0	3.5	2.2	5.5
2/17/2011	9.68	6.82	2.38	1.8	2.8	7.8	3.3	3.3	9.0
2/17/2011	9.68	7.58	1.91	3.2	4.3	4.5	4.3	5.2	7.3
2/17/2011	9.68	8.61	1.62	3.1	3.7	6.0	4.3	4.6	7.1
6/12/2011	9.68	8.94	1.88	2.8	1.0	4.8	3.2	1.4	6.5
6/12/2011	9.68	9.90	1.67	3.4	2.8	2.9	3.5	3.4	4.3
6/12/2011	9.68	7.65	2.30	1.5	1.5	4.7	2.1	2.1	6.6

Table 3-2. Results of a test of using multiple GPS Signals (L1 & L2, L2C) and GNSS (NAVSTAR & GLONASS) RTK-GPS data was collected at 1 second intervals for 600 seconds for each test. Each of the signal configurations below was conducted twice in reverse order to account for satellite configuration changes.

<b>GPS Signals</b>	<b>N Pole (cm)</b>	<b>E Pole (cm)</b>	<b>Ele Pole (cm)</b>	<b>N Max- Min (cm)</b>	<b>E Max- Min (cm)</b>	<b>Ele Max- Min (cm)</b>
L1/L2 Test #1	1.8	1.44	3.6	2.9	2.2	6.3
L1/L2 Test #2	2	2	6.2	2.4	2.3	6.5
L1/L2, L2C Test #1	1.6	1.2	3.2	2.3	2.1	4.4
L1/L2, L2C Test #2	1.6	1.8	3.7	2.3	2.3	5.7
L1/L2, GLONASS Test #1	2.3	1.3	2.7	2.7	1.7	3.8
L1/L2, GLONASS Test #2	1.4	1.7	4.8	2	2.1	7.2
L1/L2, L2C, GLONASS Test #1	1.8	2.2	4.3	2.9	2.6	5.3
L1/L2, L2C, GLONASS Test #2	1.4	1.6	3.4	2.2	2.2	6.4

Table 3-3. The difference between a walked across shore transect location of the MHW DBSL and a MHW DBSL extracted from a raster DEM created by the Slope break survey style. Positive values are those seaward the walked position of MHW DBSL; negative values landward.

UF Transect	Difference in Meters between Datum MHW and Walked MHW							
	9/5/09	5/27/10	7/28/10	8/28/10	10/9/10	11/20/10	2/18/11	5/19/11
10	0.61	1.08	-0.3	0.24	0.57	0.06	0.55	-0.5
20	1.62	-0.06	0.65	-0.09	0.63	0.07	-0.31	0.3
30	-0.16	0.28	0.55	0.06	0.44	0.7	0.49	-1.2
35	0.11	-0.52	0.4	-1.81	0.25	0.14	0.45	-1.4
40	1.41	-0.08	0.8	0.03	0.01	-0.38	0.65	0.8
50	-0.06	-0.42	1.16	0.96	0.76	1.22	1.07	0
60	0.09	0.07	0.35	0.39	1.56	-0.21	0.16	0
70	1.91	0.35	0.3	-0.16	0.97	0.22	1.23	0.6
80	0.14	-0.17	-0.05	1.92	-0.55	1.3	1.16	0.1
90	0.62	-0.18	1.1	1.41	-0.72	-0.1	0.12	0.5
Missing								
100	Data	-0.02	0.05	0.92	1.55	0.45	0.5	1.4
	No	No	No	No				
105	Transect	Transect	Transect	Transect	0.11	0.63	0.41	-0.2
110	-0.78	-0.26	0.15	-0.35	0.04	0.75	-0.11	-0.4
Missing								
120	0.08	0.07	Data	0.33	0.63	0.48	0.16	-0.5

Table 3-4. Table showing the difference in elevations between different 3-dimensional surfaces constructed from a simple TIN for each of the different survey RTK-GPS collection strategies on a simple concave-up beach. Positive elevations are those above the “idealized” surface and negative are below the “idealized” surface.

Survey Styles on Simple Concave-up Beach							
Elevation	Difference (m)	Slope Break	3 Line	Transects	Square	Sawtooth	Diamond
0.75 - 0.85							10
0.65 - 0.75							9
0.55 - 0.65							15
0.45 - 0.55			11				21
0.349 - 0.45			176			1	26
0.25 - 0.349			873		162	1	71
0.149 - 0.25		63	2011	21	501	1	435
0.05 - 0.15		812	4435	34	967	66	1531
-0.05 - 0.05		11461	4697	3563	3939	4664	6884
-0.149 - -0.05		1	16	6973	5358	5690	2424
-0.25 - -0.149				1129	816	406	299
-0.349 - -0.25				142	128	65	29
-0.45 - -0.349				20	25		12
-0.55 - -0.45				2	15		
-0.65 - -0.55					8		
-0.75 - -0.65					5		
-0.85 - -0.75					2		
> than 0.85							

Table 3-5. Table showing the difference in elevations between different 3-dimensional surfaces constructed via a simple TIN for each of the different survey RTK-GPS collection strategies for a complex beach with cusps and berm. Positive elevations are those above the “idealized” surface and negative are below the “idealized” surface.

Survey Styles on Complex Beach with Multiple Breaks						
Elevation	Slope Break	3 Line	Transects	Square	Sawtooth	Diamond
Difference (m)						
0.45 - 0.55			6	5		
0.349 - 0.45		18	44	81	1	
0.25 - 0.349		168	122	288	26	15
0.149 - 0.25	3	376	353	524	120	65
0.05 - 0.15	343	480	1067	1265	493	248
-0.05 - 0.05	9107	4802	4544	3919	2317	1877
-0.149 - -0.05	930	1835	3351	2197	3771	5233
-0.25 - -0.149	361	958	688	1030	1810	1468
-0.349 - -0.25	204	843	179	636	810	635
-0.45 - -0.349		697	73	318	337	394
-0.55 - -0.45		495	16	147	78	244
-0.65 - -0.55		225	1	106	20	111
-0.75 - -0.65		56		64		23
-0.85 - -0.75		2		32		2
-0.95 - -0.85				3		

## CHAPTER 4

### ANNUAL VARIANCE IN DATUM BASED SHORELINE POSITION

#### **4.1 Introduction**

The effects of climate change on sea level and ocean wave conditions will produce changes in spatial and temporal patterns of nearshore water levels and sediment transport, resulting in morphologic adjustment of beach and dune systems. As coastlines adjust to these changes, coastal studies documenting the shoreline response to changes in forcing will become increasingly important, especially for establishing a net change in the rate of shoreline motion (i.e., signal-to-noise). Recent studies have benefitted from the advent and increased use of new technologies such as LIDAR, GPS and high-resolution (< 1m pixel size) satellite imagery. Collection of these new data types, along with shoreline analysis from historical imagery, has increased appreciably in the past decade. Regardless of the methods used to collect and produce shoreline data, understanding the uncertainties involved in establishing shoreline position is important. The temporal and spatial variance in annual changes in shoreline position and its relationship to net change derived from longer-term studies is particularly important for understanding long-term shoreline change rates, regardless of the data type studied. Establishing annual variation in shoreline position may also provide insight into the variance about the mean found in previous long-term studies. Documenting seasonal variance in shoreline position also can provide a basis to minimize uncertainty in future data collection by acquiring data during the least variable seasons and assigning uncertainty to previously collected data.

Although substantial variability in alongshore coastal change has been well documented in the long term (>10 years) (Dolan et al., 1979a; Guillen et al., 1999; Stive

et al., 2002) and short term (monthly or storm) (List et al., 2006), studies that provide information on temporal and spatial variability of annual change are rare. Understanding the pattern, magnitude and seasonality of these variations is required to understand coastal change patterns and to make predictions using other techniques such as LIDAR, GPS, aerial photogrammetry or high-resolution satellite imagery. Regardless of the technique used to generate a shoreline position, uncertainties associated with the annual variation in shoreline position have to be taken into account. Uncertainties associated with shoreline position studies were defined by Fletcher et al. (2003)

Formula 4-1 as:

Formula 4-1

$$U_t = \pm(T^2 + S^2 + t^2 + RMS^2 + O^2)^{1/2}$$

where  $U_t$  is the total uncertainty, T is the uncertainty associated with cartographic errors such as that on T-Sheets, S is the uncertainty related to the annual variation in shoreline position, t is the uncertainty associated with variation in a visual-based determination, resulting from tidal cycle water-level changes, RMS error is the uncertainty of shoreline position associated with the ortho-rectification process and O is the uncertainty associated with delineating a visual-based shoreline. For most long-term shoreline position studies, the uncertainty associated with annual shoreline position is estimated or produced from limited data (Fletcher et al., 2003), and has not been quantified using datum-based shoreline (DBS) techniques. Datum-based shoreline position studies of alongshore variability generally fall into two categories; long-term (~ 10 year) LIDAR studies, with several years between observations (Sallenger et al., 2003) or monthly (Barnard et al., 2009; Hansen and Barnard, 2009, 2010) pre- and

post-storm assessments, using RTK-GPS (List et al., 2006). Measurements of the shoreline change envelope compared to net coastal change and beach morphodynamics provide a better understanding of the datum-based shoreline position uncertainties used in long-term coastal change studies employing LIDAR, RTK-GPS and aerial photography.

To quantify and compare the spatial and temporal variability in the annual shoreline change envelope and the net annual shoreline change, a series of monthly RTK-GPS studies over a two-year period was conducted during continuous collection of monthly data. These studies were undertaken during the full moon spring tidal cycle along a 10 km section of coastline at the Kennedy Space Center (KSC), located on Cape Canaveral, FL. During these monthly surveys, a datum-based shoreline was extracted at the MHW (0.28 m) elevation and was evaluated at 10-m intervals along the coast. By completing these surveys, I hoped to provide a better understanding of the uncertainties involved with using less frequently acquired shoreline positions in long-term coastal change studies. I also examined the spatial and seasonal variability of SCEs in three-month time intervals to assess the most desirable period for collection of LIDAR or imagery data. I consider several hypotheses for the spatial and temporal variation in SCE and net change. I also evaluate the uncertainties associated with seasonal variability as it is applied to uncertainties in the shoreline position of long-term data, and examine the wave climate for the study area and discuss seasonality associated with major weather systems. Finally, I discuss the most desirable three-month period for long-term data collection.

The effects of climate change on sea level and ocean wave conditions will produce changes in spatial and temporal patterns of nearshore water levels and sediment transport, resulting in morphologic adjustment of beach and dune systems. As coastlines adjust to these changes, coastal studies documenting the shoreline response to changes in forcing have become increasingly important, especially when trying to establish a net increase or decrease in the rate of shoreline motion (i.e., signal-to-noise). These studies have benefitted by the advent and increased use of new technologies such as LIDAR, GPS and high-resolution (< 1m pixel size) satellite imagery. The collection of these new data types along with shoreline analysis from historical imagery has increased significantly in the past decade. Regardless of the methods used to collect and produce shoreline data, understanding the uncertainties involved in establishing shoreline position is of significant importance. The temporal and spatial variance in annual changes in shoreline position and its relationship to net change derived from longer time-scale studies is of particular importance in understanding long-term shoreline change rates regardless of the type of data studied. Establishing annual variation in shoreline position may also provide insight into the variance about the mean found in previous long-term studies. Documenting seasonal variance in shoreline position also can provide a basis to minimize uncertainty in future data collection by acquiring data during the least variable seasons and to assign uncertainty to previously collected data.

Although substantial variability in alongshore coastal change has been well documented in the long-term (>10 years) (Dolan et al., 1979b; Guillen et al., 1999; Stive et al., 2002) and in the short-term (monthly or storm) (List et al., 2006) studies

undertaken to provide information on temporal and spatial variability of annual change are rare. Understanding the pattern, magnitude and seasonality of these variations are required to understand coastal change patterns and to make predictions using other techniques such as LIDAR, GPS, aerial photogrammetry or high-resolution satellite imagery. Regardless of the technique used to generate a shoreline position the uncertainties associated with the annual variation in shoreline position have to be taken into account. Uncertainties associated with shoreline position studies have been defined as (Fletcher et al., 2003):

$$U_t = \pm(T^2 + S^2 + t^2 + RMS^2 + O^2)^{1/2}$$

where  $U_t$  is defined as the total uncertainty,  $T$  is the uncertainties associated with cartographic errors such as those on T-Sheets,  $S$  is the uncertainty related to the annual variation in shoreline position,  $t$  is the uncertainty due to variation of a visual based proxy due to tidal cycle water level changes, RMS error is the uncertainties of shoreline position associated with the orthorectification process and  $O$  is the uncertainty associated with delineating a visual based shoreline proxy. For most long-term shoreline position studies the uncertainty associated with annual shoreline position is estimated or produced from limited data (Fletcher et al., 2003), and have not been quantified using datum-based shoreline (DBS) techniques. Datum-based shoreline position studies of alongshore variability generally fall into two categories; long-term (~10 year) LIDAR studies with several years between observations (Sallenger et al., 2003) or monthly (Barnard et al., 2009; Hansen and Barnard, 2009, 2010) pre- and post- storm assessments using RTK-GPS (List et al., 2006). Measurements of the shoreline change envelope compared to net coastal change and beach

morphodynamics provides a better understanding of the datum based shoreline position uncertainties used in long-term coastal change studies using LIDAR, dGPS and aerial photography.

In order to quantify and compare the spatial and temporal variability in the annual shoreline change envelope and the net annual shoreline change, a series of monthly RTK-GPS studies over a two-year period were conducted during a continuing collection of monthly data. These studies were undertaken during the full moon spring tidal cycle along a 10 km section of coastline at the Kennedy Space Center (KSC) located on Cape Canaveral, FL. During these monthly surveys, a datum-based shoreline was extracted at the MHW (0.28 m) elevation and was evaluated at 10 m intervals along the coast. In doing these surveys I hope to provide a better understanding of the uncertainties involved with using less frequently acquired shoreline positions used in long-term coastal change studies. I will also examine the spatial and seasonal variability of SCEs in three-month time intervals to access the most desirable period for collection of LIDAR or imagery data. In discussion, several hypotheses for the spatial and temporal variation in SCE and net change are considered. Further discussion will also be undertaken on the uncertainties associated with the seasonal variability as it is applied to uncertainties in the shoreline position of long-term data. I will also examine the wave climate for the study area and discuss seasonality associated with major weather systems. Finally, the most desirable three-month period for long-term data collection will also be discussed.

#### **4.2 Physical Setting**

Recent geomorphic changes to the coastal zone at Kennedy Space Center (KSC), Cape Canaveral, Florida, are threatening NASA infrastructure and have altered

endangered wildlife habitat. Since 2008, the U.S. Geologic Survey (USGS) has been conducting a dune vulnerability study at this site to provide a decision support system to the environmental management team at NASA-KSC. A major component of this project requires observations of shoreline and beach morphologic variability, to assess current risk and to help predict and evaluate future risk.

The beach at the John F. Kennedy Space Center (KSC) is part of the Cape Canaveral-Merritt Island sedimentary complex (Figure 4-1). The ~10 km coastline of KSC is bordered on the north by the Cape Canaveral National Seashore and on the south by the Cape Canaveral Air Force Station. This 10-km area contains critical infrastructure, including Launch Complex 39B, which is currently being retrofitted for the next American heavy-lift space vehicle, Launch Complex 39A, which until recently was used as the Space Shuttle launch platform, and Launch Complex 41, which is a medium-lift pad used by the Air Force for Atlas V vehicles (Figure 4-1).

The Cape Canaveral coast lies in a microtidal setting, with a mean tidal range of 1.03 m and an average spring tidal range of 1.19 m ((NOAA), 2011). The nearshore zone is characterized by two bars throughout the year that migrate onshore and offshore as forcing conditions change (Kline et al., 2011). The offshore bathymetry is complex and exhibits a series of transient oblique shoals and large cape-related shoals at False Cape and Cape Canaveral (Field and Duane, 1974a; Kline et al., 2011) (Figure 4-1).

Temporal linear trends and variability in the trends of long-term shoreline positions were calculated for the study area in three discrete intervals: 1875-2008, 1875-1969 and 1969-2008 by Dean (1998) and Absalonsen and Dean (2010). These rates were

calculated from surveys conducted by the Florida Bureau of Beaches and Coastal Systems (BBCS) and the Florida Department of Environmental Protection (FDEP) at 1,000-foot intervals along the shore at virtual monuments. Long-term change rate data are sporadic at this site after 1943 because the Kennedy Space Center's was designated a federal facility and is bordered by a National Seashore and Cape Canaveral Air Force Base. These studies showed both spatial and temporal variability in long-term shoreline position trends and in deviation about the trend throughout the study area. For both the long-term interval (1875-2008) and the early interval (1875-1969), the long-term trend is towards stability from the northern extent of the study area south for the first kilometers, then an area of shoreline retreat at ~0.25 m/yr for ~5 km in the center of the study area (Figure 4-2). Deviation about the trend is ~7.0 m in the stable area and ~12.9 m in the middle, erosional area. In the southern section of the study area there is a net accretion from False Cape to the southern extent of the study area of up to 1.5 m/yr. In this area, the deviation from the trend is ~10.4 m. In the recent interval (1969-2008), no data exist for the first ~3 km in the northern part of the study area. For the next ~5 km of shoreline, from 1969 to 2008, an alternating pattern of accretion and retreat almost an order of magnitude greater than the long-term average was found with an average deviation about the trend of ~22.3 m. In the southernmost 1.5 km of the study area, retreat of 6.0 m/yr was calculated. There were not enough data points to calculate deviation about the trend for this area (Figure 4-2).

## **4.3 Methods and Data Overview**

### **4.3.1 Wave Data**

Buoy data were provided by the NOAA National Buoy Data Center (NDBC) for both annual study periods (6 May 2009 to 2 May 2010 and 2 May 2010 to 19 April 2011). Wave Data were obtained from NBDC buoy 41009, located ~25 km east of Cape Canaveral in 44.2 m of water. NOAA buoy data were sampled hourly. Three key wave parameters were measured and analyzed for NOAA buoy data: significant wave height,  $H_s$ , the average of the highest third of the waves; the dominant wave period,  $T_P$ , the period of the waves having the greatest energy; and  $T_{AVE}$ , the average period of the waves. NOAA buoy 41009 was analyzed at one-hour intervals for wave events >3 m for the two survey periods (May 2009 – April 2010 and May 2010 – April 2011) (Figures 4-5 and 4-6).

### **4.3.2 Survey, Datum and Definitions**

A detailed description of GPS data collection, data processing, naming conventions, and the determination of accuracy and precision of RTK-GPS measurements is found in Appendices 2, 3, and 4.

Three National Geodetic Survey (NGS) benchmarks, with the designations KAREN, BUDROE, and WARD and six other associated bench marks were used as the baseline for the coastal surveys (Fig. 4-1). The three main benchmarks are horizontal first-order and vertical first-order class II (NGS, 2011). Benchmark KAREN was surveyed using modern GPS methods on 26 July 2004 with 95% confidence to 0.76 cm northing, 0.69 cm easting and 1.57 cm ellipsoidal heights by Brevard County. Benchmarks BUDROE and WARD, along with the six other associated benchmarks were then surveyed in with 95% confidence to <3 cm in the northing, easting and

elevation dimensions by RTK-GPS methods for use in the study (See Appendices for complete details on methods).

Fourteen across-shore transects were established as locations for quality control for slope-break surveys (as opposed to walked backpack surveys), sediment sampling, and to provide an across-shore transect out to wading depth, using methods described in Morton et al. (1993). These transects are designated UF 5 through UF 120 and were established in places that demonstrated a range of variability in shoreline position over the first four surveys, conducted in May, June, July, and August 2009 (Figure 4-1).

Supplemental transects were established during the program in areas that demonstrated high variability (#105) or were visible by a fixed camera (#05; Kline et al., 2011). Each month, UF-designated transects were walked with a backpack-mounted GPS unit from the crest of the first dune out to a chest-deep wading depth. Dune heights were established using the same backpack approach used for across-shore transects. Elevations of dune crests and dune toes were collected over three separate periods: August, October and November 2010. To provide a higher-resolution alongshore reference frame for cross-shore beach behavior, shore-normal transects were cast every 10 m alongshore using the Digital Shoreline Analysis System (DSAS) created by the USGS (Thieler et al., 2009). Lastly, a local alongshore reference system was used by local managers and is in km north of the northernmost jetty at Port Canaveral.

Beach surveys were conducted on the full moon spring tide to obtain the furthest seaward measurements possible. Rapid response surveys were also conducted during storm events. The local mean high water (MHW) datum for the beach (Figure 4-4) was

defined by Morton and Miller (2005) at 0.28 m NADV88. DBS mean high water contours were generated with data collected using an RTK-GPS cart and trailer system (Chapter 3). Surveys were conducted alongshore to capture slope breaks, which occur where the across-shore profile slope changes noticeably, such as at a berm crest or welding bar. In instances of a concave-up beach profile with limited slope breaks, the beach was evenly divided at equal across-shore distances. Landward survey bounds were defined by the vegetation line, when using the UTV, and the seaward survey bounds were determined by the furthest measurement that could safely be made with the existing tide and wave conditions (Figure 4-4). Alongshore dual-antenna GPS passes (up the 10 km study reach and back) varied from two to four passes, producing 8 to 16 individual lines (Fig. 4-4). During each pass, one wheel was towed along a specific slope break or minimum/maximum elevation. An example of a slope-break minimum/maximum survey pass position followed this order: vegetation line, berm overwash trough, berm crest, center of foreshore slope, beach toe and furthest seaward exposure of sub-aerial beach that could be safely surveyed.

For this study, beach width is defined as the horizontal distance measured from the top of the most seaward continuous dune crest out to the intersection of the 0.28-m mean high water contour on the beach (Fig. 4-4). The first continuous dune is defined as the most seaward continuous dune ridge throughout the study area. Proto-dunes were not included. Beach slope was defined as the average slope between the 0.25 m and 0.75 m contours (Fig. 4-4). These two elevation contours were consistent in each survey, and represented the slope of the foreshore.

Data QA/QC consisted of removing data points with a reported RTK-GPS uninitialized state (i.e. no data from base station). After QA/QC, a simple TIN was generated from the remaining data points (Chapter 3), and then the TIN was converted to a 1-m<sup>2</sup> raster-based DEM using GIS. A single contour line at 0.28 m was extracted from the raster using GIS, representing a MHW DBS. Additional contours were generated at 25-cm intervals to calculate slope.

## 4.4 Results

### 4.4.1 Wave Data During Survey Periods

Average significant wave heights ( $H_s$ ) were recorded at half-hour intervals for both annual survey periods (May 2009-April 2010 and May 2010-April 2011) at NOAA buoy 41009, located ~25 km east of Cape Canaveral at a water depth of 44.2 m (Figures 4-5 and 4-6). An “event” for this data set is described as any condition when  $H_s$  equals 3 m or greater, as described by Bromirski and Kossin (2008) for the U.S. East and Gulf Coasts (Figures 4-5 and 4-6). Bromirski and Kossin (2008) related this to  $H_s$  in the 90th percentile along the U.S. East Coast, along with a record of storm erosion events. At Cape Canaveral, 3 m  $H_s$  “events” have also been observed to be approaching the threshold for wash over in areas with depleted or eroded dunes. During both survey periods, the wave climate at Cape Canaveral was very similar in nature to both extra-tropical and tropical “events,” although no significant tropical events were recorded during either survey period, i.e.  $H_s > 3$  m for 24 hours or longer (Bromirski and Kossin, 2008) (Figures 4-5 and 4-6).

Figure 4-5 shows the average significant wave heights ( $H_s$ ) recorded from March 2009 through 2 May 2010 at Buoy 41009. Data gaps occurred during two periods, from 13 December 2009 to 1 January 2010 and from 14 January 2010 to 27 January 2010,

when Buoy 41009 malfunctioned. The maximum  $H_s$  occurred during an extra-tropical northeast storm with  $H_s > 3$  m, recorded from 19-21 May 2009 and a maximum  $H_s$  of 5.57 m on 20 May 2009. Another event occurred from 9-12 November 2009 when Hurricane Ida formed in the Gulf of Mexico, causing persistent strong winds from the northeast. The “Ida Nor’Easter” caused  $H_s > 3$  m, but these conditions were sporadic, with  $H_s$  conditions not lasting more than three consecutive hours. During the first survey period, three other extra-tropical northeast storms had recorded  $H_s > 3$  m, on 5 February 2010, 25 February 2010 and 11 March 2011, but none of these events had  $H_s > 3$  m for more than two hours. Minimum wave heights were recorded during June and July 2009.

During the second survey period, May 2010-April 2011, the maximum  $H_s$  (4.81 m) was recorded during hurricane Igor on 19 September 2010 (Figure 4-6). Wave heights ( $H_s$ )  $> 3$  m persisted for ~7 hours. Hurricane Earl produced a maximum  $H_s$  of 4.58 m on 2 September 2010 and produced  $H_s > 3$  m that persisted for ~5.5 hours. Four extra-tropical northeast storms produced  $H_s > 3$  m on 13 November, 14 December, 26 December 2009 and 4 March 2011, whereas the storms on 14 and 26 December 2010 produced  $H_s > 3$  m for <2 hours, the 13 November 2010 and 4 March 2011 storms each produced  $H_s > 3$  m for ~10 hours. Minimum values for  $H_s$  were recorded in June and July 2010 (Figure 4-6).

#### **4.4.2 Slope**

The foreshore slope of beaches tends to reflect most strongly the resident sediment grain size, and is a key parameter for defining beach morphology. Spatially, the slope of the foreshore decreases from north to south along the 10 km of the KSC coastline (Figure 4-7). Over the two-year survey period, the average slope of the KSC foreshore was 0.089, with a  $1-\sigma$  deviation of 0.026. The northernmost 1.5 km section of

shoreline, hereafter Region 1, had the highest average slope (0.109) and the highest deviation in slope (0.29) of the four distinct KSC coastal regions, whereas the southernmost 1 km of shoreline (Region 4) had the lowest average slope (0.073) and deviation (0.018) (Figure 4-7). Region 2, 1.5-5 km, measured from the northern boundary, is the area of greatest concern to NASA with regard to dune overwash and erosion. It has a mixed range of slopes, with an average slope of 0.092 and a deviation of 0.027 (Figure 4-7).

During the first survey period (May 2009 - April 2010) in Region 2, i.e. the area defined by frequent overwash (>annually) and no dunes, there was a wide range of slopes (0.12-0.07). A wide range of slopes (0.10-0.07) was also found in Region 3, the area of the False Cape, where there has historically been accretion. Region 4, the area south of False Cape, with low multiple dunes, the range of slopes (0.09-0.06) was similar although lower compared to the area of stability found in the northern area (Figure 4-8).

During the second survey period (May 2010 – April 2011), slopes in each region were generally similar to those measured during the first survey period. In Region 1, the range and magnitude of slopes were similar to the first survey period (0.13-0.09), whereas in Region 2 there was a greater range of slopes (0.13 – 0.06) compared to the first survey period. Region 3, the False Cape area, had a range of slopes (0.09 – 0.06) similar to the first survey period. In Region 4, the southern reach of the study area, beach slopes (0.06 – 0.08) had a range similar to the first survey period (Figure 4-8).

#### **4.4.3 Net Shoreline Change**

Two years of shoreline position observations are insufficient to extract longer-term shoreline trends (Harley et al., 2011). They can, however, provide an indication of the

areas of a shoreline that are most sensitive to short-term forcing. It is important to consider any shoreline change in terms of the overall variability in position throughout the time period of measurement (i.e., shoreline change envelope, SCE). If the net change is larger than the SCE, the relative signal to noise ratio is high.

The relative annual shoreline change during the two survey periods (May 2009 - April 2010 and May 2010 - April 2011) is an order of magnitude greater than the long-term net change of Absalonsen and Dean (2010) (Figure 4-9). There was consistent anti-phasing throughout the entire study area between the two annual survey periods, unrelated to any specific storm event (Figure 4-9), indicating that small changes in the wave climate can have a large impact on shoreline response over short time periods.

The average net change for the entire period from May 2009 through April 2010 was 1.24 m seaward, with a standard deviation of 4.56 m. Maximum net change was found at DSAS transect 465, with a seaward advance of 12.18 m. Maximum retreat occurred at DSAS transect 175, with a retreat of 7.98 m (Figure 4-9). There is a net retreat of ~2 m from DSAS transect 0 to 300 and then a net accretion of ~8 m from DSAS transects 300 to 500. DSAS transects 500 to 800 are highly variable, with areas of retreat and accretion with ~0 m of change, whereas DSAS transects 800 to 1000 are also highly variable, with an average of ~2 m advancement (Figure 4-9).

The average net change for the second survey period for all 1000 DSAS transects was a 1.90 m advance, with a standard deviation of 3.31 m (Figure 4-9). The maximum net change occurred at DSAS transect 763, with 13.50 m of advance. The maximum retreat occurred at DSAS transect 416, with a loss of 6.10 m. DSAS transects 0 through 360 had an average accretion of ~3 m, whereas DSAS transects 350 through 500 had a

retreat of ~4 m, in antiphase with the first survey period. For DSAS transects 500 through 800 there was an area of accretion (~4 m with a maximum of 13.8 m) whereas during the first survey period, change was highly variable, with both accretion and retreat. DSAS transects 800 to 1000 were slightly accretional (~1–2 m) and were similar to the 2009 – 2010 period, with antiphasing (Figure 4-9).

#### **4.4.4 Shoreline Change Envelope**

The total maximum seaward to landward excursion of the MHW shoreline position is called the shoreline change envelope (SCE). Higher SCE values reflect a more dynamic shoreline. Over the two-year survey period, the MHW (0.28 m) shoreline positions extracted from the DEM models reveal that the four regions of the KSC beach show different spatial and temporal patterns of variability (Figure 4-10). Region 2, the region with historic shoreline retreat, has a change envelope of 17.25 m and an average standard deviation in shoreline position of 4.39 m. Region 3, with a pattern of historic shoreline advancement, has an average SCE of 19.30 m and an average shoreline position deviation of 4.99 m. Regions 2 and 3 display higher variability than the two regions at the north and south. Regions 1 and 4 have average SCEs of ~12.53 m and average standard deviations in shoreline position of ~3.15 m (Figure 4-10).

During the first survey period, the average SCE was 13.02 m, with an average standard deviation of 3.32 m (Figure 4-11). The maximum SCE was 26.10 m at DSAS transect 765, whereas the minimum SCE was 7.43 m at DSAS transect 902.

During the second survey year, areas with higher slopes generally had less variability than the flatter areas of the beach (Figure 4-10), as observed during the first survey year, although all four regions of the beach displayed greater variation in SCE. In Region 1, the range of SCEs was wider (~4.0 – 13.5 m). In Region 2, there was an even

wider range of SCE, from ~4.5 – 20.1 m, compared to the first survey period. The Region 3 False Cape area had a similar range of SCE of ~5 – 37 m when compared to the first survey period. In southernmost Region 4, there was a wider variation in SCE, from ~5.0 – 11.0 m) (Figure 4-10).

#### **4.4.5 Slope Versus Shoreline Change Envelope (SCE)**

To test the assumption that variability in shoreline position is simply a function of beach slope (i.e., lower slopes = higher variability), I compared beach slope and SCE within the four different geomorphic and historically defined areas of the beach (Figures 4-11 and 4-12). For the two-year survey period, areas with higher slopes generally had smaller SCEs and therefore less variability, although there is much scatter, indicating that factors other than beach slope influence shoreline variability. In general, during the first survey period, the northern, Region 1 stable area (DSAS transects 0-200) had higher slopes (0.13-0.09) and smaller SCEs (8.55 - 15.43 m). During the first survey period, in the Region 2 area defined by frequent (>annual) overwash and no dunes, there was a wide range of slopes (0.12-0.07) and a wide range of SCEs (7.75 – 23.50 m). The same pattern of wide range of slopes (0.10-0.07) and SCEs (7.41 – 26.01 m) is also found in Region 3, the area of False Cape, where there has historically been accretion (Figure 4-11). In Region 4, the southern extent of False Cape, the beach is flatter (slopes 0.09 – 0.06), with a narrow range of relatively small SCEs (9.20 – 14.93 m). Whereas Region 1 has a relatively small range of lower SCEs and steeper slopes, Region 4 has a relatively narrow range of lower SCEs, but has the flattest beaches in the study area.

During the second survey year, areas with higher slopes generally had less variability than the flatter areas of the beach (Figure 4-12) as observed during the first

survey year, although all four regions of the beach had a wider variation in SCE. In the northern area of the beach, the range and magnitude of slopes were similar to the first survey period (0.13-0.09), whereas the range of SCEs was wider (~4.01 – 13.53 m). In the overwash section, there was a greater range of slopes (0.13 – 0.06) and wider range of SCE (~4.51 – 20.12 m) compared to the first survey period. The False Cape area had a similar range of slopes (0.09 – 0.06) and an SCE of ~5 – 37 m, in contrast to the first survey period. In the southern reach of the study area, beach slopes (0.06 – 0.08) had a range similar to the first survey period, but had a wider variation in SCE ~5.0 – 11.01 m. Table 4-2 shows the statistics for shoreline position deviation, SCE and SCE deviation for the entire study area as well as each region.

#### **4.4.6 Seasonal Variation in Shoreline Change Envelope**

Two years of shoreline position observations allow us to determine the seasonal period when shoreline variability is smallest. This is important when considering the use of remotely sensed imagery to establish a visual-based shoreline location. Ideally, the best time to acquire imagery for this purpose is when the relative shoreline position is least variable, which allows for better year-year comparisons of shoreline position using visual data (e.g., wet-dry line). The average shoreline changes were calculated in three-month intervals for the entire two-year length of the study, along with maximum landward and seaward excursions for all 1000 DSAS transects (Figure 4-13). The maximum three-month landward excursion (shoreline retreat) of 18.03 m occurred during August-September-October 2010 and the maximum three-month seaward excursion (shoreline advance) of 24.24 m occurred during June-July-August 2010. Maximum net shoreline movement occurred in August-September-October 2010 with an envelope of 33.54 m change. June-July-August 2010 also had a difference between the

maximum landward and seaward excursions >30 m. The smallest three-month difference between peak landward and seaward change was found in March-April-May 2011, with a difference of 12.50 m. April-May-June 2010 and 2011 both had maximum and minimum differences of <15 m (Figure 4-13).

Maximum average net advancement over all 1000 DSAS transects during a three-month period occurred in February-March-April 2010 at 4.51 m. June-July-August 2010 and July-August-September 2010 also had average shoreline accretion of >3 m (Table 4-3). Maximum average shoreline retreat occurred during September-October-November 2010, with an average loss of 4.82 m. July-August-September and October-November-December 2009 averaged a loss of >4.01 m. Maximum standard deviation in average 3 month change occurred in June-July-August 2010 and August-September-October 2010, with a deviation of 5.8 m corresponding to an average shoreline accretion of 3.52 m during the first three-month period and an average shoreline retreat of 1.71 m during the second three-month period. Minimum standard deviation in three-month shoreline change occurred in March-April-May 2011, with a deviation of 2.21 m. April-May-June 2010 and 2011 had minimal standard deviations of 2.42 m.

## 4.5 Discussion

### 4.5.1 Spatial Trends in Shoreline Behavior and Morphology

Long-term shoreline change rates and geomorphic characteristics enable division of the study area into four distinct zones (Fig. 4-1). From north to south, Region 1 is the northernmost ~1.5 km of the study area and is characterized by long-term stability, with a single dune that is ~4 m in elevation (NAVD 88). This area also has the highest average foreshore slopes in the study area. The next ~5 km, Region 2, is characterized by a single, frequently overwashed dune and long-term net retreat. Foreshore slopes in

this area are highly variable relative to slopes in the northern reach and to those of False Cape. Region 3 is at False Cape and is characterized by an aspect change in the coastline, with low dune ridge sets and the presence of incipient or proto-dunes. This area also has variable foreshore slopes, but is on average flatter than the area with historic retreat. This 2.5 km is also an area of net advancement. Region 4, the southernmost 1 km of the study area is characterized by a series of low dunes, but is lacking proto-dunes. It is also characterized by historic long-term accretion, but there has been severe retreat (~5.5 m/yr) during the most recent period (1969-2008) (Figures 4-1 and 4-2). Foreshore slopes in this region are, on average, as flat as False Cape, but with less variability.

#### **4.5.2 Net Shoreline and Annual Reversals**

It is difficult to point to a simple morphodynamic explanation for the spatial variability in net change (Figure 4-9). Even though similar patterns of alongshore SCE and alongshore shoreline change have been observed at other coasts with shore-parallel offshore depth contours (List et al., 2006), the patterns in shoreline change observed at Cape Canaveral may be more related to wave refraction patterns over the offshore bars near the cape.

Temporal variability in shoreline position at KSC is not easily understood in simple terms of shoreline geometry, i.e., slope and width. Whereas slope, beach width, and wave climate remained very similar during both survey periods, there was consistent anti-phasing in the overall shoreline change between the two years. This area experiences similar storm reversal patterns, consistent with those measured from storms by List et al. (2006), but the anti-phasing here is annual in nature and not attributable to any specific storm. The wave climate was very similar through both study

periods, with a mix of both extra-tropical and tropical events. One possible explanation is that there is temporal variation in wave refraction patterns over the extensive shoals found in the area, but it is difficult to reconcile this with very distinctive 180-degree anti-phasing in shoreline change.

Spatial variation in an autonomous beach with minimal anthropogenic influence is difficult to explain. Although several periods were observed when rip cells were present in all four regions, none were large or persistent enough to explain the variability in the data. The narrow stable areas experienced as much change as the areas with historic retreat and overwash, with the exception of the area around DSAS transects 360-475. One area that may have a morphological explanation is the area at the initial aspect change of False Cape. This area is at an inflection point between historic accretion and erosion.

#### **4.5.3 Annual Shoreline Uncertainties**

Annual variability in shoreline position is important for understanding the uncertainties related to long-term shoreline analysis, regardless of whether the shoreline data are datum-based (LIDAR, GPS) or visual-based (imagery). Shoreline Regions 1 and 4 had the highest and lowest slopes, respectively, but had the smallest SCE. In the northern reach of the study area, where the most stable beaches and highest slopes are found, this may be related to a more typical on-shore/off-shore migration of sand bars or to the intersection of beach parallel bars with the beach. In the area of the lowest slopes south of the False Cape protrusion, the low values for SCE may be related to the orientation of the shoreline and the protection from northeast storm-wave fields by the offshore shoals. The areas that have the highest SCEs are the areas that have the highest long-term shoreline change. Larger SCEs are also

associated with areas of historic accretion. These areas typically have a wide variety of low-angle beach slopes. The area where the dunes have been overwashed and where there is problematic erosion (Region 2) have a wide variety of slopes and a broad range of SCEs. This may be related to the disruption of the onshore-offshore migration of sand or loss of sand from the system. In many areas of Region 2, sand has been overwashed behind the dunes or to swales behind the dunes, thereby removing it from the active shoreline system.

These results point to a dilemma for coastal scientists and managers - areas with the most stability have the lowest uncertainties associated with shoreline measurement, whereas areas of greatest change, usually the areas of highest concern or interest, have the highest uncertainties associated with them. Deviation of shoreline position (i.e., variance about a linear regression) in long-term shoreline studies, suggest several explanatory factors: storms, changes in wave climate or seasonal effects. In Brevard County, the average standard deviation in shoreline position from 1874-2008 was 14.1 meters (Absalonsen and Dean, 2010; Dean et al., 1998). For the two-survey period of this study (May 2009 – April 2011), the average SCE along the entire study area was 12.4 m, a similar value. This result demonstrates that much of the variance about a linear regression in long-term shoreline studies may be explained by seasonal variation in shoreline position over the period in which the measurement was made.

#### **4.5.4 Three-Month Variation in Shoreline Change**

Two years of shoreline position observations allowed us to determine the seasonal period when shoreline variability is smallest. This is important when considering use of remotely sensed imagery to establish a visual-based shoreline position. Ideally, the

best time to acquire imagery for this purpose is when the relative shoreline position is least variable. This allows for better year-to-year comparison of net shoreline position.

The best time to acquire coastal data is determined by the type of data desired. Data for best delineating a beach at maximum annual seaward growth, where berms are most prevalent, are best acquired late in the June-July-August time period. This allows for berm construction and is typically before major tropical storms affect this region. The best time to acquire beach data where the shoreline is at its most landward position is early in the April-May-June interval. This time period has the lowest SCE, SCE deviation, shoreline change and shoreline change deviation. This may be associated with higher winter wave energy, which removes the berm, leading to foreshore flattening, thereby maintaining a high-energy, concave-up profile with less variability.

#### **4.6 Conclusions**

Four distinct regions were defined along the 10 km of NASA's False Cape coast, each with different morphologic characteristics and behaving in a different and distinct manner. Region 1 is characterized by long-term stability, relatively high slopes, a single primary dune and a relatively narrow SCE. Region 2 is characterized by long-term retreat, has mixed slopes, overtopped dunes and a relatively wide range of SCEs. Region 3 is characterized by long-term accretion, relatively low slopes, several low dunes, and the highest SCEs in the study area. Region 4 is characterized by mixed long-term change rates, relatively low slopes, a low dune and relatively small SCEs. The manner in which each of these regions responds to forcing has consequences relating to remediation strategies. For example, in Region 2, where most of the primary dunes are missing and dune washover is prevalent during storms, there is more

uncertainty in shoreline position, as expressed in SCE. This increased uncertainty must be taken into account when planning remediation strategies, such as beach renourishment, especially when only a few temporal data points, such as shorelines extracted from infrequent LIDAR, are used to compute retreat rates.

The average SCE for the entire study area over the two years of the study was 12.4 m. This relates very well to the 14.1 m deviation found in long-term data (1878-2010) of Dean (1998) and Absalonsen and Dean (2010). This may indicate that much of the variation in shoreline position used by these authors to calculate linear retreat rates is readily explained by the annual variability in shoreline position. The SCEs for each of the annual study periods also revealed, not unexpectedly, that areas with the largest net change (either accretion or retreat), have the largest SCE. Although it is difficult to identify the causal factor in the spatial variability of the SCE, one plausible explanation may be the wave diffraction patterns over the complex bathymetry found offshore. The variability in the wave energy flux may also explain the antiphasing found in the annual net shoreline change.

Seasonal (3-month) SCEs can contribute to understanding the uncertainties related to both datum and visual-based shoreline positions. Seasonal surveys in this study indicate that data collected during April-May-June have lower SCE values than those collected during June-July-August. This means that comparisons between years when data is acquired during the former time period will have the least uncertainty resulting from shoreline dynamics.

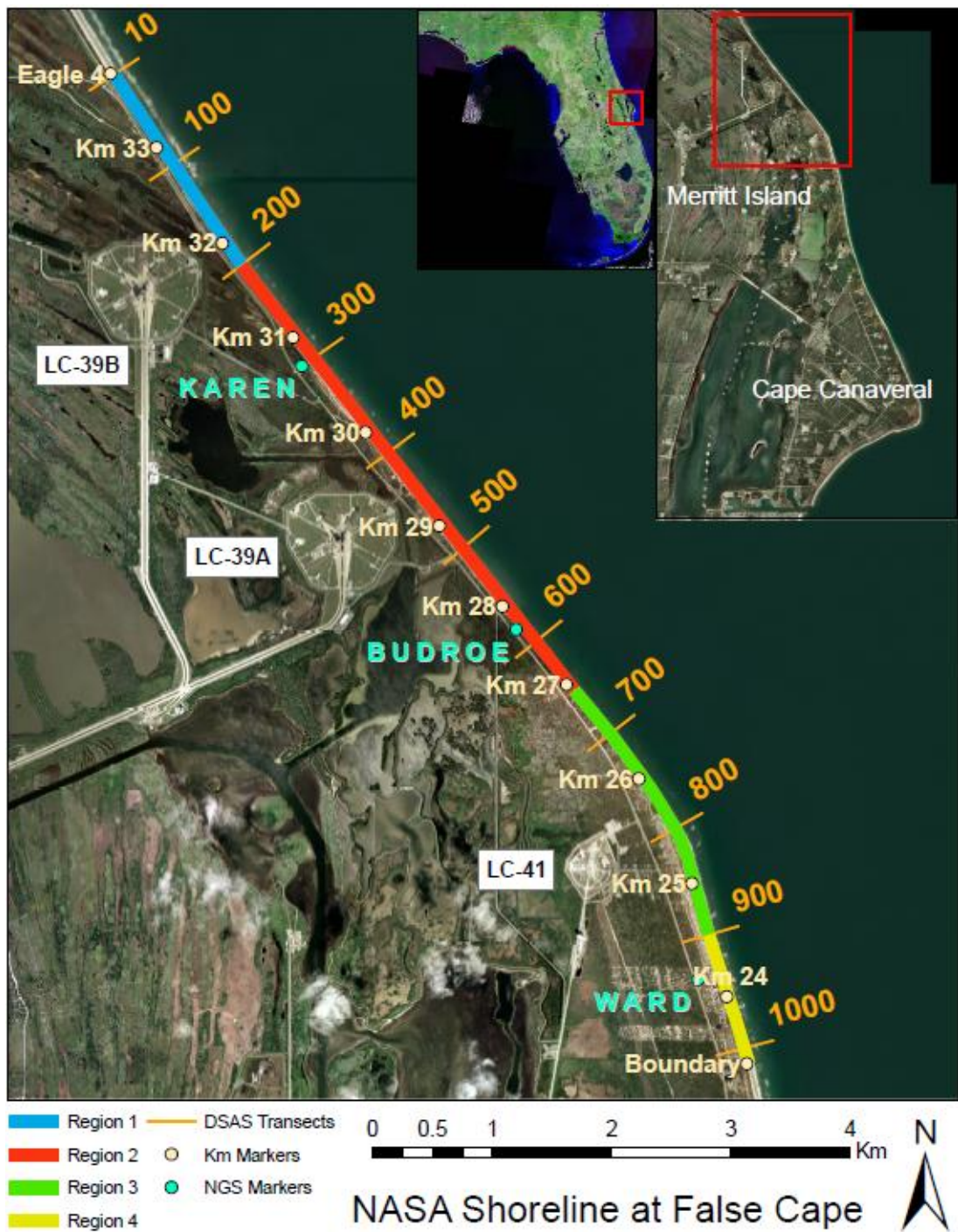


Figure 4-1. Area of study including NASA critical coastal launch facilities. DSAS transects (red) are spaced 10 m apart, here referenced at 100 m increments. Alongshore reference markers (km markers) also noted. NGS benchmarks used during surveys are shown.

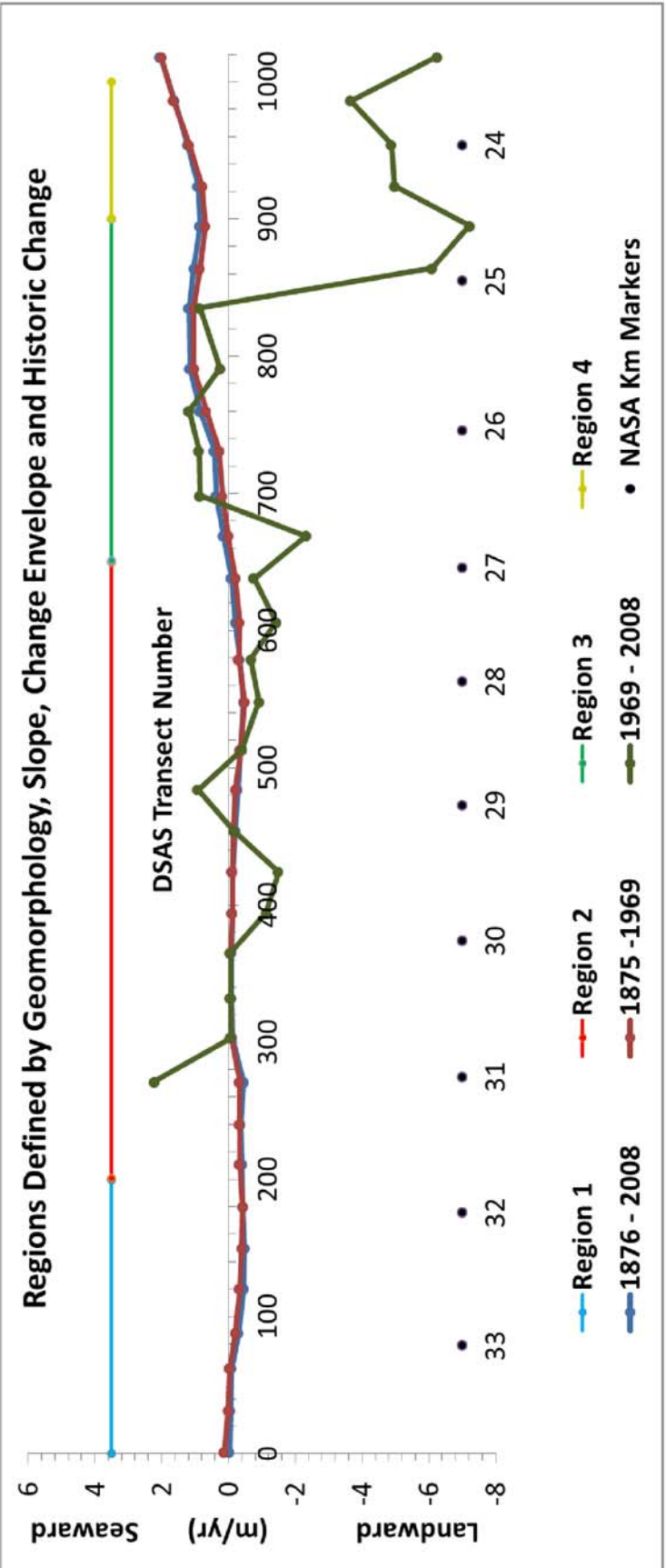


Figure 4-2. Long-term shoreline change rates for study area after Absalonsen and Dean (2010). The more recent change rates (1969-2008) do not reflect the longer-term rates (1876-2008). The four regions of shoreline behavior and locations of UF sampling transects are also noted.

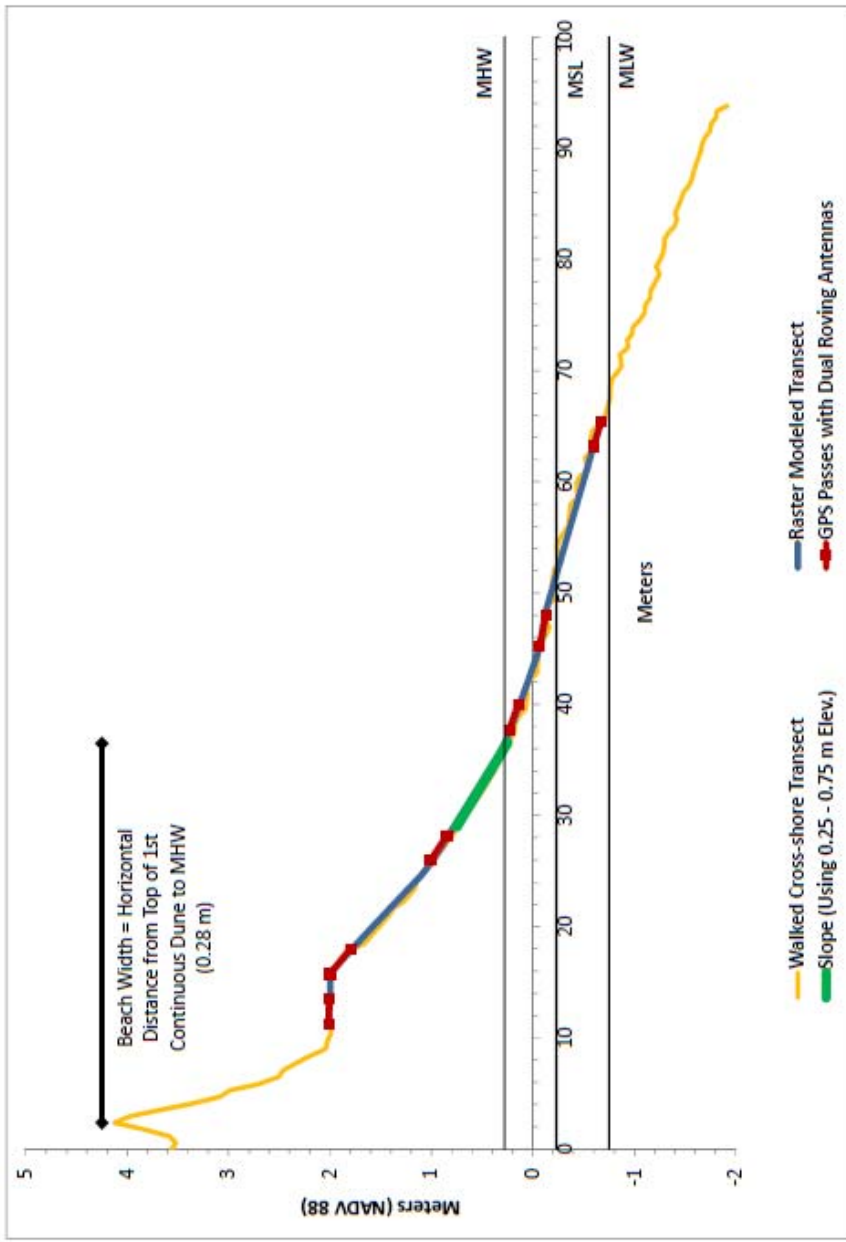


Figure 4-3. Example of data collection strategy and relevant vertical datums. Tidal datum for Cape Canaveral MHW is 0.28 m, MSL is -0.23 m and MLW is -0.68 m. Beach width (as defined in this study) is the horizontal distance measured from the top of the first continuous dune out to the MHW (0.28 m) contour. Red segments represent the two measurements taken by the GPS trailer at each slope break. The blue line indicates the across shore profile generated from the GPS measurements modeled with a TIN then converted to a raster. Red line indicates a UF sample transect measured from the landward of the first continuous dune out to wading depth. Slopes were measured between the 0.75 m and 0.25 m contours.

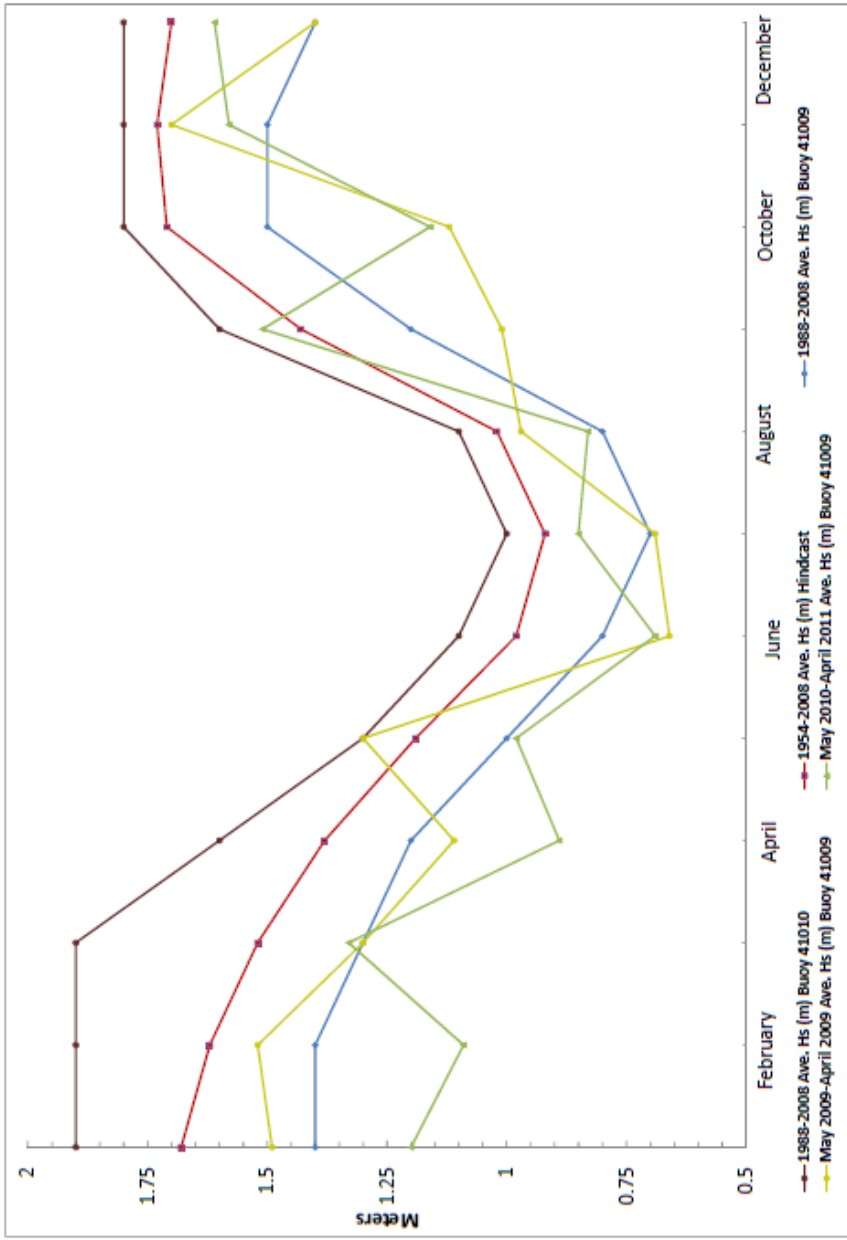


Figure 4-4. Monthly average significant wave heights measured ~37.04 km east of Cape Canaveral in a water depth of 44.2 m. Blue line indicates average significant wave heights from the WIS hindcast for the time period of 1988–2008. Red line is monthly average significant wave height measured at NOAA buoy 41009 from May 2009 through April 2010. Green line indicates average significant wave height measured at NOAA buoy 41009 from May 2010 through April 2011. Lowest average significant wave height were measured in the June July August period (“summer condition”) whereas the highest average significant wave heights were measured in the December-January-February period (“winter condition”). Transitions from summer to winter to summer occur in the months of September-October-November and March-April-May.

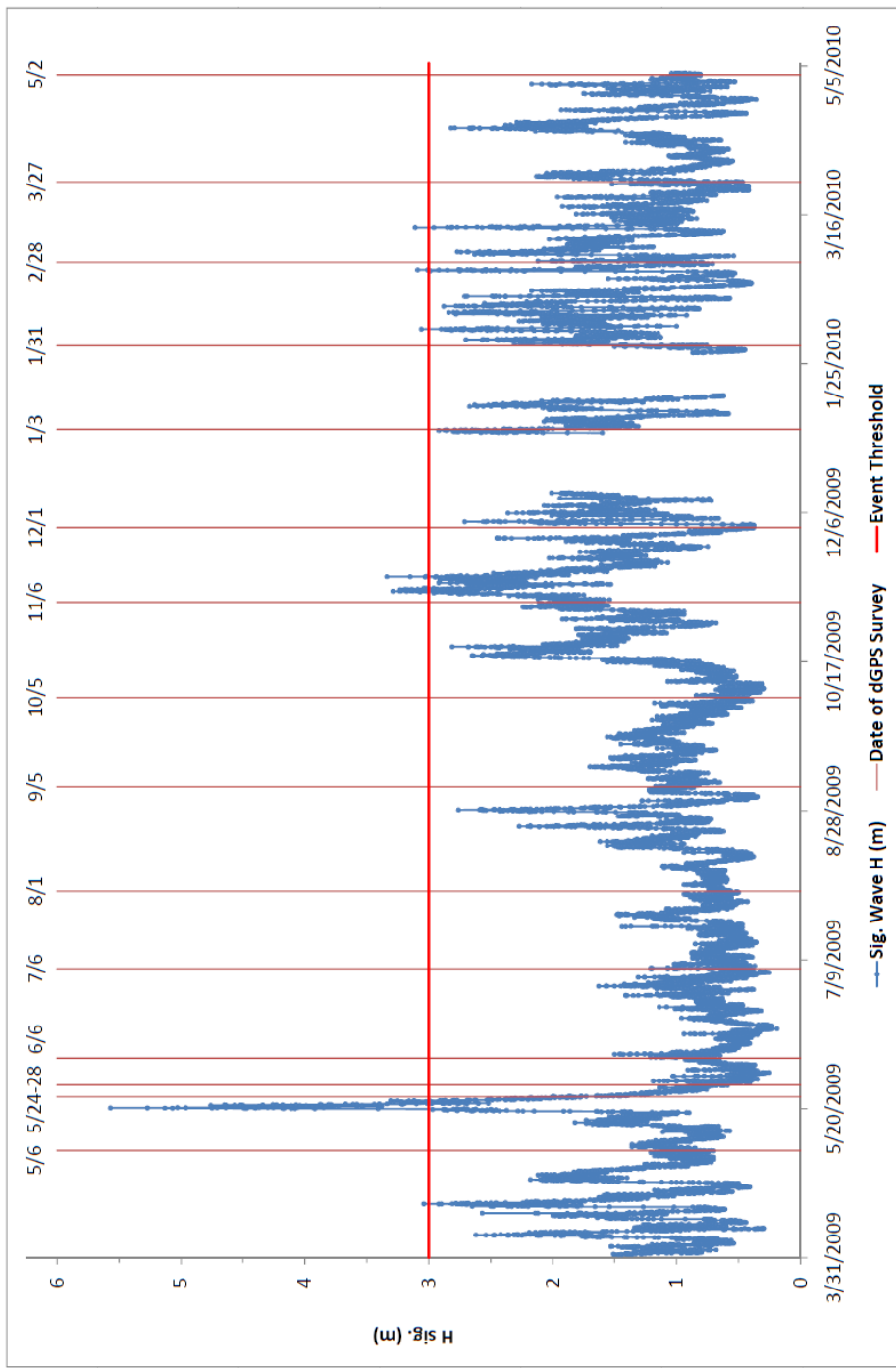


Figure 4-5. Average significant wave heights for the period of 1 April 2009 through 2 May 2010 with GPS survey times in red. The highest significant wave heights recorded for this period occurred on 20 May 2009 and were caused by a persistent northeast storm that affected the Cape Canaveral area from 19 May through 21 May 2009. Hurricane Ida in the Gulf of Mexico set up persistent northeast storm conditions with wave heights greater than 3.25 m in the Cape Canaveral area from November 9–14 November 2009. The horizontal red line is the cutoff waves heights associated with storm “events”  $>3$  m.

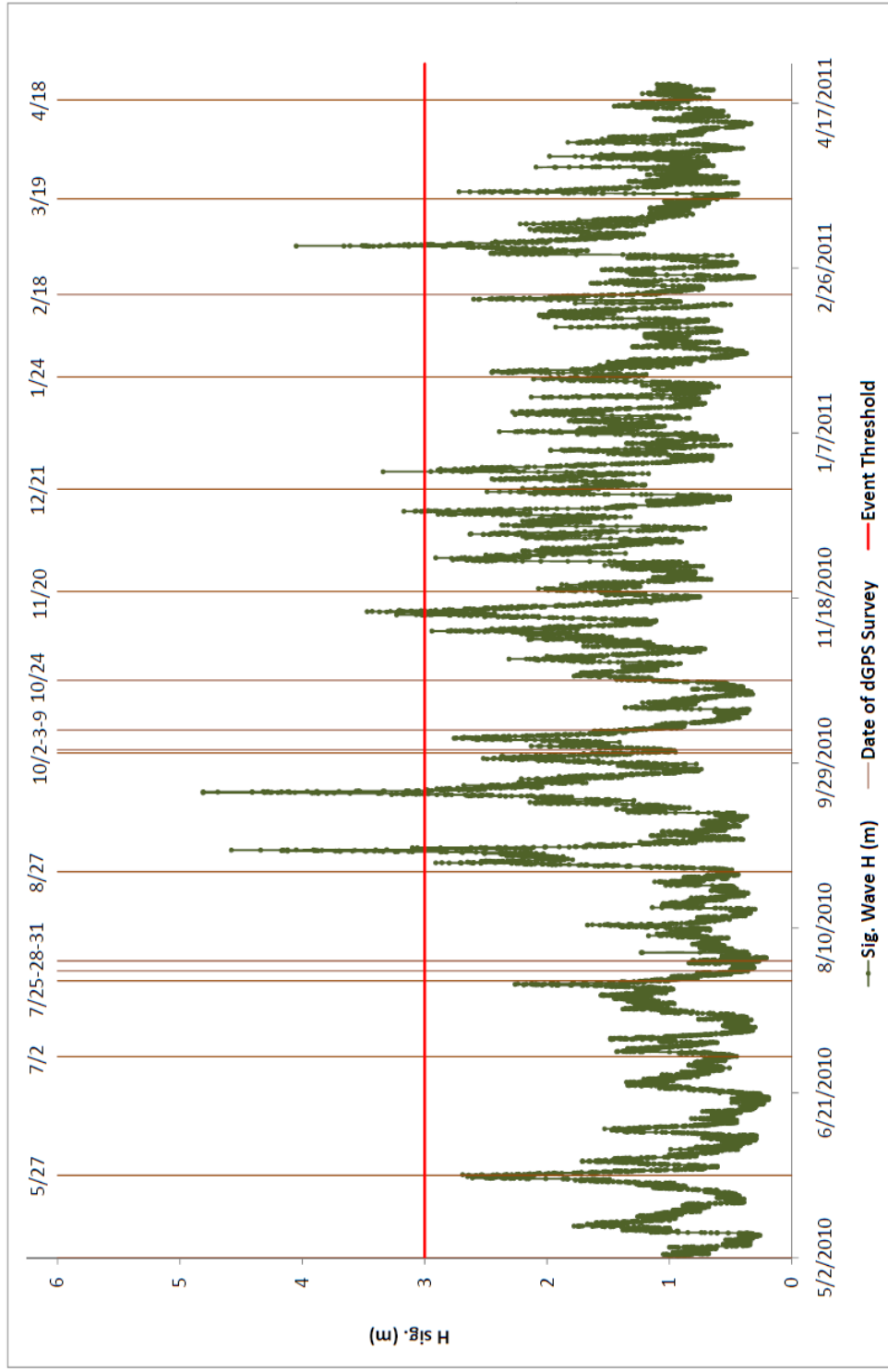
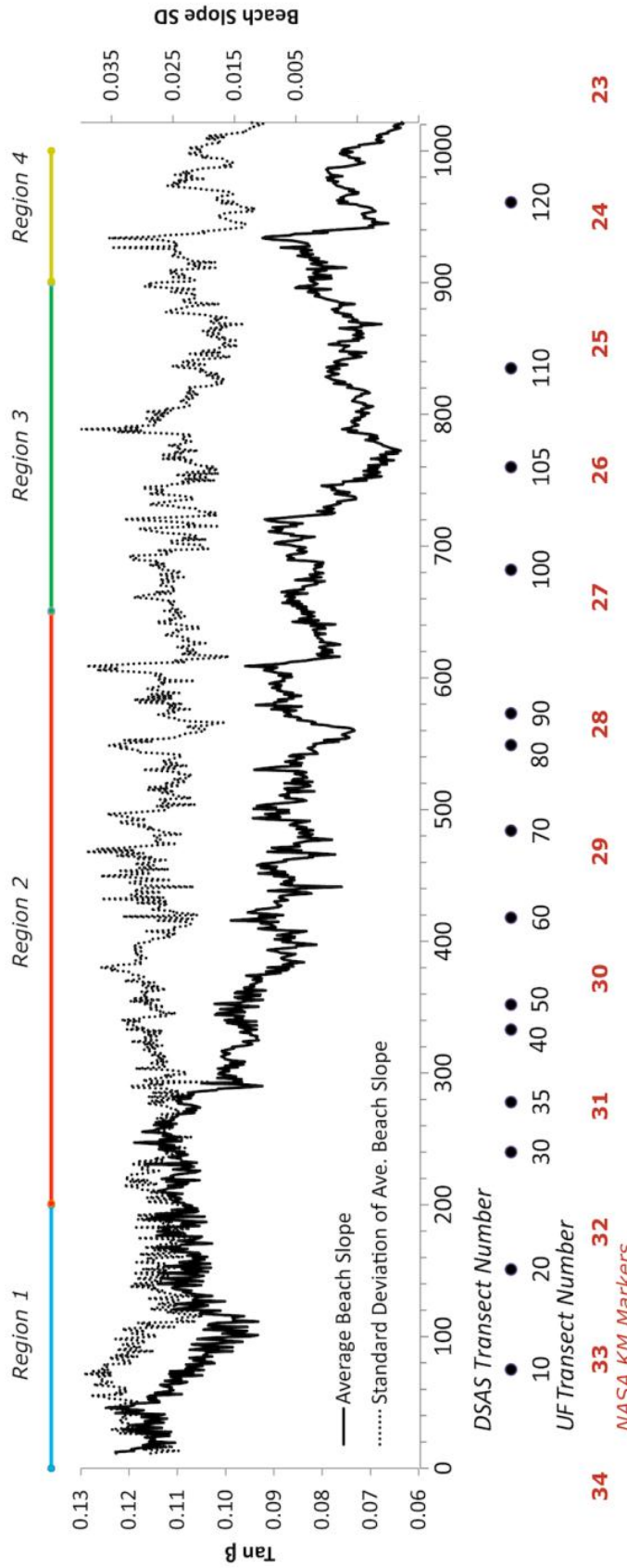


Figure 4-6. Average significant wave heights for the period of 2 May 2010 through 2 May 2011 with GPS surveys noted in red. The highest significant wave heights recorded for this period occurred on 19 September 2010 and were caused by Hurricane Igor. Hurricane Earl also caused average significant wave heights of >4 m (4.58 m max.) on 9 September 2010. Horizontal is the red line same as that shown in Figure 4-5.



**Figure 4-7.** Average slope and deviation of the slope of the foreshore (0.25 m – 0.75 m contours) for surveys conducted from May 2009 through April 2011 (25 individual surveys). Different regions of the beach are indicated at the top of the figure (four colored bars). Note that slope decreases (beach flattens) from north to south (left to right in figure). Also note that there is more variability (higher standard deviation) in the foreshore slope in Regions 2 and 3 (region of erosion and accretion). DSAS transect numbers, UF transect numbers and NASA-IHA kilometer numbers are provided for reference.

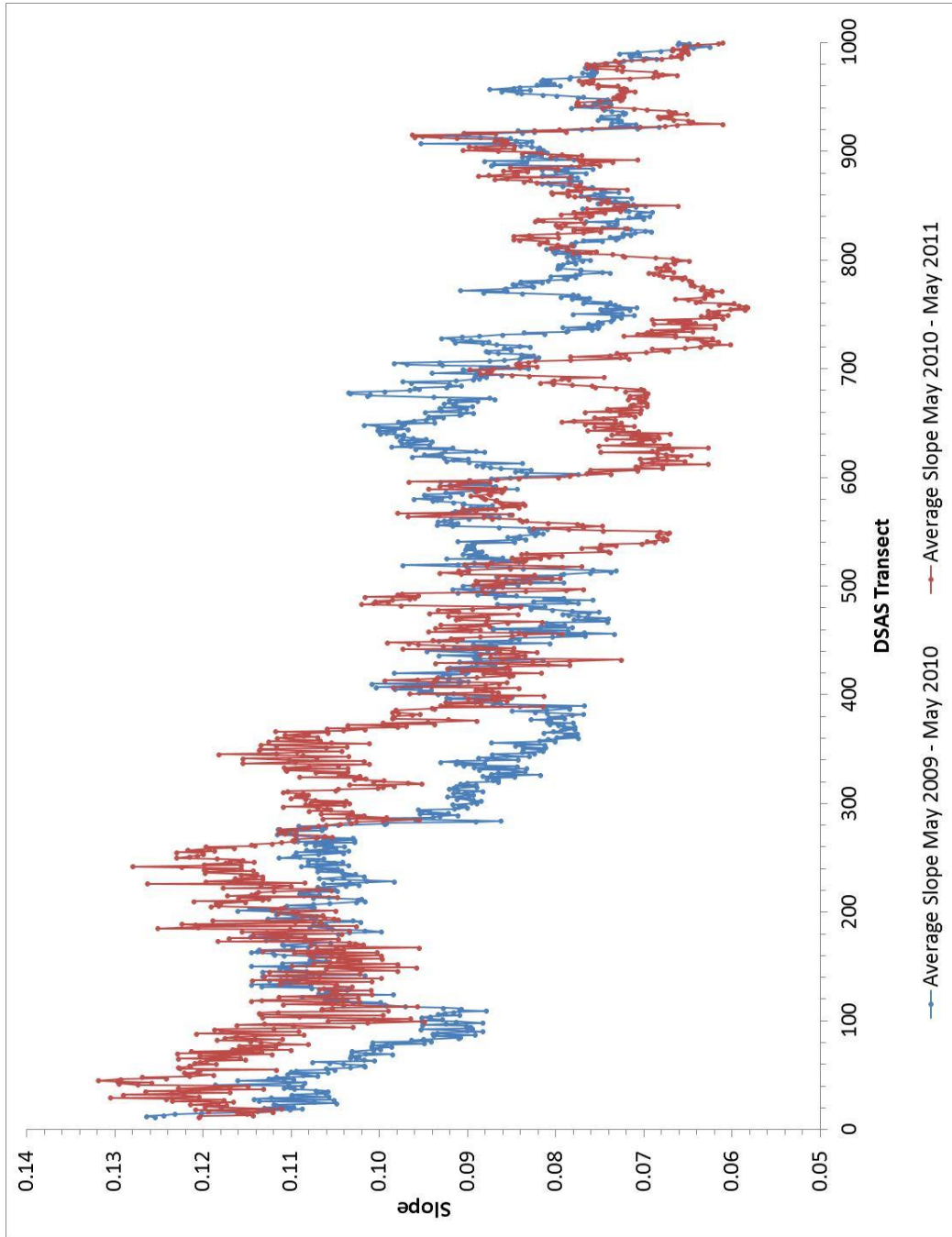


Figure 4-8. Average slope of the foreshore (0.25 m – 0.75 m contours) for surveys conducted from May 2009 through April 2010 and May 2010 through April 2011.

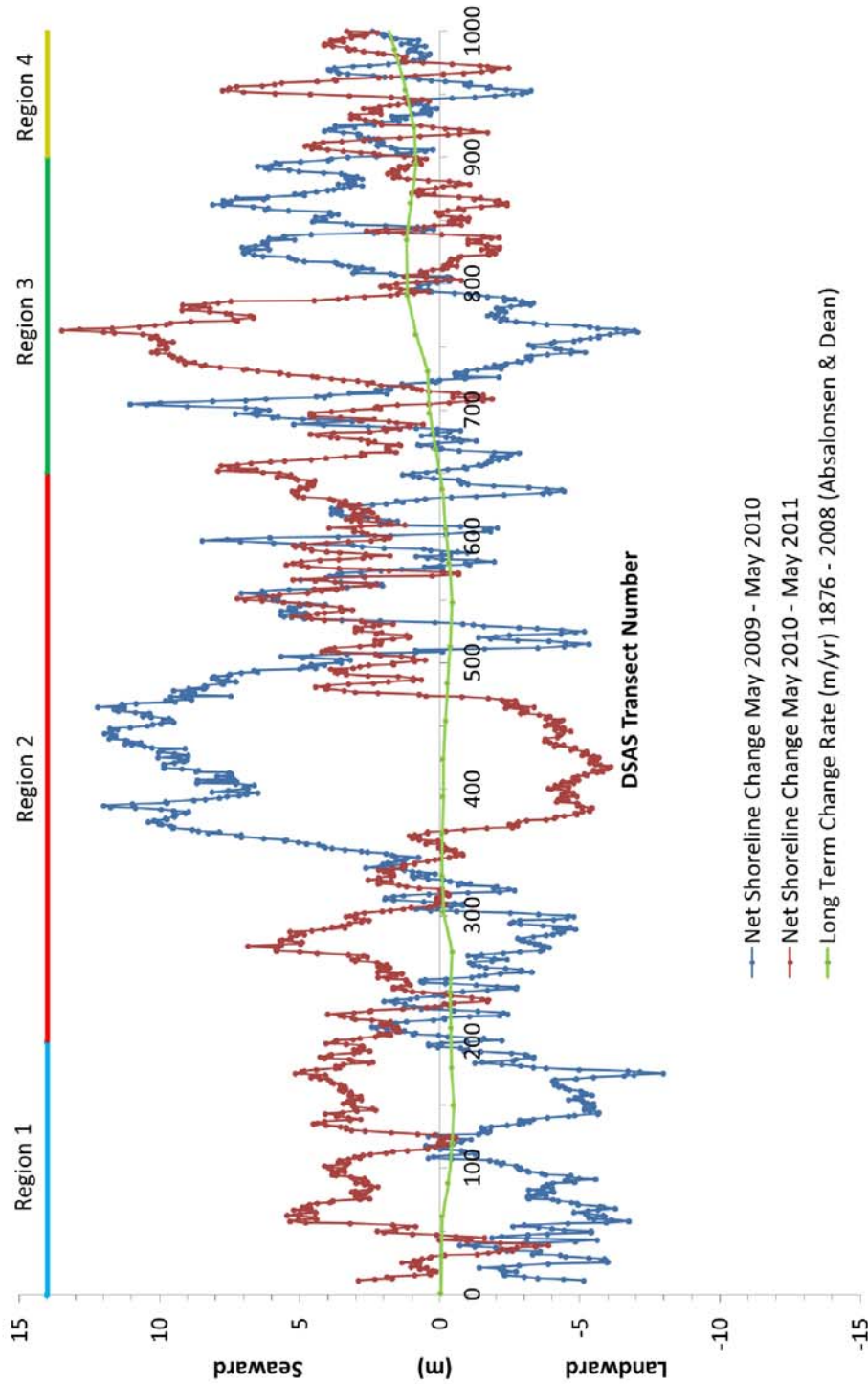


Figure 4-9. Annual shoreline change for the two survey periods of May 2009 – April 2010 and May 2010 – April 2011. Note that annual changes recorded for the two survey periods are an order of magnitude greater than the long-term (1876 – 2008) changes reported by Absalonsen & Dean (2010). Also note that there is increased variability in the annual shoreline change in Regions 2 and 3 and the entire region shows consistent anti-phasing between survey periods. Different regions of the beach are indicated at the top of the figure (four-colored bar).

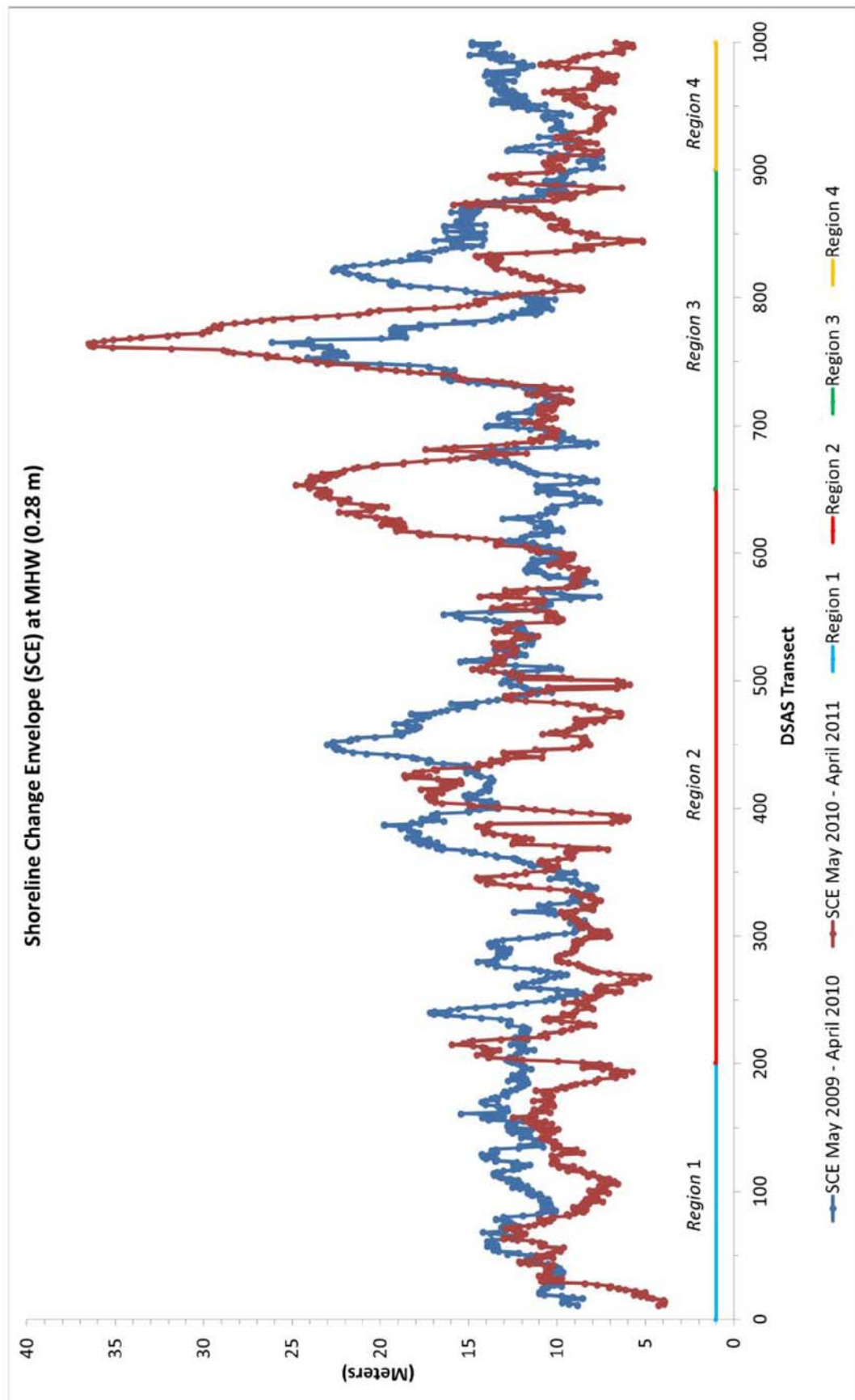


Figure 4-10. Comparison of the 2 year (May 2009 – April 2010 and May 2010 – April 2011) shoreline change envelope (SCE). Solid blue line indicates shoreline change envelope for May 2009 – April 2010. Solid red line indicates SCE for May 2010 – April 2011 for 31 individual surveys. Different regions of the beach are indicated at the top of the figure. DSAS transect location are provided for reference.

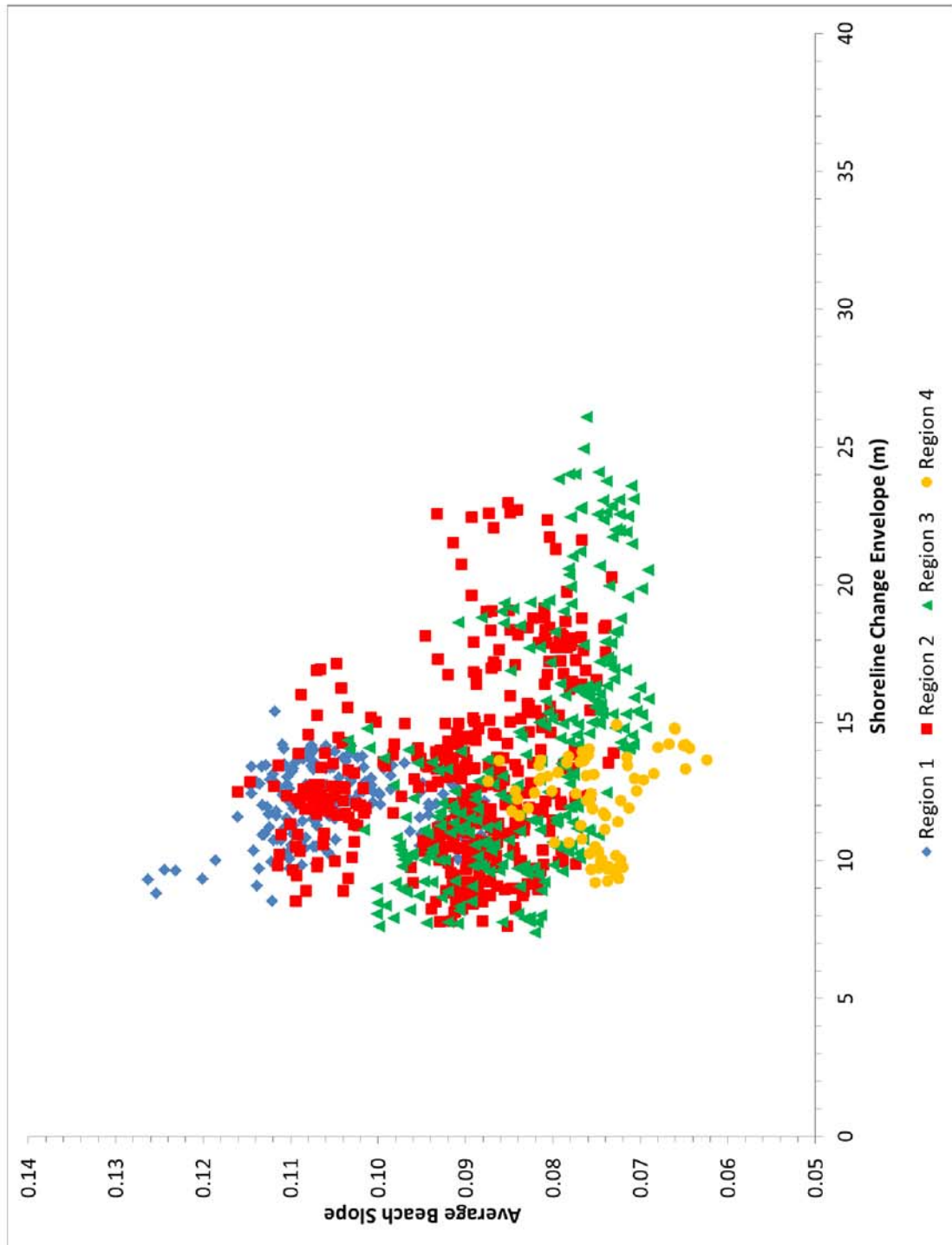


Figure 4-11. Comparison of the average beach slope and the SCE for the survey period May 2009 – April 2010. Note the increased variability in SCE in Regions 2 and 3 and that variability in SCE also increase as average beach slope decreases. SCE is greatest for Regions 2 and 3.

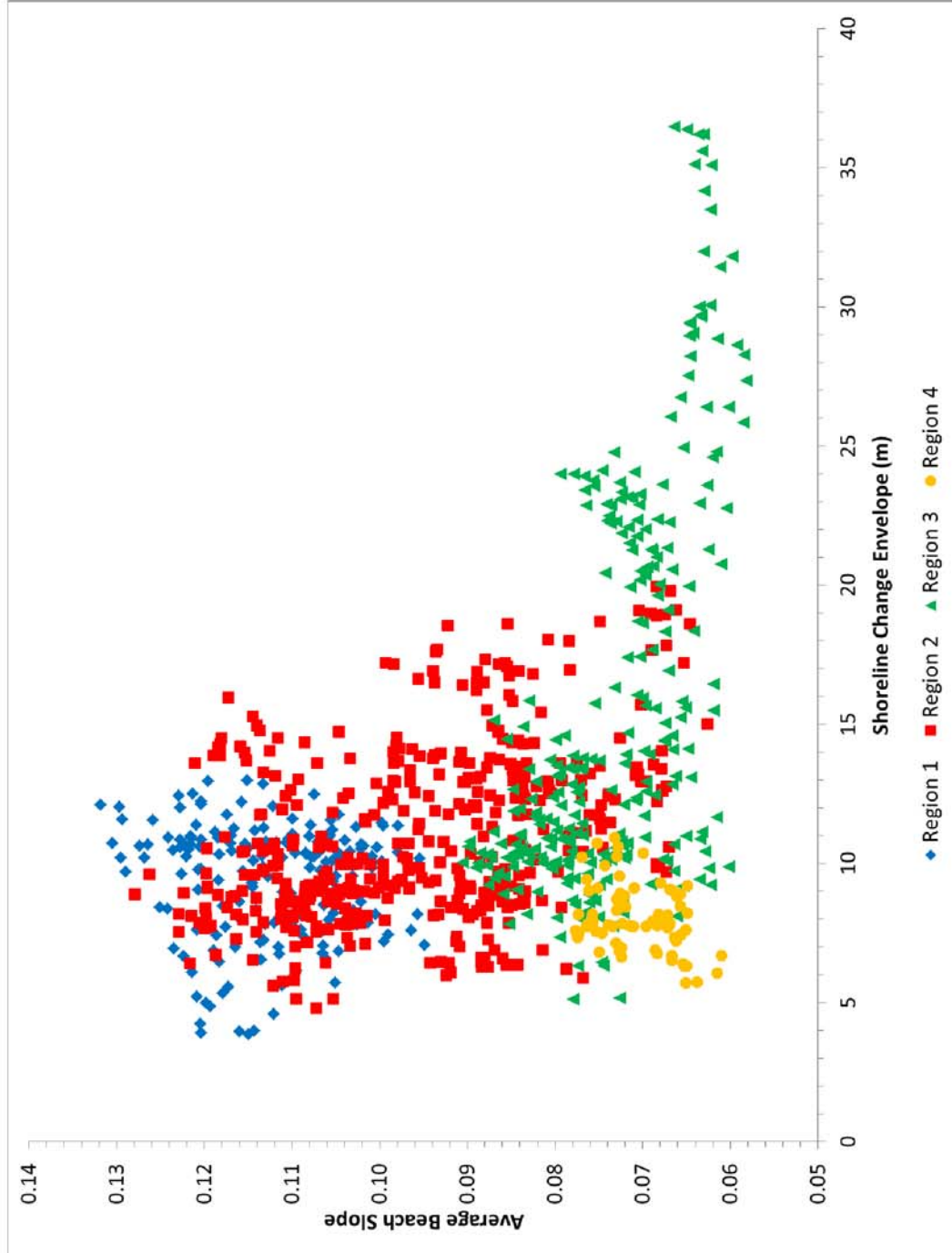


Figure 4-12. Comparison of the average beach slope and the SCE for the survey period May 2010 – April 2011. Note the increased variability in SCE in Regions 2 and 3 and that variability in SCE also increase as average beach slope decreases.

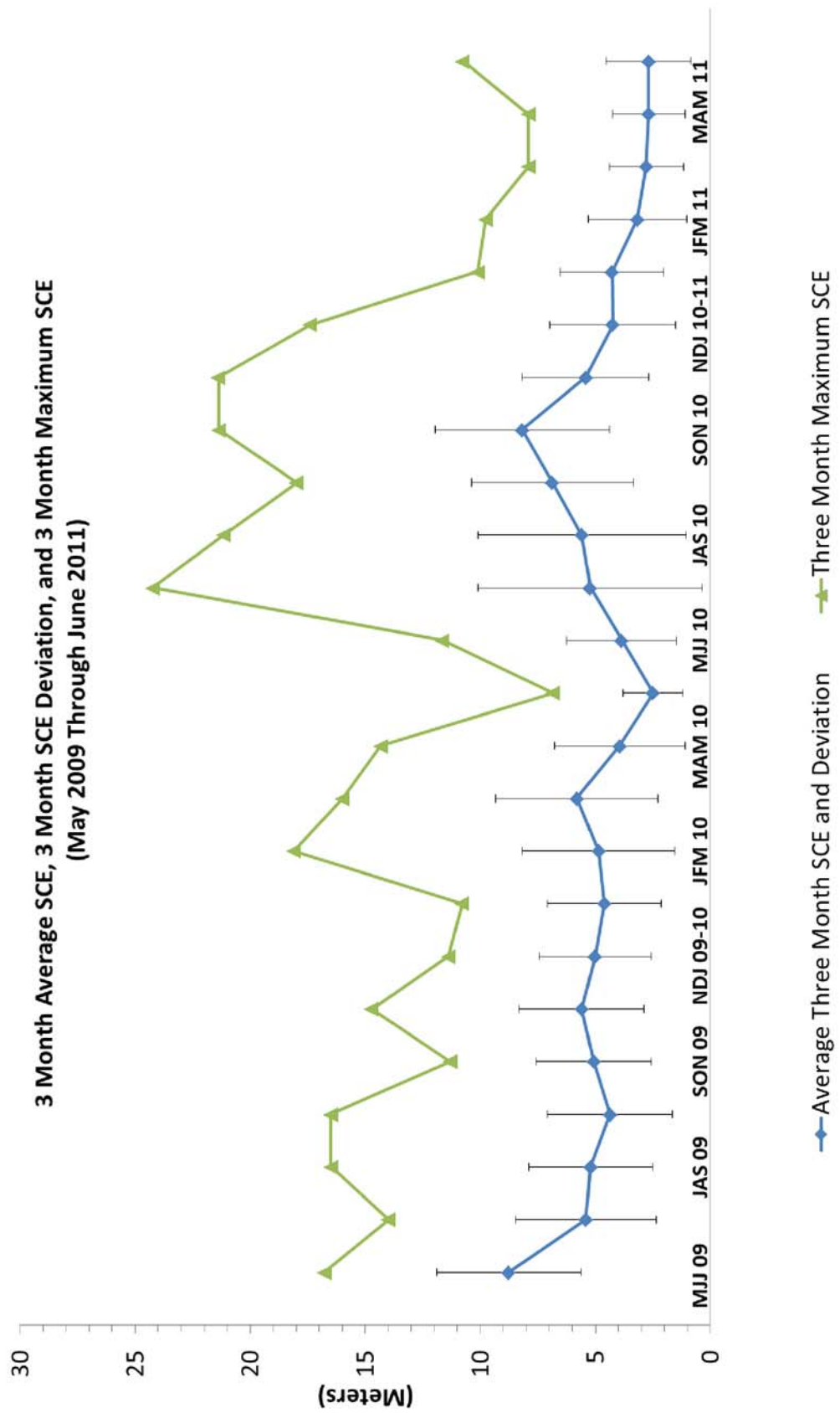


Figure 4-13. Three-month interval shoreline change envelopes (blue) with maximum individual transect SCE values (green). Black bars indicate deviation for all 1000 DSAS transects. Note that the three-month interval of April-May-June has the minimum values for SCE and deviation.

**Table 4-1. Table of survey dates**

<b>Survey Date</b>	<b>Full Moon Date</b>	<b>Survey Period</b>	<b>Notes</b>
May 6, 2009	May 9, 2009	1st	Begin First Survey Period
May 24, 2009		1st	Storm Response
May 28, 2009		1st	Storm Response
June 6, 2009	June 7, 2009	1st	
July 6, 2009	July 7, 2009	1st	
August 1, 2009	August 6, 2009	1st	
September 5, 2009	September 4, 2009	1st	
October 5, 2009	October 4, 2009	1st	
November 6, 2009	November 2, 2009	1st	
December 1, 2009	December 2, 2009	1st	
January 3, 2010	December 31, 2009	1st	
January 31, 2010	January 30, 2010	1st	
February 28, 2010	February 28, 2010	1st	
March 27, 2010	March 30, 2010	1st	
May 2, 2010	April 28, 2010	1st	End First Survey Period
May 27, 2010	May 27, 2010	2nd	Begin Second Survey Period
July 2, 2010	June 26, 2010	2nd	
July 25, 2010	July 26, 2010	2nd	
July 28, 2010		2nd	Geoeye Image Capture
July 31, 2010		2nd	Geoeye Image Capture
August 28, 2010	August 24, 2010	2nd	
October 2, 2010	September 23, 2010	2nd	
October 3, 2010		2nd	Daily Change Test
October 9, 2010		2nd	Weekly Change Test
October 24, 2010	October 23, 2010	2nd	
November 20, 2010	November 21, 2010	2nd	
December 21, 2010	December 21, 2010	2nd	
January 24, 2011	January 19, 2011	2nd	
February 18, 2011	February 18, 2011	2nd	
March 19, 2011	March 19, 2011	2nd	
April 18, 2011	April 18, 2011	2nd	End Second Survey Period

**Table 4-2. Standard deviation of average significant wave height ( $H_s$ )**

Month	1988-2008 (m)	May 09-April 10 (m)	May 10-April 11 (m)
January	0.7	0.62	0.45
February	0.7	0.61	0.42
March	0.7	0.47	0.6
April	0.6	0.48	0.28
May	0.5	0.89	0.48
June	0.4	0.24	0.3
July	0.3	0.22	0.39
August	0.5	0.41	0.49
September	0.7	0.24	0.87
October	0.8	0.59	0.54
November	0.7	0.6	0.6
December	0.6	0.49	0.56
Annual	0.7	0.49	0.5

Table 4-3. Net change values for three-month intervals for May 2009 – June 2011.

Dates	Average Three-Month Net (m)	Average Three-Month SD (m)	Maximum Seaward Net (m)	Maximum Landward Net (m)
MJJ 09	-2.2	4.0	7.5	-13.7
JJA 09	1.0	4.4	13.5	-8.2
JAS 09	-4.1	3.3	3.4	-12.3
ASO 09	0.4	3.9	9.8	-15.1
SON 09	-2.1	3.5	7.3	-11.3
OND 09	-4.1	3.6	10.0	-14.7
NDJ 09-10	-2.8	3.8	9.3	-10.4
DJF 09-10	-1.6	4.2	8.5	-10.8
JFM 10	3.2	4.3	18.1	-7.4
FMA 10	4.5	4.4	16.0	-8.2
MAM 10	2.4	3.7	12.4	-7.1
AMJ 10	0.3	2.4	5.9	-6.8
MJJ 10	2.7	3.0	11.6	-5.8
JJA 10	3.5	5.8	24.2	-6.7
JAS 10	3.2	5.5	21.1	-7.7
ASO 10	-1.7	5.8	15.5	-18.0
SON 10	-4.8	3.9	9.0	-16.0
OND 10	-3.0	2.7	4.2	-13.6
NDJ 10-11	-1.3	3.9	7.7	-14.9
DJF 10-11	-0.2	3.8	10.1	-9.1
JFM 11	1.0	3.2	9.0	-8.5
FMA 11	1.3	2.6	7.6	-5.5
MAM 11	1.1	2.2	7.7	-4.8
AMJ 11	1.6	2.4	10.8	-3.8

Table 4-4. Shoreline change envelope values for three-month intervals for May 2009 – June 2011.

Dates	Three-Month Average SCE	Three-Month Average SCE SD	Three-Month Maximum SCE	Three-Month Minimum SCE
MJJ 09	8.8	3.1	16.8	1.5
JJA 09	5.4	3.1	14.0	0.3
JAS 09	5.2	2.7	16.5	0.3
ASO 09	4.4	2.7	16.5	0.3
SON 09	5.1	2.5	11.3	0.0
OND 09	5.6	2.7	14.7	0.3
NDJ 09-10	5.0	2.4	11.4	0.0
DJF 09-10	4.6	2.5	10.8	0.2
JFM 10	4.9	3.3	18.1	0.0
FMA 10	5.8	3.5	16.0	0.3
MAM 10	3.9	2.8	14.3	0.1
AMJ 10	2.5	1.3	6.8	0.1
MJJ 10	3.9	2.4	11.6	0.1
JJA 10	5.2	4.9	24.2	0.2
JAS 10	5.6	4.5	21.1	0.2
ASO 10	6.9	3.5	18.0	0.0
SON 10	8.2	3.8	21.4	1.1
OND 10	5.4	2.8	21.4	0.3
NDJ 10-11	4.2	2.7	17.4	0.0
DJF 10-11	4.3	2.3	10.1	0.1
JFM 11	3.2	2.1	9.8	0.0
FMA 11	2.8	1.6	7.9	0.1
MAM 11	2.7	1.6	7.9	0.1
AMJ 11	2.7	1.8	10.8	0.2

CHAPTER 5  
IMPROVEMENTS OF VISUALLY BASED SHORELINE (VBSL) ACCURACY FROM  
SIMULTANEOUS SATELLITE IMAGERY COLLECTION AND DIFFERENTIAL RTK-  
GPS SURVEYS: CAPE CANAVERAL, FLORIDA

**5.1 Introduction**

As climate change and sea level rise play an increasingly important role in coastal science and management, scientists and managers have begun to rely heavily on surveying techniques such as LIDAR (Robertson et al., 2004; Sallenger et al., 2003; Stockdon et al., 2002) and RTK-GPS (Barnard et al., 2009; Barnard et al., 2007; Dornbusch, 2010; Hansen and Barnard, 2010; Huang, 2002; List and Farris, 1999; Ruggiero et al., 2005) to document shoreline change. LIDAR has rapidly become the preferred tool for coastal studies, with its high data density, ability to survey 100s of kilometers of coast (Sallenger et al., 2003; Stockdon et al., 2002) and moderate vertical accuracy (~30 cm) (NOAA1, 2011). LIDAR datasets are available for most of the continental U.S. coast beginning in 1997, with a typical sampling frequency of ~5 years (NOAA1, 2011). RTK-GPS surveys are another technique used to produce DBSLs. These surveys have a higher vertical accuracy (~10 cm) than LIDAR (see Chapter 3) and may be conducted at more frequent intervals than LIDAR. RTK-GPS surveys, however, have a lower data density than LIDAR and the effective length of the coastline studied is less than that of LIDAR. These techniques provide relatively high-precision, high-spatial-resolution elevation data that can be interrogated to produce datum-based shorelines (DBSL) (e.g., mean high water, MHW) (Barnard et al., 2007; Dail et al., 2000; Hansen and Barnard, 2010; Ruggiero et al., 2005). Using these techniques reduces the relative uncertainty in establishing shoreline position, allowing for better documentation of the actual trajectory of shoreline change.

Although GPS/LIDAR-based surveying can provide shoreline positions with reduced uncertainty, they only have been used for the past two decades, which limits the temporal coverage of shoreline data. This results in shoreline trend analyses that use only a few points, which creates a different class of uncertainty. To overcome this temporal data paucity, decades of remotely sensed imagery and even older survey data (NOAA t-sheets) are available for many shorelines. Remotely sensed imagery has been primarily used to produce VBSLs because of its historical significance, with images available from the 1940s onward. A benefit of using VBSL techniques for shoreline change analysis is the availability of remotely sensed imagery covering many decades coupled with a higher sampling frequency, which provides an opportunity to gain insight into geomorphic evolution and system dynamics that may be difficult to extract from DBSL survey methods alone. In many cases, however, use of remote-sensing techniques (e.g. aerial and satellite imagery) to establish historical shoreline positions has been deemphasized, in part because of higher uncertainties and difficulty in relating visual based shoreline proxies to DBSL (Adams et al., 2007; Boak and Turner, 2005; Moore et al., 2006a; Ruggiero et al., 2003; Ruggiero and Lists, 2009). Whereas DBSL-generating techniques such as LIDAR or RTK-GPS can produce shorelines at several different datums such as Mean High Water (MHW), Mean Low Water (MLW) and Mean Sea Level (MSL), VBSL proxies such as the “wet/dry” line are subjectively assigned and may or may not relate well to these datums. This is a consequence, in part, of different visual based shoreline (VBS) measures (e.g. vegetation line, debris line, high water mark, wet/dry line, low water mark) not being visible on all beaches at all times. Also, creation of these visual measures (e.g. high-water mark) on the beach is dependent on

the relative wave climate, tidal range, and beach morphology, which vary in space and time (Boak and Turner, 2005; Crowell et al., 1991; Douglas et al., 1998; Moore, 2000; Ruggiero et al., 2003; Ruggiero and Lists, 2009). To relate VBSL and DBSL, an offset correction (bias) has been developed that allows for translation of VBSLs to DBSL positions and has been applied to a wide range of beach morphologies (slopes from 0.01 to 0.25), significant wave heights (0.75 to 2.5 m), and deep-water wave periods of 10-14 sec (Moore et al., 2006a; Ruggiero and Lists, 2009). By evaluating the direct relationship between VBSL and DBSL for a particular beach, it may be possible to choose a VBSL measure that best matches the position of a DBSL, thus negating the need to apply an offset correction.

To examine the relationship between a VBSL and DBSL, I tested the approach of Ruggerio and List (2009) at the Kennedy Space Center shoreline, Cape Canaveral, Florida. This shoreline has beach and wave characteristics that fall within the range used in previous bias studies, making it a reasonable test area. A benefit of working at KSC is that it is closed to the public, making preservation and identification of visual shoreline measures easier than where the sand surface is reworked by beachgoers. DBSL and VBSL shorelines were compared using two Geoeye I (0.5 m resolution) satellite images, one collected three days post DBS survey (June 2010) and another concurrently with a DBS survey (July 2010). The months of June and July were selected because of the stability in beach states and because they have the lowest average monthly significant wave height ( $H_s$ ) and least variability in  $H_s$ , providing the highest likelihood of minimal beach morphologic change during experiments. In the second experiment, the location of the HWL was traced in the field with RTK-GPS and

the bias correction of Ruggerio and List (2009) was applied to document the applicability of this approach at KSC. Knowledge of the beach geomorphology gathered from 32 prior RTK-GPS surveys was used to provide geomorphic guidance of placement of a VBSL (wet/dry line) that may result in a clearer relationship between DBSLs and a VBSL and may also minimize uncertainties in using VBSL methods along the Florida coastline.

## 5.2 Study Area

The beach at the John F. Kennedy Space Center is part of Cape Canaveral-Merritt Island sedimentary complex (Figure 5-1). The ~10 km coastline of the space center is bordered on the north by the Cape Canaveral National Seashore and on the south by the Cape Canaveral Air Force Station. The Cape Canaveral coast experiences a microtidal setting with a mean tidal range of 1.03 m and an average spring tidal range of 1.19 m (NOAA, 2011b). The beach along the KSC shoreline is classified as an intermediate beach following the classification scheme by Wright and Short (1984), although in the northern 1 km of the study area the beach tends toward a reflective end member and in the southern 3.5 km it tends toward a dissipative end member (Chapter 4). The nearshore zone is characterized by two bars throughout the year that migrate onshore and offshore as forcing conditions change (Kline et al., 2011). The offshore bathymetry is complex, exhibiting a series of transient oblique shoals and large cape-related shoals at False Cape and Cape Canaveral (Kline et al., 2011).

Based on long-term shoreline change rates (Absalonsen and Dean, 2010; Dean et al., 1998) and geomorphic characteristics (Chapter 4), the study area can be divided into four distinct zones (Figure 5-1). From north to south, Region 1 is the northernmost ~1.5 km of the study area and is characterized by long-term stability with a single dune

~4m in elevation (NAVD 88). This area also has the highest average foreshore slopes in the study area. The next ~5 km, Region 2, is characterized by a single, frequently overwashed dune and long-term net retreat. Foreshore slopes in this area are highly variable relative to similar slopes in the northern reach. Region 3 is at False Cape and is characterized by an aspect change in the coastline, with low dune ridge sets and proto-dunes. This area also has variable foreshore slopes, but is on average flatter than the area with historic retreat. This 2.5 km is also an area of net advance. Region 4, the southernmost 1 km of the study area is characterized by a series of low dunes, but is lacking proto-dunes. It is also characterized by historic long-term accretion, but severe retreat (~5.5 m/yr) during the recent period (1969-2008) (Fig. 4-4). Foreshore slopes in this region are on average as flat as False Cape, but with less spatial variability.

### **5.3 Delineating Shoreline Proxies and Uncertainty**

#### **5.3.1 Datum-Based Shoreline (DBSL) Proxies**

LIDAR has become the standard evaluation tool for shoreline change over the regional scale (Leatherman et al., 1997; Robertson et al., 2004; Sallenger et al., 2003; Stockdon et al., 2002), whereas RTK-GPS has become the tool of choice for higher-frequency kilometer-scale studies (Hansen and Barnard, 2010; Huang, 2002; List and Farris, 1999; List et al., 2006; Morton et al., 1993; Plant and Holman, 1997; Ruggiero et al., 2005; Ruggiero et al., 2003). Both methods can be used to develop elevation models from which datum-based shorelines can be extracted (Baganha Baptista et al., 2011; Barnard et al., 2009; Dornbusch, 2010; Hansen and Barnard, 2010; Ruggiero et al., 2005), or from which a datum-based shoreline can be extrapolated (List and Farris, 1999; List et al., 2006). The most common datum extracted from these methods is the MHW line, which is defined as the average tide gauge high water elevation over a

period of time, usually 19 years. The USGS has defined MHW elevations for the United States to have a common datum for comparison (Weber et al., 2005). The MHW calculated from tide gauge information is typically converted into a vertical datum such as NAVD88.

### **5.3.2 Visual Based Shoreline (VBSL) Proxies**

Boak and Turner (2005) provide a comprehensive and useful review of the VBSL definitions and detection. Several authors have defined dozens of examples of VBSLs (Boak and Turner, 2005), of which there can be multiples for any remotely sensed image, depending on wave conditions, water level, and beach state. Of the multitude of VBSLs, the most commonly used VBSL proxy is the high water line (HWL) (Anders and Byrnes, 1991; Boak and Turner, 2005; Crowell et al., 1991; Dolan et al., 1980; Hansen and Barnard, 2010; Morton, 1991; Ruggiero and Lists, 2009). The definition of the HWL varies from author to author and is often confused with or used synonymously with the wet/dry line. The most common definition of the HWL is the landward extent of the last high tide, and may be represented in imagery as a color or tonal contrast between wet sand and dry sand (Boak and Turner, 2005; Dolan and Hayden, 1983; Morton, 1979; Zhang et al., 2002). Historically, the HWL line was used to delineate the boundary between land and sea in National Oceanic Service (NOS) T-Sheet maps (Shalowitz, 1964). The T-Sheets provide historical information back to the late 1800s.

The wet/dry line may be considered a distinct VBSL. It represents a tonal contrast in images, reflecting the saturation state of the beach face at the time the image was taken. On a rising tide, it represents the average extent of wave run-up and on a falling tide, it represents the wetted beach face, but it may be seaward of the instantaneous

run-up limit (Boak and Turner, 2005). Additional tonal contrasts that mimic the wet-dry line may be a consequence of changes in sediment composition or grain size.

Figure 5-3, Panel 1 provides an example of multiple VBSLs found on a typical beach, as defined by Boak and Turner (2005). Figure 4-3, Panel 2 provides an example of the uncertainties involved in interpreting the same HWL VBSL. In an experiment involving tracing the same HWL along Assateague Island, MD, Moore, Ruggiero, and List (2006a) demonstrated that plan-view uncertainties among three independently traced HWLs were as high as 20 m and averaged ~5 m. Pajak and Leatherman (2002) note that the uncertainty in delineating a VBSL can be reduced with prior knowledge of beach morphology and the most likely position of the mean high water level on a beach face.

In addition to the multiple VBSL proxies on a coastline, there are other uncertainties associated with VBSLs. Rectification error results from placing an image or set of images into a map coordinate system and is related to the size of the image pixels and uncertainties from the digital elevation model (DEM) (Fletcher et al., 2003; Genz et al., 2007). An additional uncertainty with the use of a VBSL proxy is the shoreline change envelope (SCE) or the uncertainty associated with the annual change in shoreline position that stem from seasonal changes in forcing (see chapter 4) (Fletcher et al., 2003; Genz et al., 2007; Moore, 2000; Moore et al., 2006a; Romine et al., 2009). There is also error associated with digitization of a shoreline proxy, relating to the resolution of the image and the digitization tool (i.e. GIS program and computer screen size) and the scale of digitization (Genz et al., 2007; Moore, 2000; Moore et al.,

2006a). The errors associated with image uncertainties can be expressed by the following formula, after Fletcher et al. (2003) and Genz et al. (2007) (Formula 5-1).

**Formula 5-1**

$$U_t = \pm(Er^2 + Ed^2 + Ep^2 + Etd^2 + Es^2)^{1/2} \quad (1)$$

Where  $U_t$  is defined as the total uncertainty,  $Er$  is defined as the rectification error,  $Ed$  is defined as the digitizing error,  $Ep$  is defined as the error associated with pixel size,  $Etd$  is defined as the error associated with tidal fluctuations, and  $Es$  is the error associated with the annual change in shoreline position or SCE.

### **5.3.3 VBSL/DBSL Bias Corrections**

DBSLs such as MHW vary only with sediment transport gradients and the resulting morphological change, whereas VBSL such as the HWL vary with beach composition, beach slope, tide level, wave set-up, and swash run-up, therefore MHW datum-based shorelines have less uncertainty associated with them and have increased repeatability (Moore et al., 2006b; Ruggiero and Lists, 2009). Several studies have examined the relationship between these two approaches for estimating MHW and showed that the VBSL HWL is dominantly found shoreward of the DBSL MHW (Moore et al., 2006b; Morton and Miller, 2005; Ruggiero et al., 2003; Ruggiero and Lists, 2009). Moore, Ruggiero, and List (2006) indicate that the horizontal offset between VBSL HWL and DBSL MHW averaged 18.8 m over 40 km of coastline on Assateague Island, MD. This study also demonstrated a strong correlation between vertical offset and beach slope. Other studies showed similar results, with average horizontal offsets ranging from 8 to 49 m (Moore et al., 2006a; Morton and Speed, 1998; Pajak and Leatherman, 2002; Ruggiero et al., 2003; Ruggiero and Lists, 2009). These offsets are thought to be a function of differences in water level, i.e. tidal water level, wave set-up, and swash run-

up (Moore et al., 2006a; Ruggiero et al., 2003; Ruggiero and Lists, 2009). Moore, Ruggiero, and List (2006) and Ruggiero and List (2009) developed numerical relationships to predict the horizontal offset between the visual HWL and MHW datum using the foreshore beach slope, the deep-water wave height, and the deep-water wavelength. Ruggiero and List (2009), and Moore, Ruggiero, and List (2006a) demonstrated that the high water VBSL and MHW DBSL bias on beaches with a slope greater than  $\sim 0.05$  is sensitive to variations in wave height and period, whereas the bias on beaches with a slope  $<\sim 0.05$  is more sensitive to the slope of the beach. This indicates that on beaches with slopes  $<0.05$ , an average slope calculated from minimal data produces more uncertainty than on steeper beaches, whereas on beaches with a slope  $>0.05$ , use of average wave and water levels produces greater uncertainty.

Although some studies have concluded that the horizontal offsets may be a small source of error (Moore, Ruggerio, and List, 2006), these offsets become more critical to calculating shoreline change rates as the slope of the foreshore decreases and the time interval between shoreline observations decrease. Recent work by Ruggiero and List (2009) using previous work by Hapke et al. (2006) and Hapke, Reid, and Richmond (2009) on the California coast, provided evidence of the importance of bias correction when using VBSL proxies. The authors found that with uncorrected bias, using a mix of HWL VBSL and MHW DBSL, only 1 of 15 analysis regions was retreating over the long term ( $\sim 117$  years), whereas after correcting for bias, 9 of 15 analysis regions showed long-term retreat. As shoreline position estimates and shoreline change rates using DBSL proxies are increasingly derived from LIDAR and RTK-GPS studies, testing methods to reduce uncertainties involved in VBSL proxies becomes more critical,

especially if imagery-based VBSL proxies are used to bridge the gap between longer-interval DBSL studies.

## 5.4 Methods

### 5.4.1 Remotely Sensed Image Capture and Analysis

Collection of remotely sensed and RTK-GPS survey data was coordinated with GeoEye Inc., Herndon, VA. GeoEye operates both the Ikonos satellite (1 m resolution) and the GeoEye I satellite (0.5-m resolution) (GeoEye, 2011). During the first experiment, a remotely sensed image was captured on 6 June 2009 using the Ikonos satellite and a RTK-GPS survey was conducted on 9 June 2009. Images were not collected concurrently because of a retaking of the Geoeye I satellite for national security reasons. During the second experiment, concurrent image capture by the GeoEye I satellite and RTK-GPS surveys was conducted on 28 July 2011. Both the Ikonos and Geoeye I satellites captured four bands; red, blue, green, and near-infrared. These image bands were provided in separate files and were “stacked” using ERDAS Imagine software into a 4-band composite imagine (.img) file. Remotely sensed image files were provided with coarse ortho-rectification (within 4 m). Further ortho-rectification was accomplished with a master image of the Kennedy Space Center and Cape Canaveral Air Force Station, surveyed to 95% confidence to 0.25 m. Ortho-rectification was done on each image using a minimum of 25 additional rectification points, and a simple first order polynomial correction. Each image was then tested with at least 20 additional test points selected along the coast and at easily recognized image locations. The corrected Geoeye I image test points were compared to the test point locations from the February 2007 image, with all test points fitting into a circle with a 1.5 m radius. The across-shore positions of VBSLs (HWL, wet/dry line) were traced at a scale of

1:1000 from the imagery in ArcGIS 9.3 at alongshore transects spaced at 10-m intervals along the 10 km study area.

#### **5.4.2 RTK-GPS Surveys**

A detailed description of GPS data collection, data processing, naming conventions, and the determination of accuracy and precision of RTK-GPS measurements can be found in Chapter 3 of this dissertation. Two surveys were conducted in association with remotely sensed image capture and an additional 32 surveys were conducted as part of a larger study of shoreline change at KSC. The monthly and event (storm) surveys provide a larger spatial and temporal context in which to guide placement of visual-based proxies. Surveys were conducted using two RTK-GPS antennas, with a distance of 2.25 m between them, towed behind an ATV on a trailer. Surveys were conducted on all beach slope breaks with a slope break defined as anywhere the across-shore slope breaks or changes noticeably. In instances of a concave-up beach profile with limited slope breaks, the beach was surveyed at equal across-shore distances (Figure 5-6). Landward survey bounds were defined by the vegetation line and seaward survey bounds were determined by the furthest seaward measurement that could safely be made with the prevailing tide and wave conditions. Alongshore, dual-antenna GPS passes (up the 10 km study reach and back) varied from two to four passes, producing 8 to 16 individual lines. During each pass, one wheel was towed along a specific slope break or minimum/maximum line. An example of a slope-break min/max survey pass position followed this order: vegetation line, berm overwash trough, berm crest, center of foreshore slope, beach toe and furthest seaward exposure of sub-aerial beach that could be surveyed safely (Figure 5-6).

RTK-GPS elevation points were used to generate a geomorphic surface using a Triangulated Irregular Network (TIN) in ArcGIS. Individual TINs were converted to a raster with 1 m<sup>2</sup> resolution. DBSLs were extracted at the local mean high water (MHW) datum for the beach, as defined by Morton and Miller (2005), at 0.28 m NAVD88 along the central Florida coastline. The high water line (HWL) VBSL from the previous high tide was traced in the field by the UTV during the RTK-GPS survey on 28 July 2010.

#### **5.4.3 HW Geomorphology**

To establish the offset between HW VBSL and the MHW DBSL, the conditions and time of formation of the HWL had to be identified, and the HW line had to be traced during the RTK-GPS survey conducted on 28 July 2010. After observing the formation of the HWL, it was traced with the RTK-GPS system described above (Figure 5-8).

The Geoeye I remotely sensed image was captured at 11:01 EDT, approximately 1 hour and 10 minutes after conditions responsible for the formation of the HWL. This difference in time between the capture of the image and the conditions responsible for the deposition of the HW line had no observed effect. The HWL position in the Geoeye I image was then digitized at 10 m alongshore intervals at each DSAS transect (Figure 5-8, Panel 2).

A VBSL other than the HWL was digitized from the Geoeye I imagery using previous knowledge of the geomorphology of the beach from 32 RTK-GPS surveys and visual observations as a guide, along with the tonal contrast of a feature I believe to be related to groundwater or tidal water exfiltration. To use the beach morphology as a guide, the MHW DBSL was compared to the raster of each of the 32 RTK-GPS surveys conducted, and the location of the intersection of beach morphology with the MHW

DBSL was observed. This allows for placement of a geomorphically guided VBSL very near the MHW DBSL, as shown in Figure 5-8, Panel 3.

#### **5.4.4 Water Level, Wave Height, and Wave Length**

To establish the offset between HW VBSL and the MHW DBSL, the conditions and time of formation of the HWL had to be identified. Therefore, observations were taken during the RTK-GPS survey conducted on 28 July 2010 to determine the time of formation for the HWL. After the RTK-GPS survey, the wave and water level recorded at NOAA buoy 41010 and Trident Pier tide gauge were collected for the time of HW formation. *In situ* water level measurements from NOAA Tides & Currents (NOAA, 2011) were extracted for Trident Pier station 8721604, located ~20 km south of the study area (Figure 5-1). Deep-water significant wave heights ( $H_s$ ) and periods ( $T_0$ ) are required to calculate HW/MHW offsets. *In situ* wave statistics are provided by The National Data Buoy Center (NDBC) at half-hour intervals for significant wave height and dominant period (NDBC, 2011). Figure 5-1 shows the location of NDBC buoy 41010, which is located ~222 km due east of Cape Canaveral in 872.6 m of water. Wavelength was calculated using Airy wave theory (Formula 5-2) and dominant period after Stockdon et al. (2006):

Formula 5-2

$$L_o = (g/2\pi)T^2$$

where  $g$  is the acceleration of gravity ( $9.8 \text{ m/s}^2$ ) and  $T$  is the dominant wave period (s) corresponding to the value of  $H_o$  selected above, recorded at Buoy 41010.

#### **5.4.5 Slope**

DBSL/VBSL offsets have been shown to be sensitive to slope in the vicinity of MHW (Ruggiero and List, 2009). For this study, beach slope was defined as the

average slope between the 0.25 m and 0.75 m NAVD88 contours. These two elevation contours were observed in each RTK-GPS survey, and represented the slope of the foreshore near the HWM (Figure 5-5). Slopes were then calculated at the same 10-m alongshore intervals used for digitization during the concurrent survey image capture on 28 July 2010. Additionally, to test offset biases resulting from the use of average beach slopes rather than instantaneous slopes, average values from the two-year study period were calculated at the same 10-m intervals and then averaged into 1-km blocks as described in (Ruggiero and Lists, 2009). One-km intervals were used to remove biases associated with inter-annual morphologic features such as cusps, rip cell embayments, and sand waves that are common in this study area.

#### **5.4.6 DBSL MHW – VBSL HWL Offset Calculation**

The offset between the VBSL HW proxy and a DBSL MHW proxy was originally based on estimated water levels on the beach and validated by several field experiments (Moore et al., 2006a; Ruggiero et al., 2003). Stockdon et al. (2006) updated the empirical relationship for the extreme run-up that is thought to cause the HW line on beaches. Ruggiero and List (2009) combined these approaches and developed two formulas for HW/MHW offset corrections, one using the measured tidal water levels and a simplified version using the MHW level as an estimate for the water level responsible for the HW line. Because these equations are applied to image-based VBSLs, the VBSL digitized in the Geoeye I satellite image at 10-m intervals was used in the experiments, instead of the VBSL traced using RTK-GPS in the field.

In our experiment, the first method is used to explore the offset between the HW VBSL and MWH DBSL (Formula 5-3).

### Formula 5-3

HW/MHW Offset (with tidal correction and slope measured every 10 m) =

$$\left( \left[ Z_T + 1.1 \left\{ 0.35 \tan \beta (H_O L_O)^{\frac{1}{2}} + \frac{[H_O L_O (0.563 \tan \beta^2 + 0.004)]^{\frac{1}{2}}}{2} \right\} \right] - Z_{MHW} \right) / (\tan \beta)$$

where  $Z_T$  is the tidal or water level during the formation of the HW VBSL,  $Z_T$  was measured at the Trident Pier tide gauge located ~20 km south of the study area.  $\tan \beta$  is the foreshore beach slope measured between the 0.25 m and 0.75 m contours, calculated at 10-m intervals along the entire 10-km study area.  $H_O$  is the deep-water significant wave height measured at NOAA buoy 41010, the value for  $H_O$  was selected as the highest wave height that occurred 20 minutes before or after high tide.  $L_O$  is the deep-water wavelength for the selected significant wave height at NOAA buoy 41010, using equation 5-2.  $Z_{MHW}$  is the mean high water value for the study area of 0.28 m (Weber et al., 2005).

Method 2 was used to calculate the HW VBSL and MWH DBSL offset using the image-traced HW line, single average slope value ( $\beta = 0.089$ ; 2009-2010) and wave values recorded at NOAA Buoy 41009 on 28 July 2010 (Formula 5-4).

### Formula 5-4

HW/MHW Offset (with no tidal correction and general slope) =

$$\left[ 1.1 \left\{ 0.35 \tan \beta_{(ave)} (H_O L_O)^{\frac{1}{2}} + \frac{[H_O L_O (0.563 \tan \beta_{(ave})^2 + 0.004)]^{\frac{1}{2}}}{2} \right\} / \tan \beta_{(ave)} \right]$$

$\text{Tan } \beta_{(\text{ave})}$  was calculated with the method outlined in Ruggiero and List (2009), using the foreshore beach slopes for all 32 surveys, measured between the 0.25 m and 0.75 m contours and averaged at 10-m intervals along the entire 10-km study area. The 10 m averaged slopes were then averaged again at 1-km intervals as described in Ruggiero and List (2009) to provide the average slope for each of the ten 1-km sections of the study areas.

## 5.5 Results

### 5.5.1 Visual-Based Versus Datum-Based Shorelines

Thirty-five image sets are available for the Cape Canaveral study site from 1943 to 2011, which potentially could be used to conduct a decadal shoreline change study (Figure 5-4). To perform such a study, one or more appropriate VBSLs must be selected that can be identified in several remotely sensed image types. Figure 5-5 provides an example of the different imagery types in the collection of Cape Canaveral images. Figure 5-4 Panel 1 is a typical historical aerial black and white image, scanned from a positive plate. In this image, it is difficult to delineate the different VBSLs that are closely related to each HWL, i.e. old high tide, previous high tide, wet/dry, or storm line, although the wet/dry line is obvious. Figure 5-4, Panel 2 is an example of a false color infra-red aerial positive plate, scanned at a resolution comparable to 1.0-m pixel size. In this type of image, vegetation is easily identified by its red color, but again, it is difficult to find or relate similar HWL VBSLs. Finally, in Figure 5-4 Panel 3, a Geoeye I (0.5 m resolution) satellite image is shown, in which multiple VBSLs can be identified. Several color contrast lines could be identified as the HW line. In all the images, a vegetation line can clearly be discerned, along with a tonal contrast delineating a “wet/dry” line that may be related to wetting by wave run-up or groundwater exfiltration. Consequently, I

chose to use the wet-dry line as the feature most likely to be observed in all types of remotely sensed imagery.

Both the HWL and wet/dry VBSL were traced in the satellite imagery using the geomorphology of the beach as a guide to where each feature was likely to be found, as described in the methods section. As an example, it was observed that the MHW DBSL always intersected cuspatate features at their base, very near the tonal contrast, likely related to groundwater exfiltration or continuously wetted sand. Also, the MHW was found seaward of berms, where they are present. This allows for placement of a geomorphically guided VBSL very near the MHW DBSL, as shown in Figure 5-8 Panel 3.

### **5.5.2 DBSL Versus Wet/Dry VBSL**

During a concurrent and near-concurrent RTK-GPS survey, the uncorrected offset between the VBSL and DBSL was observed with the VBSL almost always landward of the MHW DBSL. During the nearly concurrent survey on June 6, 2009 and Geoeye I image capture on 9 June 2009, the VBSL offset was landward of the DBSL (Figure 5-10). The RMS error for all 1,000 10 m spaced cross-shore transects was 5.97 m, with a maximum offset of 13.43 m. During the concurrent RTK-GPS survey and Geoeye I image capture on 28 July 2010, the VBSL offset was both landward and seaward of the DBSL, with a majority of offsets landward of the DBSL (Figure 5-10). RMS offset was 3.57 m, with a maximum offset of 8.94 m (Figure 5-10).

### **5.5.3 DBSL Versus HW VBSL**

During the concurrent RTK-GPS survey and Geoeye I image collection, the HW line was surveyed using RTK-GPS and digitized on the Geoeye I image. Although an attempt was made to trace the same HW feature on the ground (RTK-GPS) and in the

imagery, there was an offset (Figure 5-11). The maximum landward offset of the Digitized HW VBSL, when compared to the RTK-GPS HW VBSL, was 12.39 m, whereas the maximum seaward offset of the digitized HW VBSL, compared to the RTK-GPS HW VBSL, was a maximum of 11.42 m. The RMS offset of the entire 10-km study area at 10 m intervals was 2.53 m.

#### **5.5.4 DBSL Versus HWL offsets**

The experiment to relate the traditional image-based digitized high-water line (HWL) with the MHW datum, via an offset correction, used the traced HWL (section 5.5.2) and corrected its position for the relative slope and wave/water level characteristics of the beach. HW VBSLs were corrected by the methods discussed in both Moore, Ruggiero, and List (2006a) and Ruggiero and List (2009), using both slope measured at 10-m intervals on the day of image collection and a median slope at 1 km intervals, calculated from all 32 surveys, water level, and wave conditions for the 10 km study area. Using the median slope for each 1 km section of the study area and the best estimate for water levels, the RMS offset was 4.51 m, with a maximum offset of 15.2 m (Figure 5-12). Using the measured water level and the wave conditions responsible for the formation of the HW VBSL and the beach slope measured at 10-m intervals, the RMS offset was 3.63 m, with a maximum offset of 18.6 m (Figure 5-12).

The highest water level, 0.164 m, was recorded on a rising tide at 09:36 AM EST at the tide gauge (Figure 5-7). Local meteorological conditions caused the highest water levels before estimated high tide. The nearest recorded measurement of significant wave height at the buoy that corresponded to the highest water was 0.69 m at 09:20 AM EDT. The dominant period recorded at the buoy at 09:20 EDT was 7.69 seconds. This

result was used to calculate the deep-water wavelength, using Equation 5-1. The image was captured on a falling tide, whereas predicted high tide occurred at 10:06 AM EDT

Ruggiero and List (2009) discussed the importance of foreshore beach slope on the offset between the HW VBSL and MHW DBSL as being inversely related to the slope of the beach, following Equation 5-3 after Moore, Ruggiero, and List (2006a). Ruggiero and List (2009) tested the sensitivity of the HW offset to the slope of the beach under several wave conditions and demonstrated that the offset is most pronounced where slopes are <0.05. The beaches in the study area exhibit a wide range of slopes, but average slopes calculated over a two-year interval at each 10-m alongshore transect were never <0.05, although several areas along the study area did have instantaneous (not temporally averaged) slopes that occasionally were less than the 0.05 threshold, including the experiment day in July 2010 (Figure 5-7). Spatially, the slope of the foreshore decreases from north to south along the 10 km of the KSC coastline. Over the initial two-year survey period, the average slope of the KSC foreshore was 0.089, with a deviation of 0.026. Region 1 had the highest average slope (0.109) and the highest deviation in slope (0.29) of the four distinct KSC coastal regions, whereas Region 4 had the lowest average slope (0.073) and deviation (0.018) (Figure 5-7 and Table 5-2). Reach 2 (area of greatest concern with regard to dune overwash and erosion) had a mixed range of slopes, with an average slope of 0.092 and a deviation of 0.027 (Figure 5-7 and Table 5-2). Slopes calculated during the image capture on 28 July 2010 ranged from 0.02 to 0.25. Unlike the average slope trend that generally flattens from the northern region of the study area to the south, the slopes calculated on 28 July 2010 are steepest and have the highest variability in Region 2

(Figure 5-7). The lowest slopes were found at the southern end of Region 2, in Region 3, and in Region 4 (Figure 5-7).

The offset between HW VBSL and MHW DBSL was calculated using both the measured and 1 km-median (Ruggiero and List, 2009) for beach slope, water level, and wave conditions at 1 km intervals for the 10-km study areas. The median beach slope was calculated as “best estimate” for beach slope using the median beach slope for all RTK-GPS surveys at 1 km intervals (Ruggiero and List, 2009). Using the measured water level and the wave conditions responsible for the formation of the HW VBSL, and the beach slope measured at each of the 10-m intervals on 28 July 2010, the RMS offset was 3.63 m, with a maximum offset of 18.6 m. Using the median slope for each 1 km section of the study area and the estimated water levels, the RMS offset was 4.51 m with a maximum single transect offset of 15.2 m.

Figures 5-13 through 5-18 illustrate the relationship between DBSL/VBSL offsets (both measured and estimated corrected HWL and wet-dry line) and beach slope in July 2010 divided into the different regions and morphologies of the beach. In general, DBSL/VBSL offsets increase as the slope of the beach becomes flatter. The same trend can be found in the variability of the offsets relative to the beach slope, i.e. the higher the slope, the less variability in DBSL/VBSL offset (both measured and estimated corrected HWL and wet-dry line). For the wet/dry VBSL, the offset may be landward or seaward of the DBSL, regardless of slope. For the HWL VBSL offset, higher slopes generally have a corrected VBSL offset landward of the DBSL, with the lower slopes having an offset seaward of the DBSL.

In Region 1, with a range of beach slopes from 0.18 to 0.07, the wet/dry-DBSL offset ranged from -7.0 to 2.1 m. For the HWL offset corrections using 10-m measured slope values, the offsets ranged from -2.9 to 2.3 m, and for the HW offsets using the best averages, the offset range was 11.8 m (-8.5 m to 3.3 m). Region 2 had the widest range of beach slopes (0.27 - 0.03), and the wet/dry-DBSL offset had a range of 11.6 m (-9.2 to 2.4 m). For the HWL offset correction using 10-m measured slope values, there was a 19.0-m range (-15.1 to 3.9 m), and for the HWL offsets using the best averages, the offset range was 18.1 m (-13.7 m to 4.4 m). For Region 3, with a relatively wide range of beach slopes (0.16 - 0.02), the wet/dry-DBSL offset range was 14.3 m (-9.5 to 4.8 m). For the HWL offset corrections using individual slope values, the offset ranged 16.0 m (-14.3 to 1.7 m), and for the HWL, offsets using the best averages ranged 23.8 m (-18.6 m to 5.2 m). Region 4 had the narrowest range of beach slopes (0.07 - 0.05), and the wet/dry-DBSL offset range was 3.0 m (-7.0 to -4.0 m). For the HWL offset correction using measured 10 m slope values, there was a 2.3 m range (-1.0 to 1.3 m), and for the HWL offsets using the best averages, the range was 3.5 m (2.4 m to 5.9 m).

#### **5.5.6 VBSL/DBSL Offset Versus Beach Morphology**

Figures 5-16 through 5-18 illustrate the relationship between beach slope and DBSL/VBSL offsets as a function of beach morphology. In the area of the beach dominated by complex cuspatate morphology (Figure 5-9), and a high range of beach slopes (0.02 – 0.21), there was a 14 m range of offsets between the wet/dry VBSL and MHW DBSL (-9.2 to 4.8 m). For the HWL offsets using measured 10 m slope values, the cuspatate areas of the beach had a 17.2 m range of offsets (-15.0 to 2.2 m), and for the HWL offsets, using the 1-km section median slope, the offset range was 23.2 m (-18.6 to 4.6 m). In the area of the beach with a simple concave-up beach and the lowest

range of beach slopes (0.04 – 0.12), the wet/dry VBSL and MHW DBSL offset ranged 11.8 m (-9.5 to 2.3 m). For the HWL offsets using 10 m measured slope values, the simple concave-up area had a 5.7 m range (-3.4 to 2.3 m), and for the HWL offsets using the 1 km section median slope values, the range was 10.3 m (-4.4 m to 5.9 m). In the area of the beach with a pronounced berm and a relatively wide range of slopes (0.05 - 0.27), the wet/dry VBSL and MHW DBSL offset ranged 8.4 m (-6.0 to 2.4 m). For the HWL offsets using 1 km-section median slope values, there was an 11.0 m range (-7.1 to 3.9 m), and for the HWL offsets using the 1 km section median slope values, the offset range was 11.8 m (-7.4 m to 4.4 m). In the areas of the beach with a less pronounced berm and a range of slopes between 0.06 to 0.22, the wet/dry VBSL and MHW DBSL offset had a 4.9 m range (-4.5 to 0.4 m). For the HWL offsets using 10-m measured slope values, there was a 6.3 m range (-2.9 to 3.4 m), and for the HWL offsets using the 1-km section median values, the range was 9.1 m (-5.5 m to 3.6 m).

## 5.6 Discussion

### 5.6.1 Offsets

Comparing the offset associated with the wet/dry VBSL and MHW DBSL during the concurrent image capture and RTK-GPS survey (28 July 2010) and the offset from the near-concurrent RTK-GPS survey and image capture (6 June and 9 June 2009), the concurrently collected VBSL and DBSL have less RMS than the RMS offset of the nearly concurrent data collection (5.97 m). The concurrently collected VBSL/DBSL offsets also had a much smaller maximum offset (8.94 m) when compared to the near concurrent VBSL/DBSL (13.43 m). This is attributed to an observed berm construction event that occurred between the image capture on 9 June 2009 and the RTK-GPS survey completed on 6 June 2009. Although an attempt was made to trace the HW

VBSL during the RTK-GPS survey that would be visible in the satellite image, there was still an RMS offset of >2.50 m over the 10 km study area, with maximum landward and seaward digitized RTK-GPS VBSLs of 12.39 and 11.42 m, respectively. This is further evidence of the difficulties using a HW-based VBSL. Just as Moore et al. (2006) demonstrated uncertainties in tracing the HW VBSL in the same image, this study shows that additional uncertainties occur when trying to compare ground-based and image-based HW VBSLs.

Region 1 (historically stable and higher slopes) and Region 4 (mixed historic record of accretion and retreat and lower slopes) have less VBSL/DBSL offset, whereas areas of greater change with low to mixed slopes have higher offsets. Complex beach morphologies such as cuspatate features have the highest range of VBSL/DBSL offsets, whereas those with simple concave morphologies have a smaller range of offsets and smaller total offset. The measured bias uncertainty between the MHW DBSL and the digitized HWL at Cape Canaveral was 10.03 m RMS, with a minimum offset of 2.99 m and a maximum offset of 23.94 m. These values are very similar to the values reported by Ruggerio and List (2009) for their experiment in California (averaged alongshore uncertainty of 8.7 m, with a minimum bias uncertainty of 4.9 m and a maximum of 28.3 m. This is in agreement with both studied beaches having >90% of the beach slopes >0.05. Ruggiero and List (2009) also showed that on beaches with slopes <0.05, there is much greater uncertainty. Their experiment on the Washington coasts, with fine-grained sediments and low slopes, had a mean observed bias of 30.6 m. In our study, only Region 3 had slopes <0.05, and this region had the highest HWL VSBL/MHW DBSL offsets.

Even after directly observing the conditions that resulted in the creation of the HWL, and having measured water level and wave data on the same day, the utility in using an offset for HWL is questioned, as the offsets between the wet/dry VBSL and the MHW are comparable to the calculated offsets of the HWL. Established methodology using visual HWL offsets is a viable means to correct VBSL/DBSL offsets at KSC, but the assumption of 1-km median beach slopes and estimated water levels increases DBSL/VBSL offset uncertainties. Our study demonstrated that slopes can vary by 0.5-2.0 times the average values on any single day (Figure 5-8). Although the beach slope averaged monthly over two years displays a somewhat linear trend throughout the study region, with higher slopes in the northern region and lower slopes in the southern region, the slope measured on a single day can be unrelated to the average trend if the beach is in a highly erosive or constructional phase, driven by short-term changes in wave energy. The use of median slopes at 1 km intervals is even more problematic in areas that have rhythmic topography (Figure 5-9).

When compared to the errors in Formula 5-1, the largest uncertainties related to either VBSL or DBSL position are related to the annual shoreline change envelope, with an uncertainty of ~15 m (see chapter 4). For historic imagery, the HWL VBSL has a bias or uncertainty of ~10 m RMS compared to a MHW DBSL. This bias offset can be corrected using the methods described in this chapter, with corrected uncertainties or bias of 3.63 m RMS for measured values and 4.51 m RMS for averaged values. Uncertainties associated with an uncorrected wet/dry VBSL, compared to a MHW DBSL, are ~5.00 m RMS. Uncertainties with the position of DBSLs extracted from LIDAR or RTK-GPS, average ~2.00 m. Georeferencing errors for Geoeye I imagery

averaged 1.12 m RMS for the two images used in this study. Digitizing errors for all imagery was ~0.50 using the methods described in this dissertation.

### **5.6.2 Simultaneous Image Capture and RTK-GPS Surveys**

Satellite imagery provides several benefits when coupled with RTK-GPS surveys. Several satellites have been launched that now provide a resolution of 0.5-1.0 m, required for coastal change studies. These satellites have a return interval of about three days and capture an effectively instantaneous field of view of several 10s of km, depending on offset angles, providing precise timing of image capture and ability to monitor event-scale change and recovery. Satellite image collection times can be coordinated with satellite providers to maximize coastal collection strategies relating to optimal seasonal atmospheric and tidal conditions.

Whereas a RTK-GPS survey enables direct comparison of how different datums and beach morphology relate, the addition of a simultaneously collected image provides a direct comparison between DBSLs and VBSLs. Understanding how DBSLs are related to beach morphology allows for the use of beach morphology as a guide for VBSL placement. In the case of the study area, the tonal change identified as a wet/dry visual feature had minimal RMS offset relative to the MHW DBSL. By knowing that the MWH datum was most often seaward of berms and cusps, the choice of which tonal feature to trace is reduced when looking for this feature. This reduces the uncertainties between VBSLs and DBSLs, thus minimizing DBSL/VBSL offsets. This information can then be used to select a VBSL or a geomorphic VBSL placement guide that best relates to a desired datum. This DBSL/VBSL correlation may also apply to micro-meso tidal sandy coastlines (e.g., U.S. East Coast). Although this visual feature appears to be persistent at KSC in across-shore locations and has been found in all images, its

relationship to actual wetting mechanisms (e.g. groundwater seepage) is an area for further investigation.

## **5.7 Conclusions**

High-resolution satellite imagery, with its large field of view and instantaneous collection capability, coupled with its high return rate and ease of scheduling, makes this type of data collection beneficial for large areas of the coast, especially between other DBSL data collection activities such as LIDAR. Geomorphically guided siting of the wet/dry VBSL performs as well as or better than a HW VBSL, when average slope and water levels are used to generate it. VBSL offsets are potentially higher in areas with lower slopes, complex morphology, or in regions of higher variability. When uncertainties related to differences in VBSL and DBSL are minimized, historic imagery and satellite imagery can be used to fill temporal gaps from less frequently collected DBSL techniques.

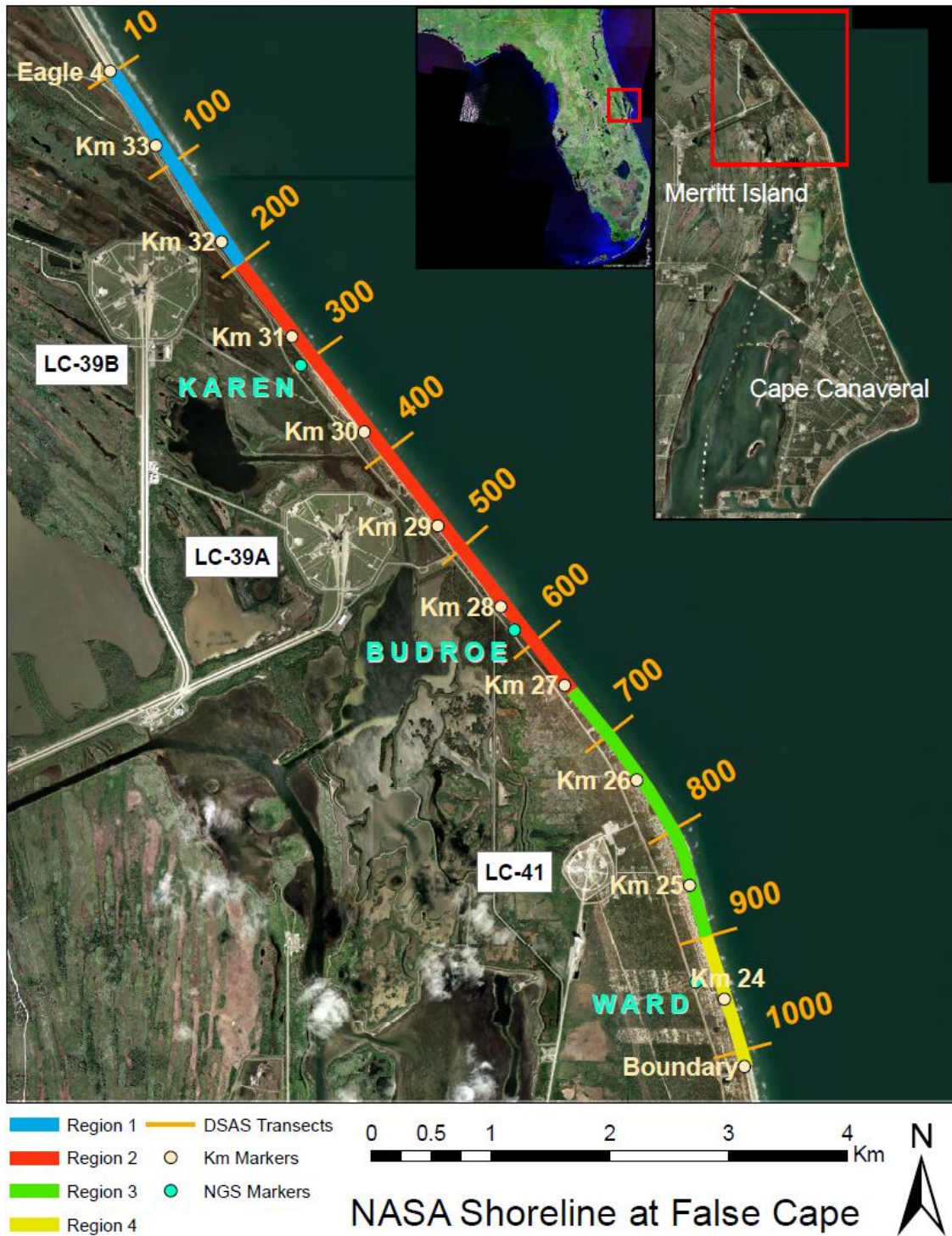


Figure 5-1. NASA coastal property at Kennedy Space Center consists of Merritt Island Capes. Four sub-regions along the KSC shoreline were established by geomorphology, historic change, and two years of monthly RTK-GPS surveys of slope, change envelope and shoreline travel path distance.

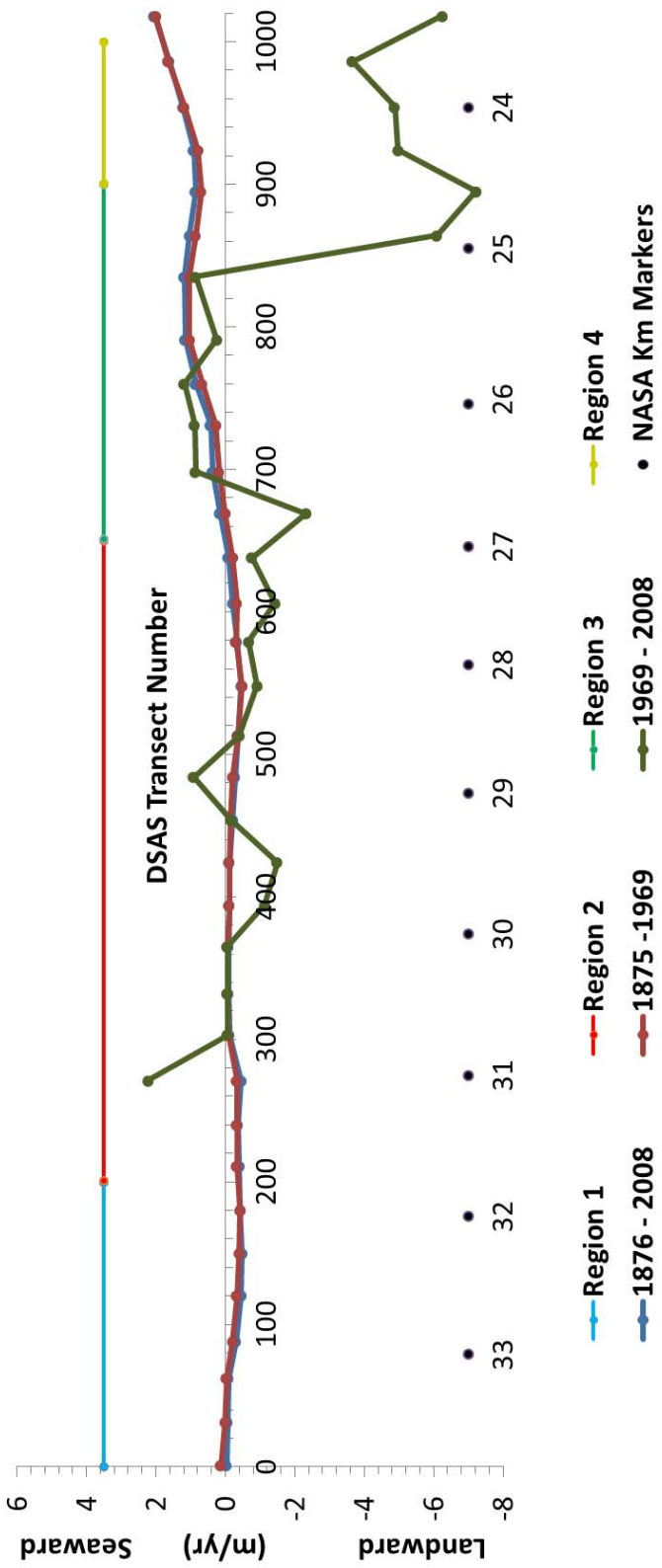


Figure 5-2. Historic shoreline change rates derived from Florida DEP across shore surveys at 1,000 ft intervals, after Absalonsen and Dean (2010). NASA km locations provided as reference. Note the higher magnitude and spatial variability in modern (1969-2008) change rates versus long-term (1875-2008) change rates.

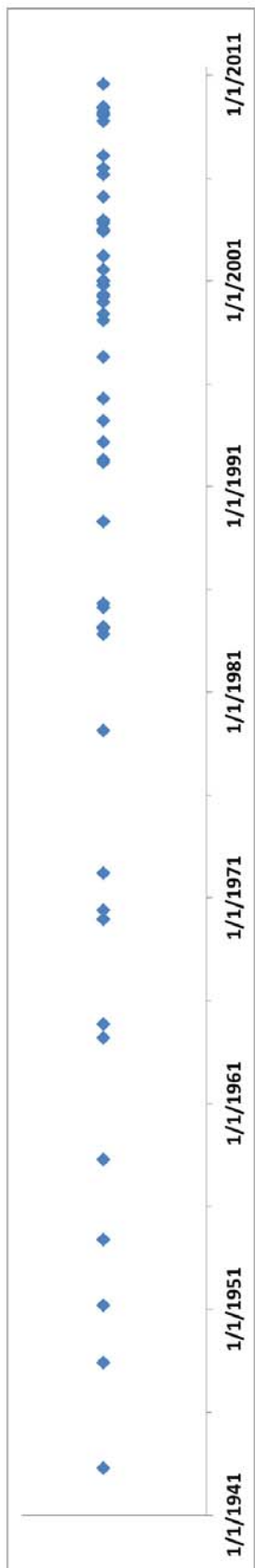


Figure 5-3. Historic and modern aerial and satellite imagery available for use in decadal-scale coastal change studies at the Kennedy Space Center, Cape Canaveral, Florida.

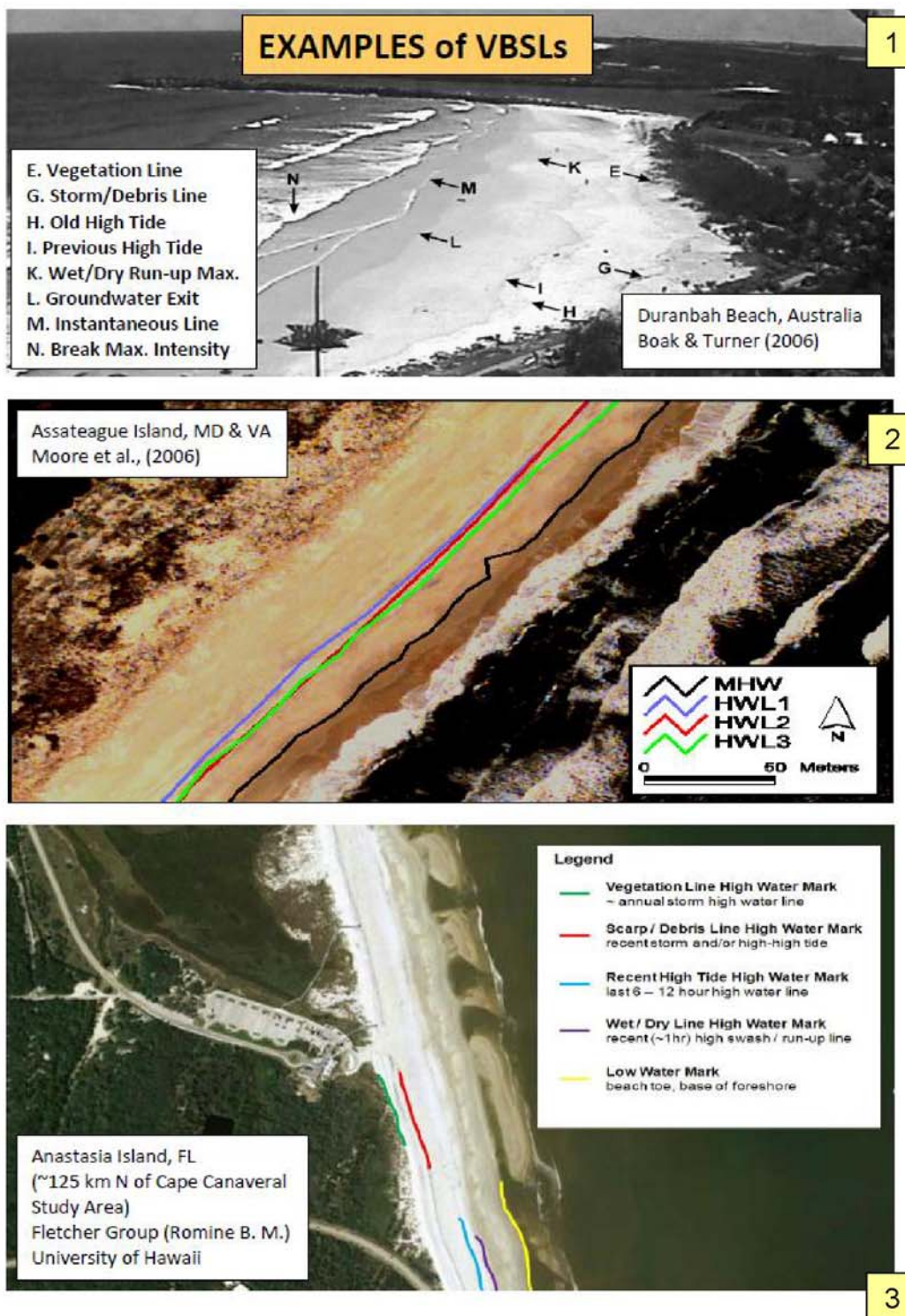


Figure 5-4. Examples of visual based shorelines (VBSLs) from previous studies. Panel 1 are VBSLs defined by Boak and Turner (2006) at Duranbah Beach, Australia, Panel 2 HW VBSL study conducted by Moore et al. (2006) at Assateague Island, Maryland and Virginia. Panel 3 preliminary VBSLs at Anastasia Island, FL from the Fletcher Group (UHI).

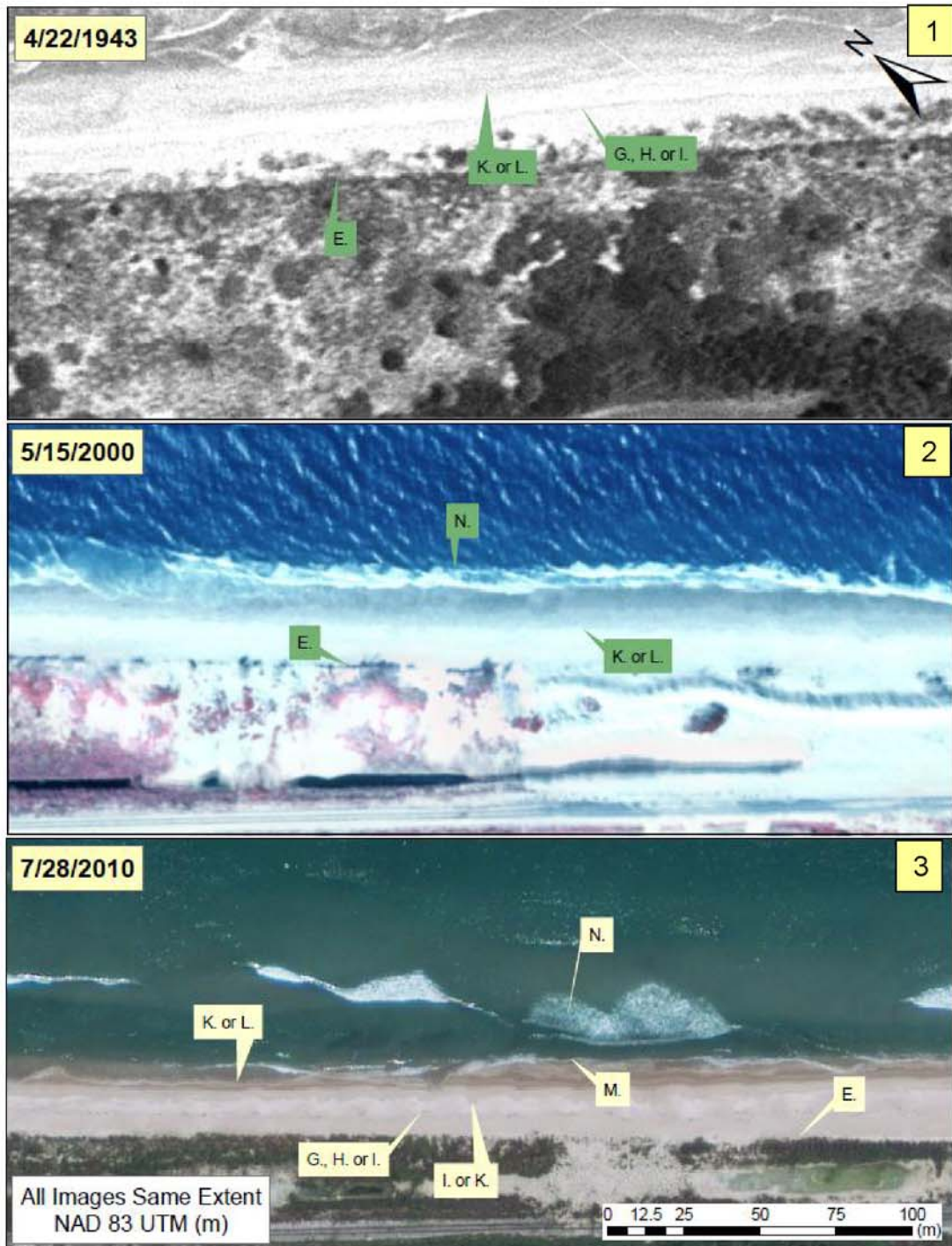


Figure 5-5. VBSLs visible in different types of imagery from the Kennedy Space Center, Cape Canaveral, Florida. Panel 1: VBSLs identified in a black and white aerial photograph. Panel 2: VBSLs identified in a false color infrared aerial photograph. Panel 3: VBSLs identified in a multi-band satellite image.

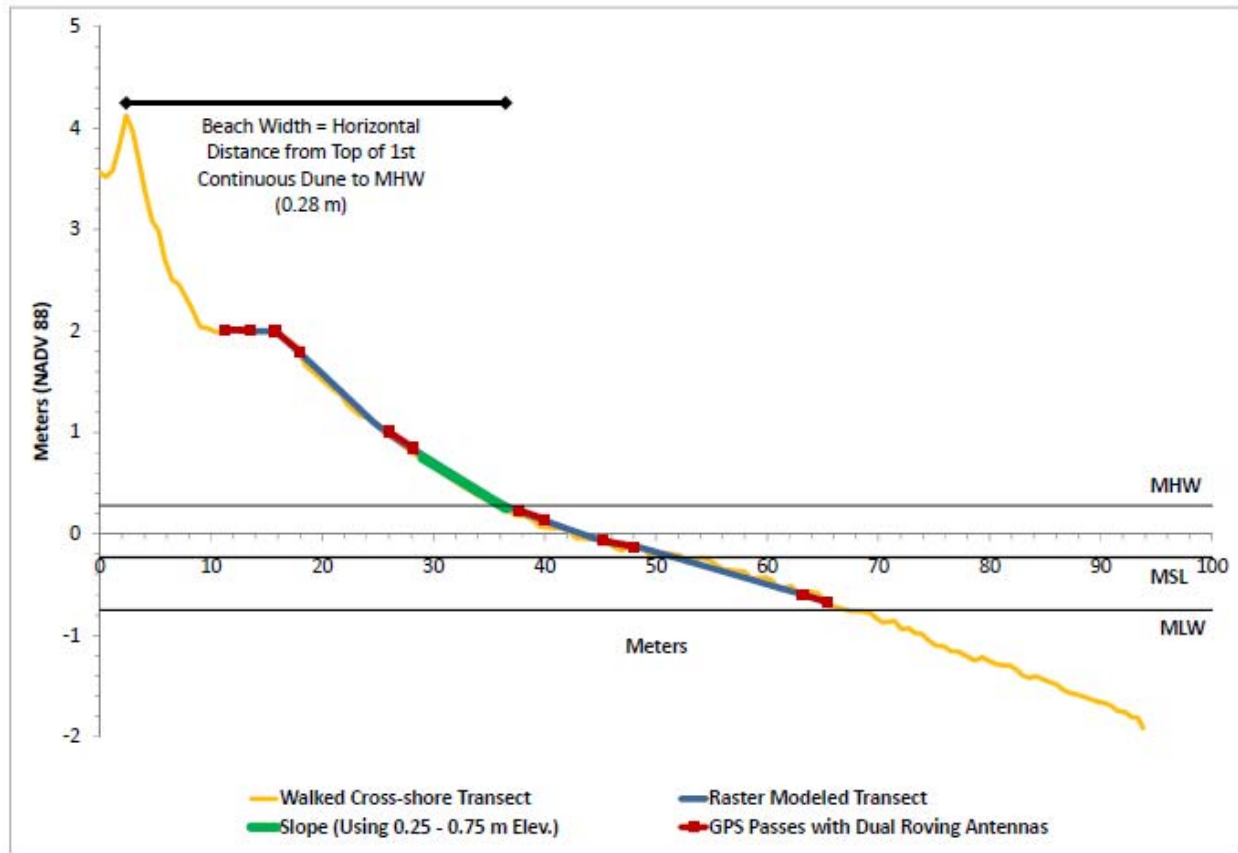


Figure 5-6. Tidal datum for Cape Canaveral MHW 0.28 m, MSL -0.23 m and MLW -0.68 m. Red segments represent the two measurements taken by the GPS trailer at each slope break. The blue line indicates the across shore profile generated from the GPS measurements modeled with a TIN converted to a raster. Orange line indicates a walked across shore profile transect measured from the base of the first continuous dune out to wading depth. Slopes were measured between the 0.75 m and 0.25 m contours.

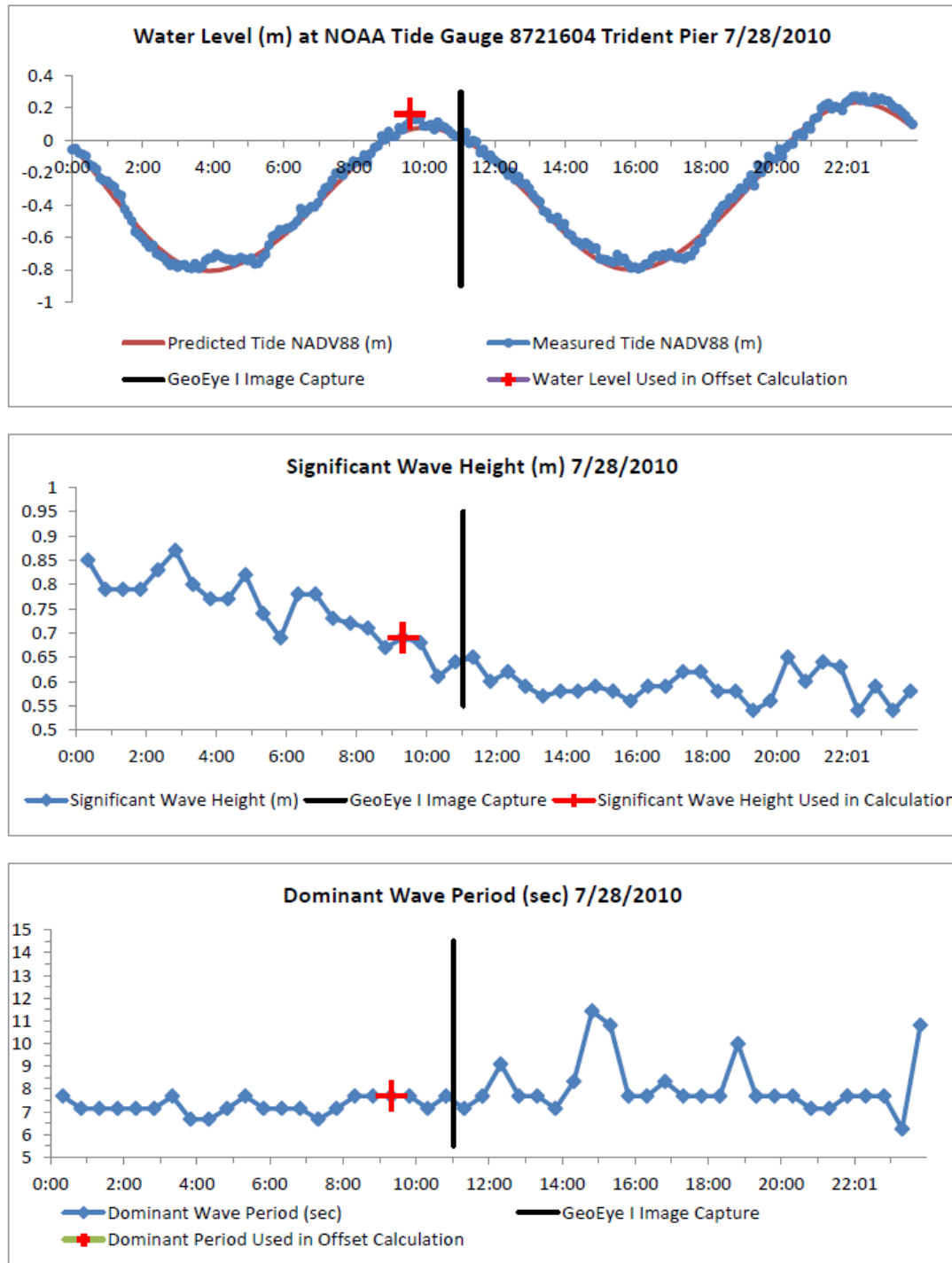


Figure 5-7. Water conditions found on the concurrent RTK-GPS survey and Geoeye I image capture on 28 July 2010. Panel 1: water level reported at Station 8721604 Trident Pier located ~ 23 km south of the study area. Panel 2: the significant wave height reported at NOAA buoy 41010 located ~140 km east of study area in 872 m of water. Panel 3: dominant wave period recorded at NOAA buoy 41010.

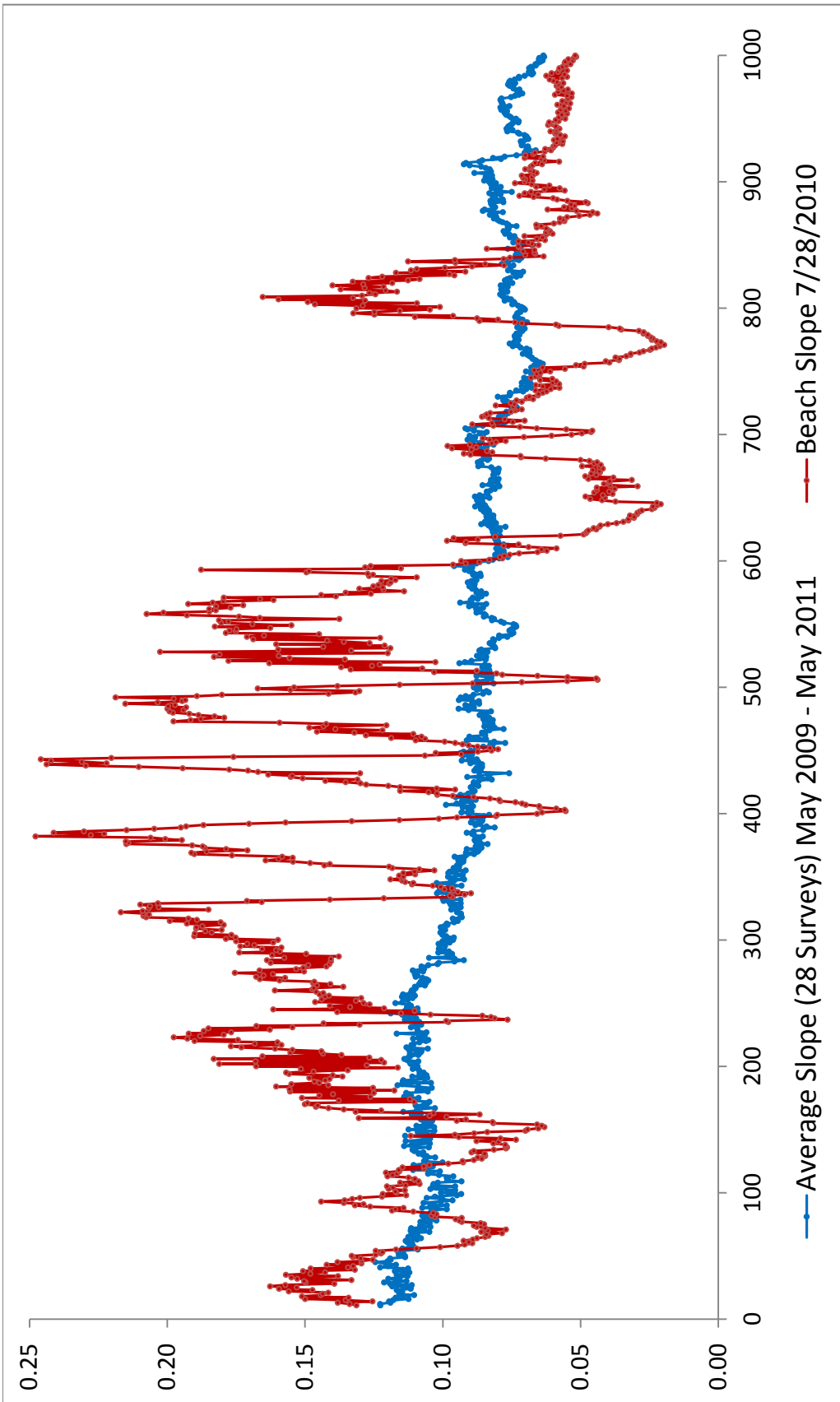


Figure 5-8. Average beach slopes for the period for 32 RTK-GPS surveys conducted between May 2009 - May 2011(blue), and the beach slope recorded on 28 July 2010 during the concurrent RTK-GPS survey and Geoeye-1 image capture (red). Beach slopes were calculated using the distance between the 0.25 and 0.75 contours (see Fig. 5-6)

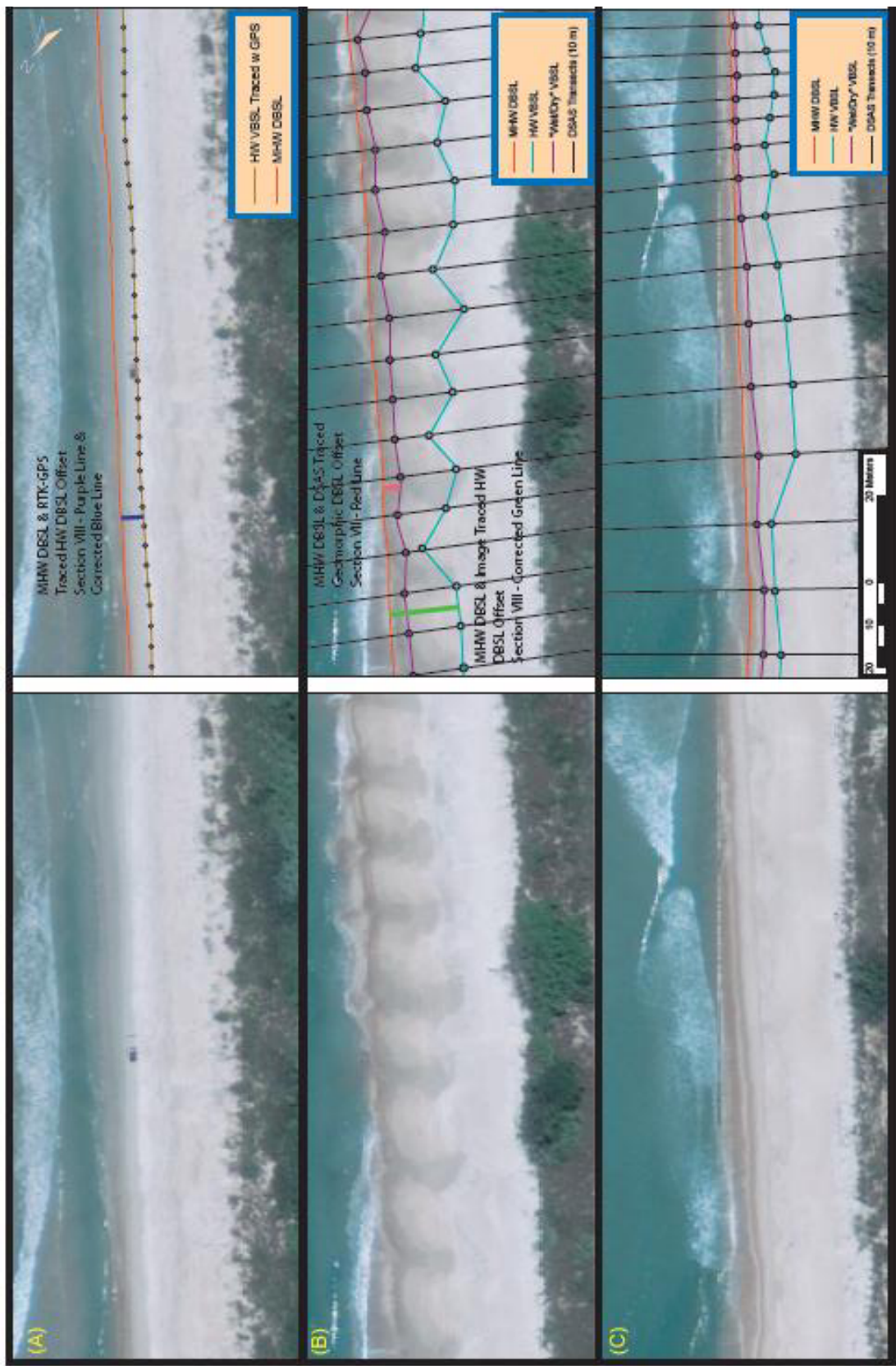


Figure 5-9. Different VBSLs and DBSLSs from concurrent image capture and RTK-GPS survey conducted on 28 July 2010.

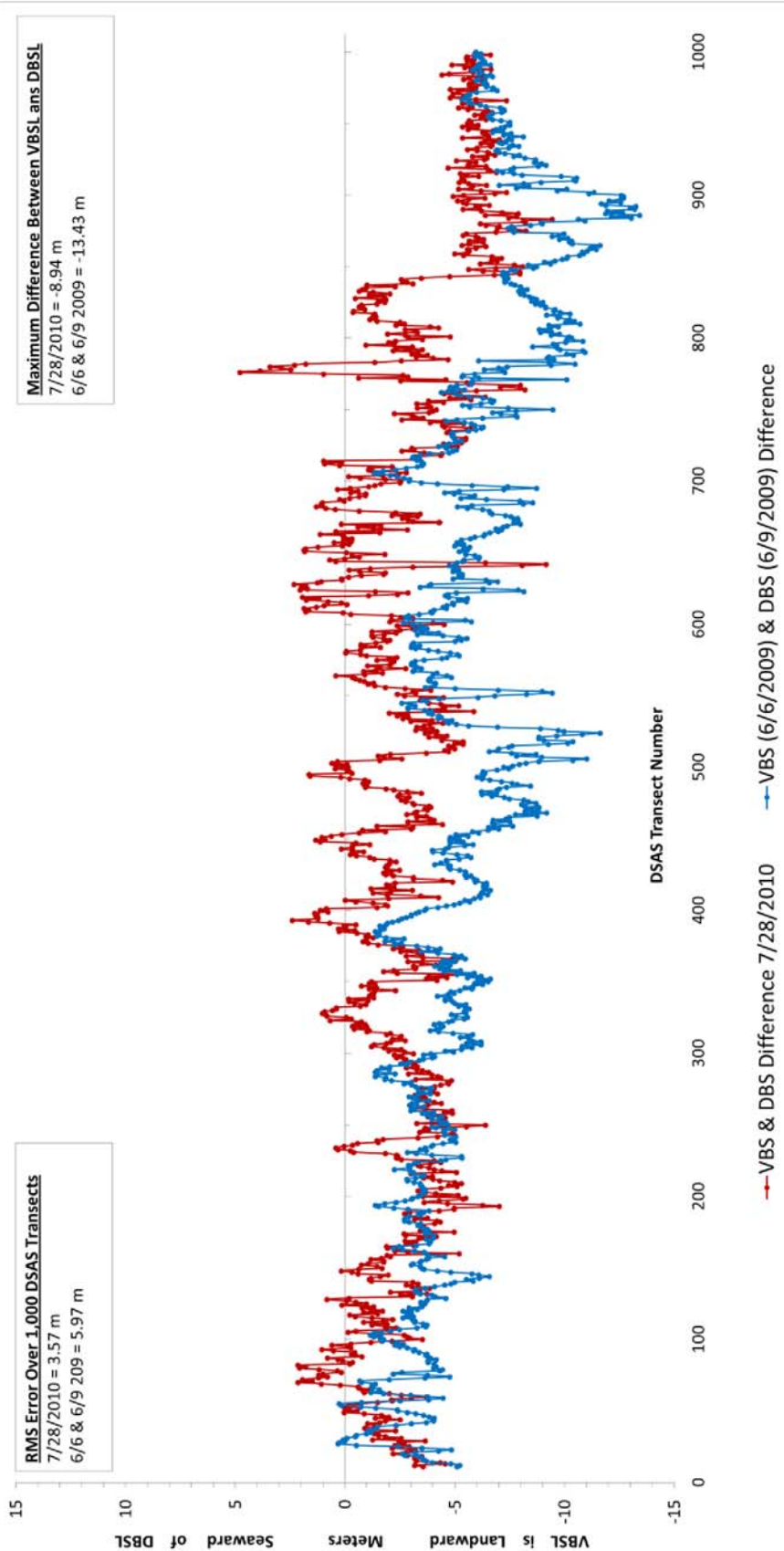


Figure 5-10. Offset digitized between the tonal change wet/dry VBSL and the MHW DBSL produced by RTK-GPS survey. For the Geoeye 1 image captured on 6 June 2009 and RTK-GPS survey conducted on 9 June 2009 (blue) the RMS offset was 5.97 m with a maximum offset of 13.43 m. For the concurrent Geoeye 1 image capture and RTK-GPS survey conducted on 28 July 2010 (red) the RMS offset was 3.57 m with a maximum offset of 8.94 m.

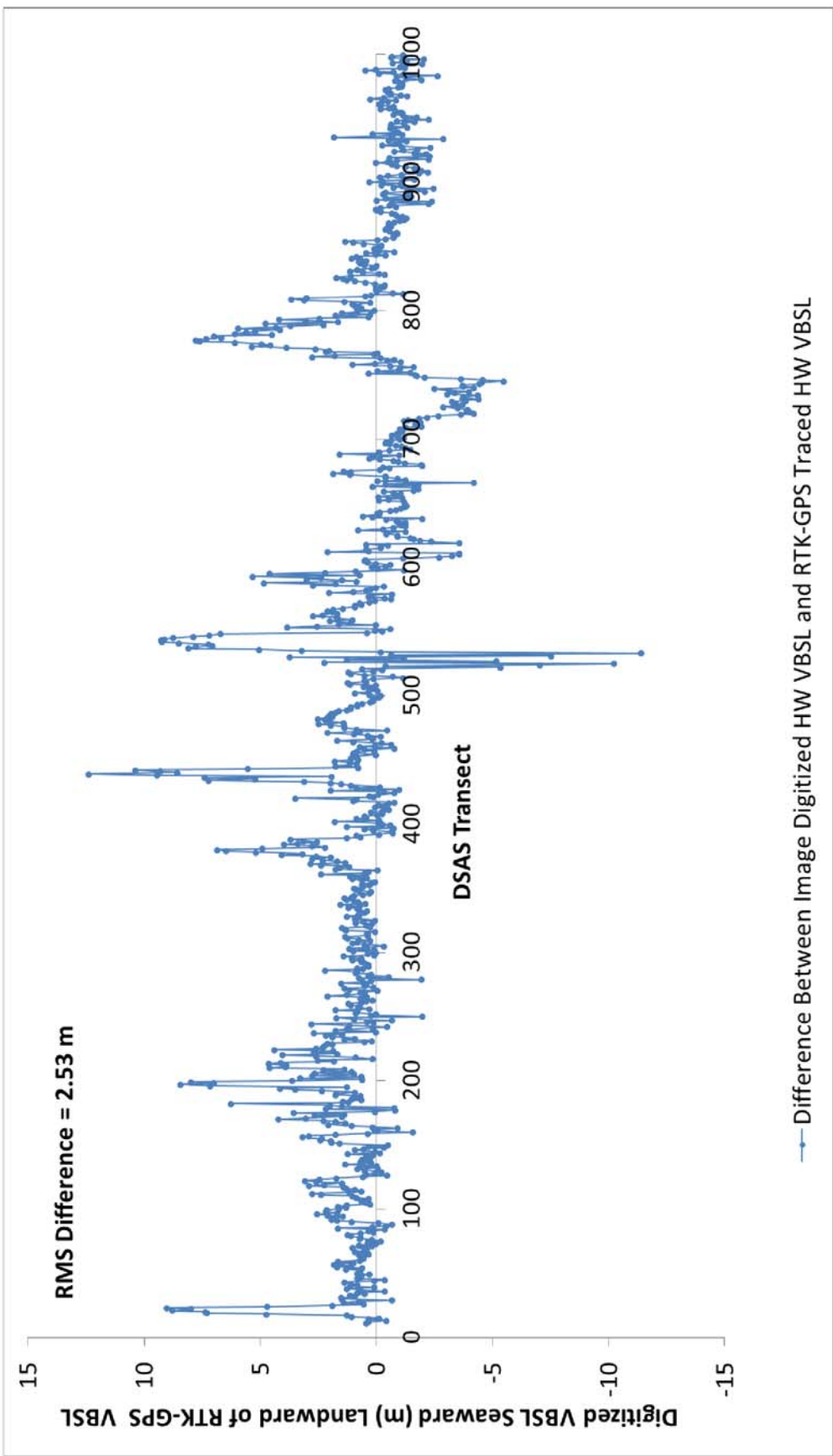


Figure 5-11. Offset between the HW VBSL traced on the ground during the RTK-GPS survey and the Geoeye I HW VBSL digitized at 10 m intervals. Both image capture and RTK-GPS survey were conducted on 28 July 2010.

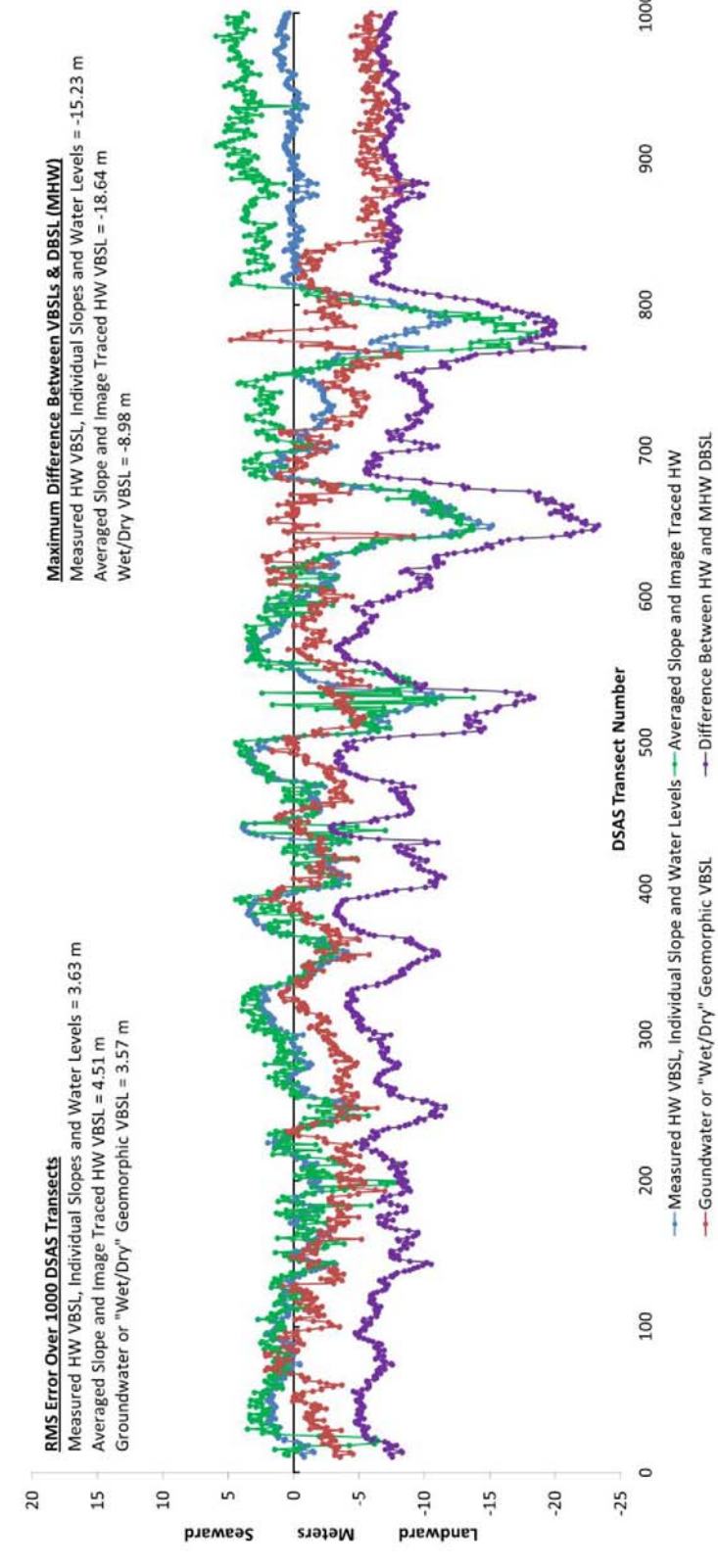


Figure 5-12. Offset between the geomorphically guided VBSL, and the MHW DBSL (red); offset between the HW VBSL with directly measured water levels and slopes measured at 10 intervals and the MHW DBSL (blue); offset between the HW VBSL with average slope measured at 1 km intervals and MHW level and the MHW DBSL Shoreline (green); and the VBSL HW and DBSL MHW offset (purple) on 28 July 2010.

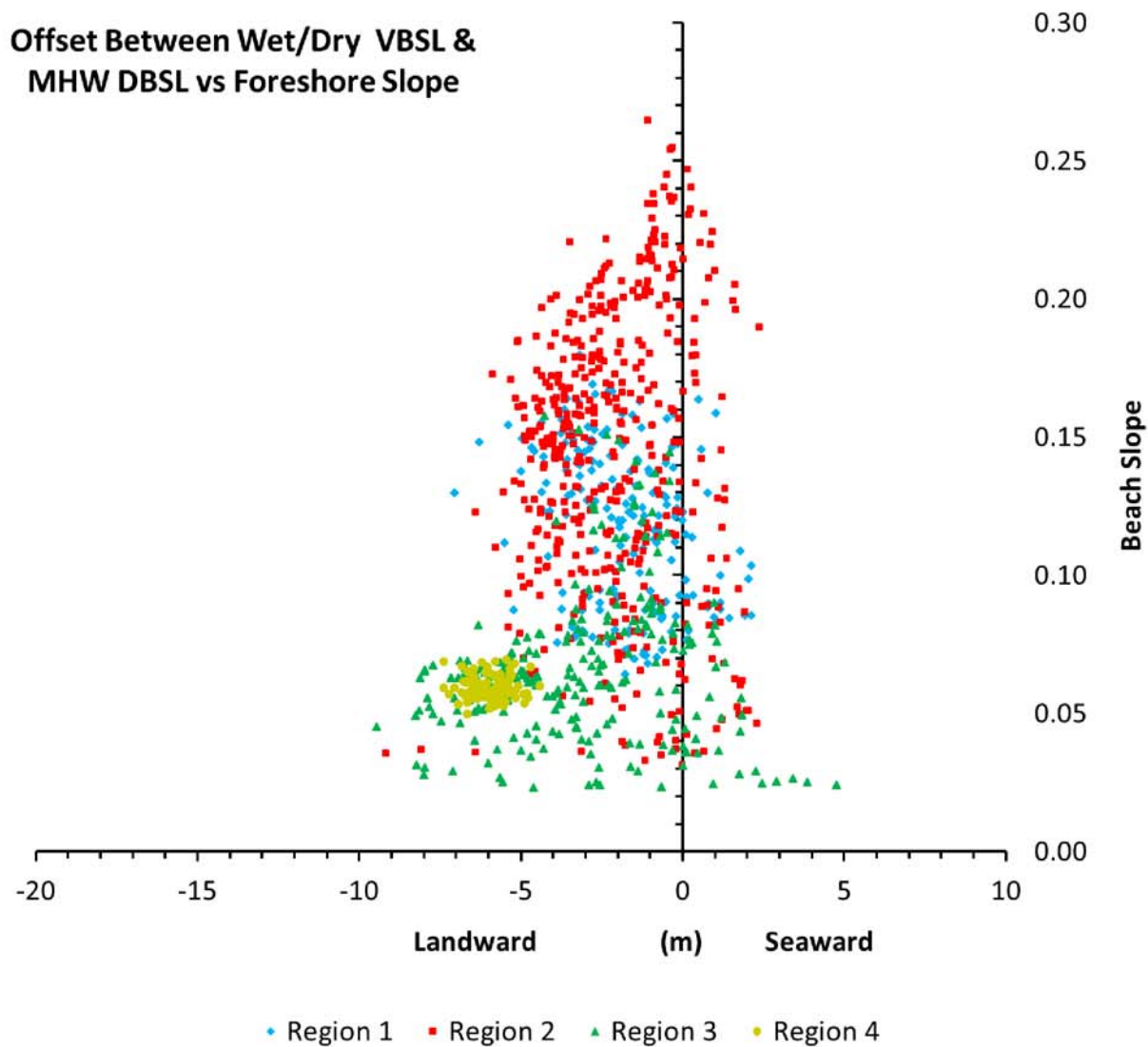


Figure 5-13. Offset between geomorphically guided tonal wet/dry VBSL and MHW DBSL vs. beach slope and further dived by beach regions on 28 July 2010.

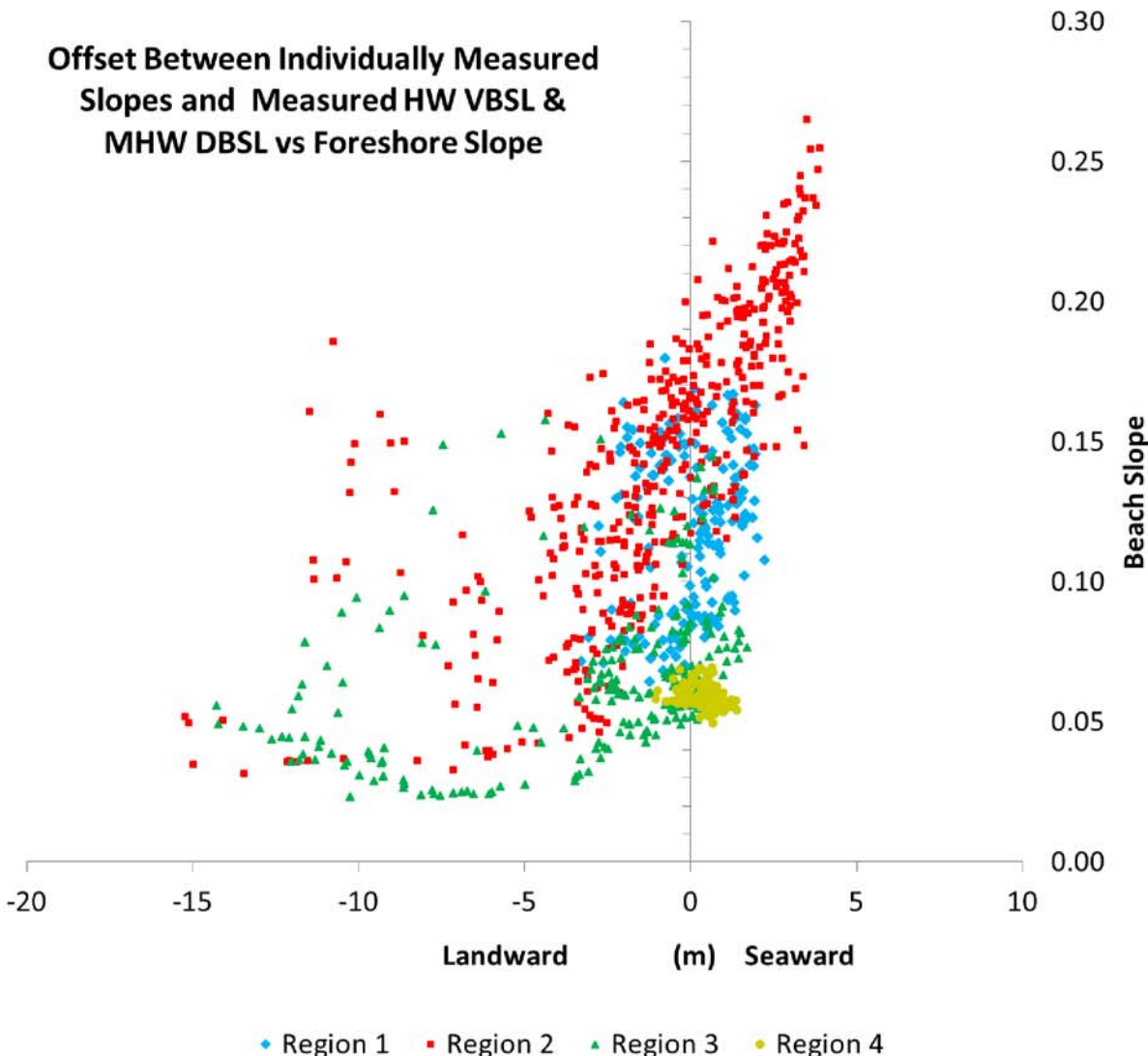


Figure 5-14. Offset between HW VBSL with offset correction applied using slopes calculated at 10 m intervals and measured water levels and MHW DBSL vs. slope and further divided by beach regions on 28 July 2010.

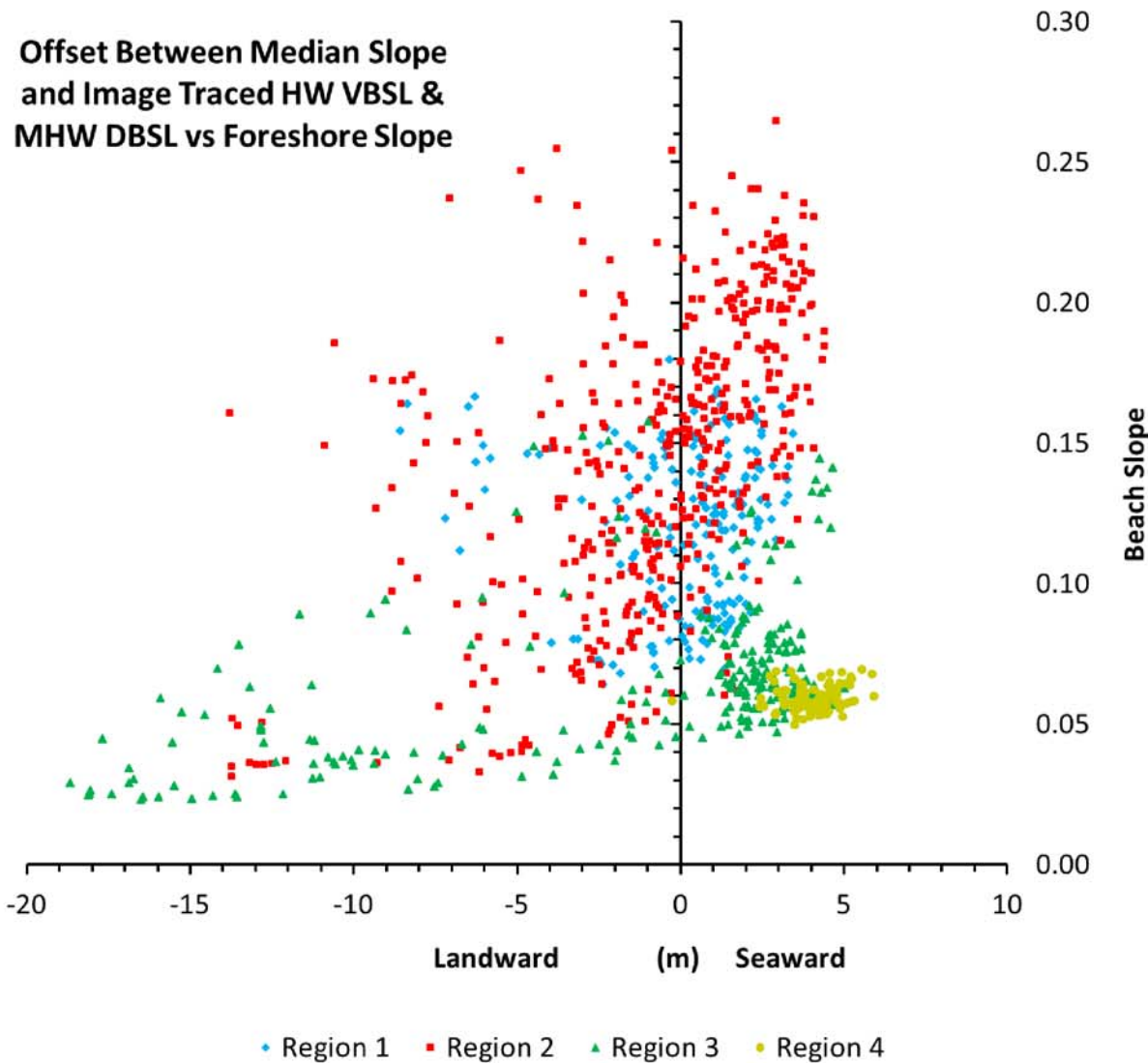


Figure 5-15. Offset between HW VBSL with offset correction applied using median slopes calculated at 1 km intervals and with MHW and MHW DBSL vs. slope and further divided by beach regions on 28 July 2010.

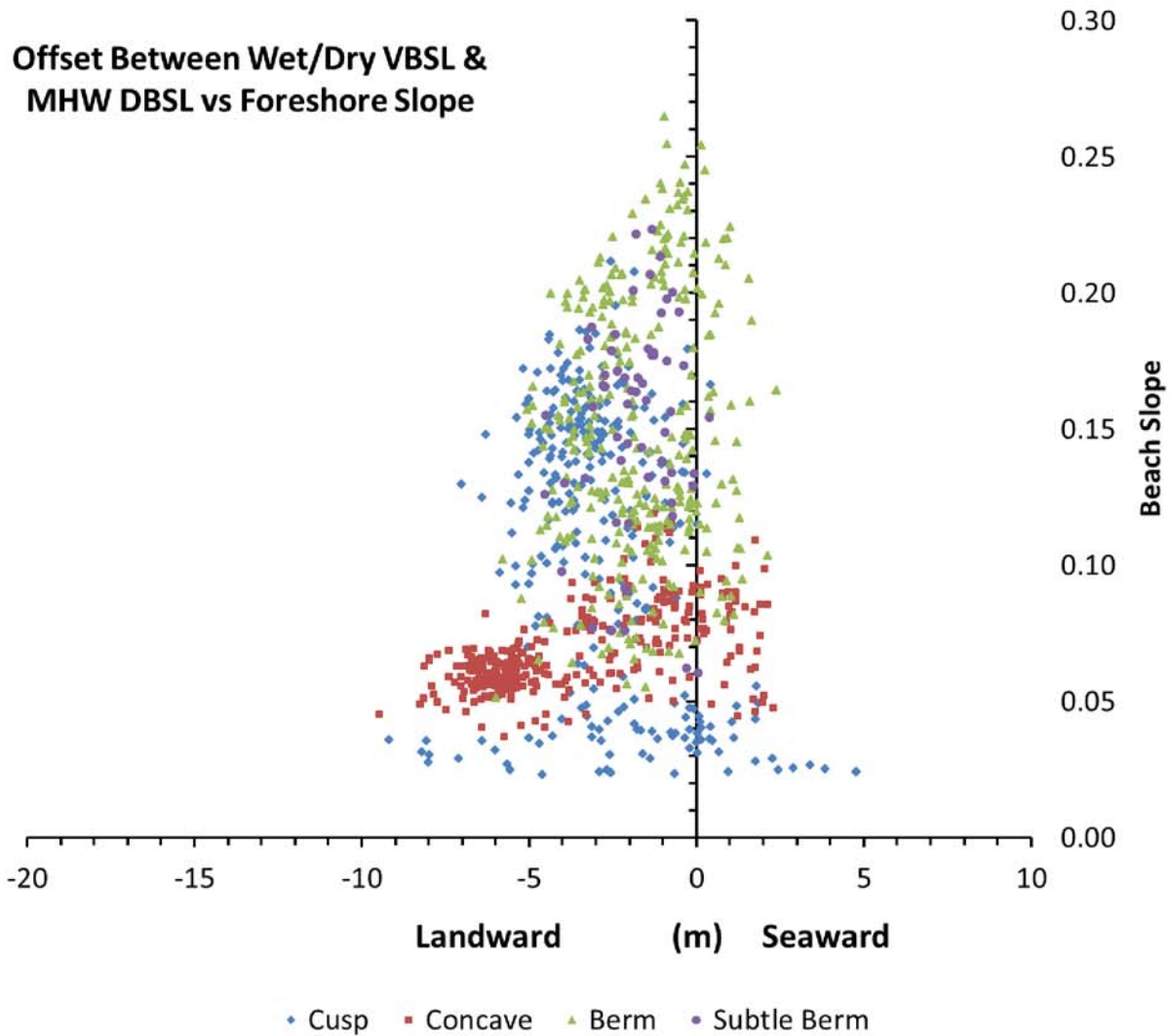


Figure 5-16. Offset between geomorphically guided tonal wet/dry VBSL and MHW DBSL vs. beach slope and further divided by beach morphology on 28 July 2010.

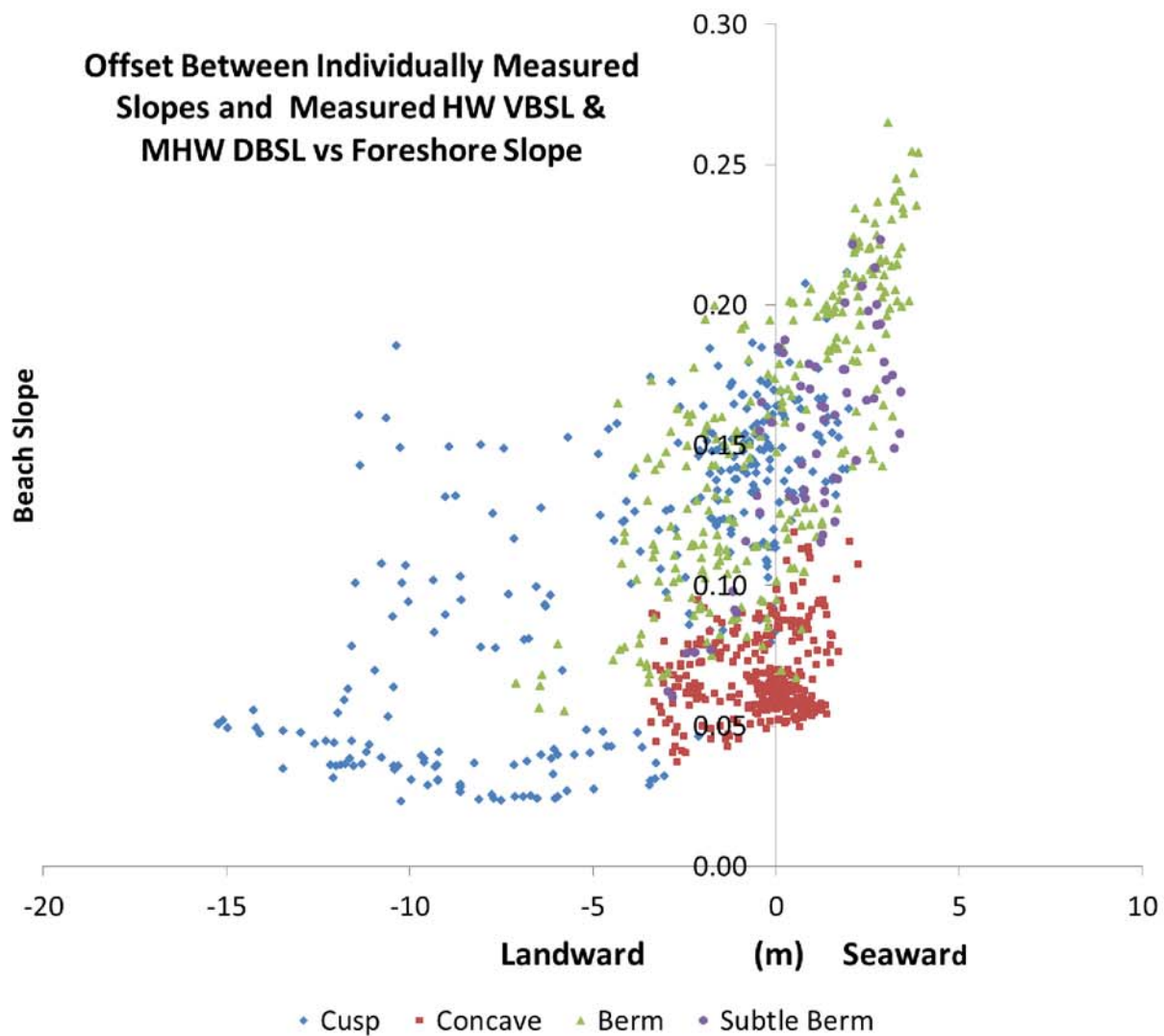


Figure 5-17. Offset between HW VBSL with offset correction applied using slopes calculated at 10 m intervals and measured water levels and MHW DBSL vs. slope and further divided by beach morphology on 28 July 2010.

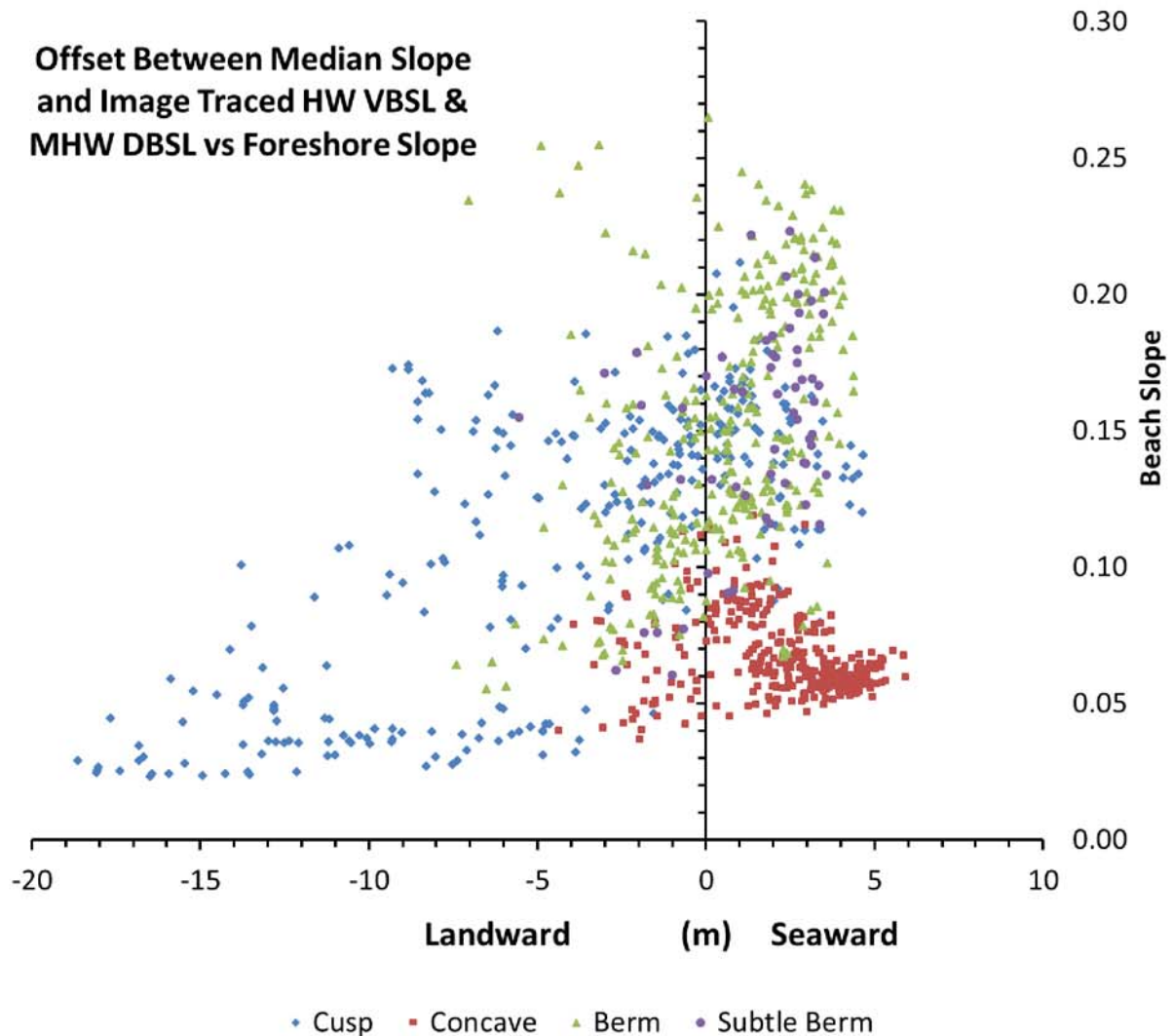


Figure 5-18. Offset between HW VBSL with offset correction applied using average slopes calculated at 1 km intervals and with MHW and MHW DBSL vs. slope and further divided by beach morphology on 28 July 2010.

Table 5-1. Average beach slopes calculated at 1 km intervals and used for HW VBSL offset corrections.

Distance Along Study Area (km)	DSAS Transects	Average Slope 09-11
1	11-104	0.11
2	105-204	0.11
3	205-311	0.11
4	312-412	0.09
5	413-512	0.09
6	513-625	0.09
7	626-728	0.09
8	729-830	0.08
9	831-928	0.07
10	929-1011	0.08
<b>Average</b>		<b>0.09</b>

## CHAPTER 6 CONCLUSIONS

The goal of this study was to provide an improved understanding of the methods employed during the collection of RTK-GPS in coastal settings under “real-world” field test conditions. Maximum values for RTK-GPS horizontal 95% confidence uncertainties are reached after ~40 minutes of surveying and are ~5 cm, whereas vertical 95% confidence uncertainties are reached after ~120 minutes and are ~10 cm. The maximum horizontal uncertainties associated with RTK-GPS measurements are ~7 cm, whereas maximum vertical uncertainties are ~20 cm. The use of multiple base station locations and multiple surveys adds an additional 1.5 cm to RTK-GPS uncertainties. These results indicate that RTK-GPS surveys without additional post-processing can provide elevation differences on the order of 20 cm, with the understanding that data with vertical uncertainties of up to 20 cm will be used in generation of the surface if more detailed QA/QC is not performed. Whereas the addition of the extra GNSS (GLONASS) and extra signal (L2C) provided no improvement on the size of the GPS uncertainty poles, anecdotally they did provide a more rapid initialization time and therefore less data and time lost to initialization.

The slope break RTK-GPS method proved to be effective for monitoring and measurement of coastal changes at many scales and intervals, especially on sandy coastlines with complex beaches. This method, along with a trailer designed specifically to operate in loose dry sand, provides a means to economically monitor and survey up to 20 km of shoreline per day. The slope break survey method provides landward and seaward constraints on the MHW DBS that the SWASH may not, although this is accomplished with additional alongshore survey data and time. The slope break method

produced MHW DBSL with average uncertainties of less than ~0.5 m and maximum uncertainties of <2 m, whereas the SWASH method produced average uncertainties of 1.8 m and maximum uncertainties of >10 m. While testing slope break versus SWASH methods, it was discovered that when using the SWASH method to generate DBSLs, it is important to stay as close to or above the MHW as possible. Surveying below the MHW can produce higher differences between the measured MHW line and the actual MHW, especially on beaches with low slopes, surveying below the MHW DBSL will project a MHW DBSL that is landward of the actual MHW datum.

Surveying along slope breaks forces a simple TIN to bend along the alongshore survey axis, allowing for an understanding of how the TIN will form while surveying. Other methods of survey styles have the possibility to form artifacts in the data, from unintended consequences of data interpolation. It is important to understand how the data collection strategy and sampling interval affects the sampling routine. Defining the length of beach to study or monitor, and knowledge of the beach morphology and beach response to forcing, are critical elements for developing a survey technique and interpolation routine that works best.

Four distinct regions were defined along the 10 km of NASA's False Cape coast, each with different morphologic characteristics and behaving in distinct ways. Region 1 with relatively high slopes displays less shoreline variability or movement with the same forcing, while Region 2 with variable slopes has more shoreline variability and movement with the same forcing. Region three has the gentlest slopes of the four regions and the highest variability in SCE, while Region 4 has low slope and less variability in SCE than Region 4. The manner in which each of these regions responds to

forcing has consequences with respect to remediation strategies. For example, in Region 2, where most of the primary dunes are missing and dune wash-over is prevalent during storms, there is more uncertainty in shoreline position as expressed in SCE. This increased uncertainty must be taken into account when planning remediation strategies, such as beach renourishment, especially when few temporal data points such as those from LIDAR are used to compute retreat rates.

The average SCE for the entire study area over the two years of the study was 12.4 m. This relates very well to the 14.1 m deviation found in the long-term data (1878-2010) of Dean (1998) and Absalonsen and Dean (2010). This may indicate that much of the variation in the shoreline position used by these authors to calculate linear retreat rates can be readily explained by the annual variability in shoreline positions. The SCEs for each of the annual study periods also revealed, not unexpectedly, that areas with the largest net change (either accretion or retreat), have the largest SCE. Although it is difficult to identify the causal factor in the spatial variability of the SCE, one plausible explanation may be the wave diffraction patterns over the complex bathymetry found offshore. The variability in the wave energy flux may also explain the anti-phasing found in the annual net shoreline change.

Seasonal (3-month) SCEs can play a significant role in the understanding of the uncertainties related to both datum-based and visual-based shoreline positions. Seasonal surveys in the study indicate that data collected during April, May, and June have lower SCE values than those collected during June, July, and August. This means that comparisons between years when data are acquired during the former time period will have the least uncertainty resulting from shoreline dynamics. These types of

surveys can provide better confidence intervals on data, depending on the season during which they were collected.

High-resolution satellite imagery, with its large field of view and instantaneous collection capability, coupled with its high return rate and ease of scheduling, makes this type of data collection beneficial for large areas of the coast between other DBSL data collection activities, such as LIDAR. A geomorphically-guided siting of the wet/dry VBSL performs as well as or better than a HW VBSL when average slope and water levels are used to generate it. VBSL offsets are potentially higher in areas with lower slopes, complex morphology, or in regions of higher variability. When uncertainties related to differences in VBSL and DBSL are minimized, historic imagery and satellite imagery can be used to fill temporal gaps from less frequently collected DBSL techniques.

**APPENDIX A**  
**TABLE OF SURVEYS AND SURVEY QUALITY**

**Table A-1. Dates of surveys and survey quality**

Survey Date	Data Points	Data Points Used (5 cm)	% of Data Lost at QA/QC (05 cm)	Data Points Used (10 cm)	% of Data Lost at QA/QC (10 cm)	File Name in Master_Survey_QC_Files
May, 6, 2009	28,346	28,265	0.29%	28,344	0.01%	CpCnv_090506_QC_Bch
May 24, 2009	16,927	16,653	1.62%	16,922	0.03%	CpCnv_090524_QC_Bch
May 28, 2009	18,954	18,327	3.31%	18,952	0.01%	CpCnv_090528_QC_Bch
June 6, 2009	28,394	24,572	13.46%	28,390	0.01%	CpCnv_090606_QC_Bch
July 6, 2009	38,925	32,349	3.19 %	37,370	0.06%	CpCnv_090706_QC_Bch
Aug. 1, 2009	50,694	48,617	4.10%	50,568	0.25%	CpCnv_090801_QC_Bch
Sept. 5, 2009	38,980	36,978	5.14%	37,866	2.86%	CpCnv_090905_QC_Bch
Oct. 5, 2009	36,853	29,362	20.33%	33,987	7.78%	CpCnv_091005_QC_Bch
Nov. 6, 2009	35,897	31,577	12.03%	35,147	2.09%	CpCnv_091106_QC_Bch
Dec. 1, 2009	34,854	33,869	2.83%	34,600	0.73%	CpCnv_091201_QC_Bch
Jan. 3, 2010	36,933	35,248	4.56%	36,932	0.00%	CpCnv_100103_QC_Bch
Jan. 31, 2010	37,472	36,624	2.26%	37,126	0.92%	CpCnv_100131_QC_Bch
Feb. 28, 2010	29,734	28,660	3.61%	29,001	2.47%	CpCnv_100228_QC_Bch
March 27, 2010	35,697	35,246	1.16%	35,526	0.47%	CpCnv_100327_QC_Bch
May 2, 2010	40,374	37,659	6.72%	38,643	4.29%	CpCnv_100502_QC_Bch
May 27, 2010	26,639	26,594	0.16%	26,626	0.05%	CpCnv_100527_QC_Bch
July 2, 2010	13,475	12,547	6.89%	12,820	4.86%	CpCnv_100702_QC_Bch
July 25, 2010	17,692	15,781	10.80%	16,590	7.64%	CpCnv_100725_QC_Bch

July 28, 2010	25,821	23,476	9.08%	24,193	6.30%	CpCnv_100728_QC_Bch
July 31, 2010	16,647	14,891	10.55%	15,682	5.80%	CpCnv_100731_QC_Bch
Aug. 28, 2010	28,310	26,922	4.90%	27,850	1.62%	CpCnv_100828_QC_Bch
Oct. 2, 2010	18,569	17,479	6.24%	18,439	0.72%	CpCnv_101002_QC_Bch
Oct. 3, 2010	18,847	18,188	3.51%	18,773	0.39%	CpCnv_101003_QC_Bch
Oct. 9, 2010	24,692	24,160	2.13%	24,621	0.29%	CpCnv_101009_QC_Bch
Oct. 24, 2010	34,338	31,605	7.96%	33,423	2.66%	CpCnv_101024_QC_Bch
Nov. 20, 2010	27,675	26,785	3.22%	27,374	1.09%	CpCnv_101120_QC_Bch
Dec. 21, 2010	102,41 9	101,636	0.76%	102,04 4	0.37%	CpCnv_101221_QC_Bch
Jan. 24, 2011	88,429	87,004	1.28%	88,409	0.02%	CpCnv_110124_QC_Bch
Feb. 18, 2011	41,209	38,999	5.36%	41,154	0.13%	CpCnv_110218_QC_Bch
March 19, 2011	72,510	71,394	1.54%	71,812	0.96%	CpCnv_110319_QC_Bch
April 18, 2011	72,808	71,527	1.76%	72,801	0.01%	CpCnv_110418_QC_Bch
May 19, 2011	61,345	52,886	13.79%	60,530	1.32%	CpCnv_110519_QC_Bch
June 13, 2011	74,034	63,214	14.61%	72,327	2.31%	CpCnv_110613_Bch_(Ty pe)

## APPENDIX B

### TRIMBLE DATA COLLECTER DATA EXTRACTION

#### Importing the Raw Data from the Trimble Data Collectors

Plug the TSC into the USB port on the computer and open the Trimble Data Transfer Utility. Once the utility opens and the TSC connects, click the “Add” button.

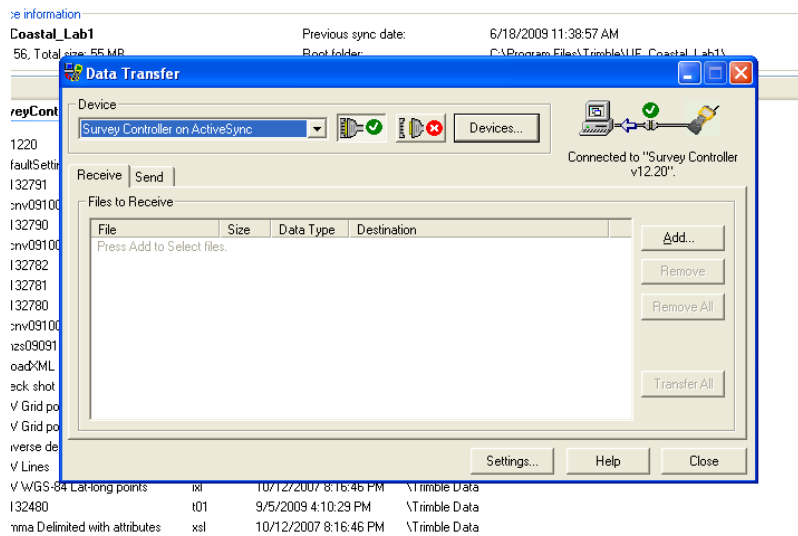


Figure B-1. Screen capture of data collector connection to PC.

This will open the “Open” box, select the file you wish to transfer, transfer files one at a time. IMPORTANT click the browse to set the file path used to transfer data, if you do not do this the files will be transferred to a ~Temp file and will be difficult to find.

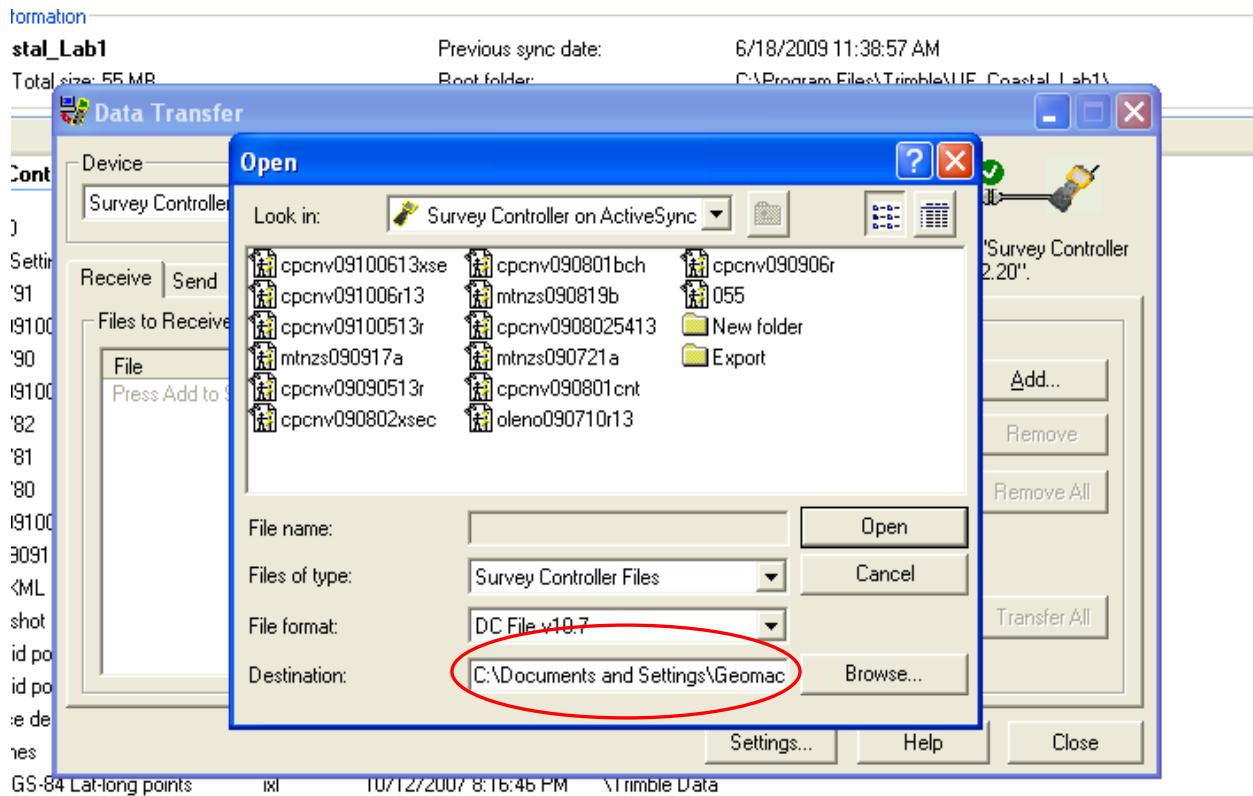


Figure B-2. Data controller destination configuration.

This will open the “Open” box, select the file you wish to transfer, transfer files one at a time. **IMPORTANT** click the browse to set the file path used to transfer data, if you do not do this the files will be transferred to a ~Temp file and will be difficult to find. Click the transfer all for the file and then check the file to ensure the transfer was completed.

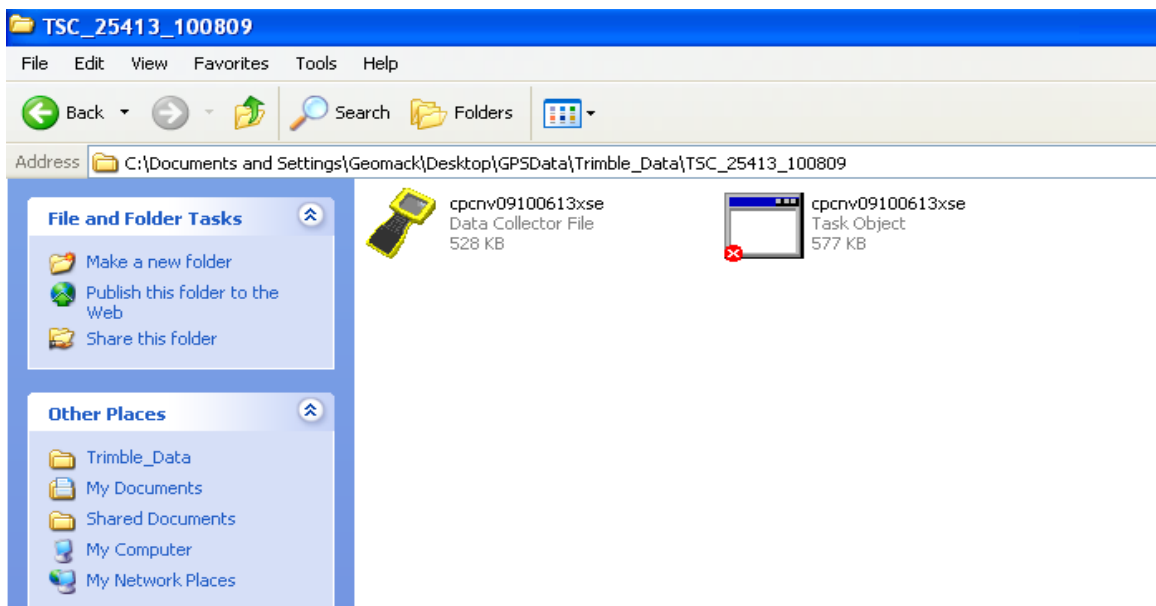


Figure B-3. Data collector files and icon structure.

There should be a “Data Collector File” and a “Task Object” file in the folder, sometimes you will see a file transfer failed message but if both files are in the folder they should be fine. Do this for each file you want to transfer and be sure to organize them so you can add more files later. Open Trimble Business Center (TBC) and the folder containing the Task Object file as seen in Fig. X. these should be located in the Folder “Trimble\_Data” “*TSC\_Collector Serial Number*” and drag the collector job that needs to be converted to a Text file into the TBC work environment. Make sure that you open a New Job in TBC before dragging the Task Object file into the TBC work environment. Ensure the correct job is open in the upper left corner of the screen and under the “Project Explorer” panel on the left hand part of the screen. Verify the data by opening the “Point Spreadsheet” and finding the Base Station used for the survey. Check Base Station coordinates against an available NGS Data Sheet or know coordinates, this will ensure the Base was in the correct position and the right kinematic

correction data was sent to the rovers. This Data\_RAW\_Text folder contains the data the is generated by the TBC Report Generator function. When the “Job” file is pulled into TBC the “Receiver Raw Data Check In” box appears, make sure all of the continuous segments are checked and hit “OK”. Once the job is drawn in TBC open a points spreadsheet and vector spreadsheet by selecting: View – New Points Spreadsheet and View – New Vector Spreadsheet. These two spreadsheets allow the user to check if the correct antenna heights were entered in the collector and if the base station data matches the location on the NGS Date sheet. Corrections to the data will be made later in Excel after the jobs have exported in a useable format. Once the data has been checked for correct base station position, antenna heights and notes about corrections have been taken the text files can be generated. To export the data open a job report by selecting: Reports – Job Report Generator. Select the job that has been opened in the “Job Report Generator” box opened at the right hand side of the screen (there should be only one available in the pull down menu). Under “Style Sheet” select the box with three dots to the right of the box, this allows you to select a job report from other than the few located in the TBC.

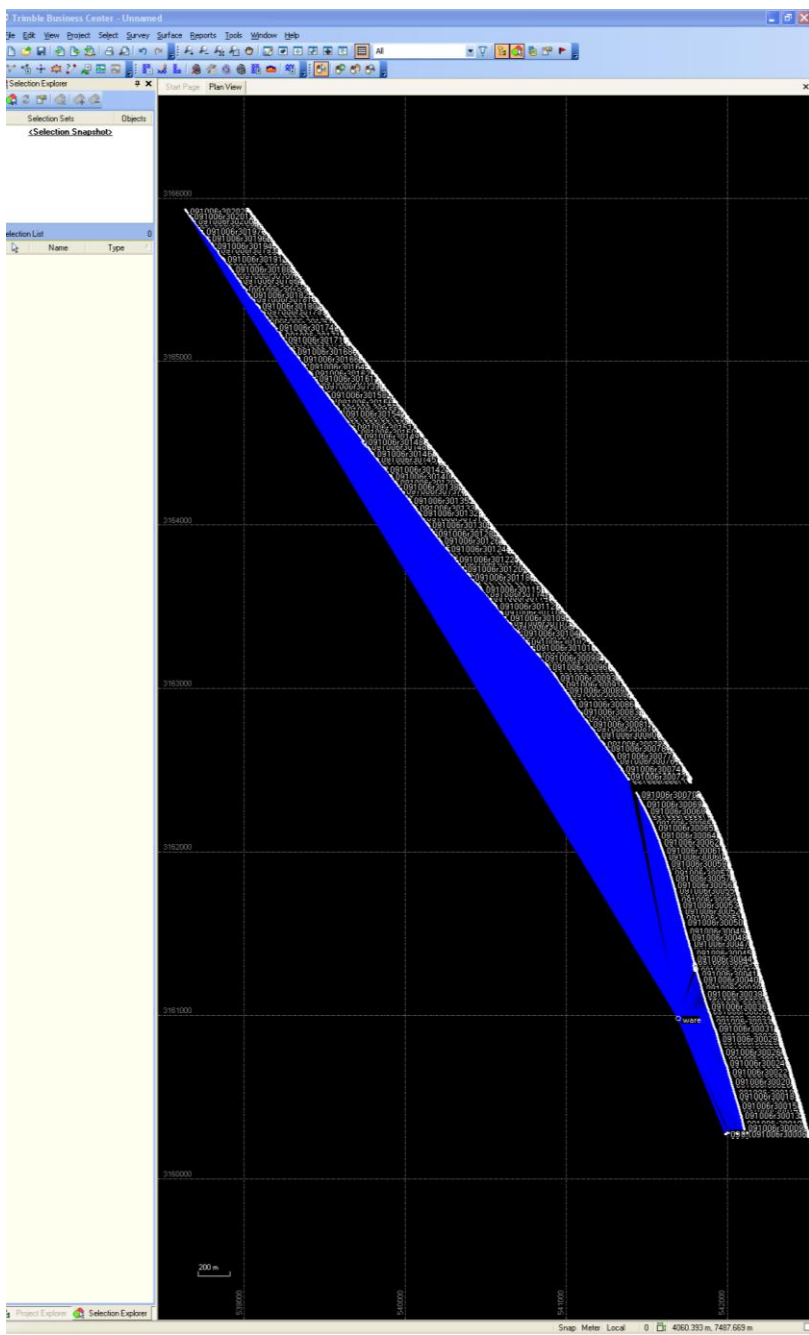


Figure B-4. Trimble Office GPS project screen shot.

There should be a “Data Collector File” and a “Task Object” file in the folder, sometimes you will see a file transfer failed message but if both files are in the folder they should be fine. Do this for each file you want to transfer and be sure to organize

them so you can add more files later. In order to get all of the categories of data needed for the Cape Canaveral Project two different job reports are used. They are both located in the “Trimble” folder. To select the first report hit the three button box and open the “Trimble” folder, select “GPS Points report” and hit “ok” at the bottom of the screen. This is an example of the output of this report (Fig. B-4). These files contain the raw data that was collected in the field by each controller, including any errors associated with incorrect base station position, antenna heights or projections these errors can be corrected later in Excel. These reports are saved in the GPSData – Reports\_Raw folder in the following sample format (CpCnv\_0907065413\_Pts) the “Pts” indicates that this is the raw data from a points report. Next follow the same directions, but use the “GPS DOP Data” report and save it in the following format: (CpCnv\_0907065413\_Dop) (Fig. B-4). Look over this file and ensure the Base Station coordinates are in the same position as the NGS Datasheet. Save this file under GPSData - Excel\_Data as an Excel Workbook and in GPSData – CSV\_Data as a comma delimited (.csv) file.

c20090607rs - Notepad

File Edit Format View Help

Point coordinates for job c20090607rs

Point	North	East	Elev	Code	Hz	Prec	Vt	Prec	PDOP	Sats
ward	3160982.777	541695.747	9.614		?	?	?	?	?	?
s906070160	3160282.759	542115.412	2.506	bch	0.007	0.012	1.9	10		
s906070161	3160283.256	542115.597	2.460	bch	0.012	0.020	1.9	10		
s906070162	3160284.324	542115.923	2.403	bch	0.010	0.018	1.9	10		
s906070163	3160285.948	542116.071	2.353	bch	0.010	0.016	1.9	10		
s906070164	3160287.570	542116.033	2.325	bch	0.011	0.019	1.9	10		
s906070165	3160289.497	542115.808	2.291	bch	0.012	0.020	1.9	10		
s906070166	3160291.549	542115.435	2.295	bch	0.008	0.013	1.9	10		
s906070167	3160293.721	542114.960	2.257	bch	0.011	0.020	1.9	10		
s906070168	3160298.868	542113.910	2.278	bch	0.014	0.024	1.9	10		
s906070169	3160301.458	542113.232	2.216	bch	0.010	0.018	1.9	10		
s906070170	3160304.065	542112.590	2.236	bch	0.012	0.021	1.9	10		
s906070171	3160306.516	542112.007	2.201	bch	0.013	0.022	1.9	10		
s906070172	3160309.627	542111.287	2.210	bch	0.015	0.026	1.9	10		
s906070173	3160315.190	542109.985	2.203	bch	0.011	0.018	1.9	10		
s906070174	3160318.369	542109.280	2.190	bch	0.013	0.021	1.9	10		
s906070175	3160321.192	542108.658	2.190	bch	0.013	0.023	1.9	10		
s906070176	3160324.054	542107.983	2.217	bch	0.016	0.028	1.9	10		
s906070177	3160327.001	542107.253	2.208	bch	0.013	0.022	1.9	10		
s906070178	3160330.006	542106.503	2.202	bch	0.014	0.024	1.9	10		
s906070179	3160333.064	542105.751	2.207	bch	0.016	0.028	1.9	10		
s906070180	3160339.562	542104.240	2.202	bch	0.017	0.029	1.9	10		

Figure B-5. Typical text file structure from Trimble Business Report Generator.

There should be a “Data Collector File” and a “Task Object” file in the folder, sometimes you will see a file transfer failed message but if both files are in the folder they should be fine. Do this for each file you want to transfer and be sure to organize them so you can add more files later.

```
0907061300000, 11:59:13, 8, 1.7, 1.0, 1.4
0907061300001, 12:12:50, 6, 2.8, 1.2, 2.5
0907061300002, 12:12:51, 6, 2.8, 1.2, 2.5
0907061300003, 12:12:52, 6, 2.8, 1.2, 2.5
0907061300004, 12:12:53, 6, 2.8, 1.2, 2.5
0907061300005, 12:12:54, 6, 2.8, 1.2, 2.5
0907061300006, 12:12:55, 6, 2.8, 1.2, 2.5
0907061300007, 12:12:56, 6, 2.8, 1.2, 2.5
0907061300008, 12:12:57, 6, 2.8, 1.2, 2.5
0907061300009, 12:12:58, 6, 2.8, 1.2, 2.5
0907061300010, 12:12:59, 6, 2.8, 1.2, 2.5
0907061300011, 12:13:00, 6, 2.8, 1.2, 2.5
0907061300012, 12:13:01, 6, 2.8, 1.2, 2.5
0907061300013, 12:13:02, 6, 2.8, 1.2, 2.5
0907061300014, 12:13:03, 6, 2.8, 1.2, 2.5
0907061300015, 12:13:04, 6, 2.8, 1.2, 2.5
0907061300016, 12:13:05, 6, 2.8, 1.2, 2.5
0907061300017, 12:13:06, 6, 2.8, 1.2, 2.5
0907061300018, 12:13:07, 6, 2.8, 1.2, 2.5
0907061300019, 12:13:08, 6, 2.8, 1.2, 2.5
0907061300020, 12:13:09, 6, 2.8, 1.2, 2.5
0907061300021, 12:13:10, 6, 2.8, 1.2, 2.5
0907061300022, 12:13:11, 6, 2.8, 1.2, 2.5
0907061300023, 12:13:12, 6, 2.8, 1.2, 2.5
0907061300024, 12:13:13, 6, 2.8, 1.2, 2.5
0907061300025, 12:13:14, 6, 2.8, 1.2, 2.5
0907061300026, 12:13:15, 6, 2.8, 1.2, 2.5
0907061300027, 12:13:16, 6, 2.8, 1.2, 2.5
0907061300028, 12:13:17, 6, 2.8, 1.2, 2.5
0907061300029, 12:13:18, 6, 2.8, 1.2, 2.5
0907061300030, 12:13:19, 6, 2.8, 1.2, 2.5
```

Figure B-6. DOP report generated by Trimble Business Job Report Generator.

There should be a “Data Collector File” and a “Task Object” file in the folder, sometimes you will see a file transfer failed message but if both files are in the folder they should be fine. Do this for each file you want to transfer and be sure to organize them so you can add more files later.

APPENDIX C  
POINT, TIN, RASTER, AND MEAN HIGH WATER SHAPEFILE GENERATION

**A-1 Generating shape files from Excel in ArcMap 9.3.**

**A-1.1 Importing (x,y) Data Into ArcGIS 9.3**

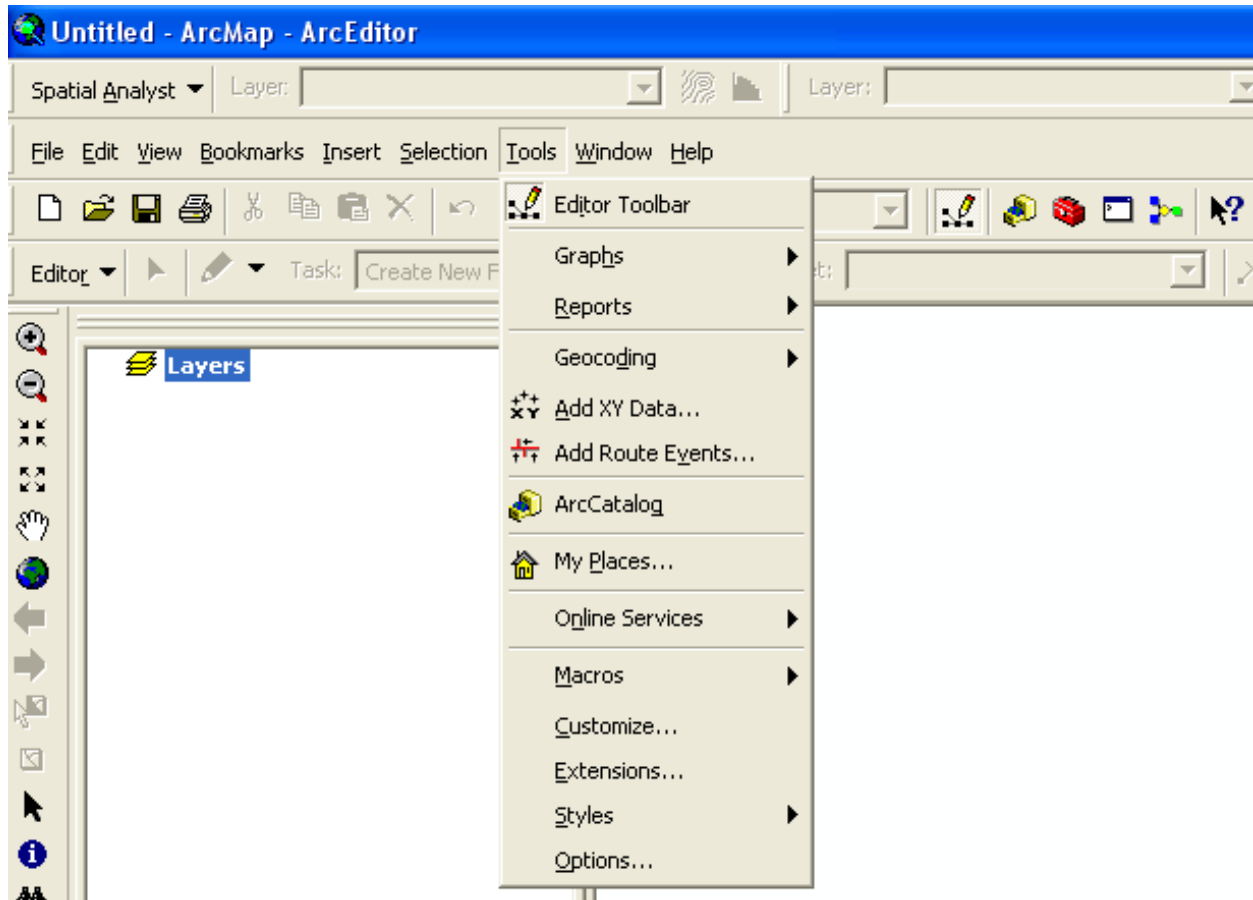


Figure C-1. ArcGIS screen shot of steps to add GPS data.

Under “Tools – Add XY Data” find the file that contains the data, and place the name of the Lon/Easting data in the “X Field” and the name of the Lat/Northing data in the “Y Field”. “Edit” the coordinate system to match the data’s coordinate system that was used to collect the data (UTM 17N – NAD83).

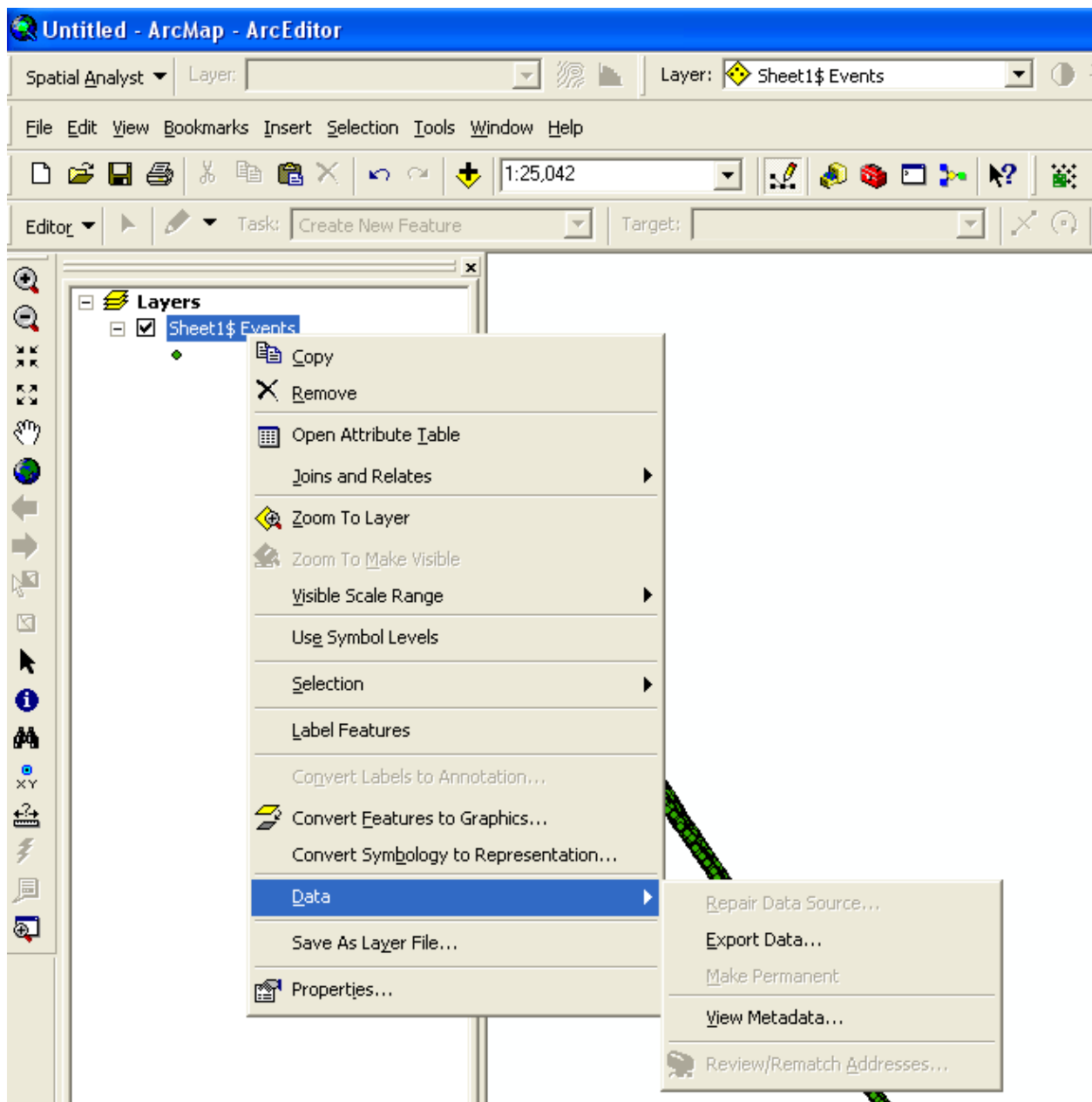


Figure C-2. Screen shot of ArcGIS demonstrating export of data.

Once the data is projected right click on the data under the layers box on the right side of the screen. Under Data use the “Export Data” feature to name the file and save the new point shape file. When the shape file has finished saving answer yes to the display on map dialog box, this will place the shapefile on the map over the data

imported from the Excel spreadsheet. It should overlay directly on the each other.

## Building a Triangulated Irregular (TIN) Network in ArcGIS 9.3 & XTools Pro

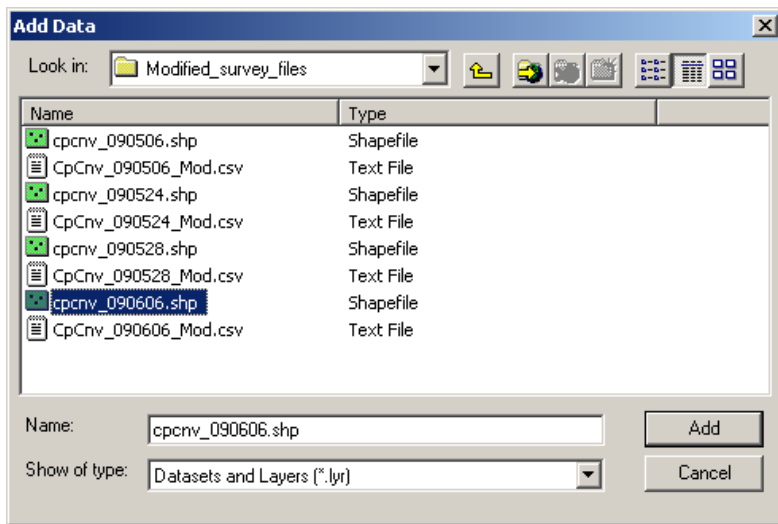


Figure C-3. Screen shot depicting how to open the desired point shape file. It may be beneficial to construct two shape files as this point shape file will be edited and changed.

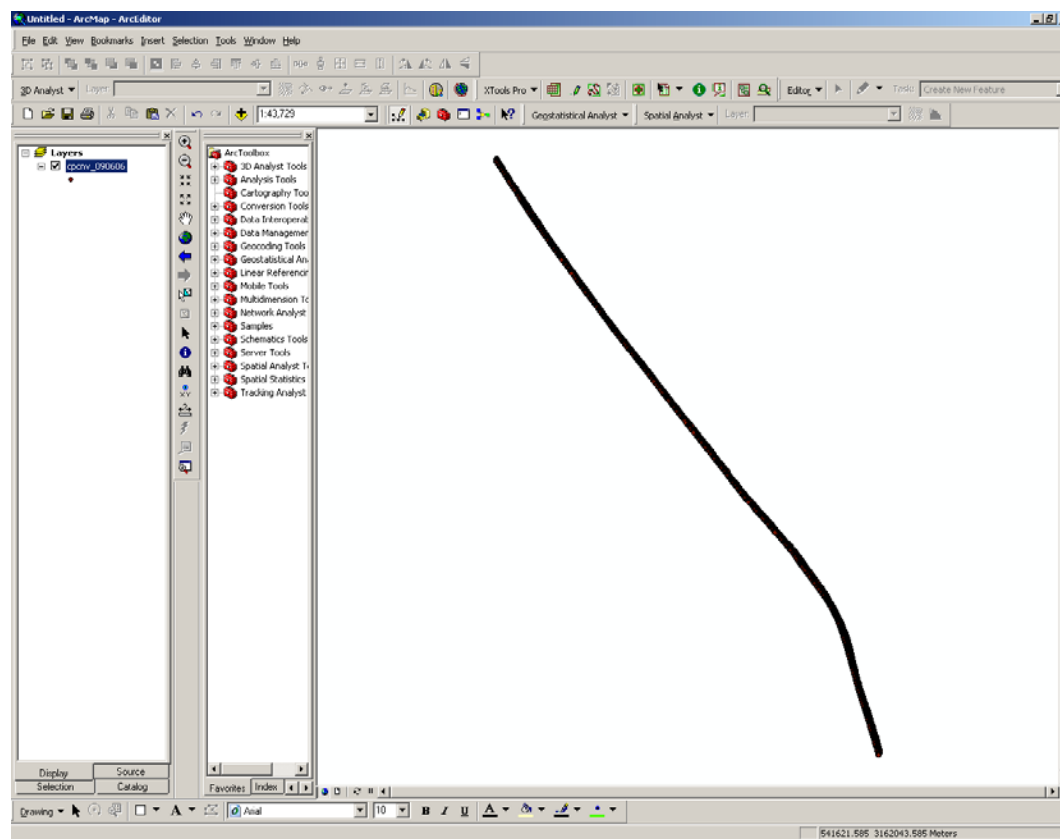


Figure C-4. Point shape file as it appears in ArcMap 9.3.

## Constructing a Single Line the Encompasses All Data Points Making a Line from Point Data

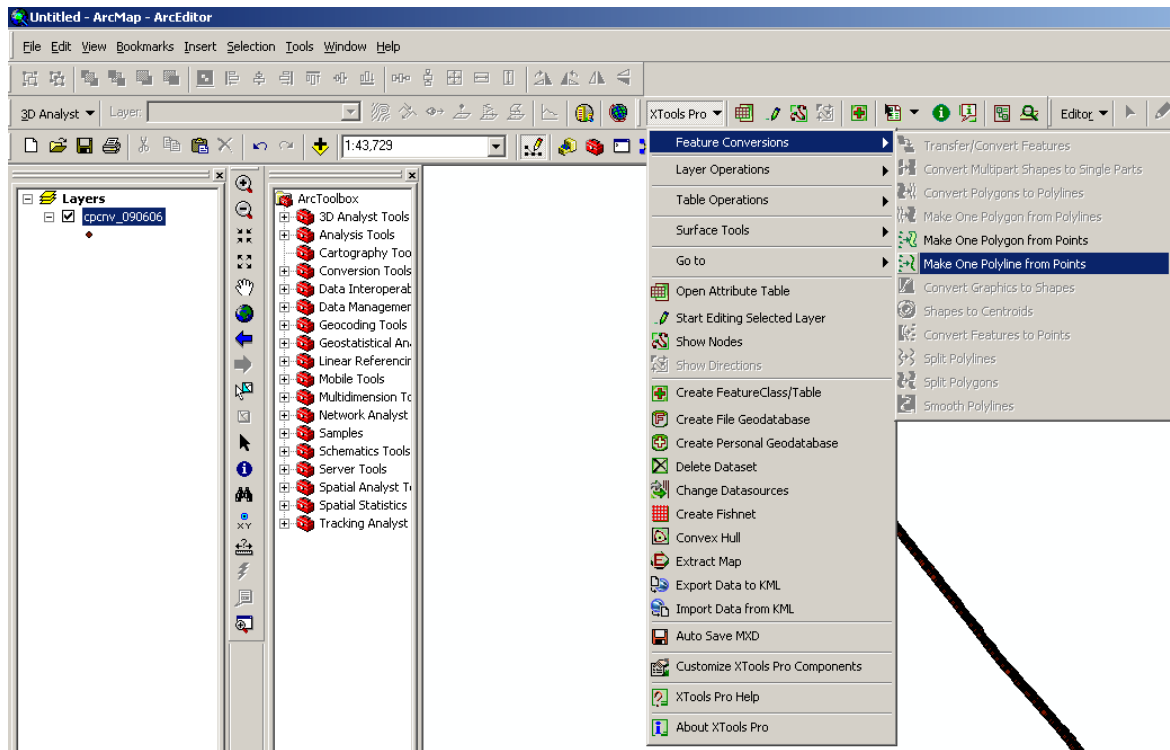


Figure C-5. Demonstration of converting data points to lines using XTools Pro. Under XTools pro tool bar, use pull down menu under “Feature Conversions” to select “Make One Polyline from Points”.

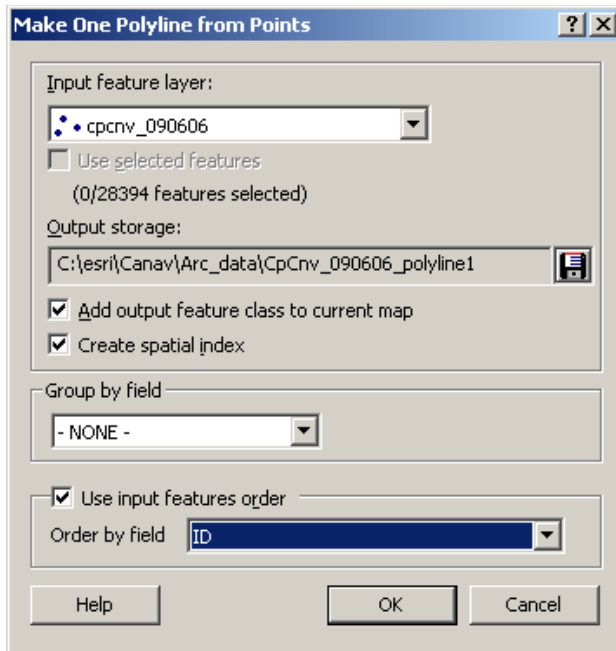


Figure C-6. Selection box for making a Polyline from Points.

In task box select “Use input features order” and select “ID” in the “Order by filed” box. This will ensure that the lines created from the points are created in the order the data was collected.

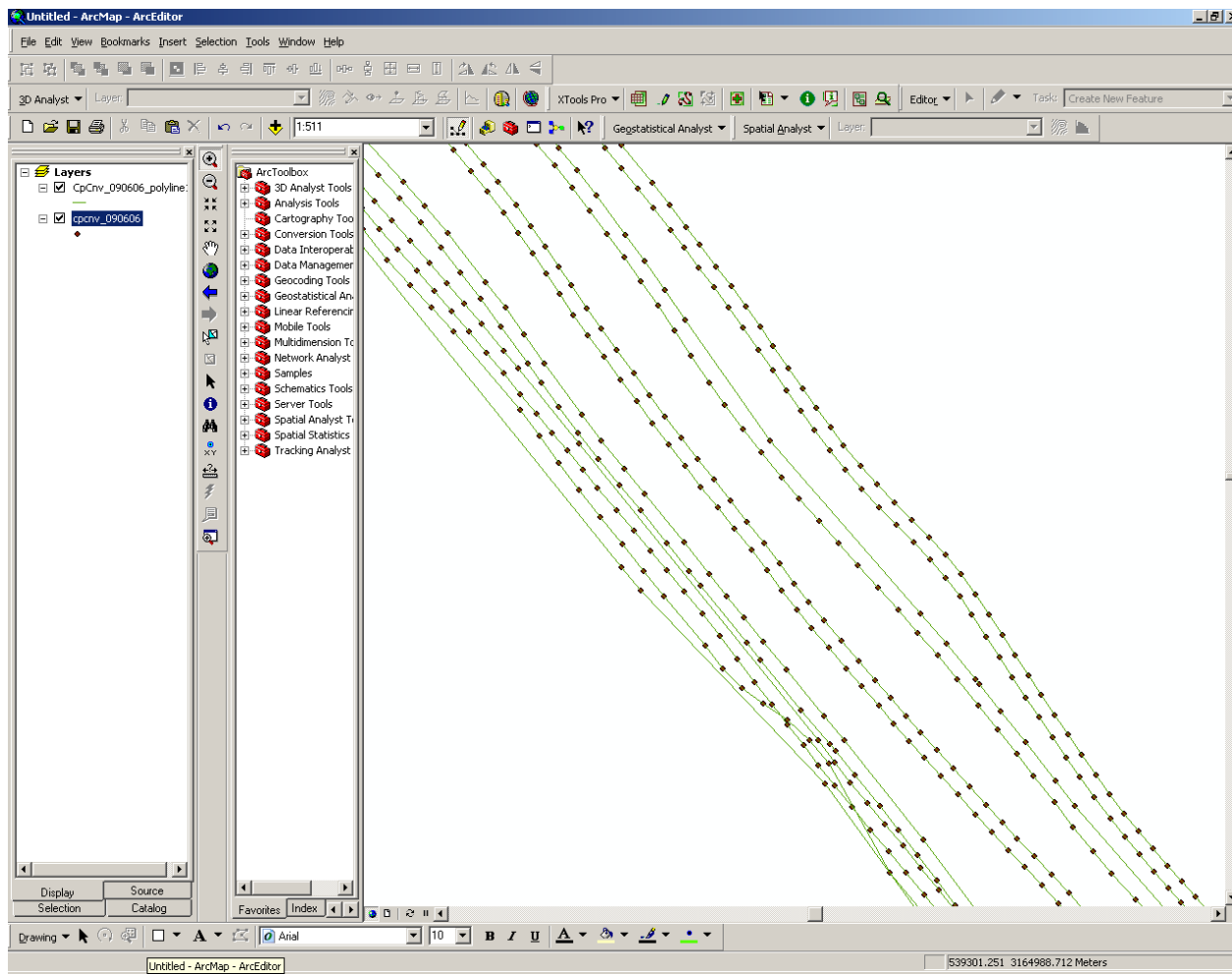


Figure C-7. An example of the polylines created from the point shape file. The polylines should follow the tracks of the towed RTK-GPS array.

## Cutting the Single Polyline Constructed in A 1.2.2.1

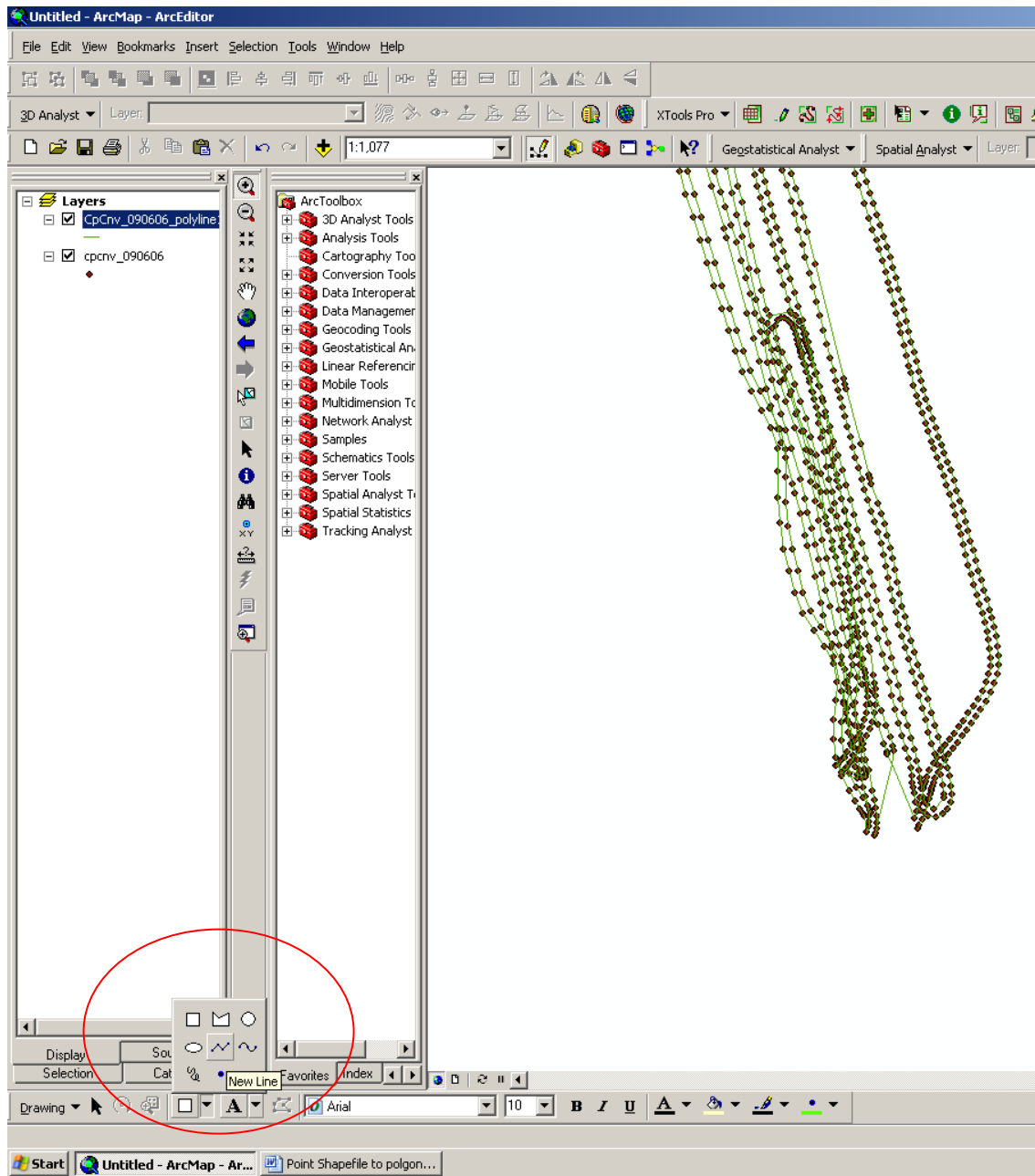


Figure C-8. Creation of a Polyline in XTools Pro. The polyline created in XTools Pro (previous step) is a single line. In order to create an a single line as an outline for a polygon containing all data points the inner segments of poly line need to be removed. To begin this process open the drawing toll in the “New Line” configuration shown above.

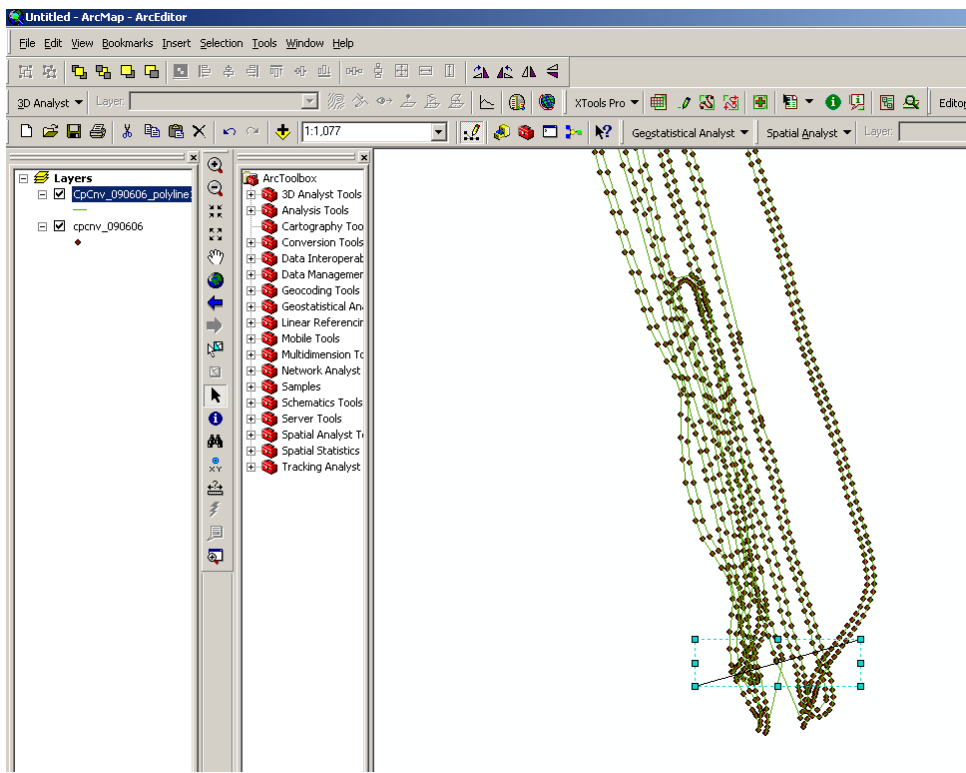


Figure C-9. Drawing a line that cuts across the Polyline at each end of the data set. In this case at the northern extent of the data as shown in this figure cutting across the souther data extent.

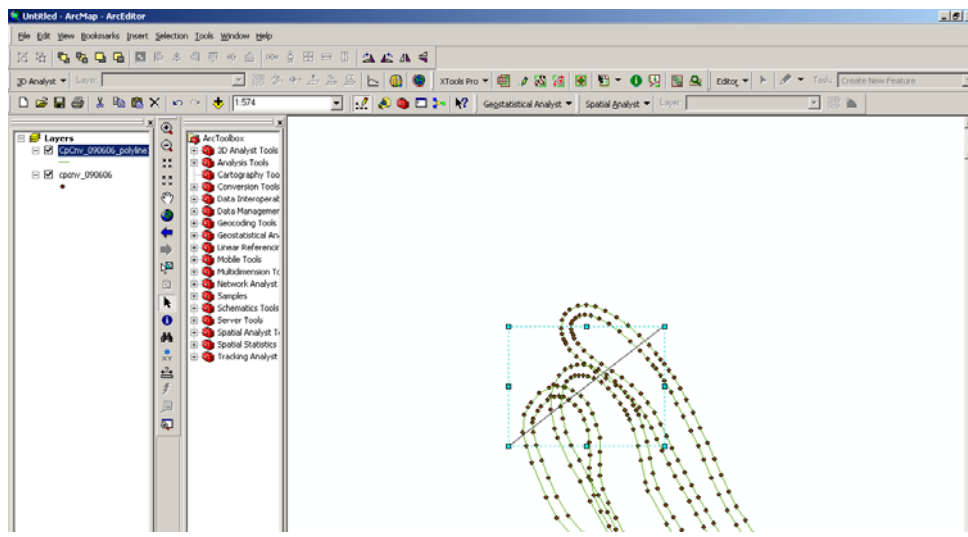


Figure C-10. Drawing a line cutting across the data at both “ends” of the data. This example shows a line cutting through the northern extent of the data. Make sure both lines are “Deselected” by clicking outside of the drawing box.

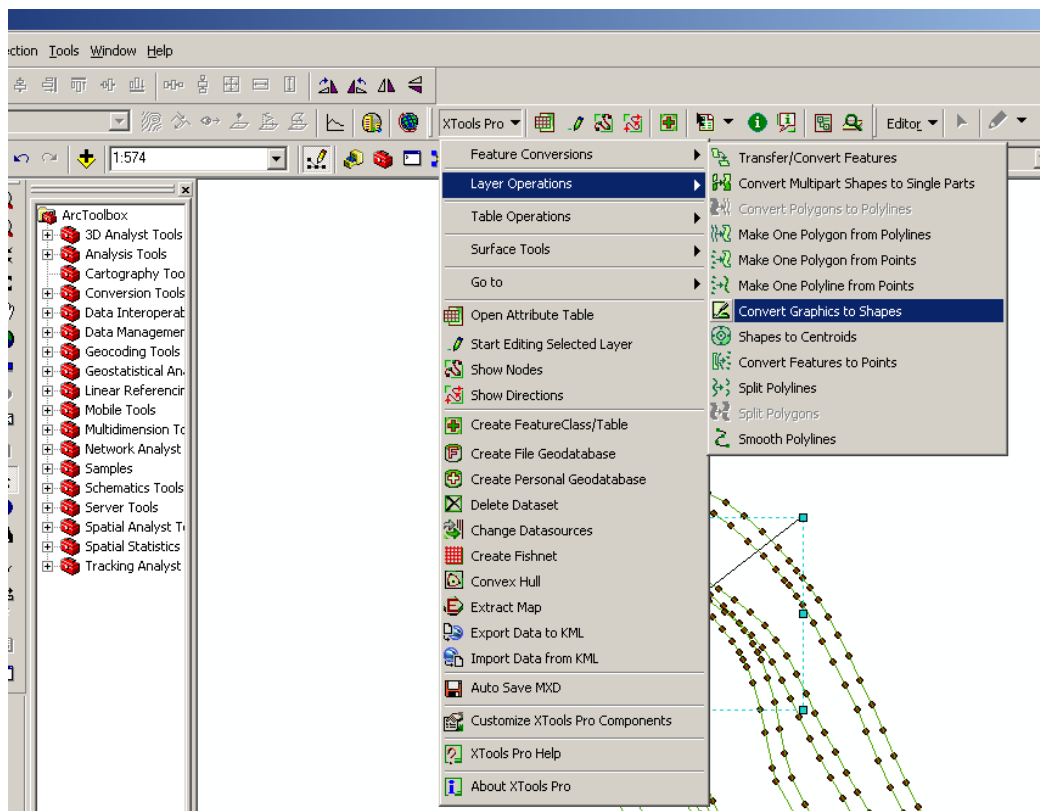


Figure C-11. Use XTools Pro to convert both of the “drawn” lines to shapefiles by selecting “Layer Operations” in the XTools Pro drop down menu. Then by selecting “Convert Graphics to Shapes” in the “Layer Operations” drop down menu.

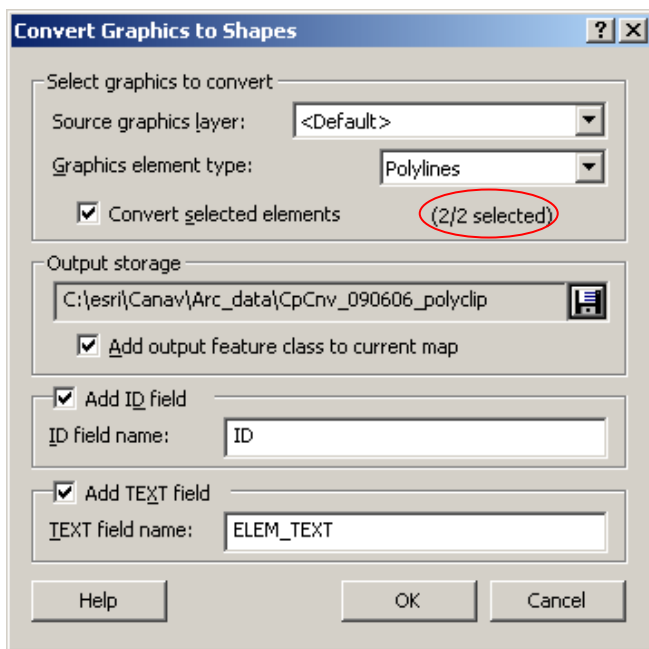


Figure C-12. Selection of the “drawn” lines. Make sure both of the drawn polylines are selected, save the shapefiles in a work folder and add to the map.

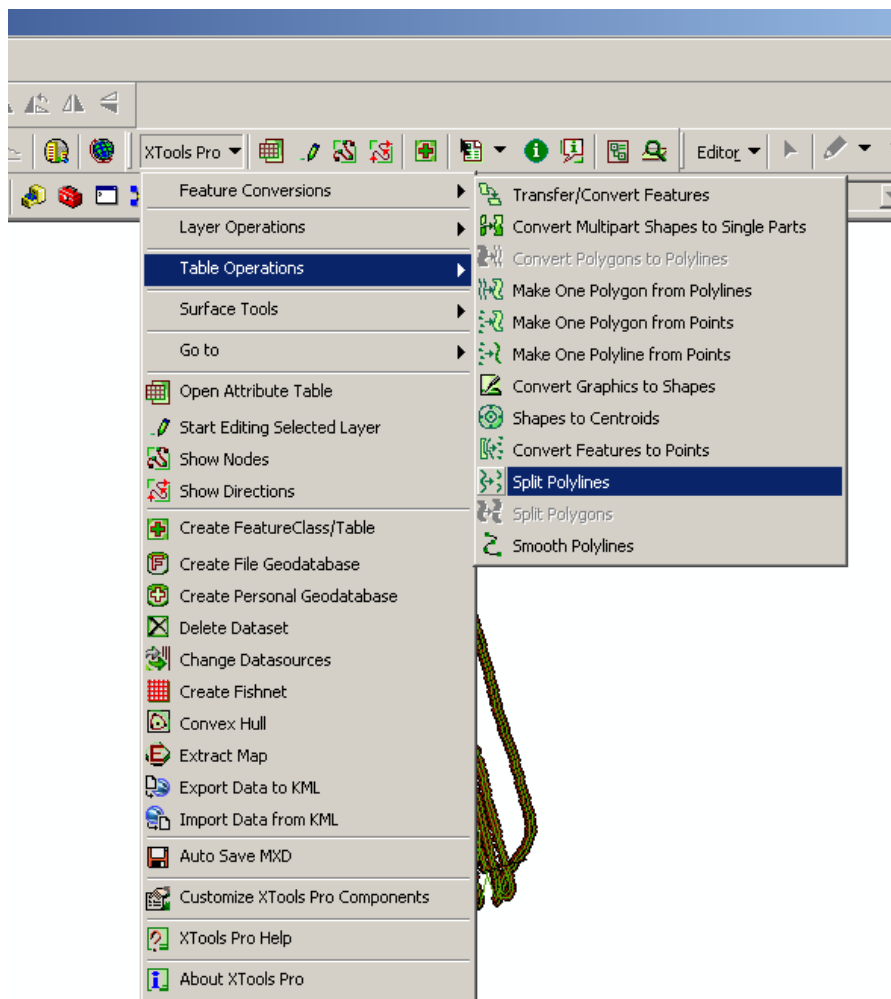


Figure C-13. Instructions for splitting the single data poly line with the two drawn shapefiles created in the previous step. This is done by selecting the “Split Polyline” option under the “Table Operations” menu in XTools Pro.

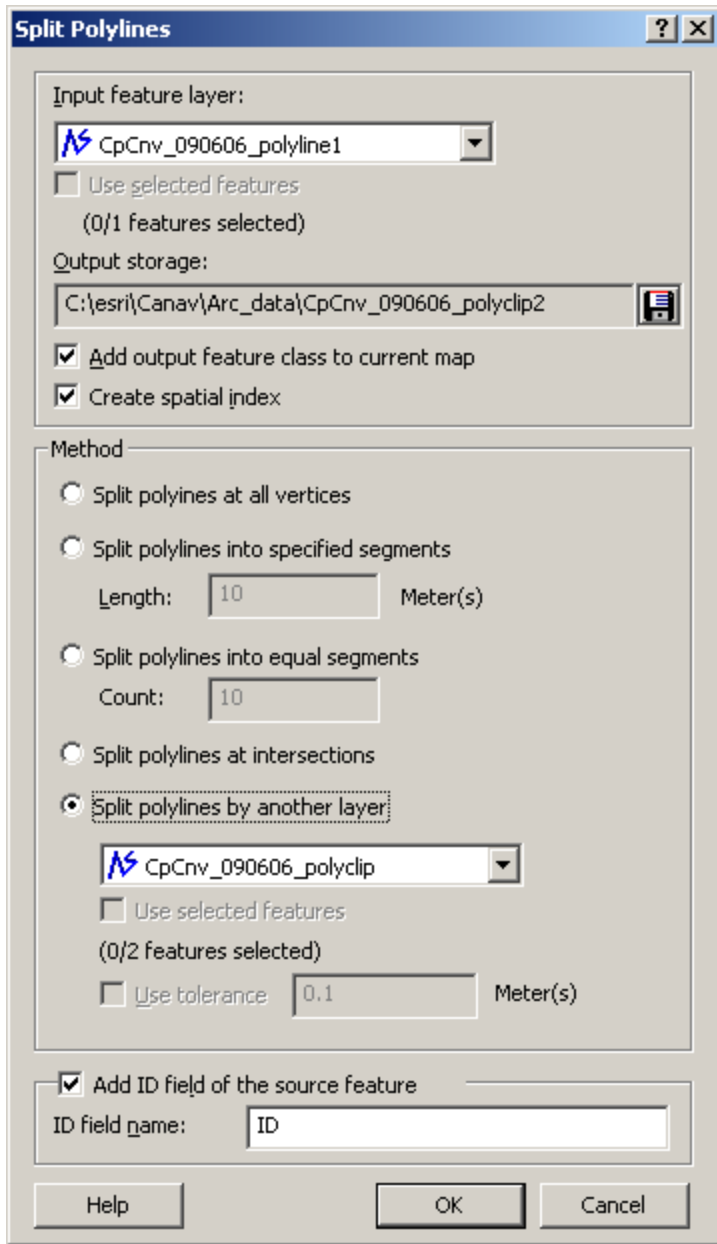


Figure C-14. Select the single polyline created from the data in step C-13, select the work folder for the data and name the Polyline shapefile that will be created.

## Editing the “Split” polyline shapefile

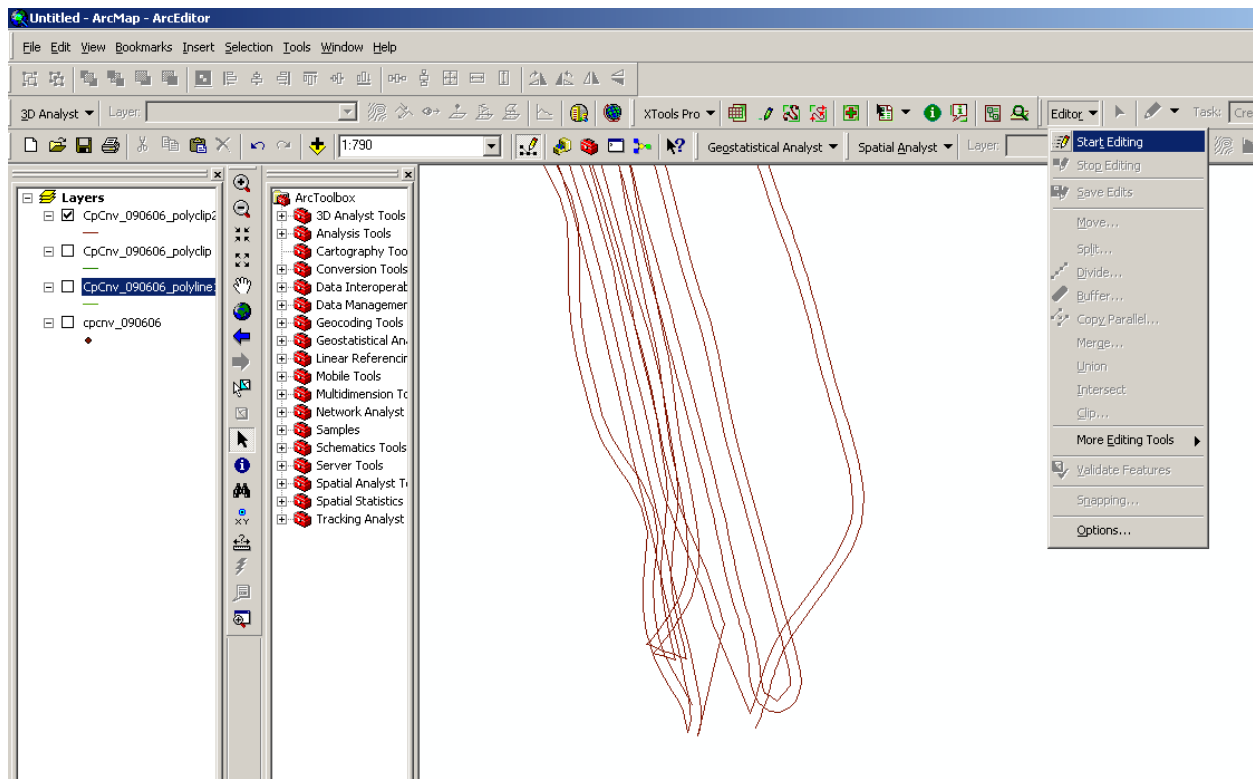


Figure C-15. Splitting of the single Polyline. In the ArcMap Editor toll bar, select “Start Editing” for the drop down menu. Be sure to select the shapefiles that contain the “Split” polyline.

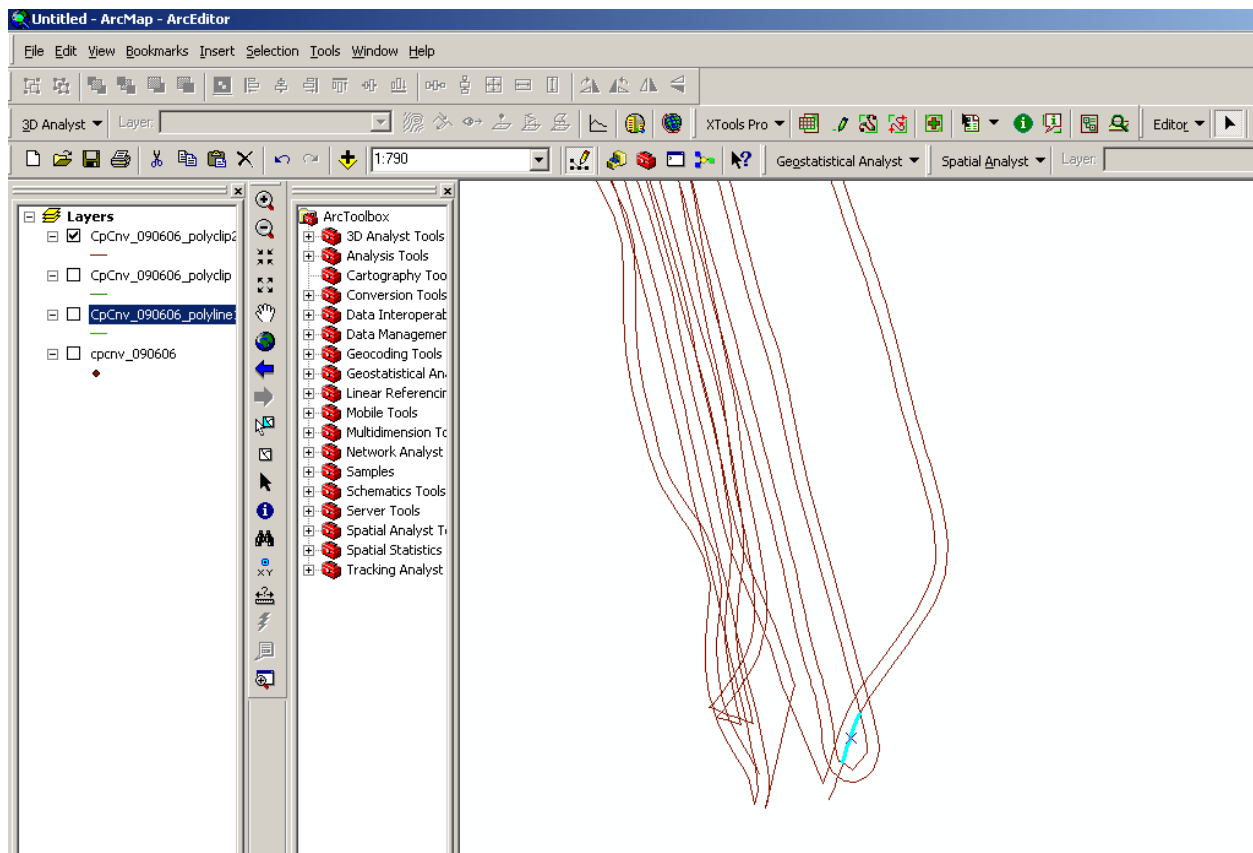


Figure C-16. Using the Edit tool to delete line segments internal to the outer lines surrounding the data. This may take up to an hour.

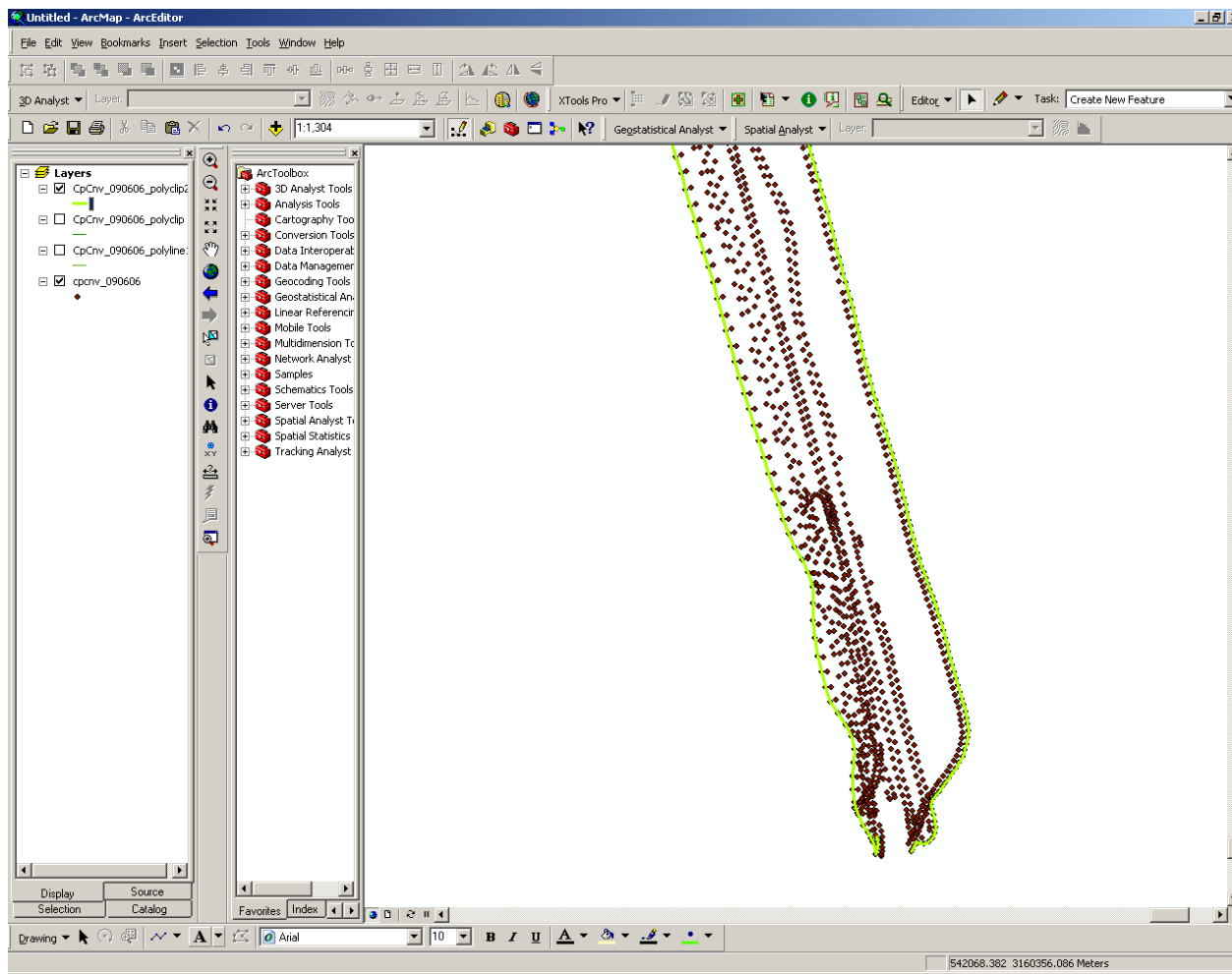


Figure C-17. Removal of extra line segments in ArcGIS. After all internal line segments are removed save your edits and ensure that the resulting polyline surrounds the point shape file data.

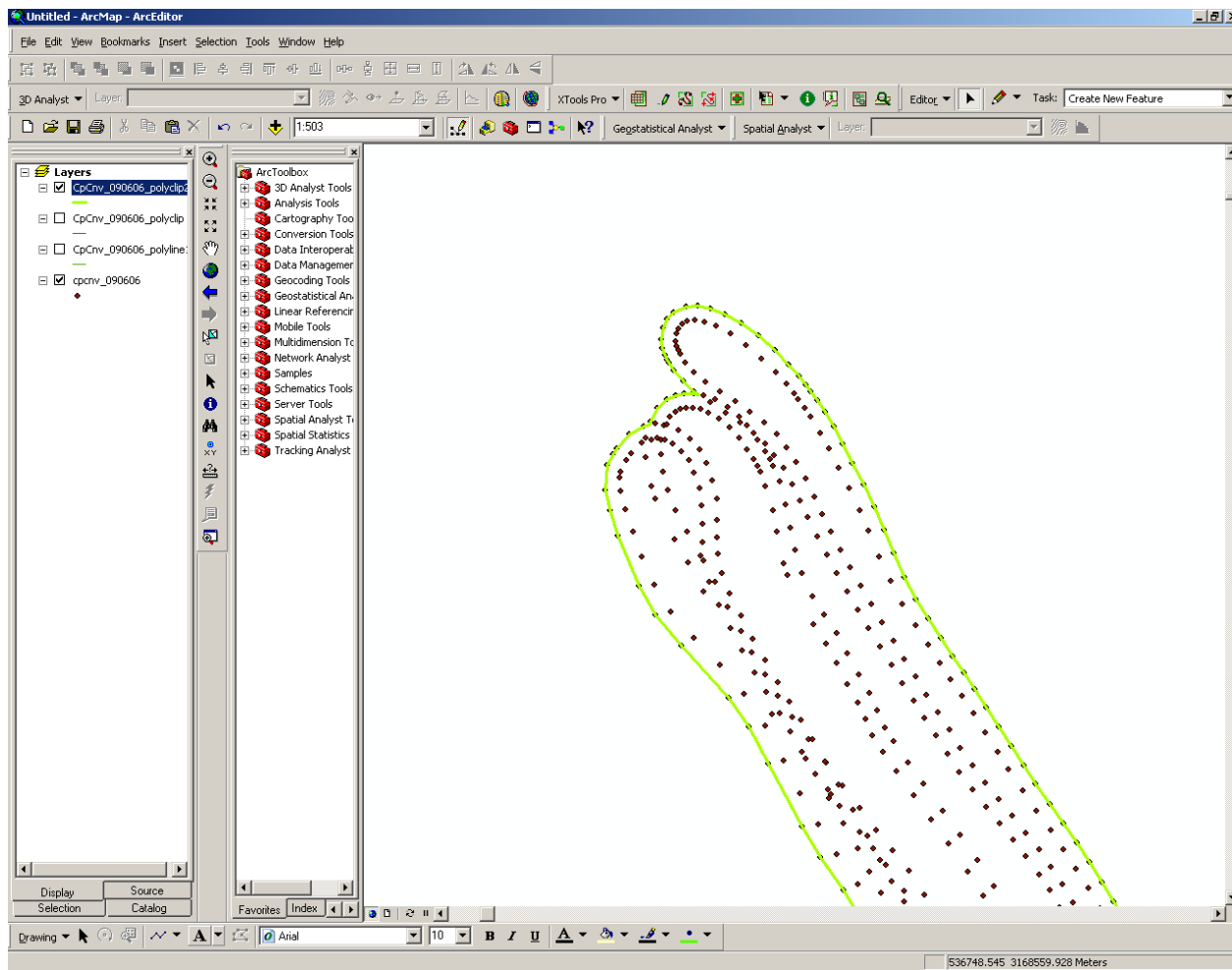


Figure C-18. Checking of the single Polyline in ArcGIS. After removing all the unwanted polyline segments, check your polyline to ensure they cover the outside-most points. Zoom in and inspect along the entire perimeter to make sure that there are no stray small segments attached to the boundary polyline. This may cause errors in the polygon construction. Again make sure that the edits have been saved and “stop editing” has been selected.

## Using XTools Pro to Make a Single Polygon Surrounding all Data from the Polyline

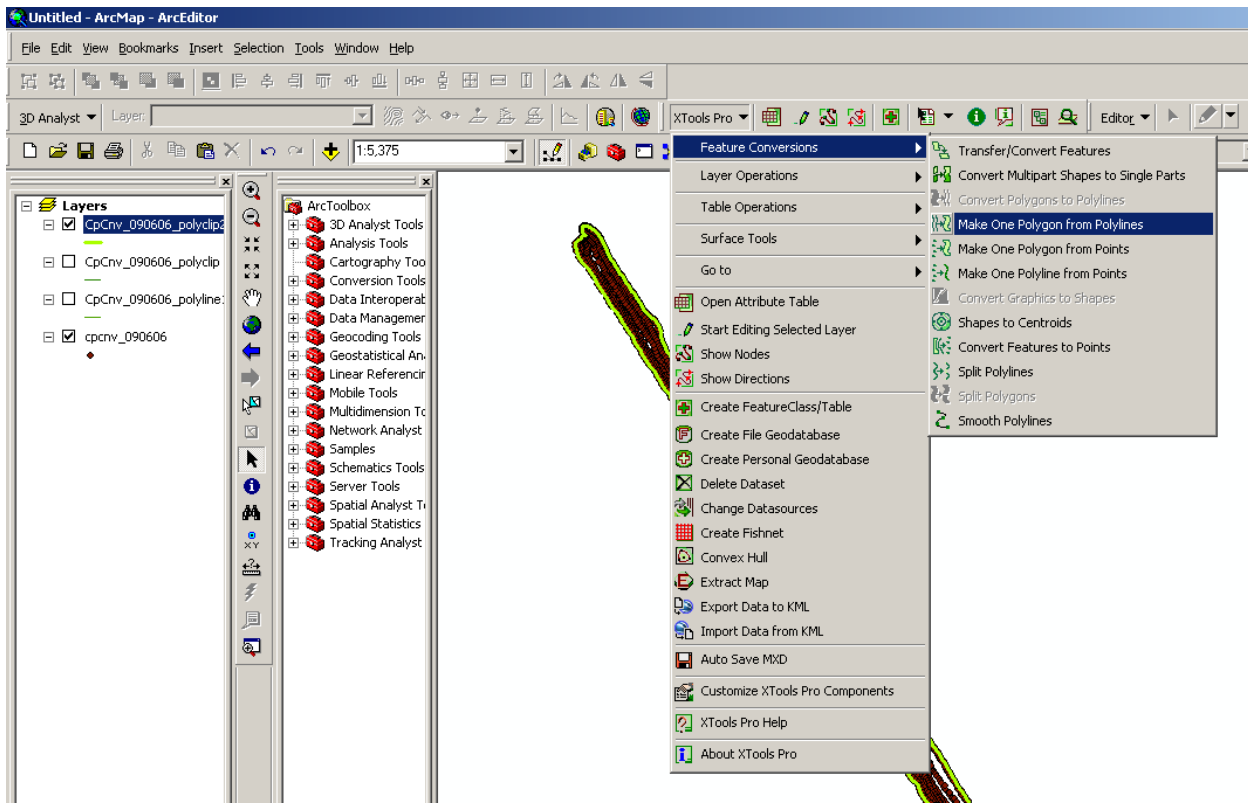


Figure C-19. Conversion of Polyline to a Polygon in ArcGIS. Under the XTools Pro drop down menu select “Feature Conversions” then “Make One Polygon from Polylines”.

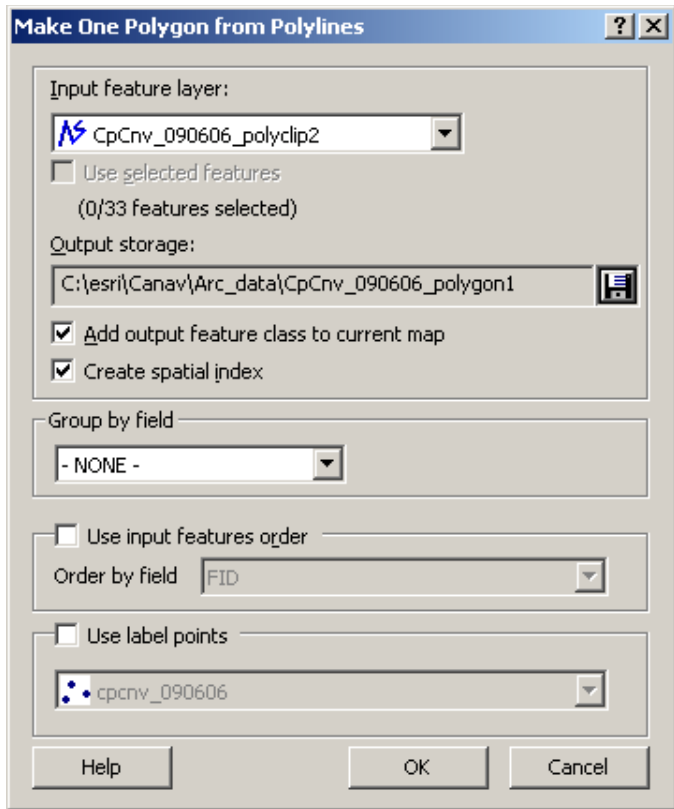


Figure C-20. Screens shot of Polygon creation settings. Use the Polyline created in the previous steps that surround the point shapefile data. Name and save the Polygon in the work folder.

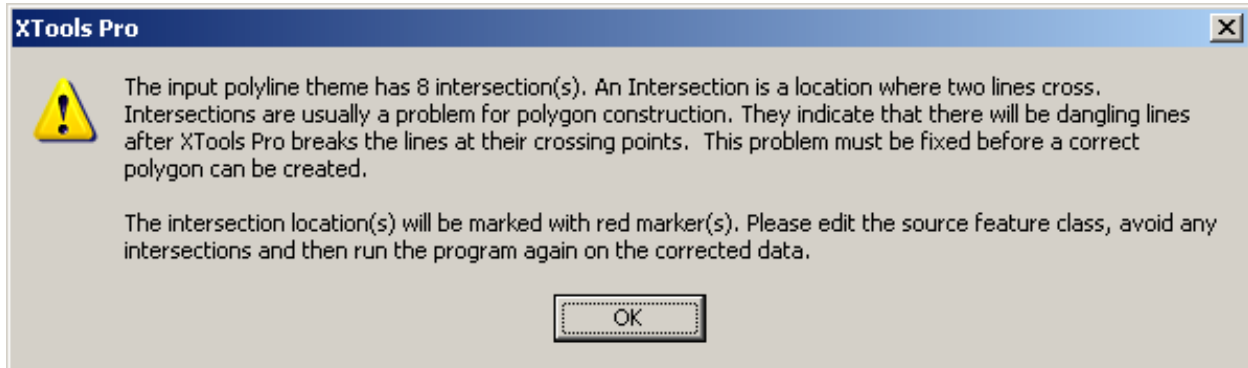


Figure C-21. Error message if spurious points are not eliminated. If you receive this error message there are intersection points and extra line segments in the polyline surrounding the data. To solve this issue return to the ArcMap Editor tool bar and “Edit” the polyline.

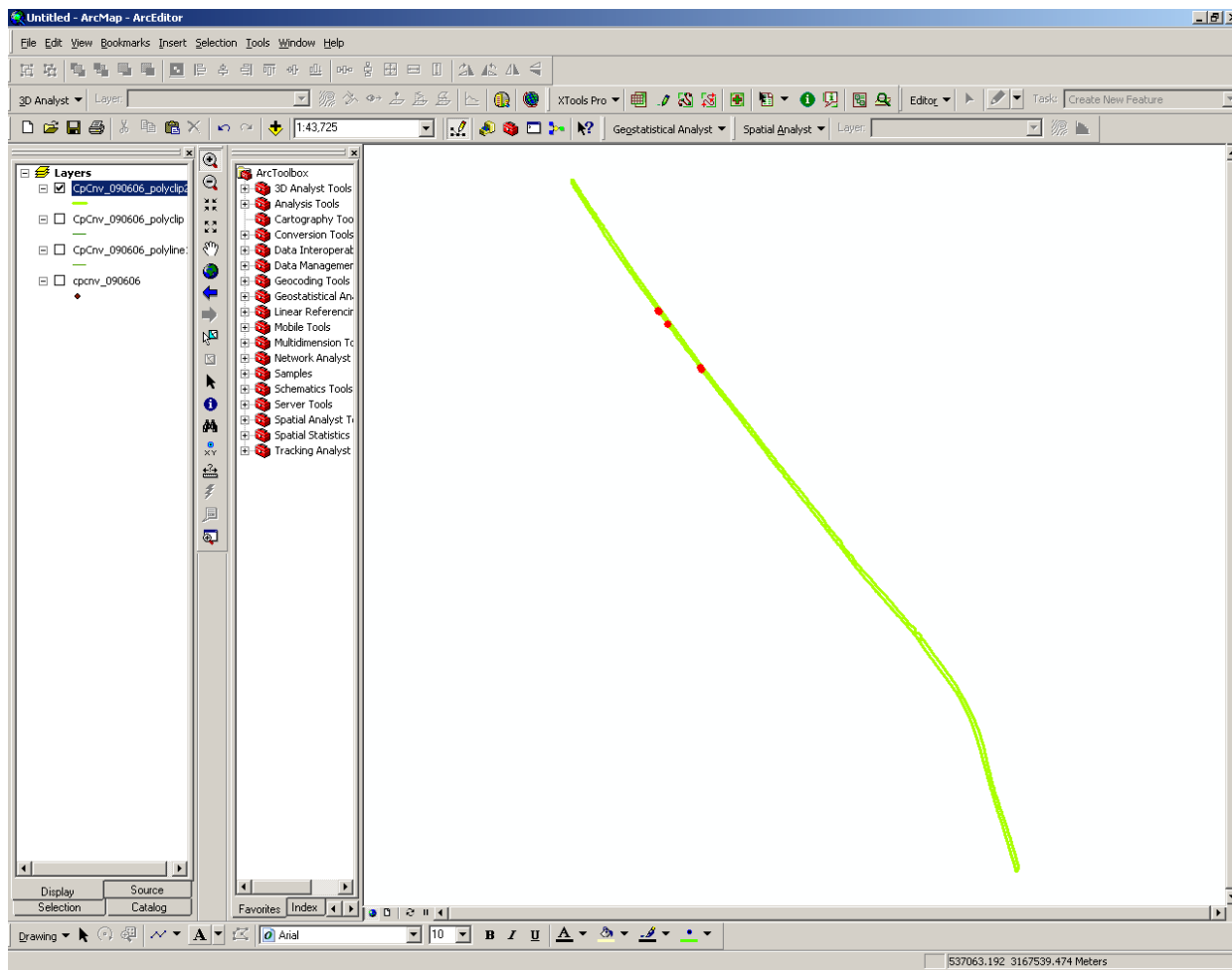


Figure C-22. Screen shot of location of extra line segments. The location of the extra line segments will be highlighted by red circles as shown above.

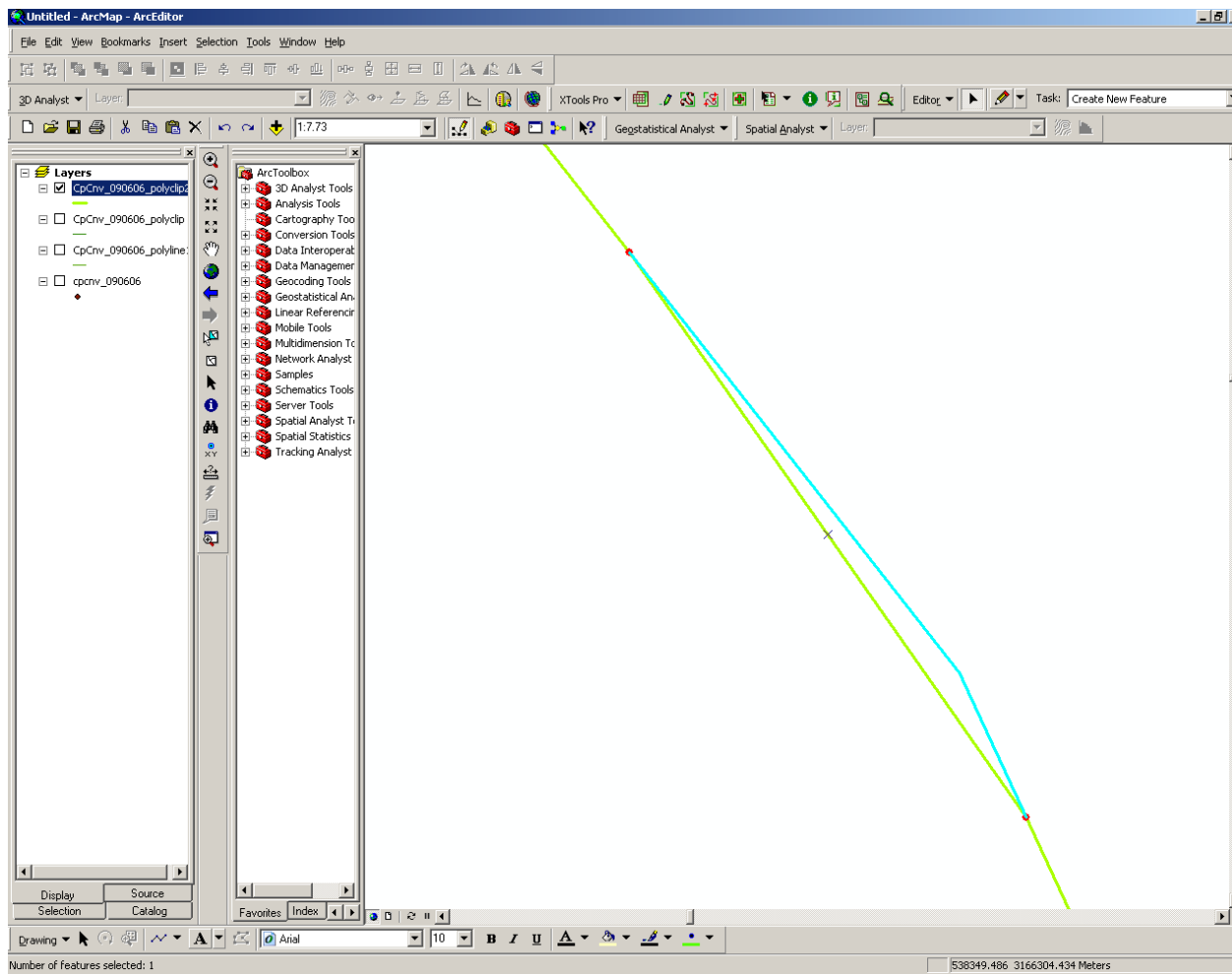


Figure C-23. Removal of extra line segments in ArcGIS. Use the ArcMap “Zoom” tool to enlarge the location of the extra line segment and use the ArcMap “Edit” tool to remove the line segment as demonstrated above. Save and stop editing, then recreate the polygon.

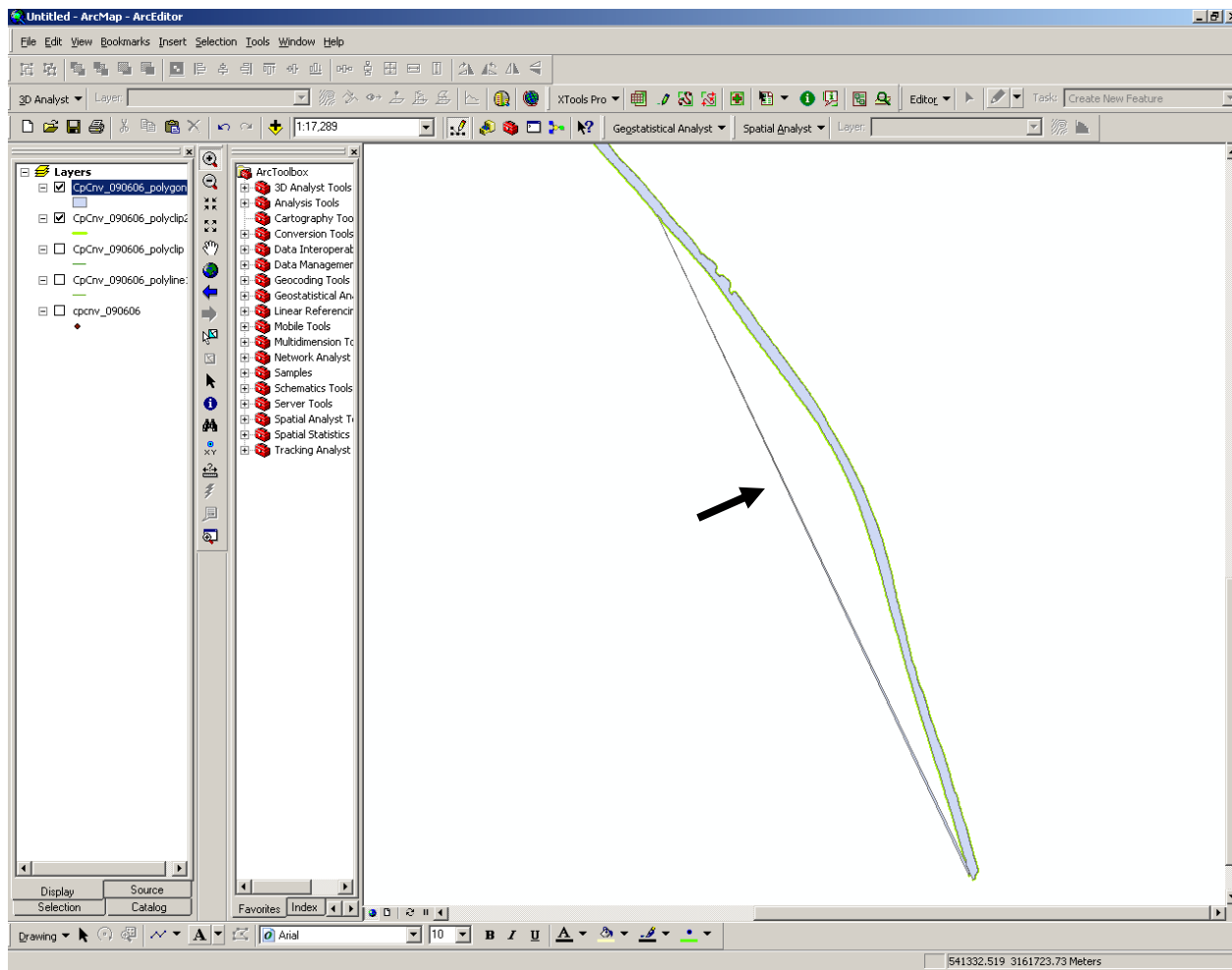


Figure C-24. Screen shot of polygon with spurious data. If the created polygon does not surround the data points or has a extra portion in a space with no point data (see arrow above) there are additional line segments that need to be removed.

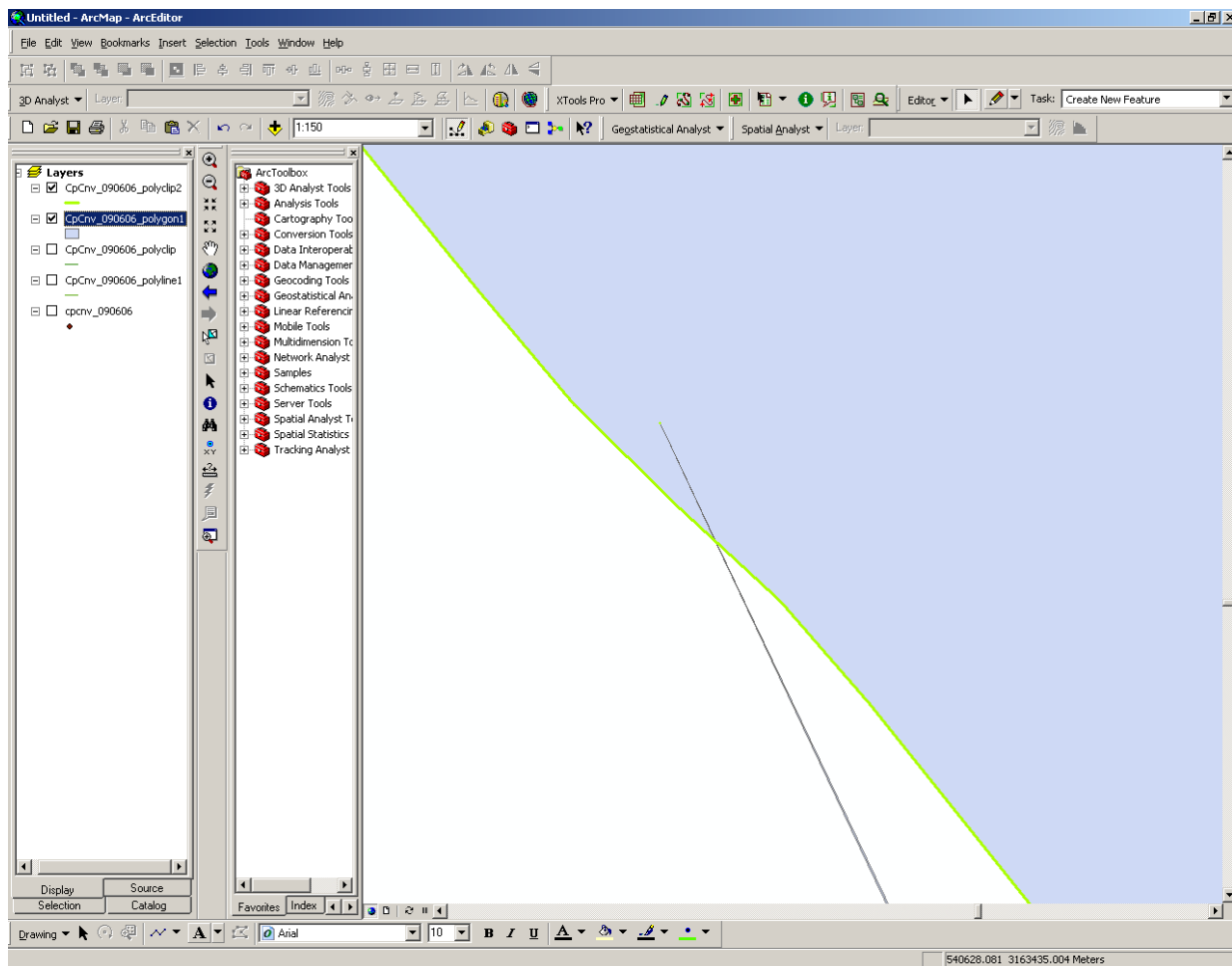


Figure C-25. Removal of polygon intersections. Zoom in on the area where the extra polygon seems to intersect a point inside the main polygon (arrow above) and activate the ArcMap Editor too. Select the polyline and remove the extra portion of the polyline. Stop and save edits. Redo the conversion of the polyline to a polygon in XTools Pro.

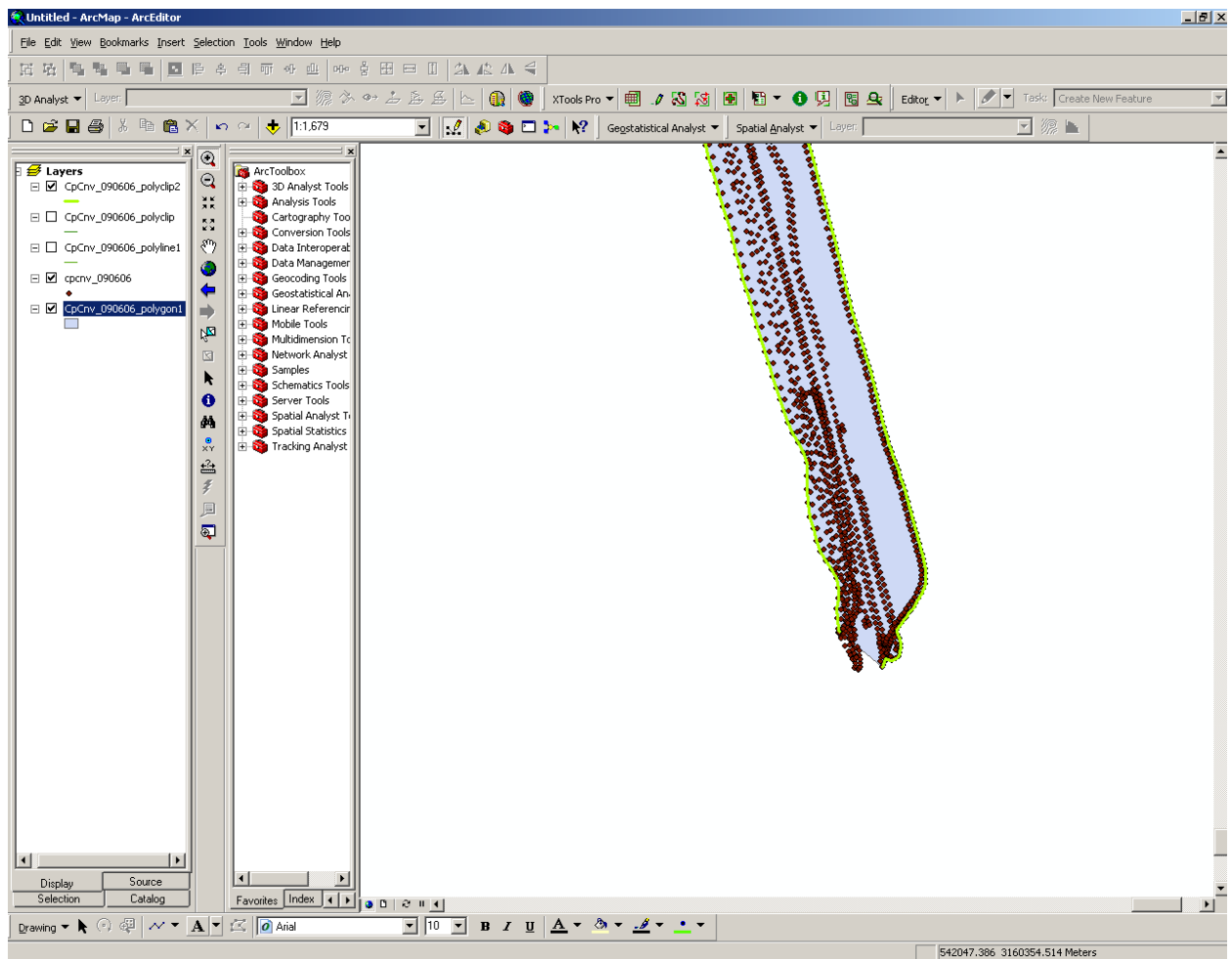


Figure C-26. Review the polygon that was created to ensure the polygon that contains all of the data points that are to be included in the construction of the TIN.

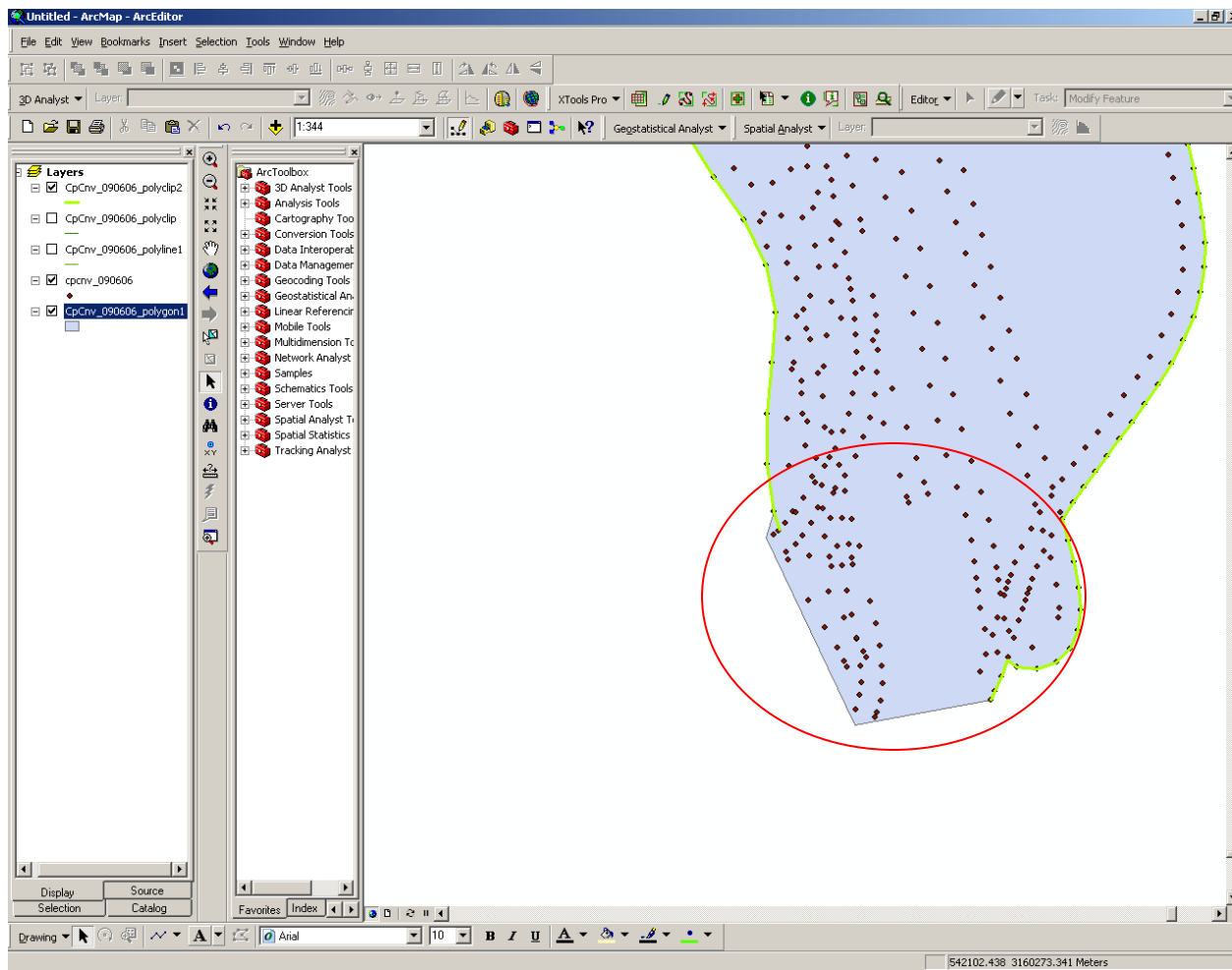


Figure C-27. Adjustment of the polygon to cover all GPS data. Once you have a polygon that contains all of the data points that are to build the TIN review the ends of the polygon to ensure it covers all of the data points. Add vertices or move vertices to cover all the desired data points.

## Creating Triangulated Irregular Network

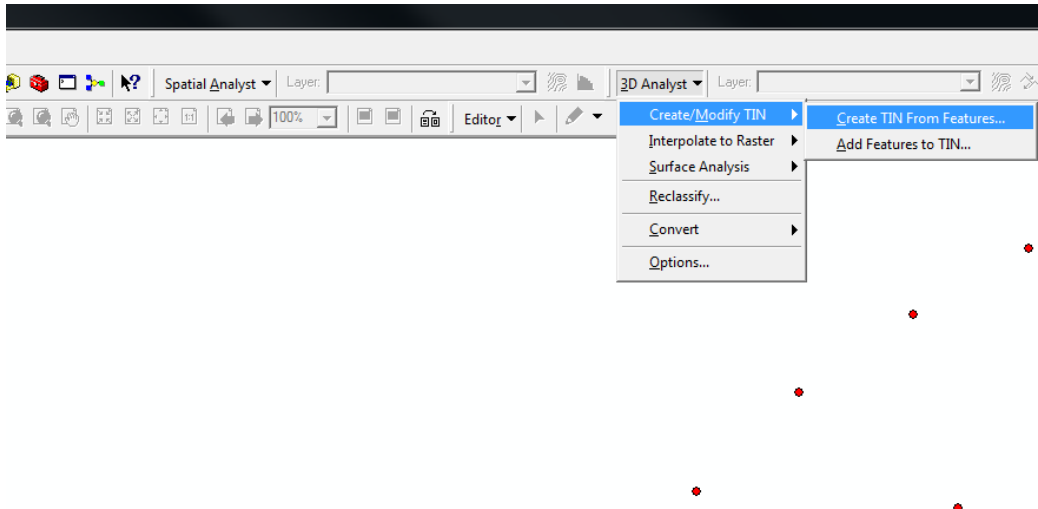


Figure C-28. Turning the GPS data into a TIN in ArcGIS. To create a TIN in ArcMap, select “Create TIN from Features” tab under the Create, Modify TIN” tab of the “3D Analysis” drop down menu.

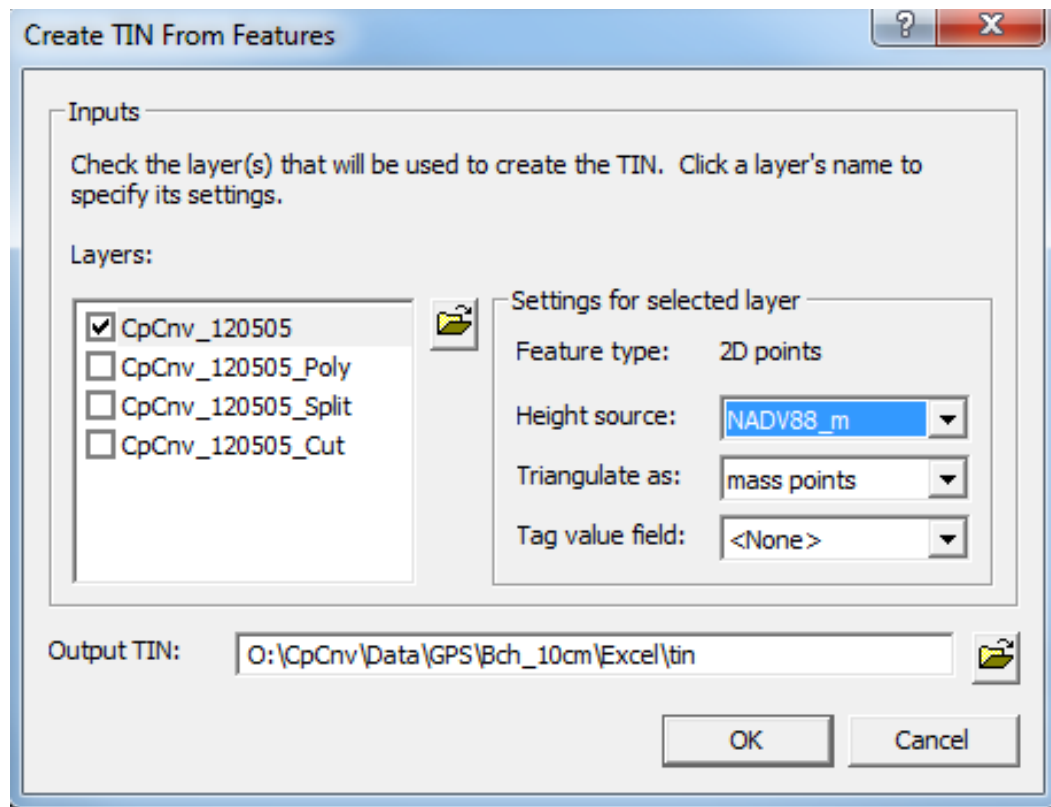


Figure C-29. Setting the height source in ArcGIS. Once “Create TIN from Selected Features” has been selected a menu box appears (see above). On the left check the box of the shapefiles that contain the point data. On the Right select “NADV88\_m” as the “Height Source” This is the elevation column in the point shape file. Under the “Triangulate as” box make sure that “mass points” is selected.

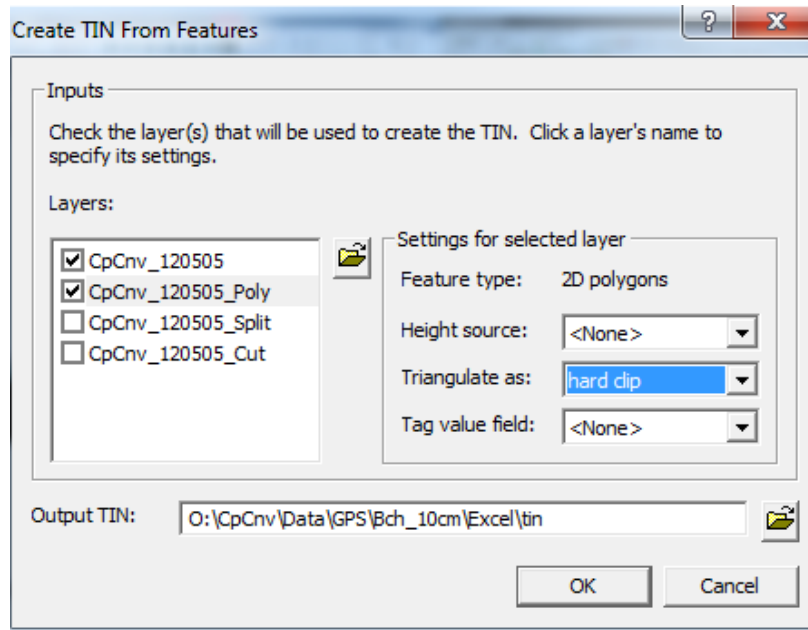


Figure C-30. Screen shot of clipping polygon settings. Next, on the left, click the box the represents the clipping polygon that surround the point data you constructed in previous steps. Make sure the “Height Source” box on the right is set to “<none>”. Set the “Triangulate as” tab to “hard clip”. This will ensure that the TIN will only calculate a surface inside the clipping polygon.

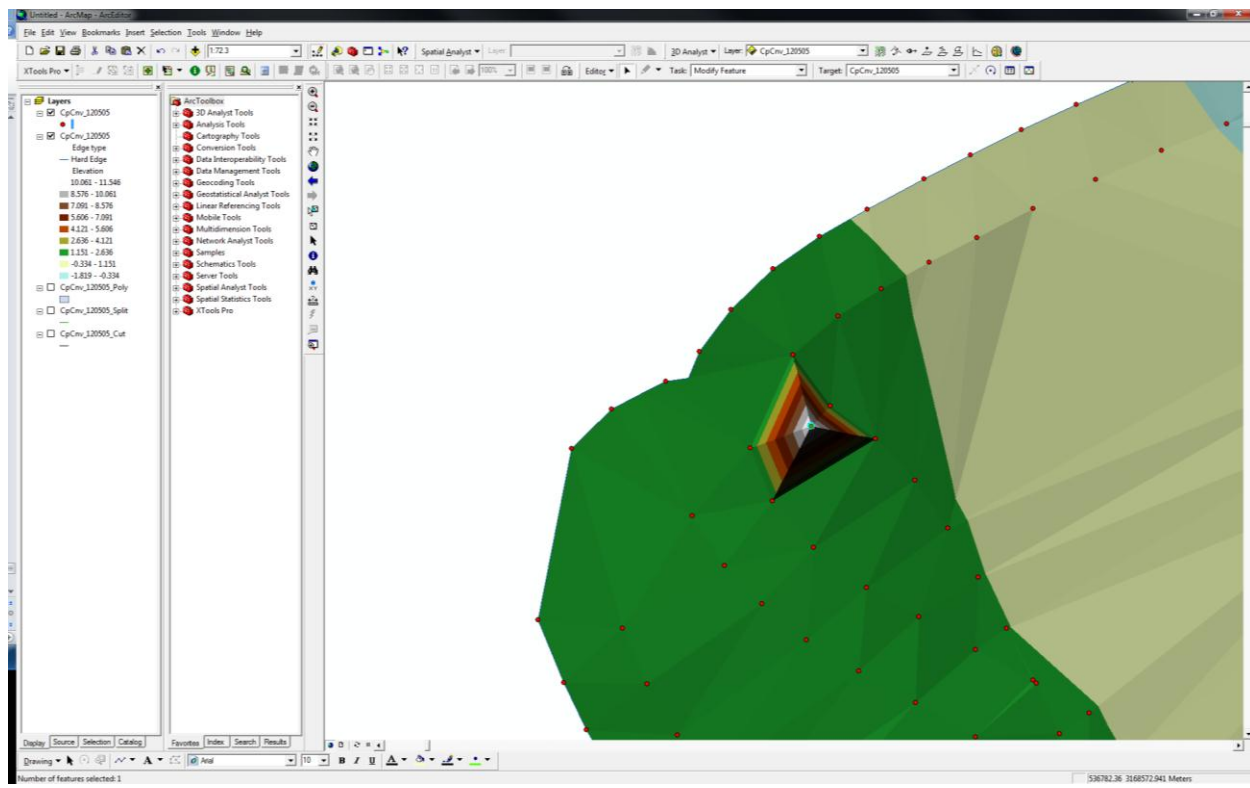


Figure C-31. Removal of spurious data from GPS data. Once the TIN is created in ArcMap review its contents for pyramids or data artifacts. If pyramids exist the points causing the pyramids must be removed by editing the point shape file. Remove the TIN from ArcMap, and delete the TIN file. Once the editing of the point shape file is complete, “stop editing” and “save edits”. Follow the steps to create a TIN, and review again. It may take several iterations to get the desirable TIN.

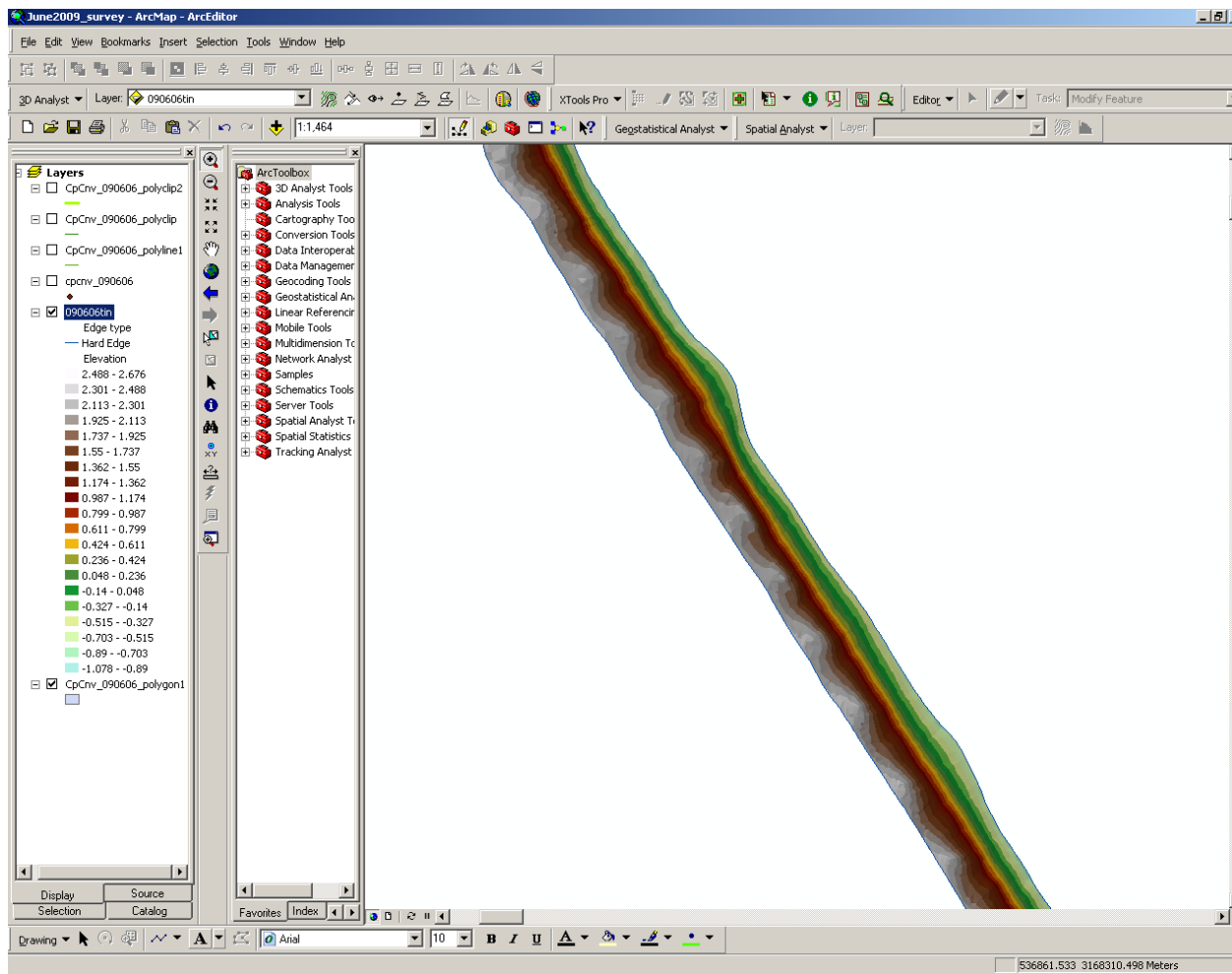


Figure C-32. Final TIN generated from GPS points. Once the TIN is complete and all edits have been completed, review it again for completeness and ensure no data artifacts or pyramids remain.

## Generate Raster from TIN

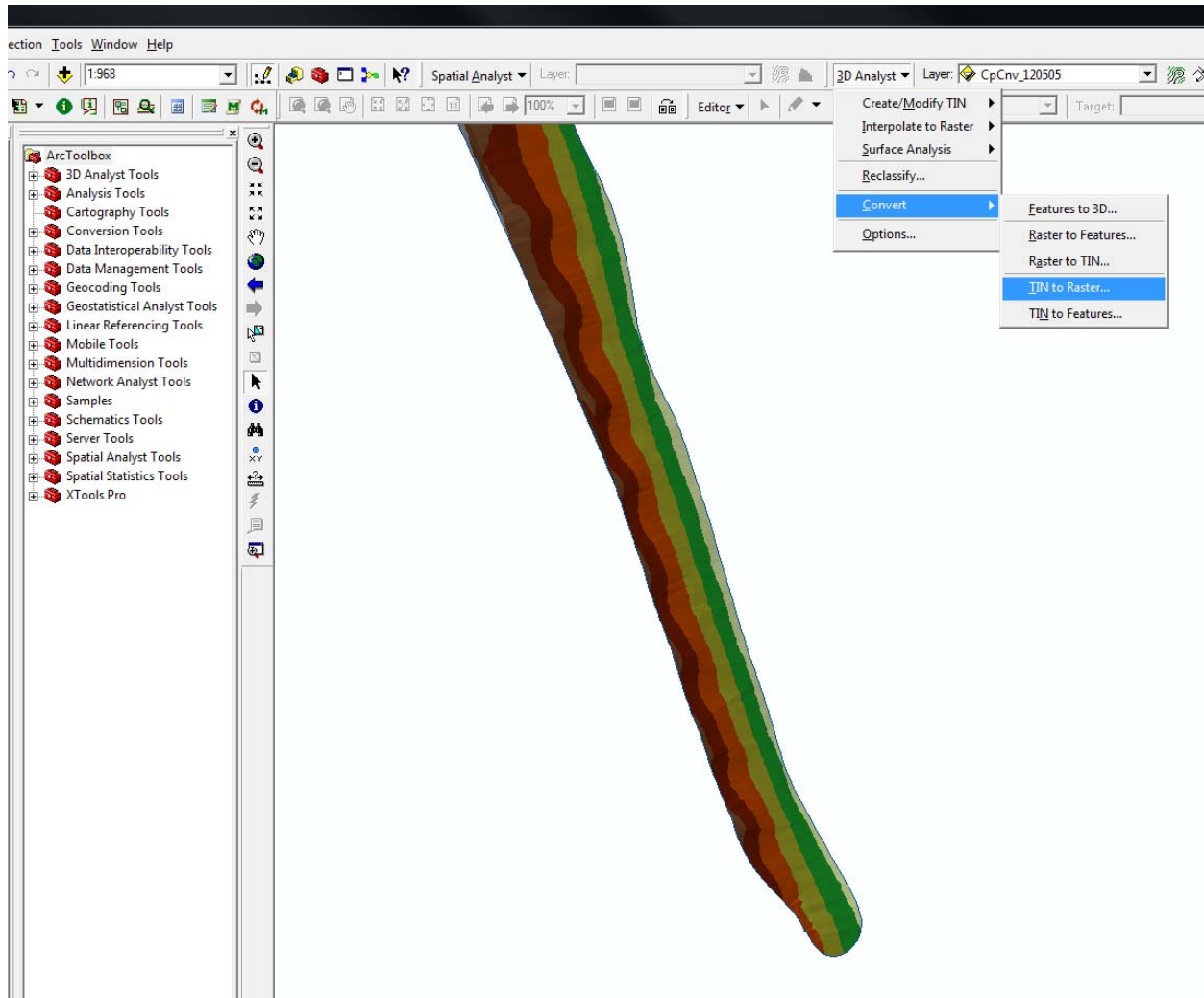


Figure C-33. Conversion of TIN to raster. Once the TIN is complete and ready for conversion to raster, click on the “3D Analysis” tool box. Select “Convert” un the pull down menu and the “TIN to Raster”. Save the Raster.

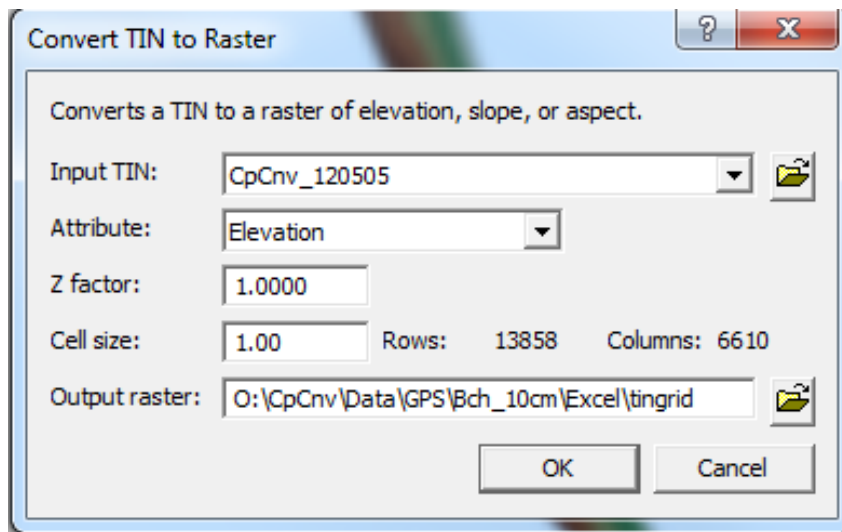


Figure C-34. Selecting the TIN used to create the raster. Under “Cell size” set size to 1.00. This sets the raster to build a grid of 1 m by 1 m squares. Save the Raster.

## Creating a Mean High Water (MHW) Contour in ArcMap

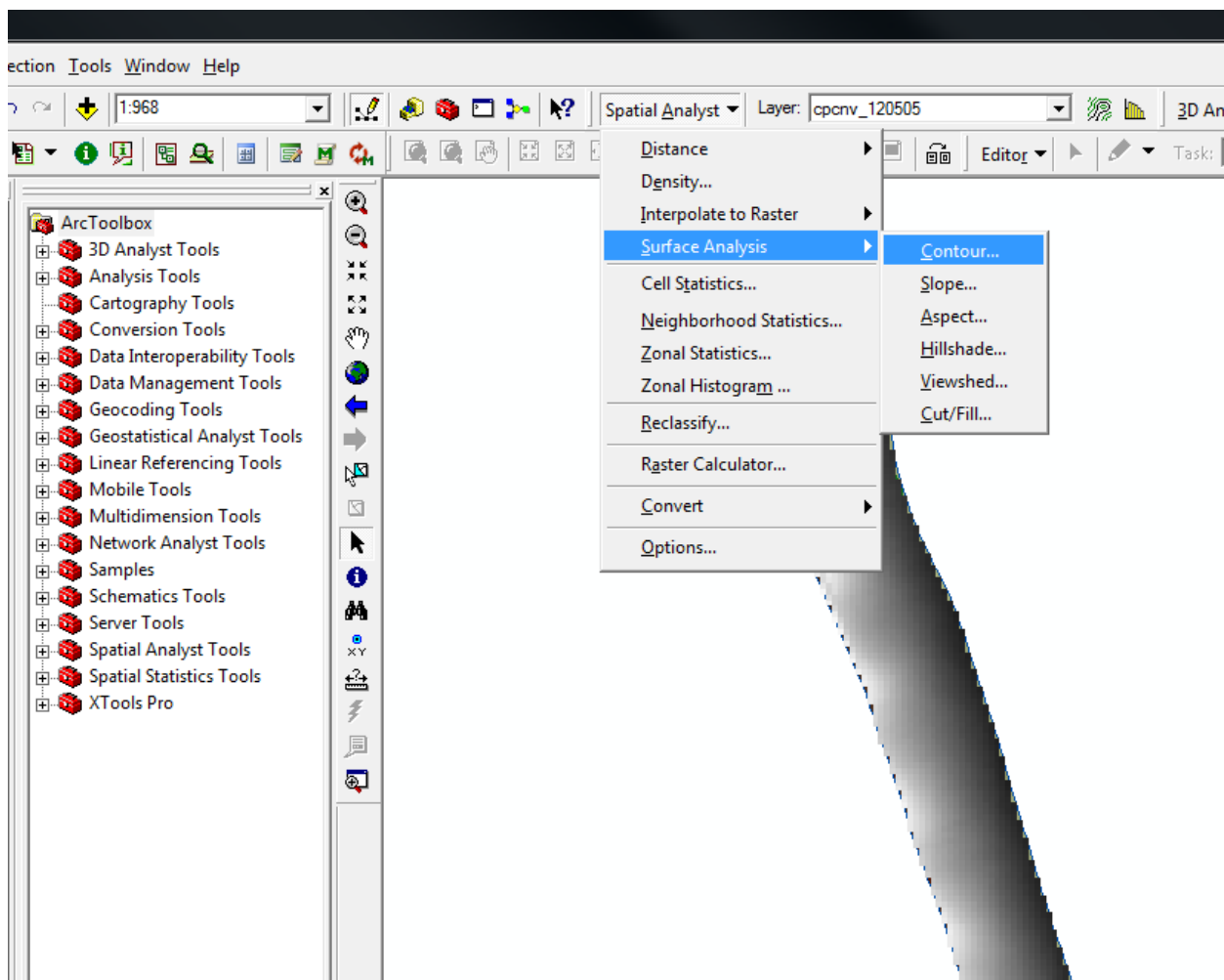


Figure C-35. Screen shot of contour settings in ArcGIS. To build a single Mean High Water (MHW) contour in ArcMap, select “Surface Analysis” under the “Spatial Analysis” pull down menu. Select “Contour” under the Surface Analysis menu.

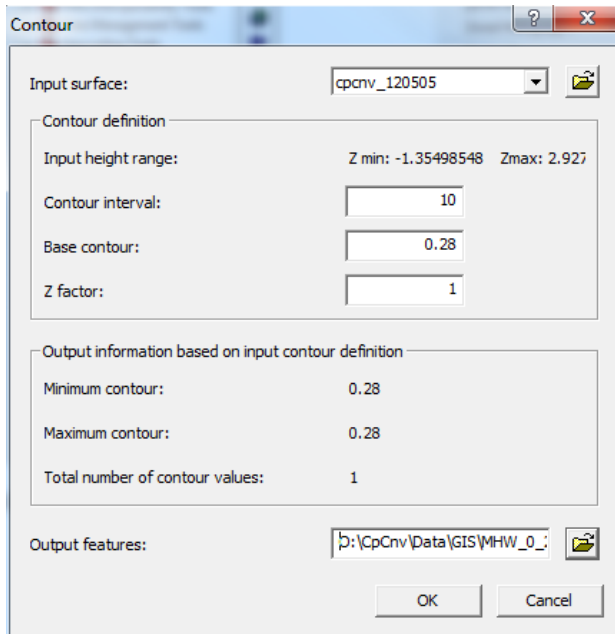


Figure C-36. Setting ArcGIS to set contour elevation. Under the “Contour” menu set the contour interval greater than the range of elevations. In this case “10” as a contour interval of 10 m is greater than the -1.445 to 2.948 m range of the raster DEM. This forces the 3D Analyst tool box to create a single contour at the elevation of the “Base Contour” set in the next box. The “Base Contour” should be set to the desired elevation, in this case it is set to 0.28 m (MHW for Cape Canaveral). Save the contour in the desired location.

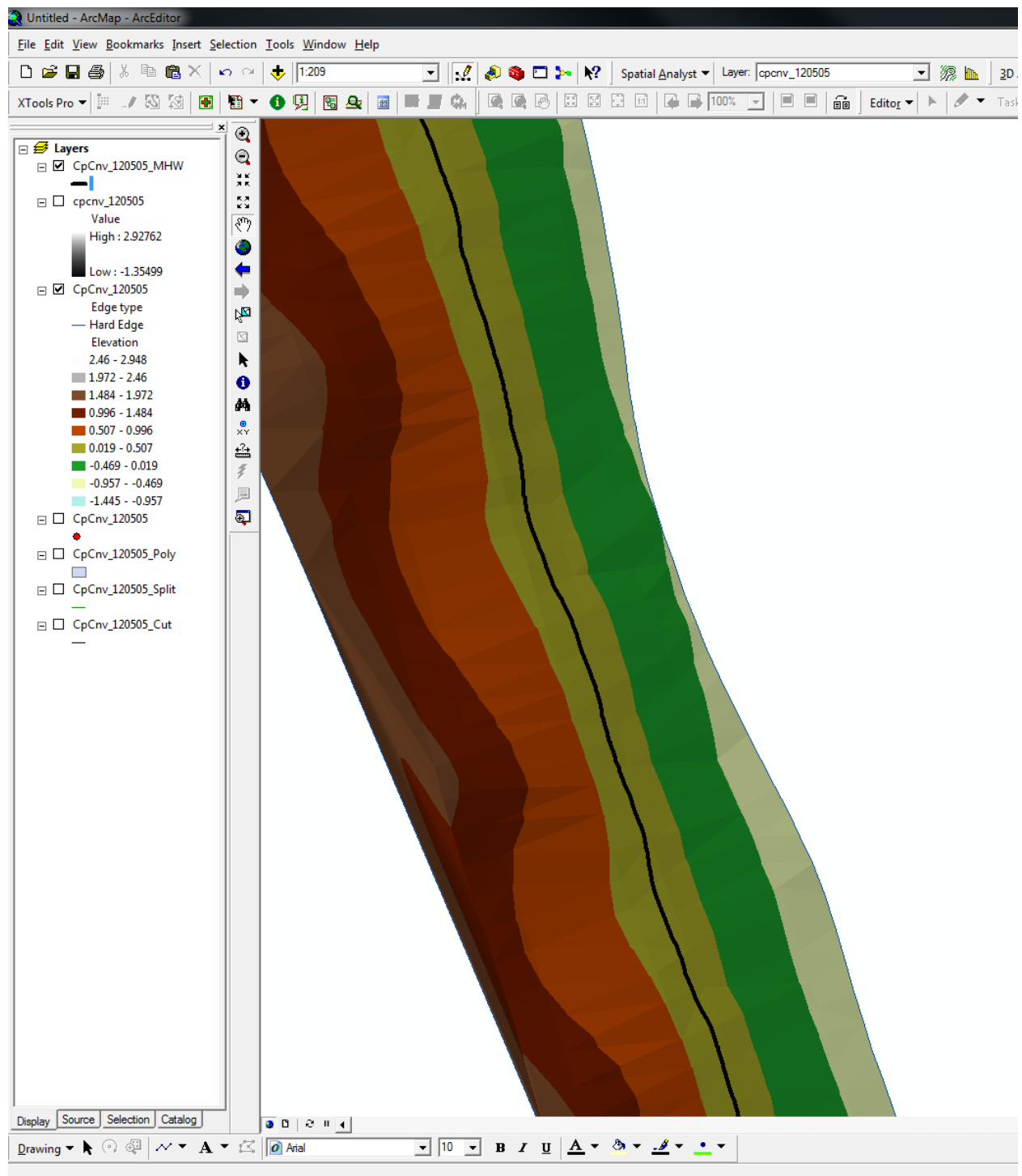


Figure C-37. MHW contour intersection with TIN. As a QA/QC measure, check the elevation of the MHW contour created in the previous step to make sure it falls in the correct color band of the TIN. In this case the MHW contour (black) is in the center of the olive bar representing elevations between 0.019 and 0.507 m. The desired countour elevation was set at 0.28, so this is a positive check.

## APPENDIX D CAPE CANAVERAL WAVE CLIMATE

Seasonal wave climate and storm patterns for the Cape Canaveral area were characterized using surface ocean buoy measurements and Oceanweather Inc. wave hind cast data. Buoy data was provided by the NOAA National Buoy Data Center (NDBC) for both annual study periods (May 6, 2009 to May 2, 2010 and May 2, 2010 to April 19, 2011) and for a monthly long-term averages (August 1998 – December 2008). Wave Data from the NBDC (<http://www.ndbc.noaa.gov>) for buoy 41009 located ~20 nm east of Cape Canaveral in 44.2 m of water (Figure D-1). The long-term averages for NOAA buoy 41010 located ~120 nm east of Cape Canaveral in 872.6 m of water were also examined for 20 year monthly averages (Figure D-1). NOAA buoy data are sampled hourly. Oceanweather, Inc. provided a hindcast of wave conditions for an extended period (1958-2008) for a location ~ 30 nm east of Cape Canaveral at a depth of 220.4 m using methods described in Oceanweather Inc. (Figure D-1) ( 2006), Cox and Swail (2000) and Swail and Cox (2001). Data for the Oceanweather, Inc. hindcast were sampled at 3 hour intervals. The Oceanweather data provided the longest (54 years) average monthly wave conditions. Three key wave parameters were measured and analyzed for NOAA buoy data: significant wave height,  $H_s$ , the average of the highest third of the waves, the dominant wave period,  $T_P$ , the period of the waves having the greatest energy and the average wave period  $T_{AVE}$ , the average period of the waves. Oceanweather data analyzed for long-term monthly averages were  $H_s$  and  $T_P$ . All data sources for this study were placed in monthly bins for monthly average analysis. NOAA buoy 41009 was analyzed at 1 hour intervals for wave events > 3 m for the two survey periods (May 2009 – April 2010 and May 2010 – April 2011).

## **Seasonal Wave Data**

To evaluate seasonal or dominant weather patterns of wave forcing at Cape Canaveral buoy and hindcast data were divided and averaged into monthly bins. At NOAA buoy 41010, the furthest of the studied data from shore (120 nm) and in the deepest water (872.6 m), the months of January, February and March have the highest  $H_s$  (1.9 m), with the months of October, November and December having a slightly lower  $H_s$  (1.8 m). June, July and August have the lowest  $H_s$  (~1.05 m) (Figure D-2). There is a pronounced decline in  $H_s$  in April and May during the transition from the higher  $H_s$  conditions into the low  $H_s$ , and a pronounced increase in  $H_s$  in September during the transition from low  $H_s$  to higher  $H_s$  conditions (Figure D-2).

The pattern at the Oceanweather, Inc., hindcast location with a longer data record (54 years) located in 220.4 m of water, ~ 32 nm from shore is similar to the deepwater buoy 41010 with October, November, December, January and February have the highest  $H_s$  (~1.70 m) and June, July and August having the lowest  $H_s$  (~0.96 m). The transition from high  $H_s$  conditions to low  $H_s$  conditions is less pronounced lasting from March through May (Figure D-2). September is still the transition from low  $H_s$  conditions to the high  $H_s$  condition.

The pattern at NOAA Buoy 41009 located nearest to shore (20 nm) and with the shallowest water depth (44.2 m) of the study is similar to the Oceanweather hindcast patterns. October, November, December, January and February have the highest  $H_s$  (~1.45 m) and June, July and August having the lowest  $H_s$  values (~0.75m). March, April and May transition into low wave energy conditions and September transitions into higher wave energy conditions (Figure D-2).

Significant wave heights (HS) for both annual survey periods (May 2009-April 2010 and May 2010-April 2011) at NOAA buoy 41009 follow the same trend as the 20 year data with a few exceptions. During the first annual survey period the May 2009 average  $H_S$  was 0.3 m greater than that of the twenty year average while in October 2009  $H_S$  was 0.38 m lower than the twenty year average. During the second annual survey period February, April, and October had lower  $H_S$  than the twenty year averages with differences of 0.31 m, 0.31 m and 0.38 m respectively, while September having a 0.31 m increase in  $H_S$  over the twenty year average (Figure D-2). During the first annual survey period the highest monthly averaged HS was recorded in November at 1.70 m, and during the second annual survey period the highest monthly averaged HS was recorded in December at 1.61 m. The lowest monthly averaged HS for both survey periods were recorded in June with HS of 0.69 m and 0.66 m respectively (Figure D-2).

At NOAA buoy 41009, the month with minimal standard deviation in  $H_S$  is July at 0.3 m and maximum standard deviation in  $H_S$  occurs in October at 0.8 m (Table D-1). During the survey period of May 2009-April 2010 the minimum standard deviation in  $H_S$  occurs in July at 0.22 m, and the maximum standard deviation in HS occurs in May with a deviation of 0.89 m. For the survey period of May 2010-April 2011 the minimum standard deviation in HS is found in June at 0.3 m, while the maximum standard deviation is found in September at 0.87 m (Table D-1). During the first survey period May had a standard deviation of  $H_S$  0.39 m higher than the twenty year average, while September had a standard deviation in HS 0.46 m lower than the twenty year average (Table D-1). The second survey period had three months (January, February and

October) with standard deviation in  $H_s$  less than 0.25 m of the twenty year average with values of 0.25 m, 0.28 m, and 0.26 m, respectively (Table D-1).

The maximum recorded significant wave height ( $H_s$ ) recorded at NOAA buoy 41009 for between 1988 and 2008 was 9.8 m in September 1999 during Hurricane Floyd (Figure D-3). During the first survey period (May 09-April 2010) a May Extra-tropical storm produced a maximum wave height 5.57 m, 99.46% of the highest  $H_s$  recorded in May during for 20 year period of 1988-2008. Maximum  $H_s$  remained 45% or less than the twenty year maximums for all months during the entire two year survey study (Figure D-3).

The average dominate wave period ( $T_p$ ) for Cape Canaveral is characterized by a maximum in September of 8.9 seconds and a minimum in June of 7.3 seconds (Figure D-3). During the first annual study period the maximum average  $T_p$  occurred in November 2009 with a recorded value of 9.22 seconds. The minimum average  $T_p$  for the first study period occurred the month following the maximum average  $T_p$  with a value of 6.53 seconds in December 2009. During the second annual study period the maximum average  $T_p$  was 9.11 seconds in September 2010, while the minimum was 6.82 seconds in January 2011.

The standard deviation in monthly averaged dominant wave period ( $T_p$ ) for the twenty year period 1988-2008 at NOAA buoy 41009 reaches a maximum of 2.7 seconds in September and a minimum of 2.1 seconds in July. During the first survey period the maximum standard deviation in  $T_p$  is recorded in August 2009 at 2.62 seconds and the minimum standard deviation in monthly  $T_p$  was recorded in December 2009 with a deviation of 1.74 seconds. The maximum standard deviation  $T_p$  for the

second survey period was recorded in September 2010 at 3.43 seconds and the minimum standard deviation in July 2010 at 1.63 seconds (Table D-2). During the first survey period May, September and December 2009 had standard deviations greater than 0.5 seconds lower than the 20 year averages at: -0.71, -0.83 and -0.86 seconds respectively (Figure D-3). March 2010 was the only month with a standard deviation 0.5 greater than the monthly 20 year average at 0.51 seconds. During the second study period October 2010 had a standard deviation -0.73 seconds less than the 20 year monthly average, and September and November 2010 had standard deviations of 0.5 seconds greater than the twenty year average at 0.73 and 0.62 seconds respectively (Figure D-4).

The 20 year (1988-2008) monthly average wave period ( $T_{AVE}$ ) at Cape Canaveral reaches maximums during September and October at 5.7 seconds, while the minimum  $T_{AVE}$  occurs in June at 4.8 seconds (Figure D-5). During the first survey period the  $T_{AVE}$  reached a maximum during November 2009 at 5.64 seconds, with its minimum value reached in September 2009 at 4.47 seconds. The maximum  $T_{AVE}$  for the second study period occurred in September 2010 at 5.67 seconds while the minimum occurred in June 2010 at 4.43 seconds (Figure D-5). During the first survey period (May 2009–April 2010) September, October, December and January all had  $T_{AVE}$  values that were more than 0.5 seconds less than the 20 year (1988-2008) monthly averages, while during the second survey period (May 2010-April 2011) January and February had  $T_{AVE}$  values less than 0.5 sec of the twenty year monthly averages (Figure D-5).

During the twenty year period 1988-2008 the maximum  $T_{AVE}$  was found in October at 15.5 seconds with the lowest maximum  $T_{AVE}$  occurring in June at 9.3 seconds. During

the first study period the maximum  $T_{AVE}$  was in August 2009 at 12.32 seconds with the lowest maximum  $T_{AVE}$  found in December 2009 at 5.5 seconds. For the second study period Maximum  $T_{AVE}$  was recorded in September at 10.58 seconds and the lowest maximum  $T_{AVE}$  found in January 2011 at 6.98 seconds (Figure D-5). For both survey periods maximum  $T_{AVE}$  values are at least 1 second or more below the 20 year monthly maximums with an average monthly difference between maximums of 4.17 seconds (Figure D-5).

During the 20 year (1988-2008) study period the standard deviation in monthly  $T_{AVE}$  ranges from 1.4 seconds in September to 1.0 second in January, June, November and December (Table D-3). For the first survey period the maximum standard deviation in  $T_{AVE}$  of 1.41 seconds occurred in August, while the minimum standard deviation in  $T_{AVE}$  occurred in December at 0.48 seconds (Table D-3). For the second survey period the maximum stand deviation in  $T_{AVE}$  was found in September (1.46 seconds) and the minimum found in January (0.68 seconds). During the first survey period there were no months with a standard deviation greater than 0.25 seconds different than the twenty year monthly averages, but the months of September, October, December, January and February had  $T_{AVE}$  values less than 0.25 seconds of the twenty year average (Table D-3). During the second survey period July, January and February had standard deviation values 0.25 seconds less than the twenty year average (Table D-3).

### **Annual Wave Data**

Average significant wave heights (HS) were recorded at half hour intervals for both survey periods (May 2009-April 2010 and May 2010-April 2011) at NOAA buoy 41009 located 20 nm east of Cape Canaveral at a water depth of 44.2 m (Figures D-6

and D-7). An “Event” for this data set is described as any condition where  $H_s$  equals 3 m or greater as described by Bromirski and Kossin, (2008) for the U.S. East and Gulf Coasts (Figures D-6 and D-7). Bromirski and Kossin, (2008) related this to  $H_s$  in the 90 percentile along the U.S. East Coast along with a record of storm erosion events. At Cape Canaveral 3 m “events” have also been observed to be the threshold for wash over in areas with depleted or eroded dunes. During both survey periods the wave climates at Cape Canaveral are very similar in nature with both extra tropical and tropical “events”, although no significant tropical events were recorded during either survey period ( $H_s > 3$  m for 24 hours or longer (Figures D-6 and D-7). Red bars also indicate dates of monthly and rapid response surveys (Figures D-6 and D-7).

Figure 3-8 consists of the average Sig. wave heights ( $H_s$ ) recorded from March 2009 through May 2, 2010 at Buoy 41009. Data gaps were found to exist during two periods (12/13/2009 to 1/1/2010 and from 1/14/2010 to 1/27/2010) due to a malfunction of Buoy 41009. The maximum  $H_s$  occurred during a extra-tropical Northeast storm with  $H_s$  greater than three meters recorded from May 19<sup>th</sup> to May 21<sup>st</sup> and a maximum  $H_s$  of 5.57 m on May 20, 2009. Hurricane Ida formed in the Gulf of Mexico causing strong winds from the north east that persisted from November 9<sup>th</sup> through November 12<sup>th</sup>, 2009. The “Ida Nor’Easter” caused  $H_s$  of greater than 3 m, but these conditions were sporadic with  $H_s$  conditions not lasting for more than 3 consecutive hours. During the first survey period three other extra tropical – northeast storms had recorded  $H_s$  of greater than 3 m (2/5/2010, 2/25/2010 and 3/11/2011), but none of these events had  $H_s$  greater than 3 m for more than 2 hours. Minimum wave heights were recorded during June and July 2009.

During the second survey period (May 2010-April 2011) the maximum  $H_s$  was record during hurricane Igor on 9/19/2010 at 4.81 m (Figure D-7). Significant wave heights ( $H_s$ ) greater than 3 m persisted for ~ 7 hours. Hurricane Earl produced a maximum  $H_s$  of 4.58 m on 9/2/2010 and produced values of  $H_s$  greater than 3 m that persisted for ~ 5.5 hours. Four extra tropical – north east storm produced  $H_s$  of greater than 3 m on the following dates: November 13<sup>th</sup>, December 14<sup>th</sup>, December 26<sup>th</sup>, 2009 and March 4<sup>th</sup>, 2011. While the storms on December 14<sup>th</sup> and 26<sup>th</sup> produced  $H_s$  greater than 3 m for less than 2 hours, the storms November 13<sup>th</sup>, 2010 and March 4<sup>th</sup>, 2011 produced  $H_s$  greater than 3 m for ~ 10 hours each. Minimum values for  $H_s$  were recorded in both June and July 2010 (Figure D-7).

### **Wave Climate Discussion**

The wave climate for the study area may be better characterized by dominant weather patterns and the transition into and out of these patterns than by the more traditional seasonal explanation that doesn't fit. The quiescent months of June, July and August are indicative of the beginning of the tropical storm season. These months are characterized by lowest average significant wave heights, lowest average periods and lowest average dominant wave periods. The wave climate here is dominated by locally generated convection cells punctuated by rare tropical storms. September stands alone as the transition from the quiescent months to the more active tropical season. It is characterized by tropical storms and is noted for the maximum HS. September also has the highest average dominant period and highest average period from tropical storms. The months of October and November also represent another transition: the transition out of the active tropical season into the frontal dominated winter or Nor'easter season.

These two months along with September have the highest standard deviations in both average wave period and average dominant wave period. October and November are characterized by a mix of late season tropical storms and early season frontal storms with a mix of long period waves from tropical storms and shorter period waves generated by the passage of frontal system. December, January, February and March are dominated by winter storms generated by passing frontal system. These storms are characterized by slightly shorter average wave periods and average dominant periods than their tropical counter parts. April and May are the transition from the frontal dominated nor'easter conditions to the locally generated quiescent period of June, July and August. These months are dominated by locally generated waves mixed with infrequent late season Nor'easters.

Wave climates for both survey periods were similar to the long-term averages with the exception of a much reduced tropical influence. Average monthly HS were always within 0.5 m of the long-term 20 year averages, but the maximum HS were greatly reduced. Maximum recorded HS values were less than half of the 20 year maximums with the exception of May 2009. The May 2009 Nor'easter was a 95 percentile event, and was the only event recorded above the 50 percentile. This would indicate that all the observations in the study were observed at nominal wave conditions, especially from a tropical standpoint.

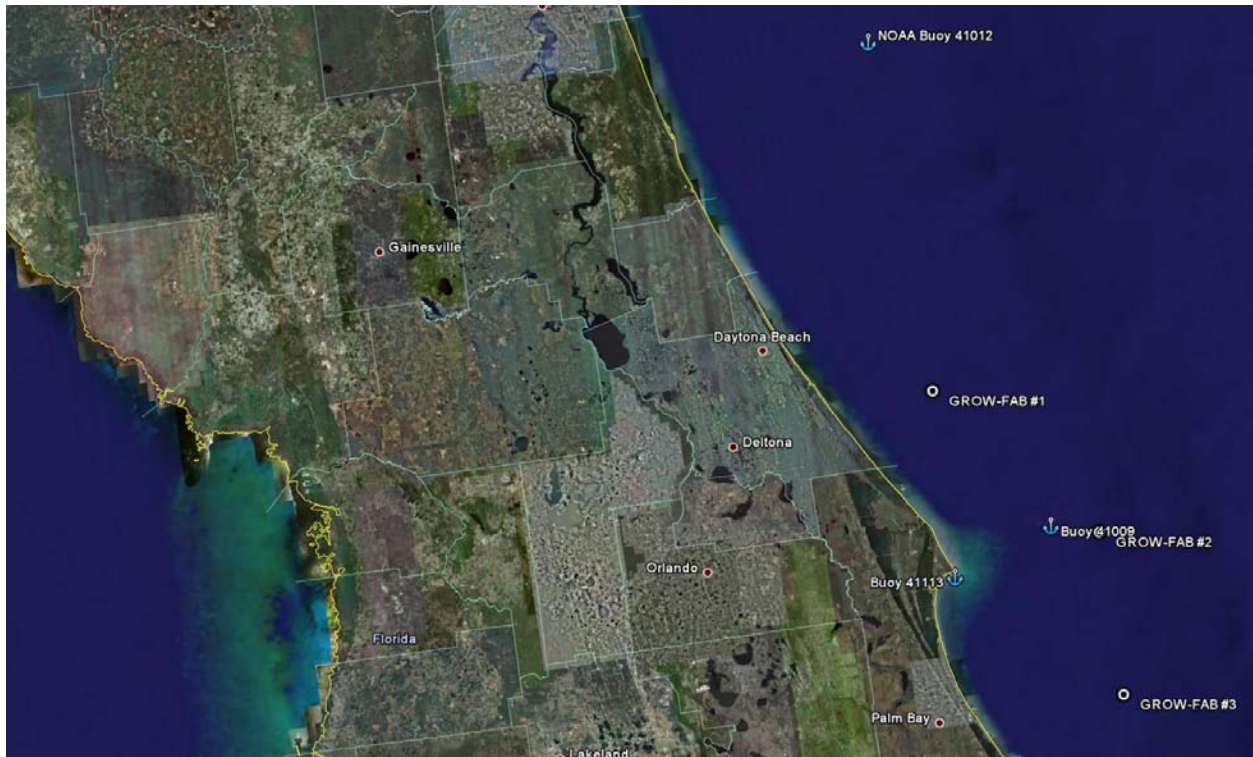


Figure D-1. Wave buoy and hindcast locations.

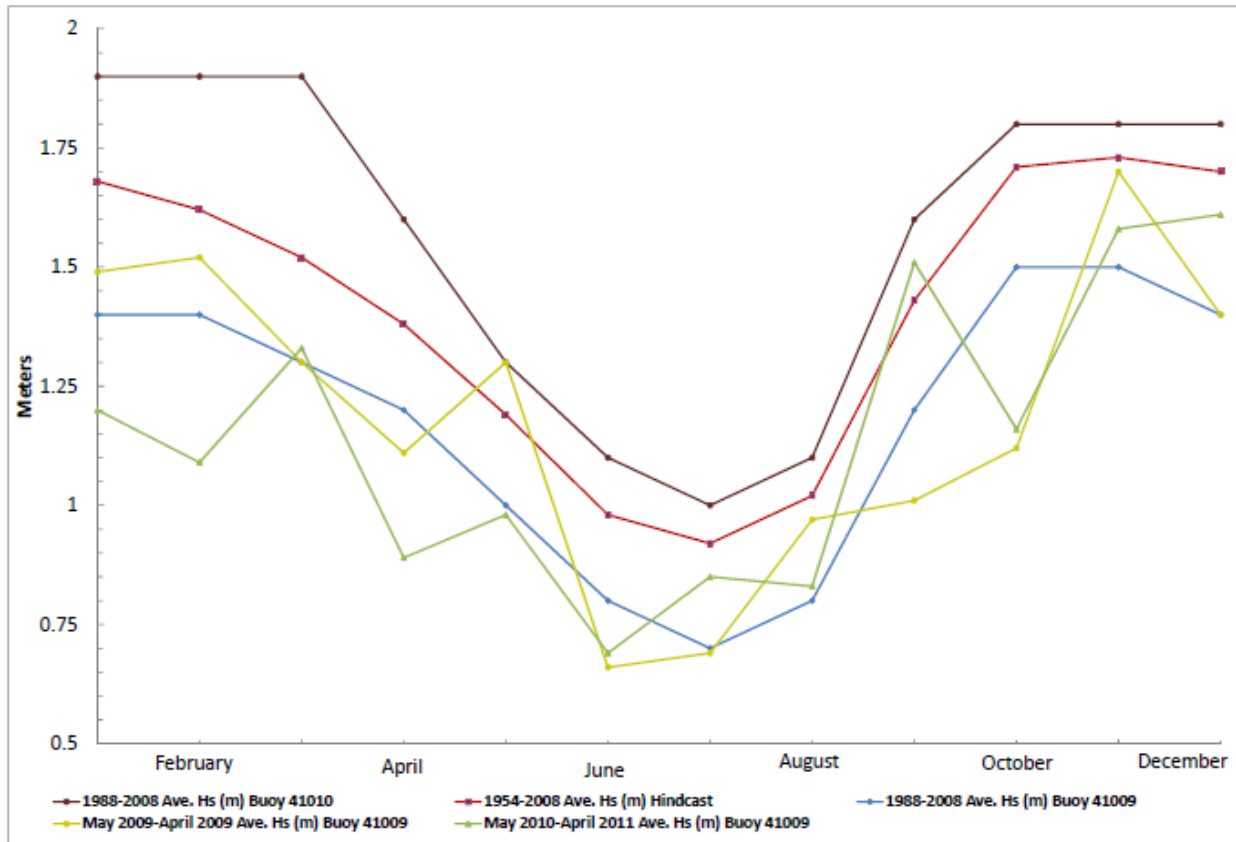


Figure D-2. Monthly average significant wave heights measured ~20 nm east of Cape Canaveral in a water depth of 44.2 m. Blue line indicates Ave. sig. wave heights from the WIS hindcast for the time period of 1988-2008. Red line are monthly Ave. sig. wave heights measured at NOAA buoy 41009 from May 2009 through April 2010. Green line indicates Ave. sig. wave heights measured at NOAA buoy 41009 from May 2010 through April 2011. Lowest average significant wave heights were measured in the June July August period (“summer condition”) While the highest average significant wave heights were measured in December January February period (“winter condition”). Transitions from summer to winter to summer occurs in the months of September October November and March April May.

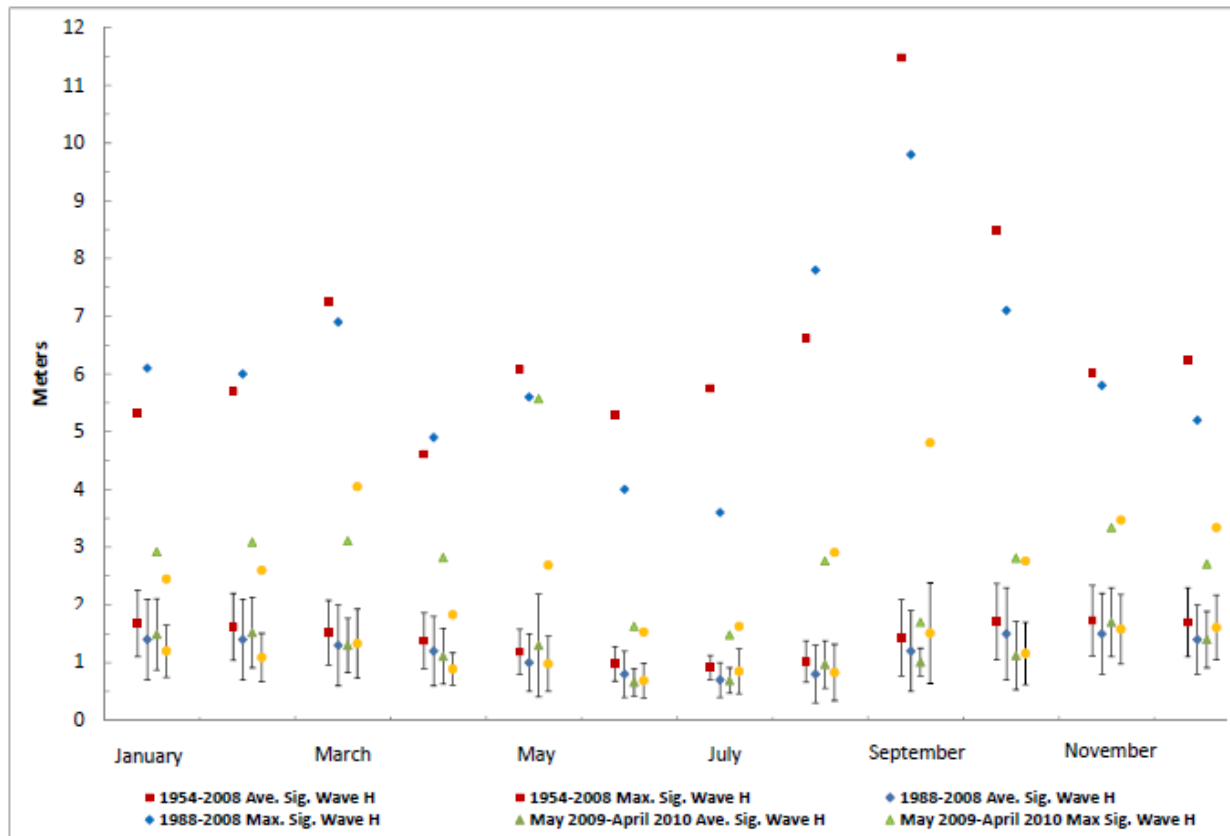


Figure D-3. Monthly comparison of average significant wave heights from NOAA Buoy 41009 collected (1988-2008) and the two annual study cycles (May 2009 - May 2010, May 2010 - May 2011). Bars indicate the monthly standard deviation in average significant wave heights. Stand-alone markers are the maximum wave heights record for that month for each of the studied times. During the two year surveys period (May 2009 – May 2011) only the May 2009 northeast storm recorded a maximum wave height comparable to the twenty year record of the WIS study (1988-2008).

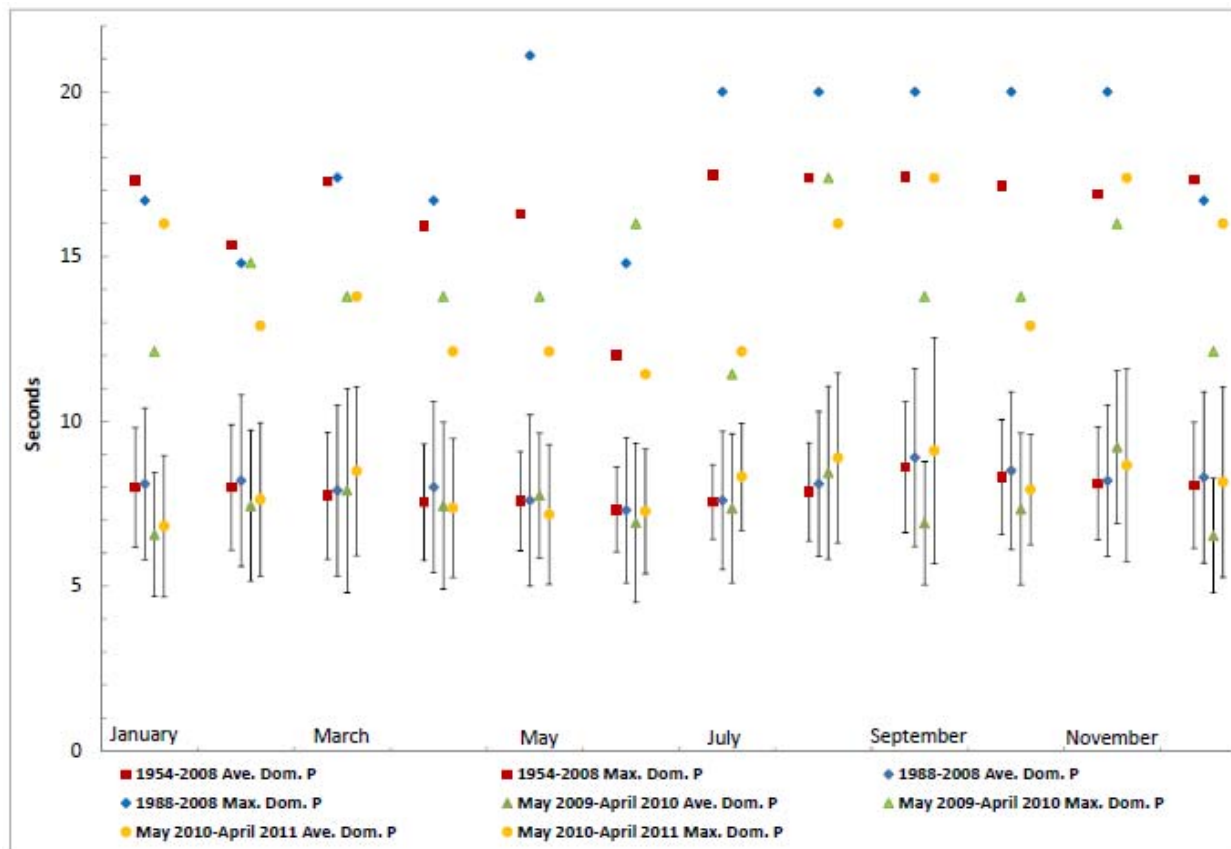


Figure D-4. Monthly comparison of dominant wave period from the WIS hindcast study (1988-2008) and the two annual study cycles (May 2009 - May 2010, May 2010 - May 2011). Bars indicate the monthly standard deviation in dominant wave periods. Stand-alone markers are the maximum dominant wave period record for that month for each of the studied times.

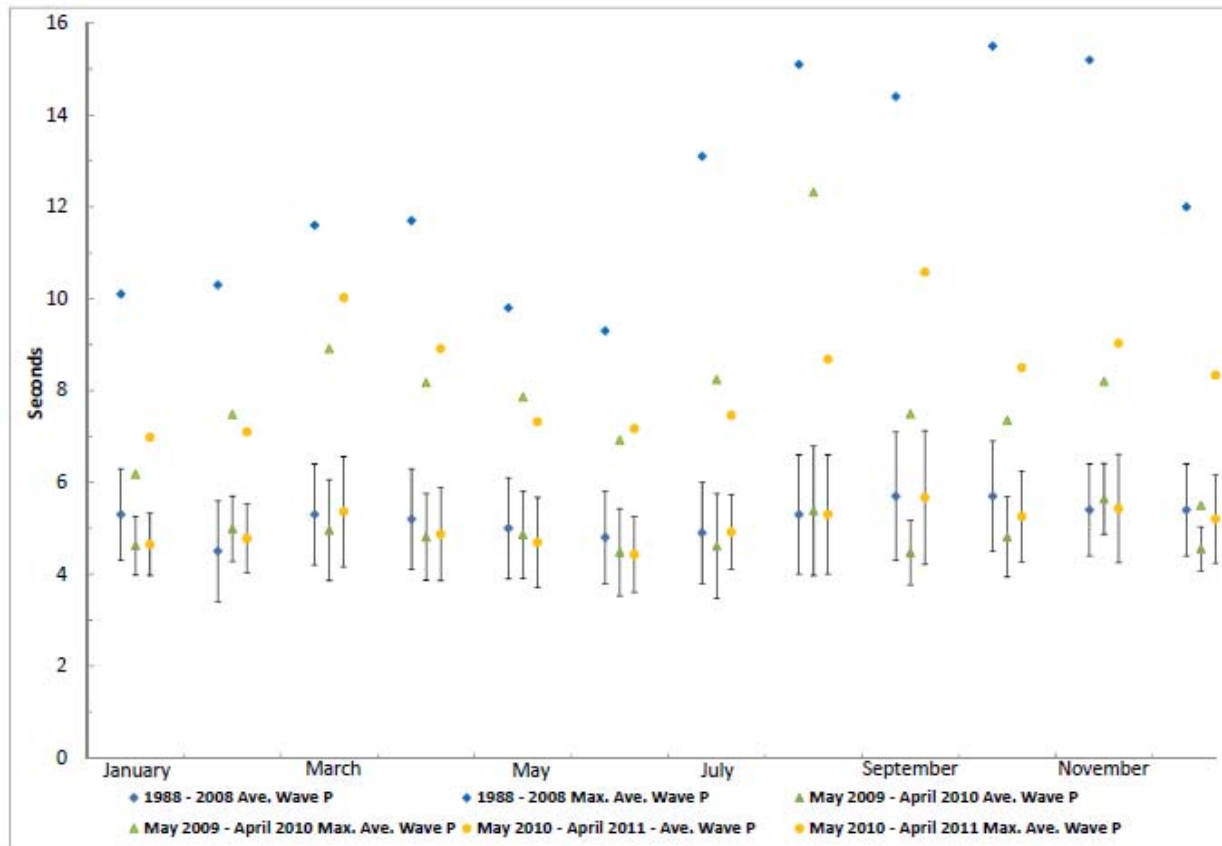


Figure D-5. Monthly comparison of average wave period from the WIS hindcast study (1988-2008) and the two annual study cycles (May 2009 - May 2010, May 2010 - May 2011). Bars indicate the monthly standard deviation in average wave periods. Stand-alone markers are the maximum average wave period record for that month for each of the studied times.

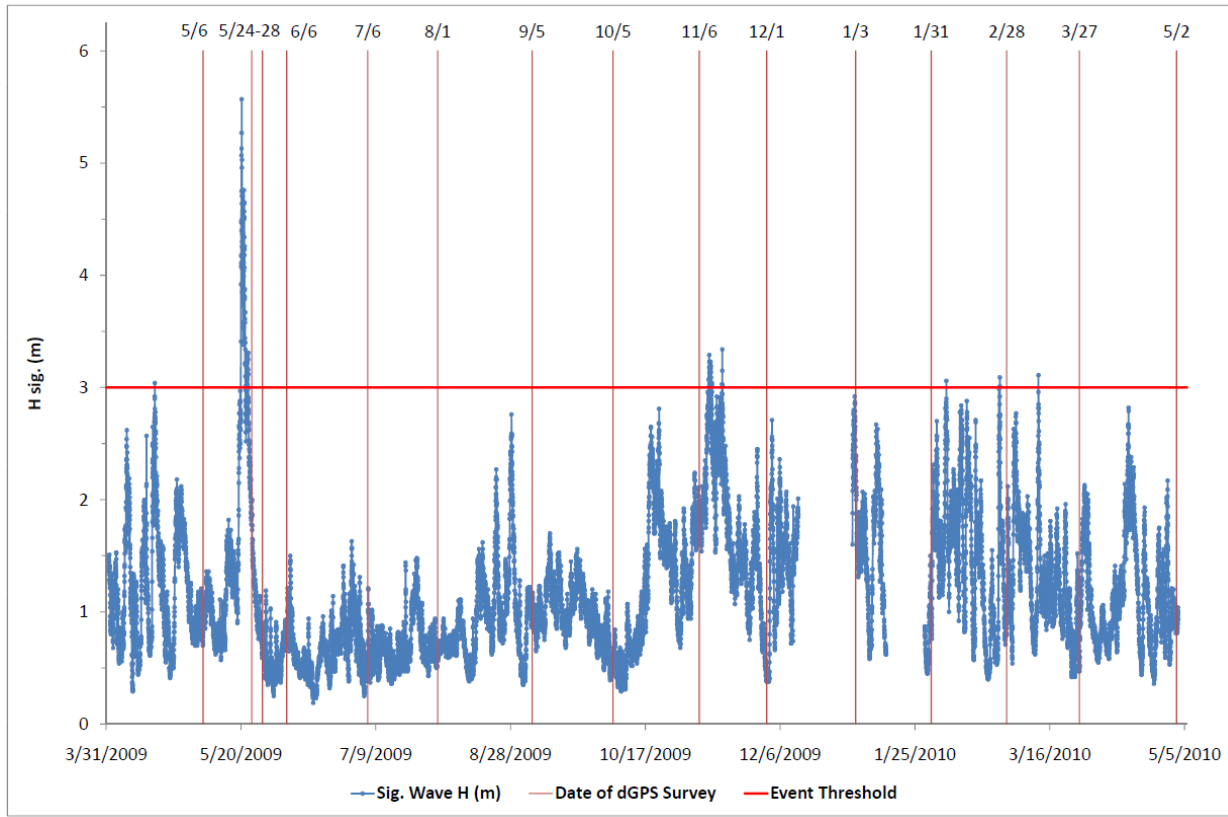


Figure D-6. Average significant wave heights for the period of April 1, 2009 through May 2, 2010 with GPS surveys lined in red. The highest significant wave heights recorded for this period occurred on May 20, 2009 and were caused by a persistent northeast storm that affected the Cape Canaveral area from May 19 through May 21, 2009. Hurricane Ida in the Gulf of Mexico set up persistent northeast storm conditions with wave heights greater than 3.25 m in the Cape Canaveral area from November 9 through November 14, 2009.

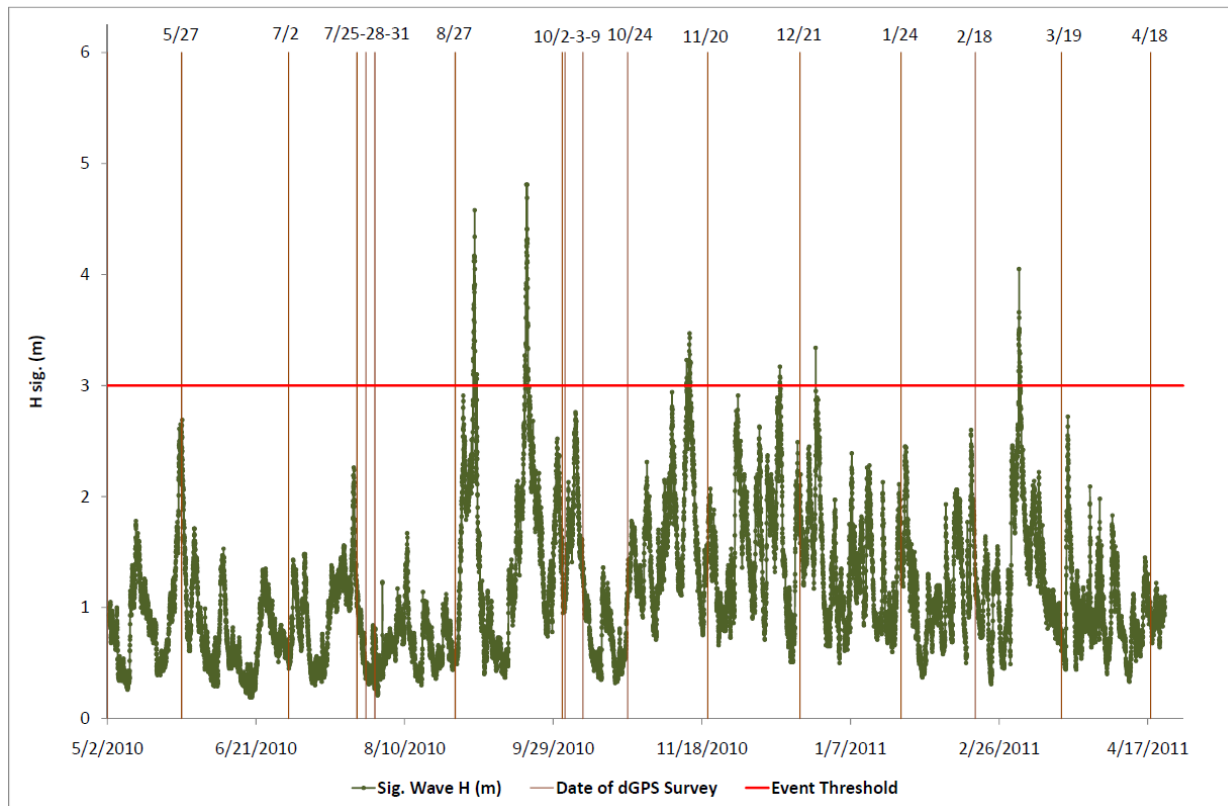


Figure D-7. Average significant wave heights for the period of May 2, 2010 through May 2, 2011 with GPS surveys lined in red. The highest significant wave heights recorded for this period occurred on September 19, 2010 and were caused by Hurricane Igor. Hurricane Earl also caused average significant wave heights of greater than 4 meters (4.58 m max.) on September 9, 2010. Series of University of Florida landmarks.

**Table D-1. Standard deviation of average significant wave height ( $H_s$ )**

Month	1988-2008 (m)	May 09-April 10 (m)	May 10-April 11 (m)
January	0.7	0.62	0.45
February	0.7	0.61	0.42
March	0.7	0.47	0.6
April	0.6	0.48	0.28
May	0.5	0.89	0.48
June	0.4	0.24	0.3
July	0.3	0.22	0.39
August	0.5	0.41	0.49
September	0.7	0.24	0.87
October	0.8	0.59	0.54
November	0.7	0.6	0.6
December	0.6	0.49	0.56
<b>Annual</b>	<b>0.7</b>	<b>0.49</b>	<b>0.5</b>

**Table D-2. Standard deviation of dominant wave period ( $T_P$ )**

Month	1988-2008 (s)	May 09-April 10 (s)	May 10-April 11 (s)
January	2.3	1.88	2.15
February	2.6	2.29	2.33
March	2.6	3.1	2.56
April	2.6	2.53	2.11
May	2.6	1.89	2.12
June	2.2	2.42	1.89
July	2.1	2.26	1.63
August	2.2	2.62	2.58
September	2.7	1.87	3.43
October	2.4	2.3	1.67
November	2.3	2.31	2.92
December	2.6	1.74	2.89
<b>Annual</b>	<b>2.5</b>	<b>2.27</b>	<b>2.36</b>

Table D-3. Standard deviation of average wave period ( $T_{AVE}$ )

Month	1988-2008 (s)	May 09-April 10 (s)	May 10-April 11 (s)
January	1	0.64	0.68
February	1.1	0.71	0.75
March	1.1	1.1	1.2
April	1.1	0.94	1.01
May	1.1	0.95	0.98
June	1	0.95	0.82
July	1.1	1.14	0.81
August	1.3	1.41	1.3
September	1.4	0.7	1.46
October	1.2	0.87	0.99
November	1	0.77	1.18
December	1	0.48	0.96
<b>Annual</b>	<b>1.1</b>	<b>0.89</b>	<b>1.01</b>

## LIST OF REFERENCES

- Abbe, C. J., 1895, Remarks on the cuspatc capes of the Carolina Coast: Proceedings of the Boston Society of Natural History, v. 26, p. 489-497.
- Absalonsen, L., and Dean, R. G., 2010, Characteristics of the Shoreline Change Along the Sandy Beaches of the State of Florida: An Atlas: University of Florida.
- Adams, P. N., Ruggiero, P., Schoch, G. C., and Gelfenbaum, G., 2007, Intertidal sand body migration along a megatidal coast, Kachemak Bay, Alaska: Journal of Geophysical Research-Earth Surface, v. 112, no. F2.
- Anders, F. J., and Byrnes, M. R., 1991, Accuracy of shoreline change rates as determined from maps and aerial photographs: Shore & Beach, v. 59, no. 1, p. 17-26.
- Ashton, A., Murray, A. B., and Arnault, O., 2001, Formation of coastline features by large-scale instabilities induced by high-angle waves: Nature, v. 414, no. 6861, p. 296-300.
- Baganha Baptista, P. R., Bernardes, C., and Cunha, T. R., 2011, The validation analysis of the INSHORE system-a precise and efficient coastal survey system: Environmental Monitoring and Assessment, v. 179, no. 1-4, p. 589-604.
- Barnard, P. L., Erikson, L. H., and Hansen, J. E., 2009, Monitoring and Modeling Shoreline Response Due to Shoreface Nourishment on a High-Energy Coast: Journal of Coastal Research, p. 29-33.
- Barnard, P. L., Eshleman, J. L., Erikson, L. H., and Hanes, D. M., 2007, Coastal processes study at Ocean Beach, San Francisco, CA: summary of data collection 2004-2006.
- Bird, E. C. F., 1985, Coastline Changes, New York, Wiley and Sons, 219 p.:
- Boak, E. H., and Turner, I. L., 2005, Shoreline definition and detection: A review: Journal of Coastal Research, v. 21, no. 4, p. 688-703.
- Brock, J. C., Wright, C. W., Sallenger, A. H., Krabill, W. B., and Swift, R. N., 2002, Basis and methods of NASA airborne topographic mapper lidar surveys for coastal studies: Journal of Coastal Research, v. 18, no. 1, p. 1-13.
- Bromirski, P. D., and Kossin, J. P., 2008, Increasing hurricane wave power along the US Atlantic and Gulf coasts: Journal of Geophysical Research-Oceans, v. 113, no. C7.

- Brooks, H. K., 1972, Geology of Cape Canaveral, Southeastern Geological Society 16th Field Conference, Volume 16: J. F. Kennedy Space Center, Florida, Southeastern Geological Society, p. 35-44.
- Brown, D. W., 1962, Water Resources of Brevard County, Florida, Volume Report of Investigation 28: Tallahassee, FL, Florida Geological Survey, p. 59.
- Bruun, P., 1962, Sea-level rise as a cause of shoreline erosion: American Society of Civil Engineering Proceedings, Journal of Waterways and Harbors Division, v. 88, p. 117-130.
- , 1988, The Bruun Rule of Erosion by Sea-Level Rise - A Discussion on Large-Scale Two-Dimensional And Three-Dimensional Usages: Journal of Coastal Research, v. 4, no. 4, p. 627-648.
- Bumpus, D. F., 1955, The circulation over the continental shelf of Cape Hatteras: Transactions of the American Geophysical Union, v. 36, p. 601-611.
- Byrnes, M. R., and Hiland, M. W., 1995, Large-Scale Sediment Transport Patterns on the Continental-Shelf and Influence on Shoreline Response - ST-Aandrew-Sound, Goergia to Nassau-Sound, Florida, USA: Marine Geology, v. 126, no. 1-4, p. 19-43.
- Cooke, C. W., 1936, Geology of the coastal plains of South Carolina, Volume U. S .Geological Survey Bulletin 867, U. S. Geological Survey, p. 196.
- Cowell, P., and Thom, B., 1994, Morphodynamics of coastal evolution: Coastal Evolution, Late Quaternary Shoreline Morphodynamics, p. 33-86.
- Cox, A. T., and Swail, V. R., 2001, A global wave hindcast over the period 1958-1997: Validation and climate assessment: Journal of Geophysical Research-Oceans, v. 106, no. C2, p. 2313-2329.
- Crowell, M., Leatherman, S. P., and Buckley, M. K., 1991, Historical Shoreline Change - Error Analysis and Mapping Accuracy: Journal of Coastal Research, v. 7, no. 3, p. 839-852.
- Dail, H. J., Merrifield, M. A., and Bevis, M., 2000, Steep beach morphology changes due to energetic wave forcing: Marine Geology, v. 162, no. 2-4, p. 443-458.
- Dean, R. G., Cheng, J., and Malakar, S., 1998, Characteristics of Shoreline Change Along the Sandy Beaches of the State of Florida: An Atlas, Florida Sea Grant Program: Gainesville, Florida 32611, University of Florida, p. 305.
- Dean, R. G., and Dalrymple, R. A., 2002, Coastal Processes with Engineering Applications, Cambridge, U. K., Cambridge University Press, 475 p.:

- Dolan, R., 1971, Coastal Landforms - Crescentic and Rhythmic: Geological Society of America Bulletin, v. 82, no. 1, p. 177-&.
- Dolan, R., and Ferm, J. C., 1968, Crescentic Landforms Along Atlantic Coast of the United States: Science, v. 159, no. 3815, p. 627-&.
- Dolan, R., and Hayden, B., 1981, Storms and Shoreline Configuration: Journal of Sedimentary Petrology, v. 51, no. 3, p. 737-744.
- Dolan, R., Hayden, B., Heywood, J., and Vincent, L., 1977, Shoreline Forms and Shoreline Dynamics: Science, v. 197, no. 4298, p. 49-51.
- Dolan, R., Hayden, B., Rea, C., and Heywood, J., 1979, Shoreline Erosion Rates Along the Middle Atlantic Coast of the United-States: Geology, v. 7, no. 12, p. 602-606.
- Dolan, R., Hayden, B. P., May, P., and May, S., 1980, The reliability of shoreline change measurements from aerial photographs: Shore & Beach, v. 48, no. 4, p. 22-29.
- Dolan, R. A., and Hayden, B., 1983, Patterns and prediction of shoreline change, *in* Komar, P. D., ed., Handbook of Coastal Processes and Erosion: Boca Raton, FL, CRC Press, p. 123-149.
- Dornbusch, U., 2010, Ground Survey Methods for Mixed Sand and Gravel Beaches in Intertidal Environments: A Comparison: Journal of Coastal Research, v. 26, no. 3, p. 451-464.
- Douglas, B. C., Crowell, M., and Leatherman, S. P., 1998, Considerations for shoreline position prediction: Journal of Coastal Research, v. 14, no. 3, p. 1025-1033.
- Field, M. E., and Duane, D. B., 1974a, Geomorphology and Sediments of the Inner Continental Shelf, Cape Canaveral, FL.
- , 1974b, Geomorphology and Sediments of the Inner Continental Shelf, Cape Canaveral, Florida, *in* Center, C. E. R., ed., Volume Technical Memorandum 42, U. S. Army Corps of Engineers, p. 87.
- Fletcher, C., Rooney, J., Barbee, M., Lim, S. C., and Richmond, B., 2003, Mapping shoreline change using digital orthophotogrammetry on Maui, Hawaii: Journal of Coastal Research, p. 106-124.
- Frazer, L. N., Anderson, T. R., and Fletcher, C. H., 2010, Modeling storms improves estimates of long-term shoreline change (vol 37, L02401, 2010): Geophysical Research Letters, v. 37.
- Genz, A. S., Fletcher, C. H., Dunn, R. A., Frazer, L. N., and Rooney, J. J., 2007, The predictive accuracy of shoreline change rate methods and alongshore beach variation on Maui, Hawaii: Journal of Coastal Research, v. 23, no. 1, p. 87-105.

- Gorman, L., Morang, A., and Larson, R., 1998, Monitoring the coastal environment; Part IV: Mapping, shoreline changes, and bathymetric analysis: *Journal of Coastal Research*, v. 14, no. 1, p. 61-92.
- Graham, N. E., 2005, Coastal Impacts of North Pacific Winter Wave Climate Variability: The Southern California Bight and the Gulf of the Farallones.: Scripps Institute of Oceanography.
- Graham, N. E., and Diaz, H. F., 2001, Evidence for intensification of North Pacific winter cyclones since 1948: *Bulletin of the American Meteorological Society*, v. 82, no. 9, p. 1869-1893.
- Guillen, J., Stive, M. J. F., and Capobianco, M., 1999, Shoreline evolution of the Holland coast on a decadal scale: *Earth Surface Processes and Landforms*, v. 24, no. 6, p. 517-536.
- Hansen, J. E., and Barnard, P. L., 2009, The Observed Relationship Between Wave Conditions and Beach Response, Ocean Beach, San Francisco, CA: *Journal of Coastal Research*, p. 1771-1775.
- , 2010, Sub-weekly to interannual variability of a high-energy shoreline: *Coastal Engineering*, v. 57, no. 11-12, p. 959-972.
- Hapke, C. J., Reid, D., and Richmond, B., 2009, Rates and Trends of Coastal Change in California and the Regional Behavior of the Beach and Cliff System: *Journal of Coastal Research*, v. 25, no. 3, p. 603-615.
- Hapke, C. J., Reid, D., Richmond, B. M., Ruggiero, P., and List, J., 2006, National Assessment of Shoreline Change: Part 3: Historical Shoreline Changes and Associated Coastal Land Loss along the Sandy Shorelines of the California Coast., *in* Survey, U. S. G., ed., Volume Open File Report 2006-1219, p. 79.
- Harley, M. D., Turner, I. L., Short, A. D., and Ranasinghe, R., 2011, Assessment and integration of conventional, RTK-GPS and image-derived beach survey methods for daily to decadal coastal monitoring: *Coastal Engineering*, v. 58, no. 2, p. 194-205.
- Hayes, M. O., 1994, The Georgia Bight Barrier System, *in* Davis, R. A., ed., *Geology of Holocene Barrier Island Systems*: New York, Springer-Verlag Publishing, p. 233-304.
- Hoyt, J. H., and Henry, V. J., 1971, Origin of Capes and Shoals Along Southeastern Coast of the United-States: *Geological Society of America Bulletin*, v. 82, no. 1, p. 59-&.
- Huang, J., 2002, Morphological Monitoring of a High Energy Beach System Using GPS and Total Station Techniques, Runkerry, CO. Antrim, Northern Ireland: *Journal of Coastal Research*, no. SI 36, p. 390-398.

- Inman, D. L., Jenkins, S. A., and Elwany, M. H. S., 1996, Wave climate cycles and coastal engineering practice., 25th International Conference, Coastal Engineering Research Council: Orlando, FL, p. 314-327.
- Kaplan, E. D., and Hegarty, C., 2006, Understandin GPS Principles and Applications, Boston, MA, Artech House, Inc., 730 p.:
- Klemas, V., 2011, Beach Profiling and LIDAR Bathymetry: An Overview with Case Studies: *Journal of Coastal Research*, v. 27, no. 6, p. 1019-1028.
- Kline, S. W., Adams, P. N., Plant, N. G., Jaeger, J. M., and MacKenzie, R. A., Seasonal and event-driven behavior of a sandy beach and bar system at Kennedy Space Center, Cape Canaveral, Florida, *in* Proceedings Tenth ARGUS Workshop, Corvallis, Oregon, 2011.
- Kofoed, J. W., 1963, Coastal development in Volusia and Brevard Counties, Florida: *Bulletin of Marine Science of the Gulf and Caribbean*, v. 13, no. 1.
- Komar, P. D., 1998, Beach Processes and Sedimentation, Upper Saddle River, NJ, Prentice Hall, 544 p.:
- Leatherman, S. P., Douglas, B. C., and Crowell, M., 1997, Beach erosion trends and shoreline forecasting: *Journal of Coastal Research*, v. 13, no. 4, p. R3-R4.
- Leatherman, S. P., Zhang, K., and Douglas, B. C., 2000, Sealevel rise shown to drive coastal erosion: *EOS*, v. 81, p. 55-77.
- List, J. H., and Farris, A. S., 1999, Large-Scale Shoreline Response to Storms and Fair Weather, *in* Kraus, N. C., and McDougal, W., G., eds., Proceedings of the 4th International Symposium on Coastal Engineering and Science of Coastal Sediment Processes, Volume Coastal Sediments '99: Long Island, NY, American Society of Civil Engineers, p. 1324-1338.
- List, J. H., Farris, A. S., and Sullivan, C., 2006, Reversing storm hotspots on sandy beaches: Spatial and temporal characteristics: *Marine Geology*, v. 226, no. 3-4, p. 261-279.
- Malone, K. K., 2011, Seasonal and spatial variability of beach morphodynamics at an autonomous tidal inlet: Matanzas Inlet, Florida Atlantic Coast [Master of Science: University of Florida, 291 p.]
- May, J. P., 1972, Age and Origin of the Cape Kennedy Area, Southeastern Geological Society16th Field Conference, Volume 16: Kennedy Space Center, Florida, Southeastern Geological Society, p. 31-34.
- Meisburger, E. P., and Duane, D. B., 1971, Geomorphology and Sediments of the Inner Continental Shelf, Palm Beach to Cape Kennedy, Florida, *in* Center, C. E. R., ed., Volume Technical Memorandum 34, U. S. Arm Corps of Engineers, p. 82.

- Miller, K. G., Kominz, M. A., Browning, J. V., Wright, J. D., Mountain, G. S., Katz, M. E., Sugarman, P. J., Cramer, B. S., Christie-Blick, N., and Pekar, S. F., 2005, The phanerozoic record of global sea-level change: *Science*, v. 310, no. 5752, p. 1293-1298.
- Moore, L. J., 2000, Shoreline mapping techniques: *Journal of Coastal Research*, v. 16, no. 1, p. 111-124.
- Moore, L. J., Ruggiero, P., and List, J. H., 2006, Comparing mean high water and high water line shorelines: Should proxy-datum offsets be incorporated into shoreline change analysis? (vol 22, pg 894, 2006): *Journal of Coastal Research*, v. 22, no. 6, p. 1452-1452.
- Morton, R. A., 1979, Temporal and Spatial Variations In Shoreline Changes and Their Implications, Examples from the Texas Gulf-Coast: *Journal of Sedimentary Petrology*, v. 49, no. 4, p. 1101-1111.
- , 1991, Accurate shoreline mapping; past, present, and future, *in* Gingerich, K. J., and Kriebel, D. L., eds., *Coastal Sediments '91*: New York, American Society of Civil Engineers, p. 997-1010.
- Morton, R. A., Leach, M. P., Paine, J. G., and Cardoza, M. A., 1993, Monitoring Beach Changes Using GPS Surveying Techniques: *Journal of Coastal Research*, v. 9, no. 3, p. 702-720.
- Morton, R. A., and Miller, T. L., 2005, National Assessment of Shoreline Change: Part 2 Historical Shoreline Changes and Associated Coastal Land Loss Along the U.S. Southeast Atlantic Coast: U.S. Geological Survey.
- Morton, R. A., and Speed, F. M., 1998, Evaluation of shorelines and legal boundaries controlled by water levels on sandy beaches: *Journal of Coastal Research*, v. 14, no. 4, p. 1373-1384.
- NGS, 2011, National Geodetic Survey Datasheet Page.
- NOAA, 2011, Tides & Currents, Center for Operational Oceanographic Products and Services.
- Osmond, J. K., May, J. P., and Tanner, W. F., 1970, Age Of Cape-Kennedy Barrier-and-Lagoon Complex: *Journal of Geophysical Research*, v. 75, no. 2, p. 469-&.
- Pajak, M. J., and Leatherman, S., 2002, The high water line as shoreline indicator: *Journal of Coastal Research*, v. 18, no. 2, p. 329-337.
- Pirkle, E. C., Yoho, W. H., and Pirkle, W. A., 1972, Geology of Cape Canaveral, Southeastern Geological Society 16th Field Conference, Volume 16: J. F. Kennedy Space Center, Florida, Southeastern Geological Society, p. 54.

- Plant, N. G., and Holman, R. A., 1997, Intertidal beach profile estimation using video images: *Marine Geology*, v. 140, no. 1-2, p. 1-24.
- Randazzo, A. F., and Jones, D. S., 1997, *The Geology of Florida*, Gainesville, FL, University Press of Florida, 327 p.:
- Rink, W. J., and Forrest, B., 2005, Dating evidence for the accretion history of beach ridges on Cape Canaveral and Merritt Island, Florida, USA: *Journal of Coastal Research*, v. 21, no. 5, p. 1000-1008.
- Robertson, W. V., Whitman, D., Zhang, K. Q., and Leatherman, S. P., 2004, Mapping shoreline position using airborne laser altimetry: *Journal of Coastal Research*, v. 20, no. 3, p. 884-892.
- Romine, B. M., Fletcher, C. H., Frazer, L. N., Genz, A. S., Barbee, M. M., and Lim, S. C., 2009, Historical Shoreline Change, Southeast Oahu, Hawaii; Applying Polynomial Models to Calculate Shoreline Change Rates: *Journal of Coastal Research*, v. 25, no. 6, p. 1236-1253.
- Ruggiero, P., Buijsman, M., Kaminsky, G. M., and Gelfenbaum, G., 2010, Modeling the effects of wave climate and sediment supply variability on large-scale shoreline change: *Marine Geology*, v. 273, no. 1-4, p. 127-140.
- Ruggiero, P., Kaminsky, G. A., Gelfenbaum, G., and Voigt, B., 2005, Seasonal to interannual morphodynamics along a high-energy dissipative littoral cell: *Journal of Coastal Research*, v. 21, no. 3, p. 553-578.
- Ruggiero, P., Kaminsky, G. M., and Gelfenbaum, G., 2003, Linking proxy-based and datum-based shorelines on a high-energy coastline: Implications for shoreline change analyses: *Journal of Coastal Research*, p. 57-82.
- Ruggiero, P., and List, J. H., 2009, Improving Accuracy and Statistical Reliability of Shoreline Position and Change Rate Estimates: *Journal of Coastal Research*, v. 25, no. 5, p. 1069-1081.
- Ruggiero, P., and Lists, J. H., 2009, Improving Accuracy and Statistical Reliability of Shoreline Position and Change Rate Estimates: *Journal of Coastal Research*, v. 25, no. 5, p. 1069-1081.
- Sallenger, A. H., Krabill, W. B., Swift, R. N., Brock, J., List, J., Hansen, M., Holman, R. A., Manizade, S., Sontag, J., Meredith, A., Morgan, K., Yunkel, J. K., Frederick, E. B., and Stockdon, H., 2003, Evaluation of airborne topographic lidar for quantifying beach changes: *Journal of Coastal Research*, v. 19, no. 1, p. 125-133.
- Seymour, R. J., Strange, R. R., Cayan, D. R., and Nathan, R. A., 1984, Influence of El Niños on California's Wave Climate, 19th International Conference on Coastal Engineering: New York, p. 577-592.

- Shalowitz, A. L., 1964, Shoreline and Sea Boundaries VI., *in* Department of Commerce, C., and Geodetic Survey, ed.: Washington D.C., U. S. Government Printing Office, p. 420.
- Shepard, F. P., and Wanless, H. R., 1971, Our Changing Coastlines, New York, McGraw-Hill Inc., 149 p.:
- Smith, G. L., and Zarillo, G. A., 1990, Calculating Long-Term Shoreline Recession Rates Using Aerial Photographic and Beach Profiling Techniques: *Journal of Coastal Research*, v. 6, no. 1, p. 111-120.
- Stive, M. J. F., 2004, How important is global warming for coastal erosion? An editorial comment: *Climatic Change*, v. 64, no. 1-2, p. 27-39.
- Stive, M. J. F., Aarninkhof, S. G. J., Hamm, L., Hanson, H., Larson, M., Wijnberg, K. M., Nicholls, R. J., and Capobianco, M., 2002, Variability of shore and shoreline evolution: *Coastal Engineering*, v. 47, no. 2, p. 211-235.
- Stockdon, H. F., Holman, R. A., Howd, P. A., and Sallenger, A. H., 2006, Empirical parameterization of setup, swash, and runup: *Coastal Engineering*, v. 53, no. 7, p. 573-588.
- Stockdon, H. F., Sallenger, A. H., List, J. H., and Holman, R. A., 2002, Estimation of shoreline position and change using airborne topographic lidar data: *Journal of Coastal Research*, v. 18, no. 3, p. 502-513.
- Swail, V. R., and Cox, A. T., 2000, On the use of NCEP-NCAR reanalysis surface marine wind fields for a long-term North Atlantic wave hindcast: *Journal of Atmospheric and Oceanic Technology*, v. 17, no. 4, p. 532-545.
- Thieler, E. R., Himmelstoss, E. A., Zichichi, J. L., and Ergul, A., 2009, Digital Shoreline Analysis System (DSAS), Open File Report 1278, U. S. Geological Survey.
- Tuomey, M., 1848, Report on the Geology of South Carolina: Charleston, South Carolina, Geological Society of South Carolina, p. 143.
- USACE, 2004, Hydrographic Surveying, Volume EM-1110-2-1003: Washington D. C., p. 511.
- , 2006, Coastal Engineering Manual, Volume EM 1110-2-1100: Washington D. C., p. 695.
- , 2010, Standards and Procedures for Referencing Project Elevation Grades to Nationwide Vertical Datums, Volume EM 1110-2-6056: Washington D.C., p. 422.
- , 2011, NAVSTAR Global Positioning System Surveying, Volume EM 1110-1-1003: Washington D. C., p. 273.

- Vernon, R. O., 1951, Geology of Citrus and Levy Counties, Florida, Volume Bulletin 33: Tallahassee, FL, Florida Geological Survey, p. 23.
- Weber, K. M., List, J. H., and Morgan, K. L. M., 2005, An Operational Mean High Water Datum for Determination of Shoreline Position from Topographic Lidar Data: U. S. Geological Survey.
- White, W. A., 1958, Some geomorphic features of central peninsular Florida, Volume 41: Tallahassee, FL, Florida Geological Survey, p. 92.
- , 1966, Drainage asymmetry and the Carolina capes: Geological Society of America Bulletin, v. 41, p. 92.
- , 1970, The geomorphology of the Florida Peninsula, Volume Bulletin 51: Tallahassee, FL, Florida Bureau of Geology, p. 164.
- Woodroffe, C. D., 2002, Coasts: Form, Process and Evolution., Cambridge, Cambridge University Press, 623 p.:
- Wright, L. D., and Short, A. D., 1983, Morphodynamics of beaches and surf zones in Australia, *in* Komar, P., ed., Handbook of Coastal Processes and Erosion: Boca Raton, FL, CRC Press, p. 35-64.
- , 1984, Morphodynamic Variability of Surf Zones and Beaches - A Synthesis: Marine Geology, v. 56, no. 1-4, p. 93-118.
- Young, A. P., and Ashford, S. A., 2006, Application of airborne LIDAR for seacliff volumetric change and beach-sediment budget contributions: Journal of Coastal Research, v. 22, no. 2, p. 307-318.
- Zenkovich, V. P., 1967, Processes of Coastal Development, Edinbourough, Scotland, Oliver and Boyd Publishing.
- Zhang, K. Q., Douglas, B., and Leatherman, S., 2002, Do storms cause long-term beach erosion along the U.S. East Barrier Coast?: Journal of Geology, v. 110, no. 4, p. 493-502.

## BIOGRAPHICAL SKETCH

Richard Allen MacKenzie III was born in Flint, Michigan. He is the eldest son of Richard and Nancy MacKenzie, and the older brother of three sisters; MaDonna Marie, Jennifer Evelyn, and Kristi Lynn MacKenzie. Richard has six children; Drake Edward Allen, Matthew Richard, Kathryn Mary, Richard Allen IV, Alexzandyr Gavin, and Alaena Renee. He attended and completed his primary education at Siple Elementary School in Davison, Michigan and completed his secondary education while attending Lakeville Memorial High School in Otisville, Michigan. Upon completion of high school, Richard enlisted in the U. S. Navy serving in the F-14 Fighter Squadron 31 "The Tomcatters" on board the U. S. S. Forrestal (CV-59). While in the Navy, Richard completed several naval schools including; Naval Nuclear Electronics Technician "A" School, Naval Nuclear Power School, F-14 Electronic and Avionics "A" School, and Tactical Airborne Reconnaissance Pod System School. While serving on board the U. S. S. Forrestal Richard took part in the Presidential Airshow and shook hands with President George Bush Sr. during his visit prior to the Malta Summit. He was also deployed for Operation Desert Storm and Operation Provide Comfort during the Gulf War. While serving in the U. S. Navy he was awarded The Armed Forces Expeditionary Medal, The Unit Citation, Good Conduct, National Defense, and Southwest Asia Service Medal. After his naval service Richard attended Mott Community College while working as the general manager for Intouch Communications, Inc. During his education at Mott College, he was part of the President's University Steering Committee and was awarded MCC's Student of the Year, The Michigan First Team All-Academic Award, and The USA Today Academic All-American Award. Richard started his geomorphic studies while attending

the University of Michigan-Flint, where he was mentored by Frederick DeGroot. During his education at the University of Michigan, he was voluntarily recalled into the Michigan Air National Guard following September 11, 2001. After graduating from the University of Michigan-Flint with a degree in Physical Geography with a concentration in Resource Planning, Richard enrolled in graduate school at Bowling Green State University (BGSU) where he studied the use of Geographic Information System (GIS) in paleontological biodiversity. While attending BGSU he was activated for Operation Iraqi Freedom. Richard was deployed to Balad Air Force Base, Iraq from January to April, 2005. While serving in the Michigan Air National Guard 127<sup>th</sup> F-16 "Red Devils" Maintenance Squadron, he was awarded the Iraq Campaign Medal, Global War on Terrorism Expeditionary Medal, National Defense Medal, and the State of Michigan Meritorious Service Medal. Richard received his Master of Science at BGSU after completing his tour in the Air National Guard. He then enrolled in the University of Florida's Department of Geological Sciences and began his Ph.D. examining geomorphic change at Cape Canaveral, Florida for NASA. After graduating, Richard plans on beginning a postdoctoral fellowship at the University of Florida to continue his work on Cape Canaveral geomorphology.